Alma Mater Studiorum – University of Bologna

SCHOOL OF SCIENCE
Department of Industrial Chemistry "Toso Montanari"

Second cycle degree in

Low Carbon Technologies and Sustainable Chemistry

Classe LM-75 - Scienze e Tecnologie per l'Ambiente e il Territorio

Electrocatalytic hydrogenation of biocrude from hydrothermal liquefaction: focus on palmitic acid as model compound

Experimental degree thesis

CANDIDATE

Francesco Longhin

SUPERVISOR

Prof. Patricia Benito Martin

CO-SUPERVISOR

Prof. Jacopo Catalano

Academic Year 2020-2021

Contents

Premise

Climate Change and Global Warming have become fundamental topics of the 21st century due to the evident impacts that they are having on the life of billion people. The global average temperatures have risen by more than 1°C since pre-industrial period. CO_2 and Green House Gases (GHG) levels in atmosphere are worrying (408,52 ppm of CO_2)[1] and with them, as Figure 1 shows, different planetary boundaries have reached or even overcome the safety thresholds of certainties[2].

In particular, food and agriculture industries, facing the continuous growth of world's population, are becoming relevant due to the huge impacts that they have globally. These systems contribute with the 26% of the global GHG emissions (CO_2eq)[3], the 70% of the global freshwater withdrawals[4] and the 78% of global ocean and freshwater pollution[3]. Furthermore, this system produces a high amount of wastes, which often remains unexploited.

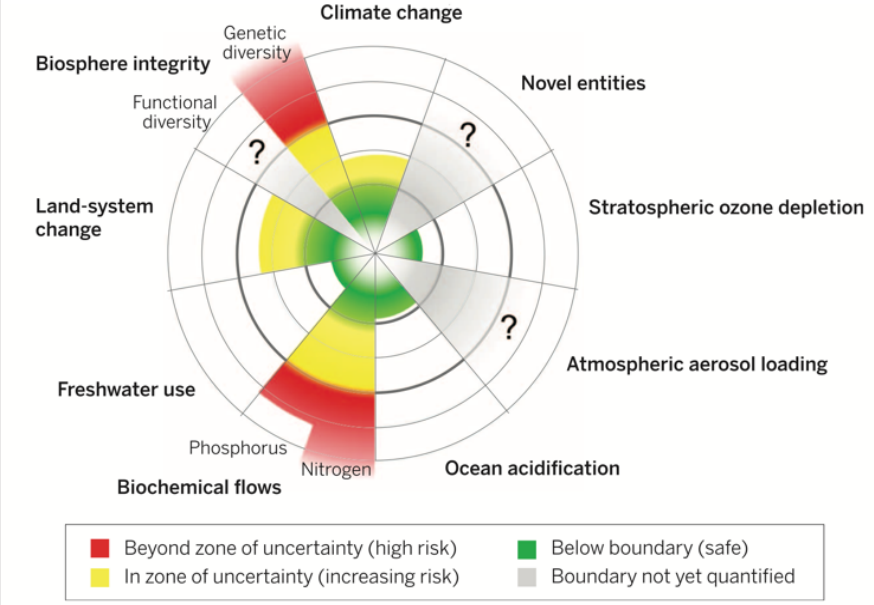

Figure 1: Status of the main planetary boundaries in 2015[2].

Concurrently another essential sector is facing a huge need of change: energy and transportation. Indeed, with a global energy demand growing, fossil fuels represent the primary source of GHG with the three-quarters (73,2%) of the overall global emissions. Of that part, the 16,2% is covered by transportation and the 24,2% by the energy use in industry (see Figure 2).

Facing these problems, innovative, energy efficient and integrated processes are needed, coupled with renewable energy and feedstocks. Moreover, the waste revalorisation is at the base of the circular economy, and it could help to reduce or even neutralised the overall GHG emission and environmental impacts of a sector.

Plant biomass together with organic-waste streams represent one of the most abundant and underutilized resources on the planet, and they can be potentially seen as a promising source of material for fuels and chemicals[5]. Indeed, biofuels and bio-based chemical will be essential for the transition toward a low carbon society, since they would be able to cut the emissions in different

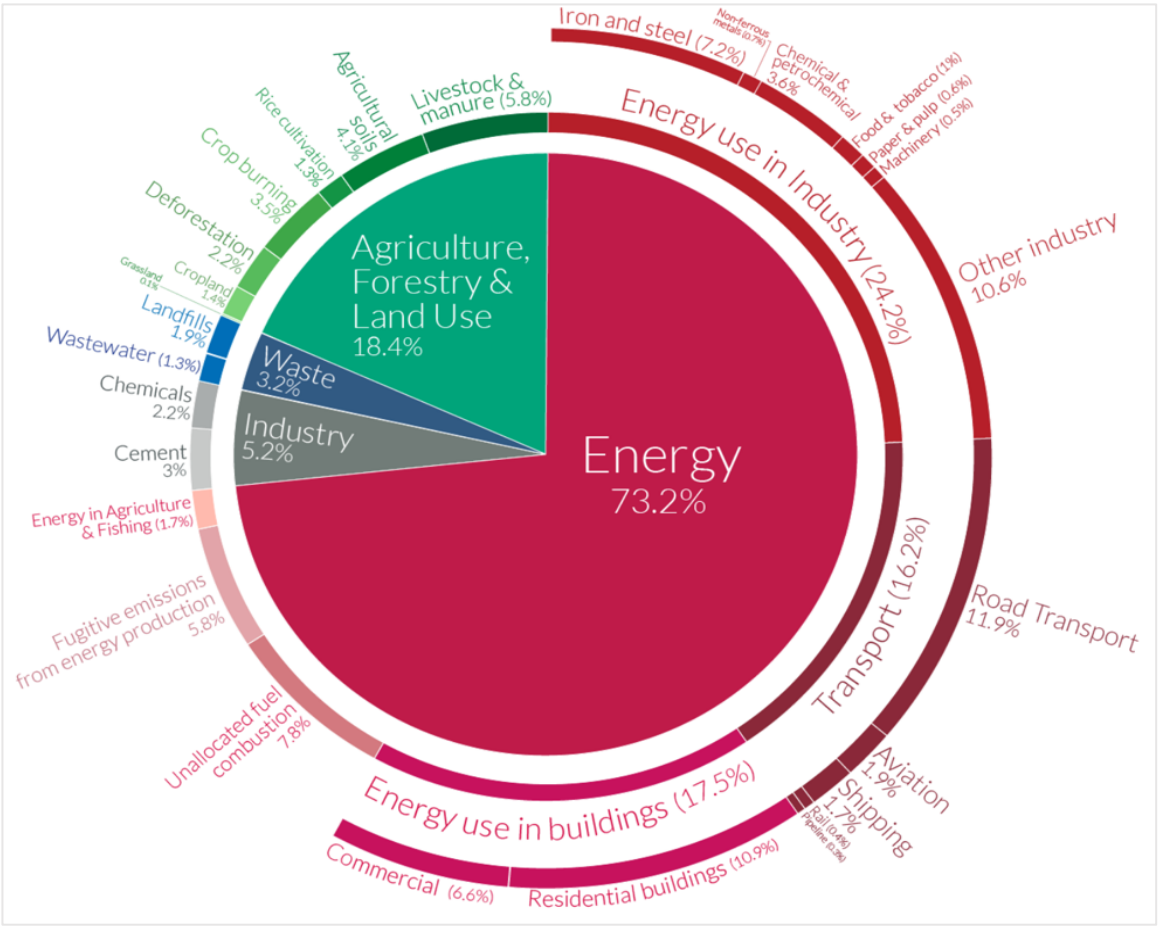

Figure 2: Global GHG emissions (CO_2eq) associated to different sectors[4].

fields. At the same time, bio-based processes and biorefineries could also guarantee the recirculation and the recycling of essential elements such as phosphorous and nitrogen, as well as efficient and integrated energy management systems. In this optic, this elaborate will tackle the complex system of bioenergy (biomass-to-liquid) and waste-to-energy systems, linking them with the electrocatalytic hydrogenation processes and the so-called power-to-X methods. These electrochemical procedures will be contextualised in the production of upgraded biofuels from the oily phase derived from thermochemical processes such as hydrothermal liquefaction (HTL). In particular, the Palmitic acid (PA) was used as model compound for this study due to the notable presence in the specific biocrudes considered, and for its low reactivity toward cathodic electrochemical processes and, therefore, a challenge compound.

The lack of literature, force the team to perform a fundamental analysis on the feasibility of the process related to the PA electrocatalytic hydrogenation (ECH). Moreover, qualitative studies on the possible reaction scheme coupled with a qualitative analysis on the products was one of the main goals of this thesis. This ambitious study starts with this work, and it has been carried out in more or less 7 months thank to the University of Bologna (IT), Department of Industrial Chemistry and the Aarhus University (DK), Department of Biological and Chemical Engineering.

1. Introduction

In the introduction chapter, the general overview useful to understand the context of the study will be shown. Therefore, the first paragraphs will discuss the field of the bioenergy with a focus on the role of the bio-feedstock in the green chemistry and circular economy. The most important thermochemical process will be mentioned with an important focus on the hydrothermal liquefaction (HTL) process for the production of biocrude from wet biomass. In this optic, the process will be introduced with a paragraph on the catalytic HTL and a focus on the HTL pilot plant of Aarhus university, one of the world's largest pilot scale plants from which the biocrude under study has been produced. Afterwards the upgrading processes will be analysed. The mention of the most used processes in industry will be followed by the analyses on the upgraded biocrudes and the specific case of the electrocatalytic upgrading of the biocrude. Finally, a theoretical electrochemical background will be provided for consultancy.

1.1 Bioenergy, biofuels, and waste-to-energy systems

With the continuous raising of the world's energy consumption, biofuels are considered a valid carbon-neutral solution for the progressively decarbonisation of society. Furthermore, they are suitable for the actual fossil-fuels infrastructures, and, at the same time, they cover the most important fossil-based applications. Therefore, even though CO_2 is emitted by combustion, it is reutilised for the biomass growth via photosynthetic pathways. Moreover, the utilisation of waste streams as innovative feedstocks for the biofuel synthesis, fulfils the principle of circular economy and Sustainable Development Goals (SDGs)[6]. While biomass technologies can provide delocalised, integrated and sustainable industrial systems with huge positive impacts on the local energy management systems, from the other hand, in base on the feedstocks, they can have conflicts with the food industry and create concerns regarding land-use, soil degradation and biodiversity loss[5].
In this paragraph, the main types of biofuels and feedstocks will be briefly introduced. After that, the concept of biorefineries will be analysed, with few words on the thermochemical treatments and a focus on the feedstocks under study.

1.1.1 Biofuels and feedstocks

Biofuels derived from plant-based biomasses can be classified on the starting feedstocks and, therefore, based on the processes used to produce them. Hereafter the four main generations of biofuels are tackled:[7]

1. First generation: they derive from oil-based plant, sugar and starch crops and genetically modified crops. They compete directly with the food industry. Some examples of biofuels that can be produced are bioethanol, biogas, and biodiesel. The plants are available at industrial scale, and they are already in the market.
2. Second generation: They are mainly produced from non-food lignocellulosic crop and agricultural and forest residues. They are quite abundant, and they do not compete with food industry. The biofuels derived are mainly lignocellulosic ethanol, butanol, bio-oil and hydrotreating oil. The industrial scale plants are not always available.
3. Third generation: They derive from aquatic biomass such as algae and they rely on a very high photosynthetic yield and a suitable composition. Nevertheless, the industrial plants are expensive and not available yet.
4. Fourth generation: They derived from genetically modified algae biomass. They are not present at large scale, also because they are not regulated by law.

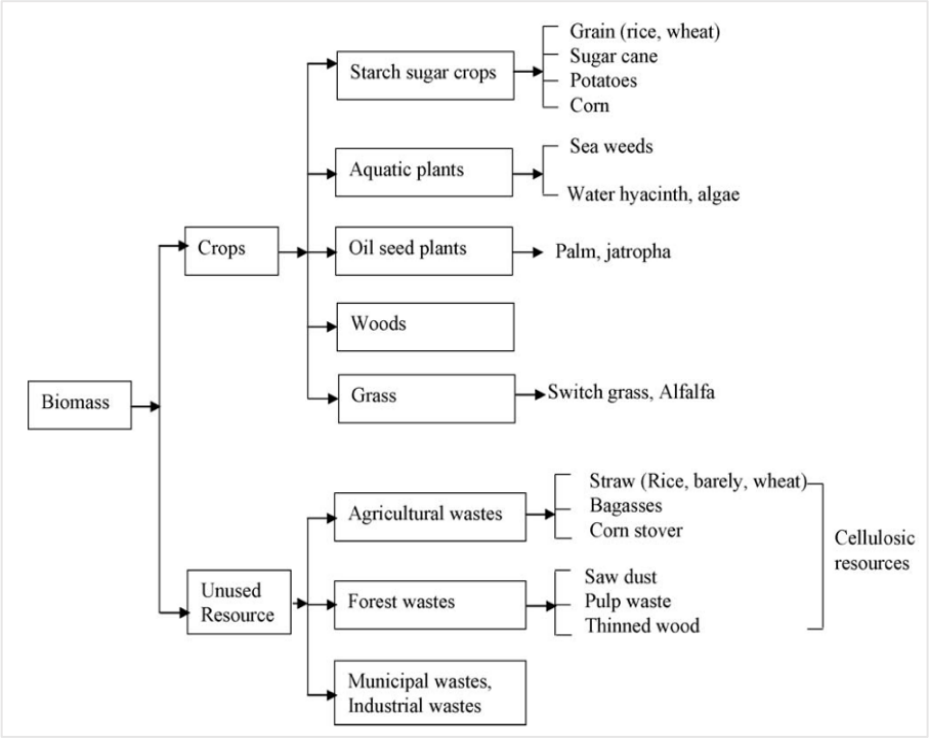

Figure 3: type of feedstocks utilised in biorefineries and for the biofuels production[5].

The most important issues regarding the different generation of biofuels are highlighted in the Annex 1. Biofuels can also derive from non-cellulosic wastes such as municipal and industrial wastes, which required specific treatments and processes in order to manage the even higher variety of organic and inorganic compounds. Those treatments usually have an overall positive impact, and they depend on the specific industrial plant. The two most interesting feedstocks are animal manure and sewage sludge derived from wastewater treatment plants. In particular, the production of biofuels from sewage sludge is feasible and economically viable[8] and it would represent a good step toward the closing of the cycle of the wastewater systems. Instead, the utilisation of animal manure is important for those zones in which farming and breeding

are spread and therefore the need of wastes' recirculation is fundamental. The Figure 3 reassumes the main feedstocks that can be used to run a biorefinery and to synthesise biofuels.

1.1.2 Biorefineries

The concept of biorefinery is related with all those integrated processes aimed to transform biological raw materials into industrial intermediates or final products with higher market value[9]. Biorefineries usually rely on a rather complex flow chart, and, at the same time, they are based on very different type of processes, from chemical-physical to microbiological treatments, arriving to the innovative electrobiochemical processes. This fact is related with the very high variety of feedstock in term of chemical composition, reactivity, and physical properties.

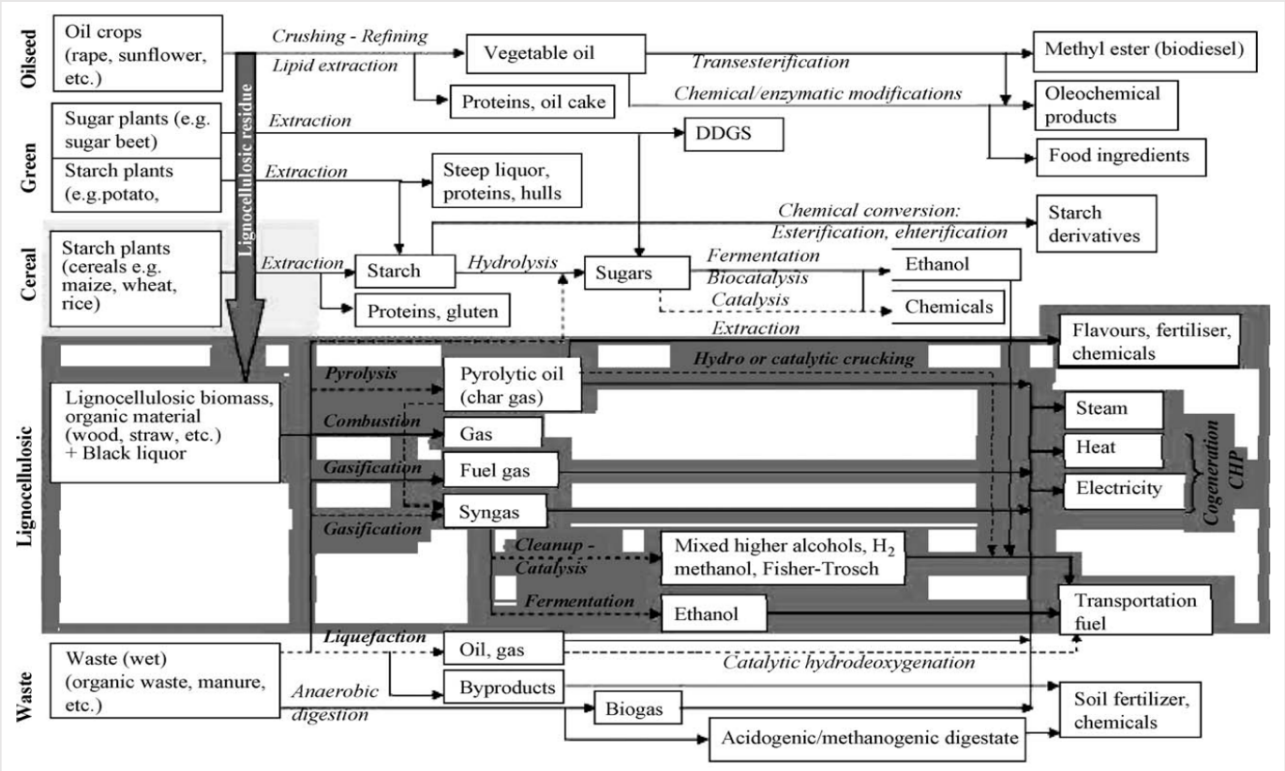

Figure 4: flow chart of a potential integrated biorefinery[5].

For this reason, the biorefineries can be customized based on the inlet feedstock flows. In this logic they can be distinguish in: (1) green biorefineries, which treat green biomass such as grass or green crops, (2) cereal biorefineries, (3) forest and lignocellulosic biorefineries, (4) algae-based biorefineries and (5) integrated biorefineries, that combine the processes in order to have benefits in term of energy requirements and final products' quality. To recognise the complexity of these systems, the Figure 4 shows the flow chart of an integrated biorefinery. As it is visible, many possible processes have integrated each other with few possible pathways. The possible final products could be biodiesel and other biofuels, oleochemical products, platform chemicals, food ingredients, fertilisers, flavours, soil amendments, hydrogen, electricity, and heat.

1.1.2.1 Thermochemical processes

In a biorefineries, as stated above, different types of processes can be found. They can be classified in mainly four categories (see Figure 5)[5]:

a) *Thermochemical processes:* such as torrefaction, pyrolysis-based processes, combustion, gasification, and hydrothermal liquefaction.

b) *Biological processes:* which comprehend all the fermentative and enzymatic processes, as well as anaerobic digestion.

c) *Chemical conversion processes:* they rely on chemical reaction of hydrolysis, solvent extractions and all those processes performed in supercritical conditions.

d) *Physical processes:* such as mechanical extraction, briquetting of biomass or distillation processes.

In this study only the thermochemical processes will be considered. These type of processes are based on the use of heat, and in some cases pressure, to promote chemical transformation of biomass into energy or chemical products[10]. The main valuable products that derived from these processes are syngas ($H_2 + CO$), bio-oil, char, tar, heat and aqueous streams.

A part the HTL that will be faced in the paragraph 1.2, the most important thermochemical processes are basically four[5]:

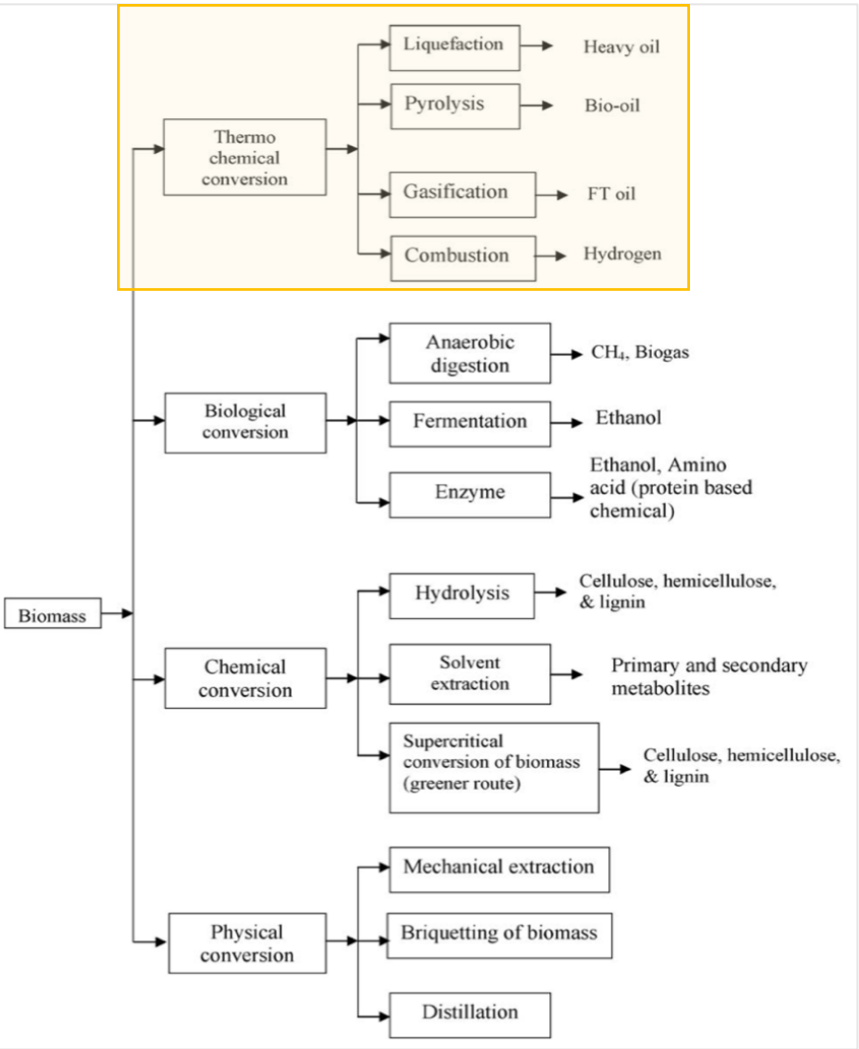

Figure 5: some of the most important biomass conversion processes[5].

1. *Combustion:* It is the oxidative reaction between oxygen and the fuel to produce CO_2, CO, H_2O, H_2S, NH_3, heat and, eventually, all the heteroatoms oxygenated derivatives such as NO_x and SO_x.

2. *Torrefaction:* this process is used for the solid fuels production from different feedstocks such lignocellulosic biomass (lignin, cellulose, and hemicellulose) and municipal solid wastes (MSW)[11]. Torrefaction is done at temperature from 180 to 300 °C and the processes is composed by five main stages (see Figure 6): (1) initial heating, (2) drying stage, (3) Intermediate heating, (4) torrefaction stage and (6) cooling stage. Moreover, it can be performed in three main ways[12]:
   Dry torrefaction: The reaction medium (carrier gas) is an inert gas (N_2 or CO_2) or an oxidative gas like air. With N_2 the solid yield (char) is higher, but the costs increase due to the air purification.
   Wet torrefaction (hydrothermal carbonisation): the reaction medium is water or diluted acid, and the product is called hydrochar. The suitable temperature is from 180-260 °C and sometimes it achieves the subcritical conditions[13]. Therefore, the changed properties of water help to degrade the biomass and the diluted acid (sulfuric acid or acetic acid) enhance the wet torrefaction performances. In this process a series of physicochemical reaction occur related to hydrolysis, decarboxylation, and dehydration. Therefore, the water phase is rich in fundamental nutrient such as phosphorus, nitrogen and ammonia, coupled with recalcitrant products like phenols and furfurals[13]. This process is seen as the most promising of all the torrefaction processes.

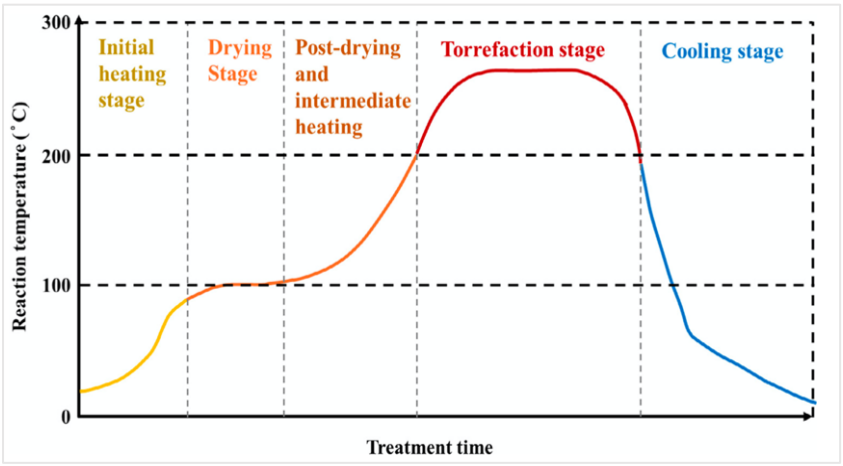

Figure 6: torrefaction's main stages[12].

   Steam torrefaction: It is based on a steam explosion at 200-260 °C and high pressures. Therefore, the biomass is in a pressurised chamber in T, the pressure is rapidly released, and the steam swells the lignocellulosic biomass with the production of more elastic and strong pellets.
3. *Pyrolysis*: It is a processes carried out in absence of gases and at *T* that can reach 1000°C[14]. It is basically a degradation of the biomass with a redistribution of the molecular weight of the particles and the production of syngas. The products are divided in three main fractions: (1) gaseous phase (syngas, CH_4 or ethylene), (2) solid fraction (ashes, char or amorphous solids) and (3) liquid fraction (bio-oil, alcohols, biodiesel and glycerol)[14]. The temperature and the residence time are set based on the target group of molecules and the final products. For example, the proteins will be degraded at 100°, but the lignin starts at 350°C until 1000°C. Two main unconventional pyrolysis are present:

Fast pyrolysis: it is performed at high temperatures with fast heating rate and short residence time. It produces mainly gaseous and liquid product; 60-75% bio-oil, 10-25% solid char and 10-20% of uncondensed gases[5].

Flash pyrolysis: it has even shorter retention time and a very high heating rate, which allows the formation of low-molecular weight products[15]. The mass balance is directed toward the gas phase, but a good percentage is also covered by the biocrude (up to 70%)[5].

4. *Gasification*: it is aimed to produce gaseous products from a partial oxidation controlled by a specific catalyst. The most desirable product is syngas, which can be used for the synthesis of fuels (Fischer-Tropsch process) or other chemicals. The temperatures are usually >700°C and in those conditions also tar is produced with CH_4, NH_3 and volatile hydrocarbons. In order to convert tar in syngas it has to work above the 1200 °C[10]. Gasification is a well-known process since it has been used for coal and the studies are focusing on the catalytic improvements. It usually can refer to two different processes:

Gasification: in which the biomass reacts with oxygen in an exothermal reaction ($\Delta H < 0$).

$$CH_4 + 1/2O_2 \rightarrow CO + 2H_2 \quad \text{(I)}$$

Steam-reforming gasification: biomass reacts with steam in an endothermal reaction ($\Delta H > 0$).

$$CH_4 + H_2O_{(g)} \rightarrow CO + 3H_2 \quad \text{(II)}$$

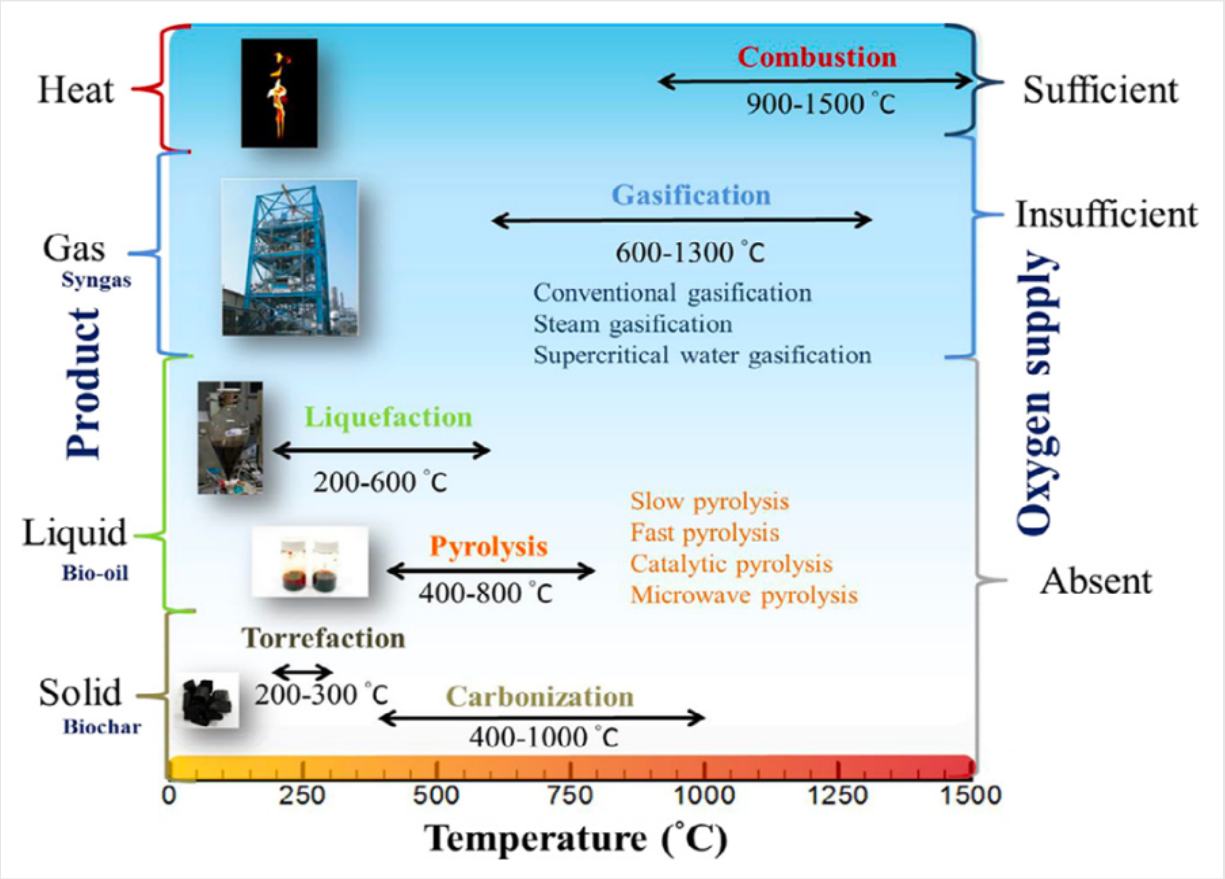

Figure 7: schematic visualisation of the main biomass thermochemical processes[12].

Figure 7 shows a schematic representation of the thermochemical processes analysed (even the HTL) in relationship with their main characteristics in term of oxygen demand, temperature, and main products.

1.1.3 Feedstocks under study

The feedstocks that have been considered are basically three: (1) *Miscanthus*, (2) *Spirulina* and sewage sludge. They have been described in some details by Anastasakis et al. in the article "Continuous Hydrothermal Liquefaction of Biomass in a Novel Pilot Plant with Heat Recovery and Hydraulic Oscillation"[16]. This article will be taken as reference for the further analysis (see also paragraph 1.2.2).

The Table 1 refers to the elemental analysis (wt%, dry) and the higher heating value (HHV) of the analysed feedstocks[16].

	Miscanthus	*Spirulina*	Sewage Sludge
Ash (wt%, dry)	2.7	6.5	12.5
C (wt%, dry)	49.1	50.6	46.5
H (wt%, dry)	3.8	7	6.1
N (wt%, dry)	0.7	11.8	3.3
S (wt%, dry)	0.2	0.8	0.4
O * (wt%, dry)	43.5	23.3	31.2
HHV (MJ/kg)	17.1	23.3	19.8

Table 1: elemental analysis and HHV of the three model biomass feedstocks. The O content has been calculated by difference[16].

Miscanthus (*Miscanthus Giganteus*) is an herbaceous perennial crop composed mainly by lignocellulosic biomass. it is characterised by high yield, environmental adaptability, and long lifecycle (from 20 to 25 years)[17]. It has been considered as model for the 2nd generation lignocellulosic feedstock. It was harvested in early-January 2018 from the Danish Center for Food and Agriculture, Foulum, Aarhus University. It presents low amount of ashes and nitrogen content, but a notable presence of oxygenated compounds. Before the processing, the fresh *Miscanthus* biomass is chopped and extruded. Carboxymethyl cellulose has been used as thickener producing long and soft fibres. The slurry is produced by adding water and KOH which acts as catalyst for decomposition of the lignocellulosic fraction. The final dry matter content is 15 wt%.

Spirulina (*spirulina platensis*), instead, is a microalga characterised by a high lipidic content and a very low nutritional requirements[18]. It represents the 3rd generation of biomass with high nitrogen content coupled with a lower O content and a higher HHV. It derives from a Chinese private company in form of dried powder. The slurry is produced by mixing *Spirulina* with water, achieving a 16,4 wt% of dry matter.

Sewage sludge, instead, represents the model waste biomass feedstock, typified by a high amount of ashes. It comes from the wastewater treatment plant of Viborg (DK), and it has been collected and processed in the same days after primary treatments. The feedstock in this case is used without any pre-treatments and it exhibited a dry matter of 4 wt%.

These three-model feedstock have been used to run the HTL plant of Aarhus University and they will be reanalysed in the paragraph 1.2.2.

1.2 Hydrothermal liquefaction

Hydrothermal Liquefaction (HTL) is an innovative and promising thermochemical conversion technology that transforms biomass into biocrude and other value-added chemicals. The first thing to highlight when speaking of HTL, is its ability to use directly wet biomass without pre-treatments, avoiding cost-intensive dewatering/drying processes.. This fact is essential, considering that only the United States alone produces annually 79 millions of dry tons of wet biowaste from animal, agriculture and food industries. Due to the high water content (80-99%) it has been stated that, by using conventional methods, the 90% of energy content in the recoverable oils would be used for the processing and the pre-treatments, jeopardising the overall benefits[19].

Another important aspect of the HTL is the possibility to use a large variety of feedstocks. One of the most promising application has been found, indeed, in the treatment of algae-based biomass such as *spirulina*. The classical method to produce fuels from algae consists in fatty acids extraction from dried biomass followed by transesterification, producing biodiesel and glycerol. In this process the 50% of the required energy is used for the drying and the distillation,[20] decreasing the overall energy efficiency of the process. Other studies highlighted the possibility to use plastic materials such as polyolefins, polycarbonates and polyesters which could be ideally treated achieving good yield comparing to the classical pyrolysis[1421]. Lignin has been demonstrated as an efficient feedstock for HTL; it can be treated in aqueous phase, but the highest yields have been achieved by using alcohols such as methanol or ethanol as solvent. Using a Co/CNT (Carbon Nanotubes) catalyst with a reaction temperature of 280°C and ethanol as solvent, the biocrude yield from lignin was 66,2 wt%[22]. Additionally, a study by Jie Yang et al. shows the feasibility to directly replace the freshwater with seawater, without jeopardising the yield, the overall efficiency of the process, and the quality of the final chemicals[23]. Hence, salt-contaminated feedstock can be converted directly without any desalinisation treatment.

The potentials of HTL are quite evident; the next paragraphs will explain this innovative method starting with a process overview and arriving to deal with the specifics of the Aarhus University's HTL pilot plan. In this plant, the three types of biomasses described in the chapter 1.1.3 are treated to produce the biocrude under study.

1.2.1 Process overview

The main products from HTL are solid residues, aqueous phase extracts, variable gas phase and biocrude (or bio-oil). With reference to Figure 8, the solid residues that are based on metal ashes, char and tar, can be recycled to produced carbon material, catalysts or recover the metals[24]. The gas phase is mainly formed by H_2, CO, CO_2 and CH_4 derived from the macromolecule degradation. The aqueous phase in this work will not be considered, but the purification of this phase is still one of the most problematic and challenging part of the overall HTL process, due to the complexity of the solution and the high variety of chemicals that could be recovered. Here is worth to note that electrochemical techniques can, and are, applied also for the purification of process water. The bio-crude is one of the most desirable products, its chemical characteristics and calorific power makes it suitable for a variety of uses. The bio-oil yield is defined by the equation (1)[25]:

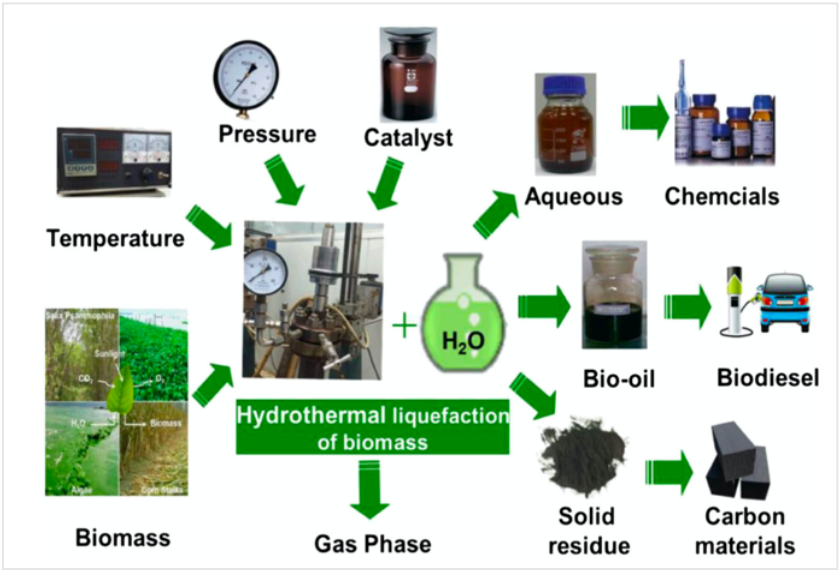

Figure 8: Overview on aqueous HTL process[24].

$$\text{Bio-oil yield} = \frac{\text{Bio-oil Mass}}{\text{Feedstock Mass (dry)} + \text{Mass of Catalyst}} 100\% \qquad (1)$$

Nevertheless, the bio-crude is not suitable for the direct use, thus further upgrades are needed to produce a good quality bio-oil. These treatments, tackled in chapter 1.3, are very important for the overall process, and the upgraded bio-oil from HTL (and from pyrolysis) could be utilised in different ways. Below some of the possible uses are listed[26]:

1. Drop-in fuels in transportation.
2. Combustion fuels in boils, furnaces, diesel engine or turbine.
3. Production of anhydro-sugars (like levoglucosan), which are used in pharmaceuticals, surfactants, and biodegradable polymers.
4. Liquid smoke and wood flavours.
5. Production of chemicals and resins.
6. Production of adhesive (e.g. asphalt bio-binder).

With reference to Table 2, HTL has many advantages. The possibility to integrate an "easy" recycling of nutrients such as P, Fe, Ca, Mg and K is fundamental when considering algae as feedstock, since they could be reused to grow the algae and close the cycle. The overall yield is acceptable, but the technology is still far to be mature. Indeed, some challenges must still be faced, such as the high capital costs due to the high pressure, temperature, as well as corrosion issues. Furthermore, it requires notable integration to be efficient, which makes this process suitable for future biorefineries.

Table 2: Advantages and disadvantages of HTL against other thermochemical processes

	Advantages	Disadvantages
HTL Process	High energy efficiency; promotion of non-spontaneous reaction using pressurised water[20]	Inevitable production of the so-called hydrothermal liquefaction aqueous phase (HTL-AP)[27]
	Wet biomass without pre-treatments such as drying	Higher viscosity of the biocrude respect to the pyrolysis one
	Effective towards the lipid fraction, but also proteins and carbohydrates	The technology is still not mature, there are basically only pilot scale plants
	Easier recycling of the nutrients such as P, Fe, Ca, Mg, K, that could be reused for the algae growth or other purposes[28]	Formation of coke, char, tar and other solid residues which can deactivate the catalysts or cause reactor plugging[24]
	In the case of the algae biomass, in comparison to lipid extraction, HTL can reduce energy requirements by at least 50%, freshwater consumption by 33%; saline groundwater by 85% and N-P demand by 44%. In comparison to fast pyrolysis, HTL bio-oil has an higher energy density, with lower O content[29]	Corrosion issues at subcritical conditions (mainly). Acidic and oxidizing environments can cause rapid corrosion, due to the dense and polar character of subcritical water[30]
	The algae-based HTL bio-crude has a higher energy content then the pyrolysis ones[25]	Further studies on kinetics must be done, to understand more in deep the complex reactions mechanism.
	Overall modest biocrude yield (40-83%)[27]	High pressure conditions that makes the HTL's economy questionable[31]
	Spontaneous phase separation (water soluble fraction and biocrude) with the consequent decreasing of the costs[32]	

1.2.1.1 Reaction conditions and mechanism

Liquefaction is the splitting of big molecules into smaller, which usually, due to the high reactivity and instability, repolymerise producing the bio-oil. Compared to other thermochemical processes, HTL works at lower temperature, from 250°C and max 400°C, with a sensible decreasing of energy supplied; furthermore, the pressure is usually maintained from 10 to 25 MPa for a reaction time

estimated from 5 to 120 min[33], being 20 minutes a characteristic residence time for a continuous HTL process. The mechanism of reaction is strictly related to the feedstock composition, reaction conditions and catalyst; in general, the HTL reaction evolution can be divided in three main steps:

1. Depolymerisation: The biomass in presence of high temperature and pressure starts to change its chemical structure. Usually, insoluble long chain polymers derived from lignocellulosic feedstock (lignin, cellulose) are transformed in shorter chain partial-soluble compounds. Another important aspect of this phase is that the energy content in the organic matter, in presence of water, can be recycled and reused.
2. Decomposition: in this phase the organic material is degraded and depending on the composition, a series of different important reaction can happen. Some of them involves water (hydrolysis and dehydration), CO_2 (decarboxylation) and/or amino group of the proteins (deamination). Water, in these conditions, can hydrolyse the macromolecule forming monomers and oligomers. An example is the hydrolysis of cellulose producing glucose monomers, which are rapidly degraded with a series of domino reactions. The products of this phase are usually soluble in water and includes furfural, phenols, glycolaldehyde, organic acids and other polar organic molecules.
3. Recombination: This phase is characterised by a lack of H_2 and a surplus of highly reactive molecules (radicals). In this reaction environment, the fragments repolymerise producing the bio-crude and the solid products of HTL (char).

Temperature is, therefore, a fundamental parameter in HTL. It has been demonstrated that when water is in subcritical conditions (280-320°C), by rising the temperature the fracture of chemical bonds and the depolymerisation of biomass increase, with the consequently repolymerisation and the rise of the biocrude yield. Instead, working in supercritical conditions (400°C or more), the yield of char and gas phase seem to increase promoting the repolymerisation, the re-decomposition of the intermediates, as well as the condensation in solid fraction, decreasing the biocrude yield[24]. This is the reason why the temperature threshold has been set at 400°C. The first reaction is usually a hydrolysis, which occurs at low temperatures; afterwards, and depending on the starting feedstock, the reaction mechanism begins to branch out. In the specific case of long chain fatty acids, such as palmitic acid, they derive from the hydrolysis of lipids (triglycerides) and depending on the reaction temperature, they will be decarboxylated producing hydrocarbons or even remain unconverted. In any cases, the elemental composition of the final biocrude changes based on the reaction temperature (see Annex 3). The Table 3[24] shows the effect of the temperature in the final elemental composition of biocrude, as well as the holding time (residence time) and the biomass/H_2O ratio.

Table 3: Effect of the reaction temperature to the final elemental composition of biocrude[24].

Parameters	C (%)	H (%)	O (%)	N (%)	H/C	O/C	HHV (MJ/kg)
Temperature (°C) [60]							
280	67.03	7.36	24.30	0.77	1.32	0.27	26.75
300	67.89	7.62	23.18	0.75	1.35	0.26	27.29
320	68.77	7.65	22.13	0.80	1.33	0.24	28.63
340	70.84	7.52	20.39	0.71	1.27	0.21	30.47
360	72.81	7.73	18.14	0.78	1.27	0.19	32.16
380	75.23	7.46	16.04	0.78	1.19	0.16	34.58
400	77.22	7.36	14.07	0.79	1.14	0.14	35.48
Holding time (min) [65]							
15	82.0	7.1	5.4	4.9	1.04	0.05	36.5
30	77.0	8.6	8.9	5.5	1.34	0.09	36.0
45	75.1	9.0	10.9	5.0	1.44	0.11	35.6
60	80.1	8.3	6.1	5.4	1.24	0.06	37.0
120	78.9	8.3	7.5	5.3	1.26	0.07	36.4
Biomass:H_2O (g/ml) [65]							
2:10	77.6	8.4	7.9	6.1	1.29	0.08	36.0
2:20	79.4	8.0	7.2	5.4	1.20	0.07	36.3
2:35	77.6	8.6	8.8	5.0	1.32	0.09	36.2
2:40	74.4	8.5	12.4	4.8	1.37	0.13	34.6

In average, increasing the *T,* the carbon content and the HHV tend to increase as well. Another important parameter is the pressure. In the case of HTL, the pressure is increased to maintain water in subcritical or supercritical conditions avoiding large enthalpy inputs required for H_2O's change of phase. In many HTL cases, pressure has no direct influence on the overall biocrude yield even though it promotes the biomass dissolution rate with the consequently increasing of decomposition and hydrolysis[24]. Hence, once the conditions for HTL are achieved, the pressure has a negligible role in enhancing the oil yield but is essential to maintain the correct environment[34].

Other parameters that largely affect the mechanism of HTL are the residence time of the feedstock and the ratio water/biomass.

1.2.1.2 Catalytic HTL

The catalytic HTL process is becoming more and more objective of study. The choice of the catalyst can influence remarkably the yield of the final bio-oil[33]. Indeed, catalysts, by reducing the activation energy of the reactions, can positively affect the overall process efficiency also decreasing the required temperature. Both homogeneous and heterogenous catalysts can be used for HTL.

In HTL homogeneous catalysis, the catalyst and the reactant/substrate are in the same phase (in this case liquid) and they interact in a solvent[35]. Different type of homogeneous catalyst can be used; the most common are alkali-catalyst such as Na, K, Ca hydroxide or carbonate, organic acid catalyst like formic and acetic acid, and finally, inorganic acid such as sulphuric acid. Table 4 shows the major advantages and disadvantages of homogeneous catalysis in HTL.

The alkali-catalyst are more widely employed due to the higher reactivity towards the heteroatom's removal, and since they can boost the liquefaction of lignin with the further depolymerisation. The

acid catalyst, instead, improve the fluid-dynamic of the system by reducing the bio-oil viscosity. Homogenous catalysts are easy to implement in a process and they are highly soluble in water. The drawbacks are, however, very significant. In fact, these catalysts are very difficult to separate and recycle. They require expensive and, sometimes, not environmentally sustainable treatments that can have impacts on the overall process value. Moreover, they can contaminate the products, as well as increase the gaseous yield, especially acid catalysts, due to decomposition reactions.

Table 4: Advantages and disadvantages of HTL homogeneous catalysts.

	Advantages	Disadvantages
HTL homogeneous catalysts	High selectivity	Products contamination
	High effectiveness	Corrosivity
	Easy to control T in exothermic or endothermic processes	Expensive processes for the separation and the purification of the solutions[33]
	Negligible diffusion problems	Low rate of recyclability
	Available with affordable costs	Sometime toxic
	Soluble in water even at low temperatures[28]	Issue related to the safety risks in hydrogenation and oxidation processes
	Less affected by coking[33]	Acid catalysts increase the gaseous
	Active towards carbohydrate rich biomass[28]	Acid catalysts less efficient to remove heteroatoms then the alkali catalysts
	KOH and K_2CO_3 enhance the lignin liquefaction, the hydrolic depolymerisation and heteroatoms removing, avoiding solid residues production.	
	Acid catalysts improve the flow properties, reducing the bio-oil viscosity	

In HTL's heterogeneous catalysis, the catalyst and the reactant/substrates are in different phases. In this case, the catalyst is always a solid material, and the reagents can be found liquid, gaseous or solid. Table 5 shows the advantages and disadvantages of heterogeneous catalysts in HTL. The strength of these catalysts is the high versatility; indeed, they can be functionalised in relationship with the reaction that one wants to boost, increasing the selectivity of the overall process.

Furthermore, they are in line with the principle of the green chemistry, since they are easy to separate, usually non-toxic and with a good recyclability. For HTL process different heterogeneous catalyst have been found. The most used are based on metals (bimetallic or monometallic) such as Pt, Pd, Ru, Ni, Mo, Co supported on carbon materials (nanotubes, active carbons, wires, or carbon black), SiO_2, Al_2O_3 or other porous materials. In addition, also zeolite and metal oxides (mixed or not) can be used. In general, the heterogenous catalysts can have acid or basic sites, or can be engineered to have both of them. Chen et al. have demonstrated that the implementation of heterogeneous catalysts like Pt/C

or Al_2O_3, CoMo/γ-Al_2O_3, Ni/SiO_2- Al_2O_3 showed to increase the HHV of the final bio-oil[36]. In particular, Pt/Al_2O_3 and CoMo/γ-Al_2O_3 seem to be more selective towards the deoxygenation of lipids, while the Ni/SiO_2- Al_2O_3 catalyst towards the carbohydrates. Ru/C, instead, uses to promote desulphurization and denitrogenation reactions[28].

Table 5: Advantages and disadvantages of HTL heterogeneous catalyst.

HTL heterogeneous catalysts	Advantages	Disadvantages
	No corrosion issues	External Mass Transfer, porosity/surface area dependent catalysts[37]
	Easy to separate from the gas and/or liquid phases	Internal mass transfer limitations
	No toxic wastes	Usually, lower yield in HTL
	Good recyclability	Coke can inactivate the catalysts
	Higher selectivity towards the HCL reactions	Difficulties to control T (hot spots due to the inconstant thermal conductivity)
	Promotion of the bio-oil stability (increasing the fraction of alkene, alkanes, and ketones)	Difficult to implement in HTL continuous reactors, with higher costs
	Increasing of the HHV promoting the deoxygenation	Base catalysts can be poisoned by air or lipids[37]
	Possibility to synthetise functional catalysts that promotes the selectivity towards the HTL reactions (silica-based catalysts, or Raney-Ni)[38]	The acid catalysts have difficulties to convert carbohydrates, since cracking reactions can occur and the small particle move to the water phase[37]

A study carried out by Lu et al. showed that using a functional porous-silica-based catalyst (or Raney-Ni) with both acid and bases sites can enhance the selectivity toward hydrocarbons and the production of low-boiling point compounds (from 68% of catalysts with only bases or acid sites to 81%). A demonstration that, in order to produce low-boiling point hydrocarbons, both acid and bases sites are needed (KOH and Na_2CO_3 are able to increase the yield low-boiling hydrocarbons too)[38].

The catalyst in HTL have a fundamental role, more studies will be carried out in order to improve and optimise this new technology.

1.2.2 Case of Aarhus University HTL Pilot Plan

At the University of Aarhus is present a pilot scale HTL plant; it has been designed *ad-hoc* and described by Anastasakis et al. in the relative article[16]. The plant is in a continuous mode with an innovative patented oscillating flow technology, a unique heat recovery system and a parallel hydraulic pressure system. It has a feed capacity of 100 L/h, one of the largest in literature, and a process volume of 20 L (see Figure 9).

Since, the biocrude produced by this plant has been used as reference for all the present study, an overview on the process, highlighting the plant design and the raw biocrude composition, is described in the following sections.

Figure 9: HTL pilot plan of Aarhus University. Centre for Circular Bioeconomy (CBIO), Foulum, Denmark.

1.2.2.1 Plant design

As we can see from the flow diagram in Figure 10, the plant is divided in seven sections, controlled by a PLC (Programmable Logic Controller): (1) feed introduction system, (2) heat exchanger, (3) trim heater, (4) reactor, (5) oscillation system (formed by 2 oscillators), (6) take-off system and (7) product collection zone.

The first pump is a progressive cavity pump, and its aim is to provide a continuous recirculation of the slurry as well as guarantee a steady flow rate in the system. The second pump, instead, feeds the slurry in the reactor. This is a particular unit that can feed high viscosity fluids and can deliver pressure of up to 476 bar and a flow rate of up to 600 L/h. In normal conditions, a flow rate of 60 L/h and a pressure of 220 bar are used. The feed is pumped in the heat exchanger, which is characterised

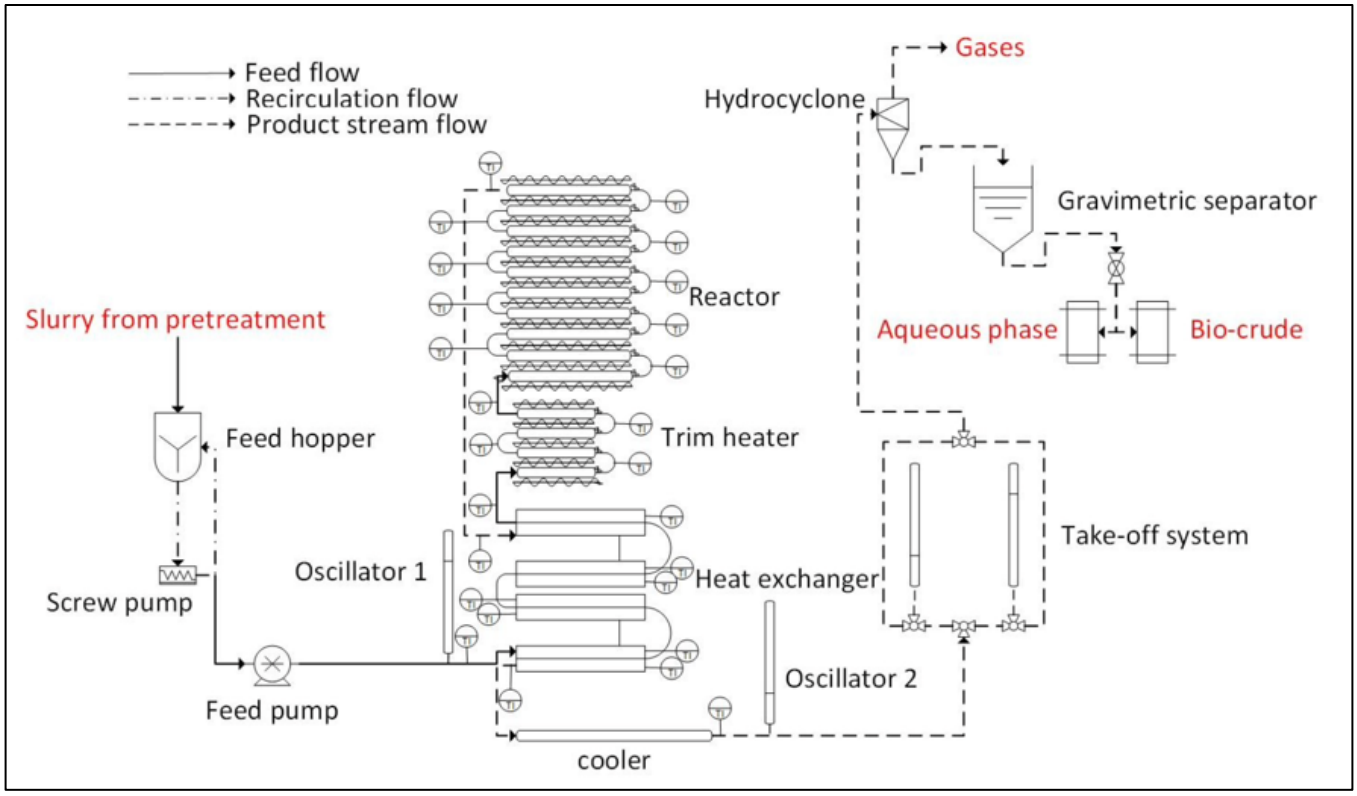

Figure 10: Flow diagram of the Aarhus University's HTL pilot plant[16].

by 8 Inconel pipes (25,4 mm of outer diameter and 5,6 mm of wall thickness) divided in 4 convolutions (12 meters each), making the "cold" and "hot" zone sides. The total length of the 2 sides is 49,2 m and some ductile heat clamps have been used to clamp the hot and cold tubes together. To monitor and control the temperature profile in the heat exchanger, 10 thermocouples are used. Hence, the slurry is pre-heated in the "cold" side before entering in the trim heater, where the feed is still heated until the reaction temperature of 350°C.

The trim heater is composed by 4 pipes divided in 2 convolutions (total length equal to 12,6 m), equipped with 32 independent electrical heaters with a heat capacity of 1 kW. Few thermocouples have been implemented to monitor the temperature profile. Before leading the reactor, the feed meets the first oscillator that enhance the turbulence and, consequentially, the local Reynold's number. It is composed of a piston and its aim is to enhance the heat transfer and improve the mixing, increasing the velocity of the slurry without changing the residence time. This is possible due to alternating the two oscillation systems, which work continuously; in other words, the system while pushes down one of the pistons, retracts the second ultimately letting the slurry to flow continuously in the plug flow reactor. A series of valves are used to maintain the suitable pressure and the movement of the pistons. At this point the slurry is ready to enter in the reactor, where the biomass conversion occurs. In this unit, 5 electrical heating tapes and 10 thermocouples are employed to maintain and control the temperature. Afterwards, the product flux is directed to the "hot" side of the heat exchanger where is cooled down and before reaching the take-off system, it meets the second oscillator.

Figure 11: 90 L separation/collection funnels (left) and Internal room (right) of the Aarhus University HTL plant

The take-off system works in a similar manner with respect to the oscillation system. It is composed by 2 pistons (0,5 L capacity) working in alternation for pressure release. They allow a continuous flow towards the collection funnel. The product collection zone is based on a hydro-cyclone for the gaseous and liquid streams separation and a 90 L separation funnel for the bio-crude and aqueous

phase separation (see Figure 11). Samples of approximately 500 mL (as the capacity of the take-off pistons) are collected directly from the product pipe at regular time intervals at temperature of ~50-60 °C and stored at 5 °C for the analysis[16].

1.2.2.2 Raw bio-crude composition

In general, the raw bio-crude composition is divided in 2 main bio-fractions[31]:

1. Dry biomass feedstock: lignin, hemicellulose, and cellulose derivatives.
2. Wet biomass feedstock: lipids/fatty acids (triglycerides) and protein/amino acids.

The composition of the raw biocrude is an important factor that influences the final upgraded product. From the mechanisms described in the chapter 1.2.1.1, there could be very different products starting from different feedstocks and using different reaction conditions (T, water content, catalyst). The Annex 2 shows the biocrude elemental composition from HTL of different feedstocks[31].

In the case of the Aarhus University HTL Pilot Plan, the three different feedstocks used for the process, *Miscanthus*, *Spirulina* and sewage sludge, show different final bio-crude composition[16]. They have been analysed using a GC-MS equipped with a suitable column, the same used for the analysis on the liquid phase of this study (see paragraph 2.4.4). From the chromatogram of Figure 12, the biocrude derived from *Miscanthus*, a lignocellulosic biomass, presents a large variety of aromatic hydrocarbons, phenols derived compounds, furfurals, aromatic alcohols, and palmitic acid.

Secondly, in the *Spirulina*-based biocrude, the aromatic hydrocarbons fraction (p-cresol, phenol, 3-ethylphenol, styrene) as well as the nitro-aromatics are present, due to the high protein content in the feedstock (indole compounds such as H1-indole and 3-methyl-1H-indole). Furthermore, a big fraction is composed by aliphatic hydrocarbons and long chain fatty acids. The most present are heptadecane, palmitic acid, linoleic acid and linolelaidic acid.

Finally, in the biocrude derived by the treatment of sewage sludges, the composition is dominated by long chain fatty acids such as palmitic acid, linoleic acid, oleic acid, stearic acid, and myristic acid. A smaller, but notable part, is also composed by aromatic alcohols (p-cresol and phenol) and long chain saturated alcohols such as 1-dodecanol, 1-tetradecanol, 1-hexadecanol and 1-octadecanol.

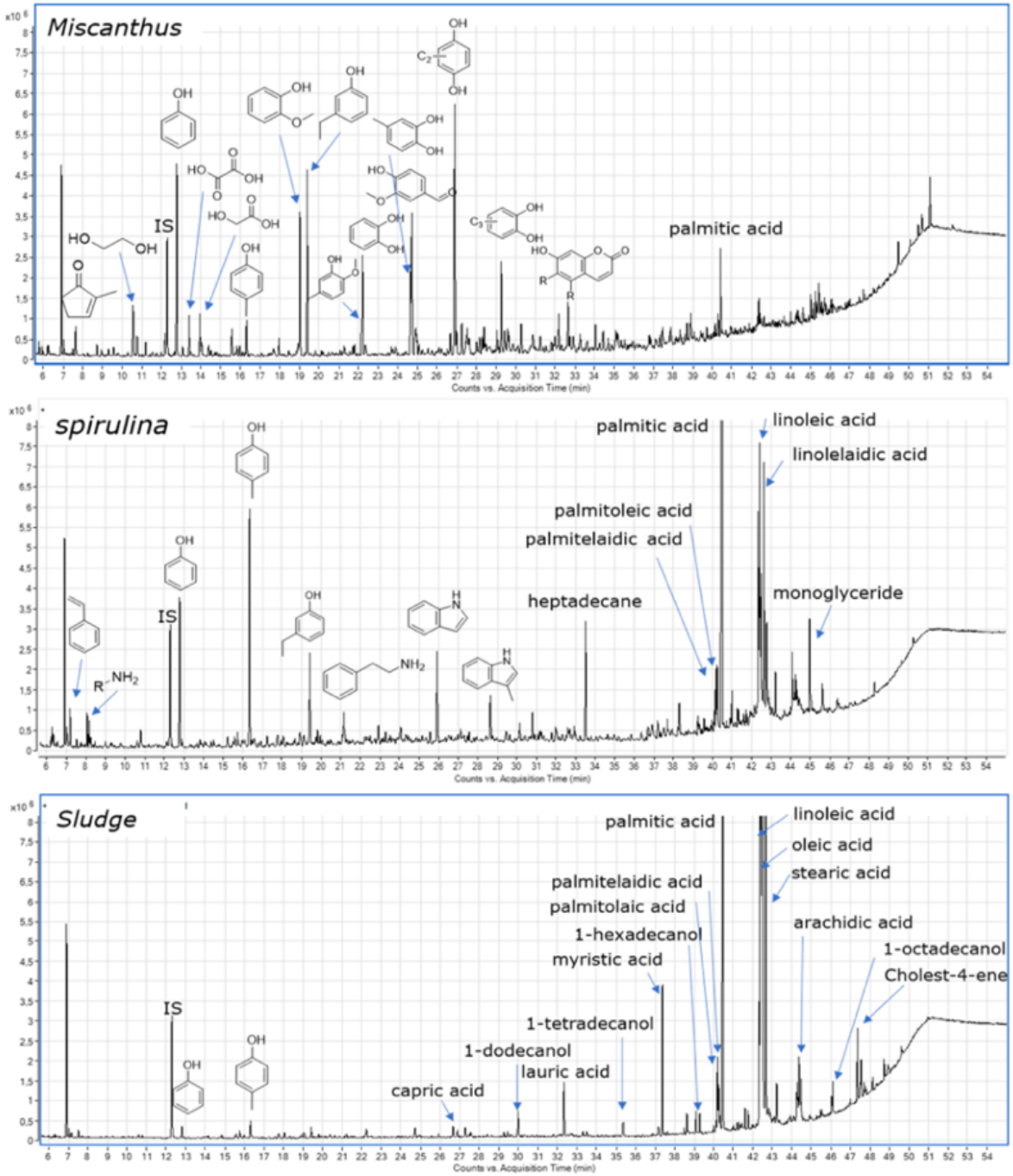

Figure 12: GC-MS chromatograms of the bio-crude derived from Aarhus University's HTL pilot plant[16].

An interesting study has been carried out by the Aalborg University in the article "Catalytic upgrading of hydrothermal liquefaction biocrudes: Different challenges for different feedstocks"[39]. In this study, the biocrudes derived from the Aarhus HTL plant have been upgraded by catalytic hydrotreating with pressurised hydrogen at 350-400°C (see paragraph 1.3.1). Nevertheless, some analysis of the different bio-crudes and upgraded bio-crudes compositions have been carried out, exploiting different analytical techniques that have been highlighted in the paragraph 1.3.2.1 dealing with the characterisation of the upgraded bio-oil.

Table 6: Yield, elemental composition, H/C ratio and HHV of the different tests[39].

Experiment	Yield (wt. %)	Elemental composition (wt. %)				H/C (–)	HHV (MJ/kg)
		C	H	N	O		
AL biocrude	–	75.0 ± 0.3	10.4 ± 0.1	7.7 ± 0.1	6.9 ± 0.3	1.66 ± 0.02	37.7 ± 0.2
AL350-4	75 ± 3	82.2 ± 0.2	11.1 ± 0.1	5.4 ± 0.0	1.3 ± 0.2	1.62 ± 0.02	41.6 ± 0.1
AL350-8	73 ± 2	84.0 ± 0.4	12.1 ± 0.1	4.0 ± 0.2	0.0 ± 0.5	1.72 ± 0.02	43.5 ± 0.2
AL400-8	63 ± 4	83.7 ± 0.4	12.3 ± 0.2	4.1 ± 0.2	0.0 ± 0.5	1.76 ± 0.03	43.7 ± 0.3
SS biocrude	–	74.5 ± 0.1	10.6 ± 0.0	3.9 ± 0.0	11.0 ± 0.1	1.71 ± 0.00	37.4 ± 0.0
SS350-4	74 ± 3	83.1 ± 0.7	12.1 ± 0.1	3.6 ± 0.0	1.2 ± 0.7	1.75 ± 0.02	43.1 ± 0.3
SS350-8	77 ± 2	84.1 ± 0.4	13.4 ± 0.0	2.5 ± 0.0	0.0 ± 0.4	1.91 ± 0.01	45.1 ± 0.1
SS400-8	72 ± 3	85.3 ± 0.2	13.8 ± 0.0	0.9 ± 0.0	0.0 ± 0.2	1.95 ± 0.00	46.1 ± 0.1
MS biocrude	–	70.5 ± 0.6	8.2 ± 0.0	1.7 ± 0.1	19.6 ± 0.6	1.40 ± 0.01	32.2 ± 0.2
MS350-4	60 ± 4	81.1 ± 0.3	8.8 ± 0.0	1.1 ± 0.1	9.0 ± 0.3	1.30 ± 0.00	37.8 ± 0.1
MS350-8	65 ± 1	84.7 ± 0.2	10.2 ± 0.1	0.8 ± 0.0	4.3 ± 0.2	1.45 ± 0.01	41.1 ± 0.1
MS400-8	61 ± 3	87.4 ± 0.0	10.3 ± 0.3	1.5 ± 0.1	0.8 ± 0.3	1.37 ± 0.04	42.2 ± 0.4

The analysis results highlight the similarities with the study carried out by Aarhus University and the three different feedstocks, *Miscanthus* (MS), *Spirulina* (AL) and sewage sludge (SS) have been evaluated. Table 6 presents the elemental composition (%) of each bio-crude and the respective three tests for the upgrading. The O content has been derived by subtraction, the H/C and the Higher Heating Value (HHV in MJ/kg) have been calculated. The analysis of this elemental composition has been done in the paragraph 1.3.2.2 about the composition of the upgraded bio-oil.

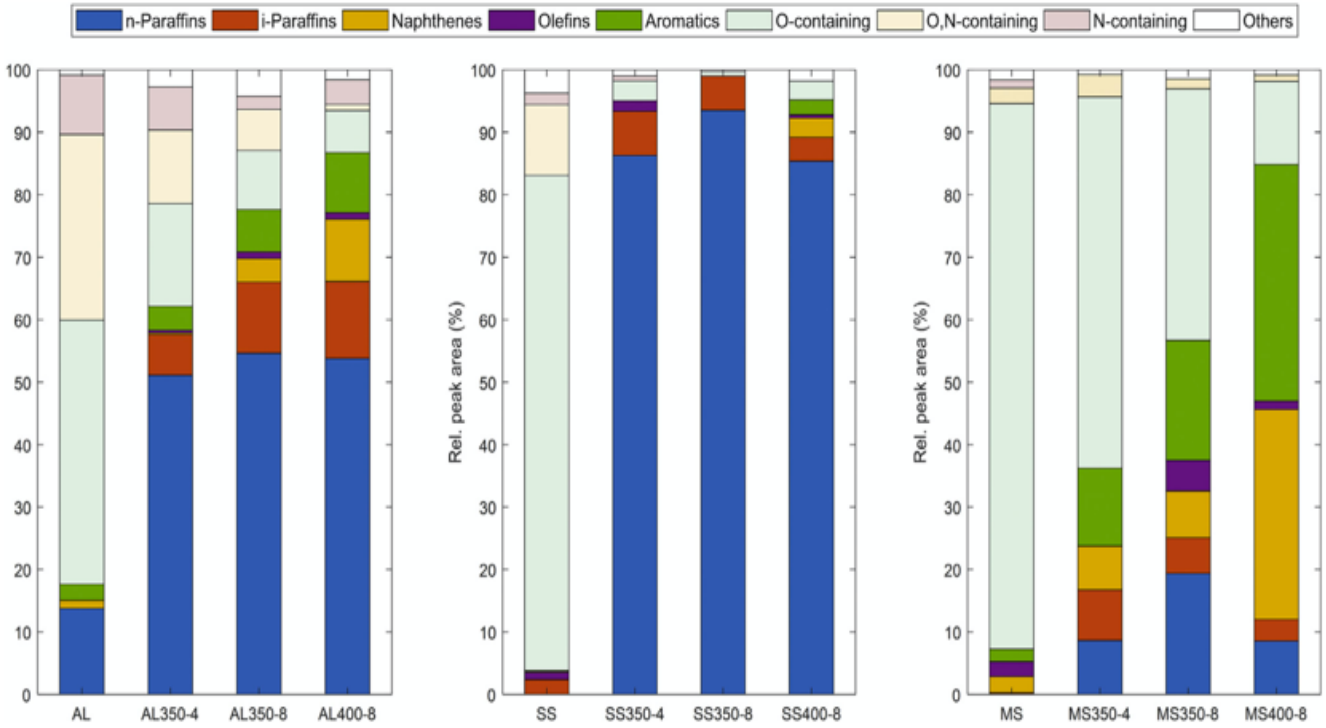

Figure 13: Raw bio-oil (AL, SS, MS) and upgraded bio-oil chemical composition in term of family compounds[39].

Figure 13 shows the composition of the bio-oils in terms of family compounds, derived from the GC-MS analysis. From the graph is easy to notice the enhanced n-paraffins, i-paraffins, aromatics and naphthenes production in the AL and SS bio-crude; coupled with the relative decreasing of the O-

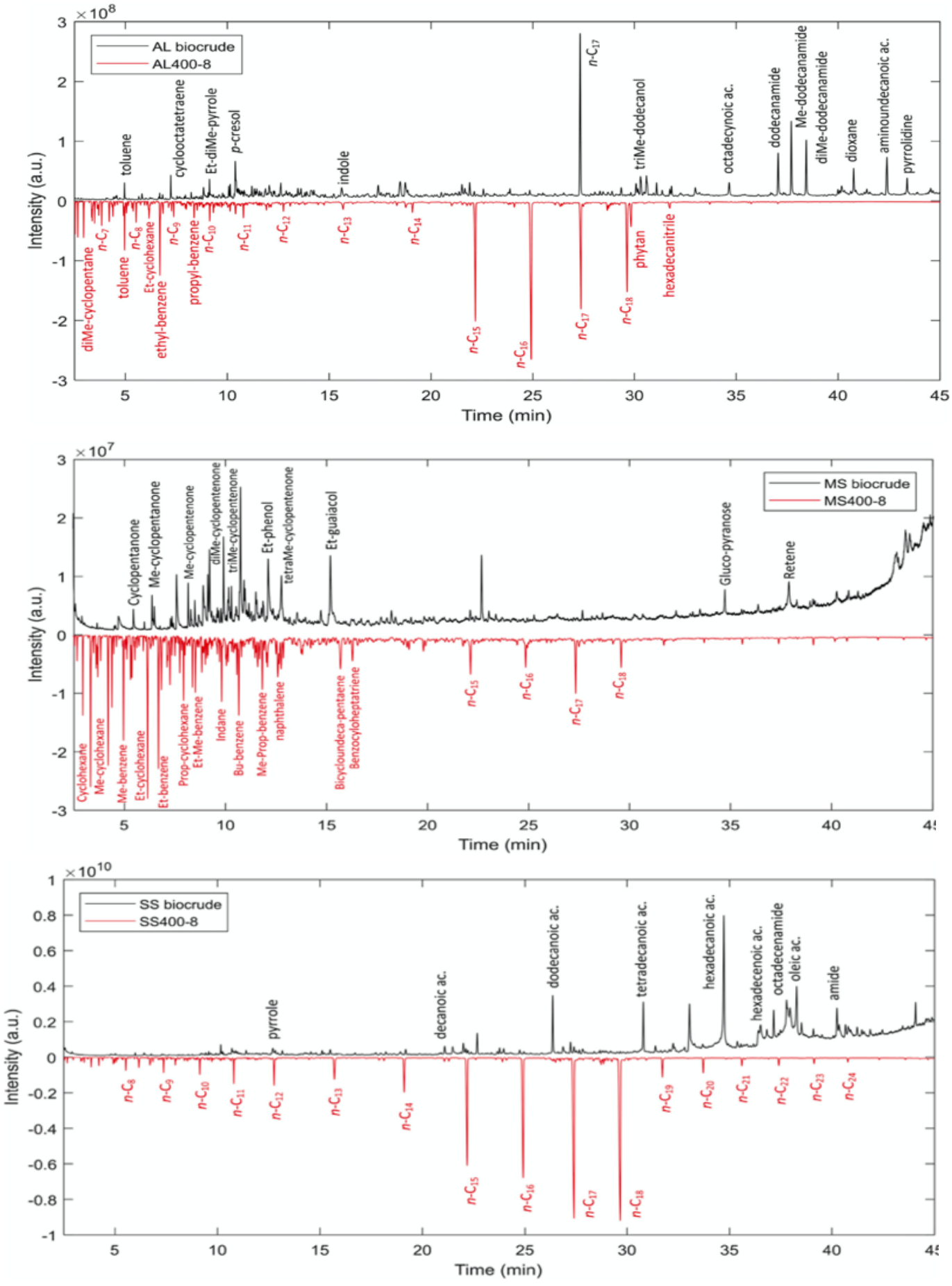

Figure 14: Chromatograms of raw biocrude (in black) and upgraded biocrude (in red)[39].

is the production of mainly aromatics and naphthenes.

A better picture of the raw and upgraded bio-crudes compositions can be drawn from GC-MS chromatograms (Figure 14). These chromatograms are in line with the study of Anastasakis et al. and can be a further confirmation of the reliability of analysis and data. The composition of the upgraded bio-crude has been analysed in the paragraph 1.3.2.2.

In summary, a deep knowledge of the composition of the initial raw bio-crude, is the first step to analyse the feasibility of possible upgrading methods trying to predict the possible products and setting up the optimal reaction conditions. Hence, these analyses have been critical for the further study of the upgrading processes, influencing the entire study project.

1.3 Biocrude upgrading

The most important and challenging problem regarding the exploitation of HTL bio-crude is, without any doubts, the upgrading. It usually represents the larger percentage of the overall costs of a typical biofuel production process. The complex and very often not well-defined composition of the bio-oil is an important problem that hampers the development of upgrading processes. Hence, the research of the most efficient and cost-effective upgrading process for HTL biocrude is becoming an essential topic to open the market for future plants and compete with other technologies already present.

Even though the high calorific power, the composition of the HTL bio-crude is typically not in line with the always more restricted regulations on biofuels.

Therefore, raw bio-oil has some unsuitable characteristics; right away has been highlighted the most important ones:

- The not negligible amount of N, especially in the algae-based bio crude, which can reach the 5-8 wt%, while the petroleum is usually between 0 and 1 wt%[37]. It is very important to maintain the N content as low as possible to avoid the NO_x emissions in atmosphere.
- The hetero-atomic contents in terms of O and S do not meet the requirements for standard biofuels.
- In many cases it could be acidic, with a high total acid number[28].
- The presence of high S and N contents can create problem of corrosion.
- The calorific power of the bio-oil can be improved, by decreasing O content.
- The viscosity is high and not suitable for direct use.
- High distillation temperature due to complex and long aliphatic chains.

To overcome these problems, there could be two main strategies: the first is to perform dewatering and deoxygenation reactions to increase the C/O ratio of the biocrude, the second is to hydrogenate the solution and rise the H/C ratio[40]. For these purposes different processes have been designed which

still entail some challenges to be solved. The next parts summarise some of the most important upgrading processes, starting with a brief overview on the most used ones, and concluding with the evaluation of the upgraded bio-oil, from the characterisation to the composition. This paragraph will introduce the target method of the electrocatalytic upgrading, in the paragraph 1.4.

1.3.1 Common processes for HTL's biocrude upgrading

For the upgrading of the biocrude from HTL, different methods have been used, some with known drawbacks, others with innovative solutions. Basically, the upgrading treatments can be clustered in three main categories[40]:

1. *Thermochemical processes:* catalytic cracking, hydrocracking, hydrotreatments (e.g. hydro-deoxygenation, hydrogenation, hydro-desulfurization). They use heat and pressure to initiate chemical reaction and they have been exploited in the petrochemical industry.
2. *Physicochemical processes:* electrochemical processes, plasma, ultrasonic cavitation, emulsification, mechanical blending.
3. *Biochemical processes:* esterification, transesterification, CTH (Catalytic Transfer Hydrogenation), biological methods.

The aim of this study is not to analyse all the possible processes, therefore, only an overview of the most important and used processes will be presented. The following mrthods have been selected based on literature and notoriety:

1. *Hydrotreating and hydrothermal upgrading:* It is well known that the higher the hydrogen content of fuels and petroleum products, the better the quality. From this principle, different processes based on hydrogenation reactions have been used to refine petroleum-derived compounds and they can be potentially exploited for the upgrading of HTL's bio-crude. Usually, it is carried out in autoclave with highly pressurised hydrogen that acts on the oxygenated compounds (like aldehydes and carboxylic acids) improving the combustion performances and stability[41]. The O in bio-crudes can be removed by hydrotreating with catalysts such as CoMo/Al2O3 or NiMo/Al2O326. Overall, these processes are the most used and convenient.
2. *Catalytic cracking and hydrocracking*: Catalytic cracking is a thermal process to produce biofuels via breakdown in low-carbon aromatics or light aliphatic hydrocarbons such as C8-C15 like diesel[40]. Usually, it used a bifunctional catalyst in which the alumina or zeolites provide the cracking function, instead the Ni, or some tungsten/platinum oxide catalyse the hydrogenation. Hydrocracking, instead, exploits a hydrogen surplus and increases the conversion towards gasoline-like compounds. It is very useful to produce light products, but it needs harsh conditions in term of temperature and hydrogen pressure to deal with less reactive compounds such as acids.

The overall process is not economically and energy efficient, as well as environmentally friendly[26].

3. *Emulsification:* this method is based on the production of emulsions of bio-crude with others fuel sources. Surfactants are needed since the initial bio-crude solution is not miscible with hydrocarbons and the process create microemulsions less corrosive and with promising ignition properties. An emulsification process with diesel oil as fuel source and octane as surfactant has been investigated by Jiang et al. confirming the feasibility and the overall treatment performances[42]. In this case, a pyrolytic-bio-oil/biodiesel ratio of 4:6 by volume has been initially used, at 30°C and 1200 rpm as stirring density. The results demonstrated the production of a stable and upgraded emulsion in term of viscosity, acidity, and water content.
4. *Esterification:* esterification is a solvent-based method that allows to transform carboxylic acid and aldehydes in their respective esters and acetals (see Figure 15). A polar solvent such as methanol, ethanol or furfural is required. They can reduce the viscosity of the bio-crude, preventing further chain growth between bio-crude particles and, at the same time, changing the physical dilution and the bio-crude microstructure. Hence, using an alcohol like ethanol, an acid catalyst and mild conditions, the bio-oil quality is enhanced. The reactions that occur in this system are basically esterification of carboxylic acids and acetalization of aldehydes. The reactive molecules are therefore transformed, reducing the acidity, increasing volatility and heating value.

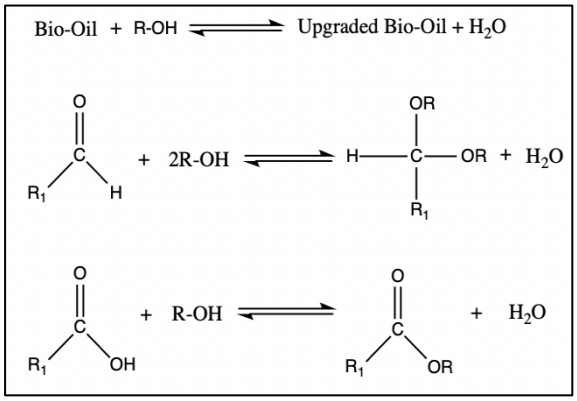

Figure 15: Esterification reaction

5. *Supercritical fluid treatment*: a fluid is defined supercritical when its temperature and pressure go above its critical point[26]. These fluids present characteristic of both liquid and gas fluids; indeed, is well known that supercritical fluids can diffuse and effuse in solid particle like a gas and dissolve compounds like a liquid. This fact overcomes problems of solubility and mass transfer that normally are present, promoting the gasification/liquefaction reactions. At the same time, they can improve the quality of the bio-crude, working in the calorific power and the viscosity of the solution. Generally, the most common, cheap and available supercritical fluid is water, but for the bio-crude upgrading, it is not suitable due to the enhancement of the O content and viscosity, as well as the lower yield toward the water-insoluble oil product. For these reasons, an organic supercritical fluid such as methanol, ethanol, butanol, or acetone must be used. This type of treatment is mainly used for HTL bio-crude, but the overall process results not

economically convenient due to the high prices of the organic solvents in supercritical conditions. Further studies have been done to study the feasibility of the process with less expensive solvent such as glycerol, a by-product of the biodiesel production from triglycerides.

1.3.2 Upgraded biocrude: characterisation and composition

1.3.2.1 Characterisation of the upgraded biocrude

The characterisation of the upgraded biocrude is usually done with different instruments and techniques. The high variability of the composition together with the complexity of biocrude, impede an easy characterisation and the identification of market-relevant fractions, as well as valuable compounds[32]. Therefore, multiple analysis from different type of techniques (thermal, spectrometry, chromatography, distillation) and general parameters that can sum-up the solution complexity, must be used. To have an overview on the quality of the upgraded bio-oil, the carbonyl concentration (CON) and the total acid number (TAN)[43] can be used. They are easy to evaluate, and they can highlight the effectiveness of the upgrading process. Another way to assess the stability of the oil is use the so-called aging studies, particularly, accelerated aging studies can help to analyse the grade of polymerisation of the biocrude. Polymerisation is an important aspect to consider in the bio-oil, it contributes to the viscosity and the overall quality of the solution. Li et el. have exploited the accelerated aging study before and after upgrading of the water-soluble fraction of biocrude by leaving it at 80°C for 48h[44]. After that, a size exclusion chromatography analyses have been done using two types of detectors, the IR detector for the molecular weight (Da) and the DAD (Diode-Array detector) to analyse the grade of polymerisation. Figure 16 shows the results of the analysis. The *a* and *b* plots are related to the crude biocrude, before ECH, and while in the IR one there is no difference, the graph of the DAD states

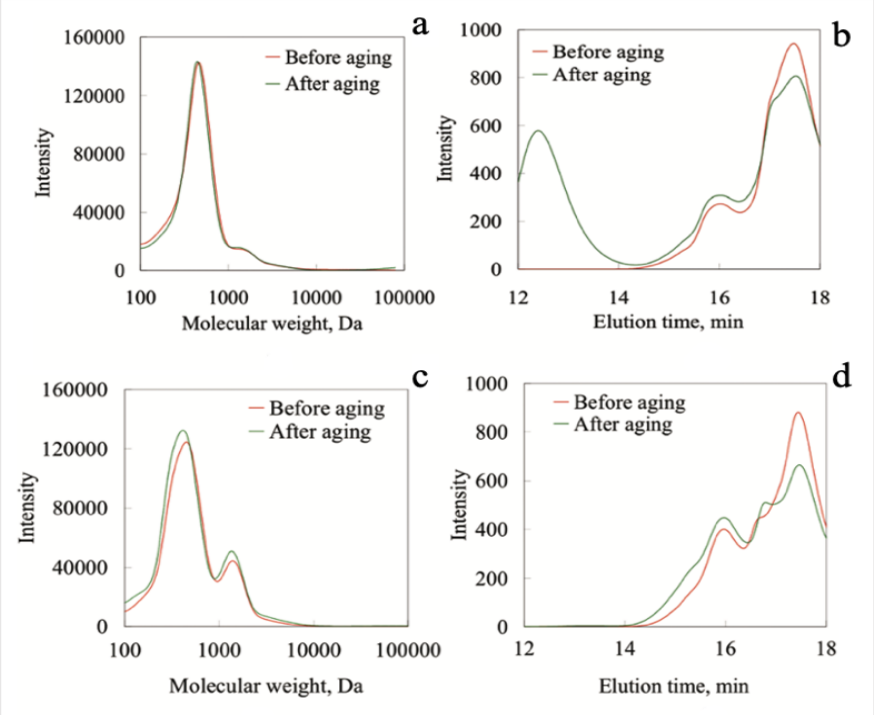

Figure 16: size exclusion chromatography results of raw bio-oil with IR detector (a), DAD (b) and upgraded bio-oil with IR detector (c) and DAD (d)[44].

that after the aging, some polymerisation phenomena have been occurred, creating a peak at 12/13 minutes. The *c* and *d* plots are, instead, related to the upgraded biocrude, and from the DAD one, the after aging is like the before aging. With this analysis they stated that in the upgrading bio-oil, the grade of polymerisation is reduced probably due to the reduction of the carbonyl group.

Other, qualitative analyses comprehend the viscosity analysis and the calorific power analysis by calorimetric bomb. They both work on the overall biocrude quality. Indeed, viscosity and the calorific power are important parameters when referring to fuels for transportations. For a more detailed analysis of the biocrude, the composition, the fractions and the residuals must be taken into account. The most used techniques to analyse these parameters are: (1) high temperature GC-MS, (2) high temperature HPLC, (3) Differential Scanning Calorimetry (DSC), (4) Thermal Gravimetric Analysis (TGA), (5). IR Spectroscopy, (6) elemental analysis, (7) traditional techniques of distillation such as fractionated distillation and (8) specific analysis on target products. For the composition, specific chromatography columns have been used. Usually, even though the resultant chromatograms are complicated and composed of several different peaks, it is still considered as one among the most valuable techniques. The method may change in base on the properties of the specific biocrude. Thermal analysis such as TGA and DSC are used to analyse the residual mass (%) and the fractions of the solution respectively. IR spectroscopy is firstly used as comparative technique, but it might be utilised as qualitative/quantitative analysis. All the distillation processes are used for separating the single fractions, but it does not give real information if not coupled with other techniques[40] (see Figure 17).

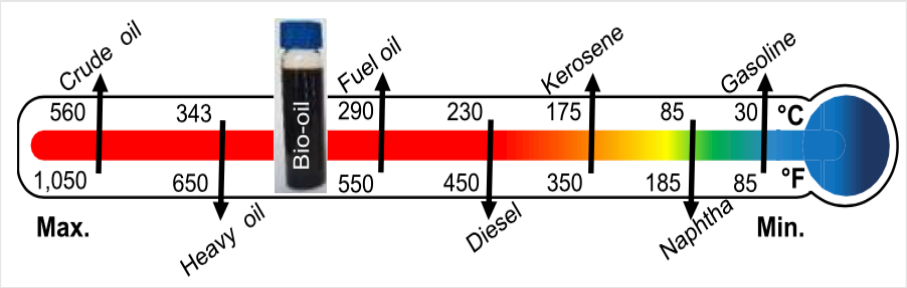

Figure 17: Distillation scale of liquid hydrocarbons mixtures and biocrude[40].

One example case has been highlighted in the paragraph 1.2.2.2 and it derived from the study of Castello et. al. on the catalytic hydrotreating upgrading[39]. They analyse the biocrude before and after the upgrading with three main techniques:

- For the gaseous phase in the upgraded system, a gas chromatography with a barrier ionization discharge detector (GC-BID) has been used. It has been manufactured by Shimadzu Inc. and equipped with a Supelco 1006 PLOT column.
- For the C, H, N and O elemental analysis, a PerkinElmer CHN-O analyser model 2400 Series II, have been utilised, following the standard ASTM D529[45].

- For the oil samples (upgraded and not), a GC-MS has been used. Samples have been diluted in 1% of diethyl-ether and injected at 300°C (split ratio 1:20) with He as carrier gas (1 ml/min). Measuring program involved heating at 10°C/min from 35°C to 120°C, holding the temperature for 5 min and then 5°C/min up to 250°C. They knew that the analysis is only limited to the volatile fraction of the sample, i.e. up to a boiling point of ca. 350°C. Nevertheless, this fraction is the one more directly involved in the production of potential drop-in fuels. The GC-MS profiles have been obtained at 400°C and 8 MPa.

1.3.2.2 Composition of the upgraded biocrude

The composition of the upgraded biocrude is highly variable and depends on the starting feedstock, as well as on the upgrading method utilised. Castello et al. have studied the composition of the upgraded biocrude by catalytic hydrotreating derived from the HTL plant of Aarhus university. The Figure 14 (in red), are the chromatograms of the upgraded biocrude derived from *Spirulina* (AL), *Miscanthus* (MS) and sewage sludge (SS), instead the Figure 13 gather the different compound based on the chemical family and in base on the upgrading reaction conditions. The results from AL's biocrude show the high presence of n-paraffins, i-paraffins and diesel-like compounds, especially n-C_{16}, n-C_{15}, n-C_{17} and n-C_{18}. Moreover, a notable number of hydrogenated aromatics such as toluene, benzene, ethylbenzene has been detected, with the presence of naphthenes like cyclohexane and cyclopentane. In the MS's upgraded biocrude a lower amount of paraffins is present, but the aromatics such as benzene, indane, methylbenzene, ethylbenzene, butylbenzene and naphthalene represent a good percentage of the overall solution. Naphthenes like cyclohexane and derivatives are present in a notable amount. It is worth to notice that by increasing the hydrotreating temperature and the hydrogen pressure (from 350 to 400 °C and from 4 to 8 MPa) the residual oxygenated compounds tend to decrease, with the consequent increasing of aromatics and naphthenes. In the SS's biocrude, the composition is almost totally dominated by the presence of different paraffins and long chain hydrocarbons. The C-content-band most present is that one that goes from C15 and C18, as the biocrude from *Spirulina*.

Other important information can be extrapolated from the elemental analysis. Table 6 shows the results of the elemental analyses of the raw and upgraded biocrudes from the three different feedstock considered in this study.

Considering the reaction conditions some conclusions can be stated:

- N and O contents tend to decrease rising the temperature and the pressure, only in the MS400-8 there is a different situation. This phenomenon is related to the degree of de-oxygenation and denitrogenation calculated with equations 2 and 3:

$$\text{de-O} = 1 - \frac{O_{product}}{O_{feed}} \quad (2)$$

$$\text{de-N} = 1 - \frac{N_{product}}{N_{feed}} \quad (3)$$

Consequently, the C and H content rise with T and P and heteroatoms removal decreases the overall bio-oil yield since they are released as gases (NO_x and CO-CO_2).

- In all the cases the HHV is increased by rising T and P.
- The H/C is, instead, a less controllable parameter. It has the tendency to increase with P and T, but it is strictly related to the H_2 consumption during the hydrogenation reaction.

1.4 Electrocatalytic systems for biomass upgrading

Power-to-X technologies, in which "X" could be heat, chemicals, fuels or molecules, refer to all those chemical processes driven by the utilisation of electricity[46]. From these processes raised the concept of the electrobiorefineries, a simplified industrial system in which electrocatalytic and electrobiochemical processes are integrated to produce green chemicals, fuels, and molecules from renewable feedstocks (or not).

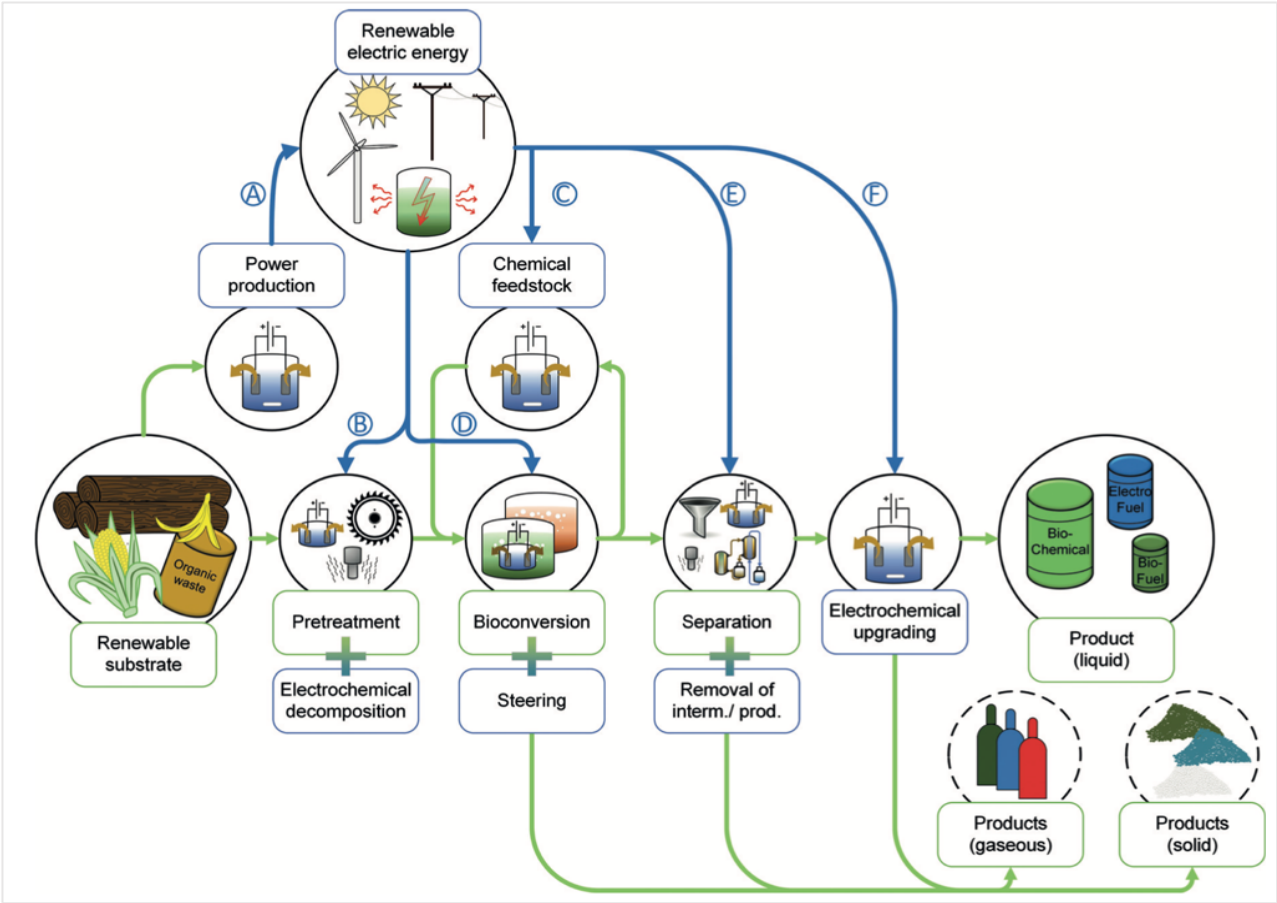

Figure 18: simplified scheme of an electrobiorefinery[46].

Figure 18 represents a possible electrobiochemical system for the treatment of renewable sources form lignocellulosic biomass, organic wastes, and plant residues[46]. This system could be integrated to biorefineries complexes in order to increase the single efficiencies of the different sub-processes. On the other hand, small-scale and decentralised electrochemical facilities for biomass upgrading and chemicals synthesis from renewables feedstocks are evolving to fulfil local demands and mitigate challenges of small realities. The Exploitation of the proton/electron transfer reaction instead of molecular hydrogen as reductant, makes these systems suitable to be coupled with the surplus-energy derived from renewables such as photovoltaics and wind turbine. Furthermore, they are carried out in mild conditions respect to the classical refinery processes. The temperature reaches a maximum of 300°C with pressures around 50 bar, where the classical large-scale processes exploit temperatures between 330 and 530 °C and pressure that can achieve 100 bar[47]. Another important aspect of these technologies is that they rely on modular, autonomous and relatively small plants, which make them easy to locate nearby the carbon source or feedstocks (energy crops, waste treatment plants, food waste and CO_2 sources)[47] cutting the inefficiencies costs of transportation (see Figure 19).

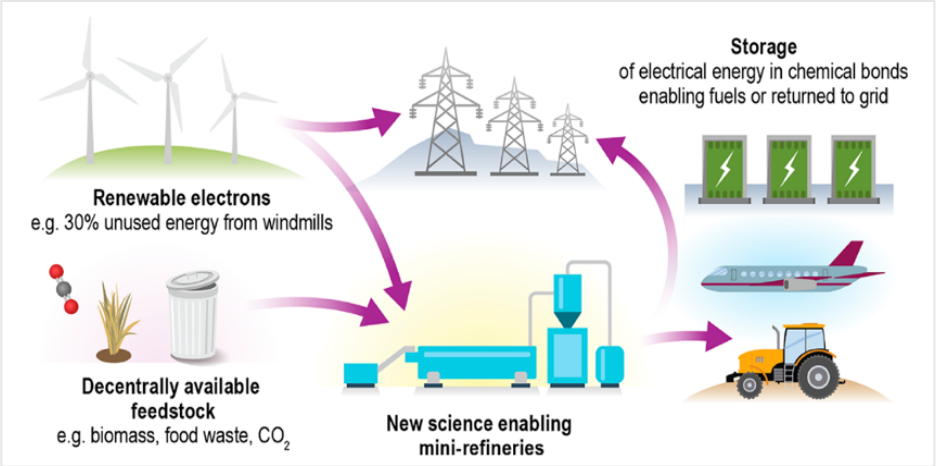

Figure 19: Utilization scheme of decentralised carbon source conversion to chemicals and fuels[47].

Electrocatalytic hydrogenation (ECH), and the equivalent classic thermo-catalytic hydrogenation (TCH), could be exploited for the upgrading of bio-oils and biocrudes from the primary conversion pathways such as HTL, fast pyrolysis and gasification (see paragraph 1.4.1). ECH is based on the theoretical aspects highlighted in the paragraph 1.5 and mainly lab scale procedures will be analysed.

1.4.1 Electrocatalytic upgrading of biocrude

This next part will tackle the specific case of the electrocatalytic upgrading of biocrude, in particular, the cathodic electro-upgrading. This method is a physicochemical treatment based on an electrochemical system in which the H_2 is not usually added but produced in-situ. It can also refer to the electrocatalytic stabilisation of biocrude, since these types of processes not always act on the C:H ratio firstly, but they can also modify some specific parameters of the raw biocrude such as the total acid number, the viscosity, or the heteroatoms presence. Here, electrocatalytic upgrading refers to

either the chemical hydrogenation with in-situ produced H_2 or the direct hydrogenation of the biocrude compounds (the preferred route).

For the first case, the hydrogen is derived from the cathodic water reduction reaction (III), also called hydrogen evolution reaction (HER), that is coupled with the anodic O_2 production (IV) also called oxygen evolution reaction (OER).

$$2H^+_{(aq)} + 2e^- \rightarrow H_{2\,(g)} \quad E^0 = 0\ V \qquad \text{(III)}$$

$$2H_2O_{(l)} \rightarrow O_{2\,(g)} + 4H^+ + 4e^- \quad E^0 = 1{,}23\ V \qquad \text{(IV)}$$

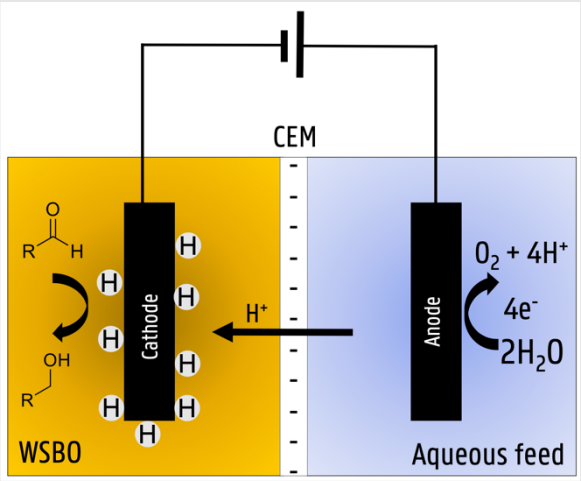

Figure 20: electrochemical cell for the upgrading of the water-soluble biocrude fraction[48].

The HER is exploited to collect the gas for energy purposes or, in this case, to carry out the downstream hydrodeoxygenation (HDO) or electrochemical hydrogenation (ECH) reactions (for convenience these two reactions will be gather under the name of ECH, even though the mechanism is different). In conventional electrochemical systems, the reduction is, though, carried out by an electricity input which allows the H^+ production at the anode, coupled with O_2 evolution. The protons are then transferred through a proton (or cation) exchange membrane (usually Nafion based) to the cathode chamber where the ECH of the biocrude molecules occur. Figure 20 shows a simple design of a cell for the electro-upgrading of the water-soluble fraction of biocrude[48]. The HER is strictly related to the pH of the solution:

$$H^+ + e^- \rightarrow H^* \text{ (In acid)} \qquad \text{(V)}$$

$$H_2O + e^- \rightarrow H^* + OH^- \text{ (In base)} \qquad \text{(VI)}$$

$$2H^* \rightarrow H_2 \qquad \text{(VII)}$$

$$H^* + H^+ + e^- \rightarrow H_2 \text{ (in acid)} \qquad \text{(VIII)}$$

$$2H^* + H_2O + e^- \rightarrow H_2 + OH^- \text{ (in base)} \qquad \text{(IX)}$$

The reactions (V) and (VI) are called Volmer steps in which the adsorbed H atom is formed electrochemically, the reaction (VII) is the so-called Tafel step which is a chemical step to produce hydrogen from two H^* adsorbed on the electrode surface, otherwise in the reactions (VIII) and (IX), the so-called Heyrovsky steps, the hydrogen is produced electrochemically. Here it is worth to note that the electrochemical reactions are all influenced by the pH, which is the parameter that selects the pathway. The rate of the HER is related with the H_2 adsorption free energy (ΔG_H). If the interaction is too strong the desorption reactions (Tafel/Heyrovsky) will be the limited steps, instead, if the

hydrogen binds the electrode surface too weakly, the limited step will be the Volmer reaction[49]. To show this phenomenon the Sabatier principle and the so-called Volcano plot is used (see Figure 21). It correlates the ΔG_H with the exchange current density of the reactions catalysed by a certain electrocatalyst. The best material must have a middle-range value of ΔG_H to do not limit any step of the HER. The best electrocatalysts are, therefore, noble metals such as Pt, Pd, Re, Ir and Rh, but also Ni, Co, Cu and MoS_2, an innovative catalyst that results to be very active mainly due to its very high surface area[49].

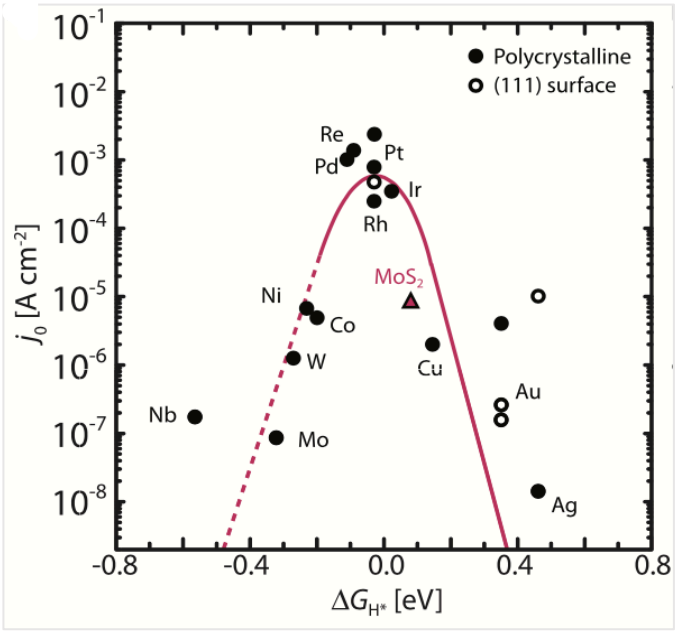

Figure 21: Volcano plot for the hydrogen evolution reaction (HER)[49].

For the second case, the direct hydrogenation of the compounds, the cathodic ECH derived can follow two main mechanism[50]: firstly, there could be a proton reduction producing adsorbed H_2, with the following reaction between the adsorbed hydrogen and the adsorbed oxygenates organic compound. Secondly there could be a direct reduction of the oxygenates organic molecules (adsorbed or not) thanks to protonation reactions (pre or post the eventual adsorption). Usually the second mechanism required higher (more negative) cathodic potentials and it happens only with electrode that have high HER overpotential since it does not require an efficient hydrogen production[47]. These two pathways are preferred that the hydrogenation with *in-situ* H_2, because it depends on the catalyst type, with more potential improvements.

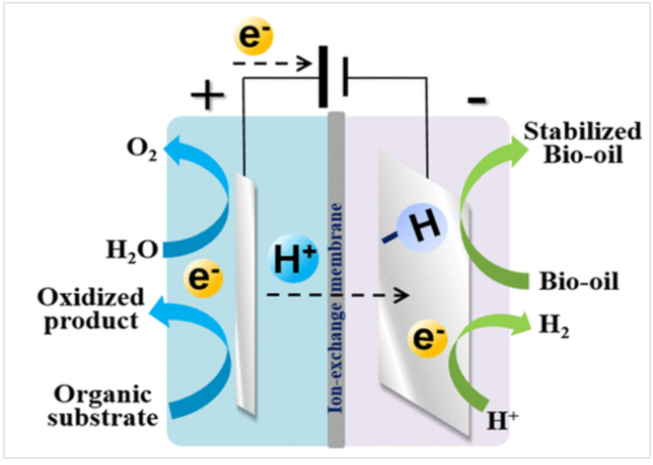

Figure 22: ECH of biocrude couple with an anodic organic oxidation reaction[43].

In ECH is important to understand the hydrogenation reduction potential of an organic species, which is the tendency to accept electrons from the cathode material. It is related to the functional group in the chemical structure and the surrounding environment where the reaction is taking place. In the case of the electrocatalytic upgrading, in order to stabilise the raw bio-crude, the first thing is to reduce the carbonyl groups, since they can condensate forming high molecular weight compounds by carbonyl condensation[51].

Another important aspect is that the cathodic ECH could be ideally coupled with another target reaction at the anode side, to perform a co-electrolysis, to integrate two processes in one (see Figure 22). Hence, this process could potentially follow the most important principle of green chemistry.

1.4.1.1 Electrode material for ECH

In the paragraph 1.5.5 the general characteristic of the electrocatalyst have been displayed with a focus on the characteristics that it must have to perform an electrochemical reaction. Many types of catalysts and electrodes material can be found, but for the specific case of the ECH of biocrude some of them result suitable.

The material used for WE's production in the ECH can be divided in three main categories[47]:

1. **Metal based catalyst**: they are mainly bulk metals or alloys with eventually deposited or coated metal nanoparticles. In this category there are all the Pt and other noble-metals-based electrodes, Ni or Raney Ni material, Cu or Devarda Cu, Co and Mo based catalysts.
2. **Metals deposited on carbon materials or solid polymer electrolyte membranes**: they are the new generation of electrocatalysts since they perform quite good towards specific biobased compounds. It comprehends the catalysts based on Pd, Rh, Pd nanoparticles, as well as Ni, Cu and Ag. The supports can be carbon nanotubes, activated carbon, carbon fibers, but there also oxide support that can be used such as alumina and $BaSO_4$.[47]
3. **Electrodes modified by conductive, redox polymers films:** in which dispersed Pt or Pd are deposited. Usually, the material modified is based on carbon, and it can be functionalised specifically for the ECH, adding acid groups or nitro groups in the pores. Indeed, Brønsted-acid sites nearby metal active sites can enhance the ECH of benzaldehyde by proton-coupled electron transfer (PCET).[52]

Reassuming, a limited number of elements can be used for the ECH of biocrude, and high engineered catalyst are needed to face the complexity of the feedstocks. Pt and Pd are the best metals, but they are also expensive and not always available, moreover they have a very low overpotential toward HER. Therefore, the research is focusing on the transitional metals or other less expensive solutions. Pb and Hg are quite active towards the carboxylic acid hydrogenation[47], but the safety issue limits their applications. Nickel is the most analysed metal for the ECH and in particular the Raney Ni has been confirmed active toward the carbonyl and nitro groups hydrogenation in alkaline conditions[47].

Indeed, as also confirmed by this study, achieving more acid pH, the Ni starts to lose activity due to its instability. Cu, instead, behaves as Ni, but it presents a lower activity in average. From the other side, it seems to be more tolerant of neutral-acid pH values. Andrews et al. has been carried out an interesting study on the usage of base and noble metal in ECH[53]. Taking as model compound benzaldehyde, they highlighted the fact that noble metal are more active towards HER and alcohol formation, while base metal are more suitable for dimerization reaction and alcohol formation (see Figure 23)[53]. A specific example is a catalyst made by ruthenium supported on activated carbon cloth, which results active in ECH of water-soluble aldehydes and ketones in mild condition and producing alcohols and diols[44]. The same approach has been used by Zhang et al. who used a well dispersed ruthenium nanoparticle anchored in ordered mesoporous carbon as electrocatalyst for ECH of the water-soluble fraction[54]. Pala et al. analysed the electro-upgrading of the water-soluble fraction of a fast pyrolysis biocrude comparing different basic metal catalysts for the conversion of carbonyl-group-based chemicals. From the study, the faradaic efficiencies towards the target reaction were CuZn > SS (stainless steel) > Ti > Pt > Ru, this because the noble metals are quite active for the HER which in the context of direct electrochemical upgrading of biocrude is a parasitic reaction. The authors claimed that electrode with medium/high hydrogen overpotential and low organics potential are, therefore, more suitable for the ECH of the biocrude compounds, since they have higher faradaic efficiencies[48]. A different approach has been used by Lister et al. who presented an electrochemical treatment of biocrude by incorporating electrodialysis separation in an electrochemical cell[51]. Here they avoided the use of liquid electrolyte by introducing a dual membrane cell (DMC), which implements a carbon cathode on an anion exchange membrane and an inert anode material on a cation

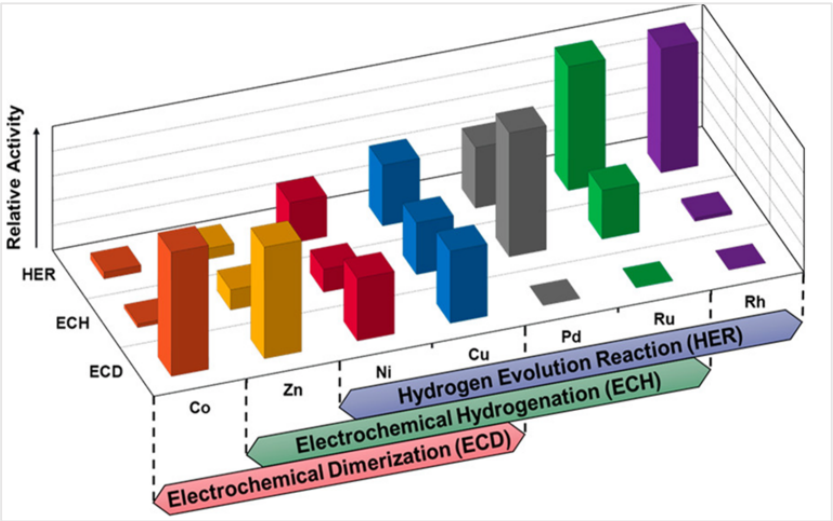

Figure 23: Relative activity of noble and base metals toward hydrogen evolution reaction (HER), electrocatalytic hydrogenation (ECH) and electrochemical dimerization (ECD)[53].

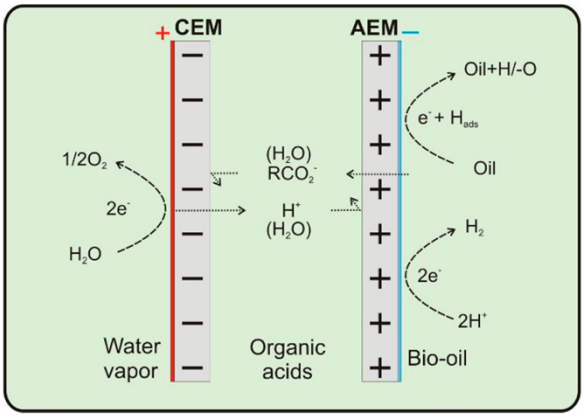

Figure 24: set-up of the dual membrane cell (DMC)[51].

exchange membrane[51]. The small acids such as formic or acetic acids can pass through the cathode by electrodialysis, decreasing the overall acidity of the catholyte and achieving an interspace between the membranes. At the same time, they can catalyse the proton movement from the OER at the anode (see Figure 24).

An issue to consider while choosing the suitable catalyst is the deactivation of the active sites. It happens mainly for supported electrocatalyst, but some problems can be also found in bulk catalysts. The most common and problematic phenomena are related with the nanoparticles, such as agglomeration, reshaping, detachment, dissolution, carbon corrosion or de-alloying. Furthermore, a problem that has been analysed in this work is the coke formation when trying to achieve more extreme conditions of reaction in term of potential. Indeed, the coke formation on the WE can block the active sites, destabilising the CA current and decreasing the ECH rate. The coke can derive from the organic radicals at the electrode-electrolyte interphase which polymerise and create carbonaceous material that can block the active sites on the surface and in the pores. It has been stated that the production of coke or carbonaceous materials can jeopardise the electrochemical performances of the system[55].

The choice of the material is therefore related to the target compound to hydrogenate and the reaction condition that are used, as well as to the deactivation phenomena that can occur for the specific material in the reaction conditions. For now, the studies are limited to the water-soluble fraction of the biocrude or some model compounds.

1.4.1.2 Efficiency for ECH and useful equations

In order to assess the efficiency of an electrochemical cell for the ECH, different equations and parameters must be used[47]:

$$\text{Faradaic Efficiency (FE)} = \frac{\text{Electrons consumed for the ECH}}{\text{Total of electron passed}} \cdot 100 = \left(\frac{n \cdot F \cdot z}{C_{total}}\right) \cdot 100 \qquad (4)$$

In which n is the mole of reactant consumed, F the Faraday constant, z the number of electrons required for the reaction and C_{total} the total charge transferred during the reaction. The FE is an essential factor to calculate the electrochemical selectivity of a certain electrocatalyst towards the target hydrogenation. It assesses the ratio of electrons that are effectively used for the target reaction. Low FE means that some side reactions are consuming the electrons that should be used for the main one. The FE is never 100% since the HER is always competing with the organics ECR[43].

$$\text{Conversion} = \frac{\text{Moles of reactant consumed}}{\text{Initial moles of reactant}} \cdot 100 \qquad (5)$$

Conversion, expressed in %, is an important parameter related to the reactants that indicate the percentage of reagent that has reacted respect to the initial amount.

$$\text{Specific ECH rate} = \frac{\text{Moles of reactants hydrogenated}}{\text{Time} \cdot \text{Mass of catalyst} \cdot \text{Metal loading}} \cdot 100 \left[\text{mol/s} \cdot \text{g}_{\text{metal}}\right] \quad (6)$$

The specific ECH rate assesses the reactants that have been hydrogenated during time in relationship with the catalyst utilised in term of mass and eventually in term of metal loading. It is specifically for the hydrogenation reactions, and it is strictly correlated with the type of electrocatalyst.

Another parameter that can be exploited while assessing the electrochemical conversion efficiency, is the lower heating value (LHV) or net calorific value (kJ g^{-1} or kJ mol^{-1}). It represents the amount of heat released by combusting a specific quantity of substance when the water is in vapour phase, and, therefore, the latent heat of evaporation of water (and eventually other reactions) is not recovered. Increasing the C:H ratio of the solution, which is one of the most important goal of the electrocatalytic upgrading of biocrude, helps the LHV to rise. The ability of a process to act on this ratio and the consequent ECH efficiency, is evaluated by the equation (7):[47]

$$E_{ECH} = \frac{P_{LHV}}{F_{LHV}\left(\frac{1}{1-X_{gas}}\right)\left(\frac{1}{1-X_{solid}}\right) + E_{LHV}\left(\frac{1}{1-X_{H_2}}\right) + O_{LHV}} \quad (7)$$

In which the P_{LHV}, F_{LHV}, E_{LHV} and O_{LHV} are respectively the lower heating value of the products, feed, electrical input, and other input required. Instead, the X_{gas} is the fraction of the feed LHV that is lost by producing light gases (CO_2, CH_4 or CO), X_{solid} is the fraction of the feed LHV that is lost due to solid formation (char, tar, coke or other solids) and the X_{H2} is the fraction of the current that has been applied (mol of electrons) that specifically contributes to the HER instead of the ECH. This last term is not negligible in the material that has a very low overpotential toward the HER such as Pt or other noble metals. Practically, the E_{LHV} represents the energy input (kJ mol^{-1}) added to the target molecule in term of H_2 equivalent, and it is defined as:

$$E_{LHV} = \frac{2AV}{CE_{gen}} \ [\text{kJ/mol}] \quad (8)$$

In which z=2 is related with the number of electrons needed to generate an H_2 molecule, A is the Avogadro number (6,02 x 10^{23} electrons mol^{-1}), C is equal to 6,24 x 10^{28} that is the number of electrons in one coulomb, V is the operating applied potential and E_{gen} is linked to the energy source, and it can be assumed as 0,6 if the electricity derives from a gas turbine combined cycle generating plant with a LHV efficiency of 60%[47]. Practically, V (and indirectly E_{LHV}) is related with the potential loss described by the equation (10). In particular, the phenomenon of the concentration polarisation, that occurs when the current is limited by the mass transfer at the electrode, and the ohmic drops are fundamental aspects to consider and try to decrease as much as possible. Summarizing, higher is X_{H2},

which means a lower FE toward the target reaction, larger will be the contribution of the E_{LHV} and lower will be the overall electrochemical conversion efficiency.

Finally, the loss occurring to other external factors (O_{LHV}) is mainly related to mechanical mixing or oil and water separation.

1.4.1.3 Target biobased compounds

The target compounds of the ECH of biocrude are all those chemicals that makes the biocrude not suitable for the direct use as drop-fuel. The complex biocrude mixture is very variable in composition and the target compounds could be not easy to activate or could react in particular conditions respect others. This paragraph will not tackle the single ECH pathway, but it is aimed to expose an overview on the most important biocrude compounds that can be electrochemically reduced. In order to simplify the highly variable mixture, the compounds will be gathered in categories in base of the chemical composition.

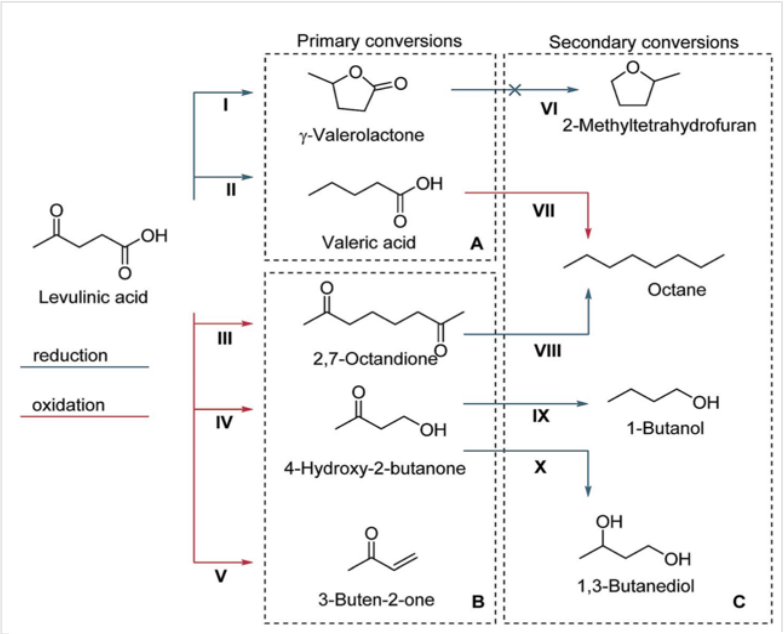

Figure 25: Electrocatalytic pathways for the treatment of levulinic acid[56].

The most studied and important categories of target compounds include:

1. Carboxylic acids: They are usually responsible of the acid pH and they must be treated for this reason. Moreover, some of them are fundamental intermediate for the production of valuable compounds such as glyoxylic acid from oxalic acid or aromatic aldehydes that are important intermediate for the pharmaceutical and agriculture industries.[47] Examples of aliphatic carboxylic acids are formic acid, pyruvic acid, acetic acid, propionic acid, levulinic acid, oxalic acid and lactic acid. Instead, within the aromatic carboxylic acids, benzoic acid is the most studied and analysed. Levulinic acid is an important compound, indeed it is one of the most present carboxylic acid in almost all the type of biocrude and it has been defined as a promising biomass-derived platform chemical. It can be transformed in valeric acid and γ-valerolactone by ECH and a further oxidation (non-kolbe electrolysis) can be performed to produce the octane (see Figure 25)[56]. It has also a carbonyl group so it can undergo multiple routes and pathways enhancing its overall reactivity.

2. Carbonyl group-based compounds: ketones and aldehydes derived mainly from cellulose and hemicellulose. They are related with the bio-crude instability; indeed, they act on the viscosity, and they can polymerise making the biocrude composition unsuitable for fuel applications[43]. Some of the most important compounds in this category are benzaldehyde, acetaldehyde, acetone, hydroxyacetone, furans family, HMF, levulinic acid, sugars like glucose and fructose. The Figure 26 shows that simple ketones and aldehydes can be reduced forming the relative alcohols[43].

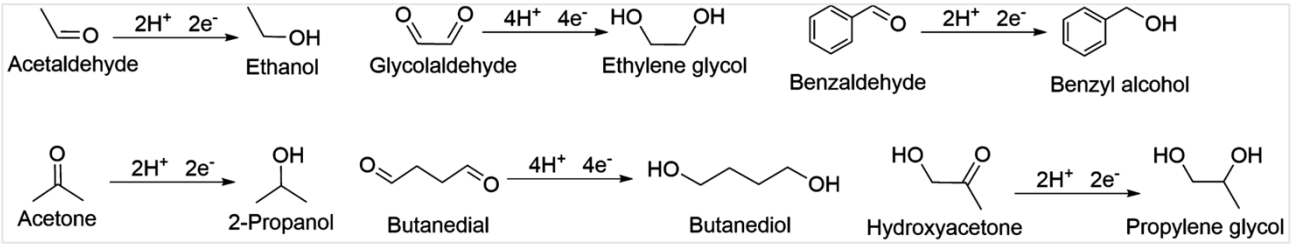

Figure 26: Examples of ECH of carbonyl group-based compounds to the respective alcohols[43].

The furans are very important to evaluate since they are quite reactive and they are related mainly to the amount of hemicellulose in the feedstock[43]. The most iconic compound is furfural that can be hydrogenated forming furfuryl alcohol and 2-methylfuran, these two compounds may undergo some side reactions such as polymerisation (see Figure 27). This latter reaction can compromise the composition of the biocrude. Furthermore, the 2-methyluran has a very low boiling point so it can evaporate. Another example is the 5-hydroxymethylfurfural (HMF) which is a representative molecule in the biocrude, and it has a similar behaviour that the furfural, indeed both, to be reduced, prefer an alkaline environment.

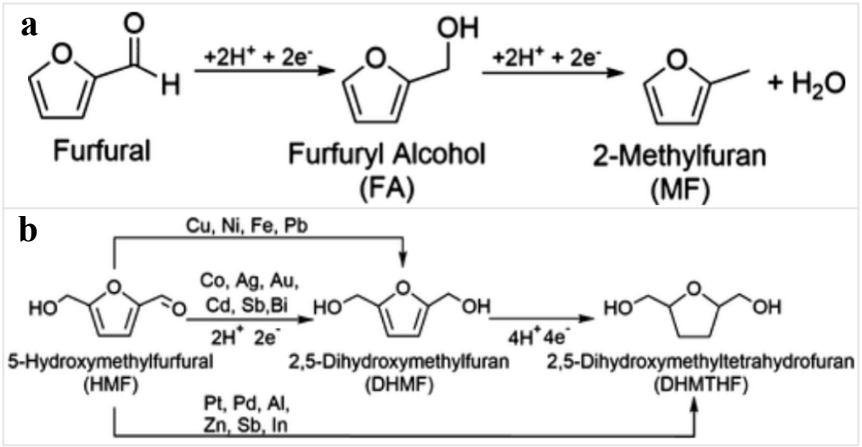

Figure 27: ECH pathways of furfural (a) and HMF (b)[43].

Sugars are also an important fraction of the biocrude. The most important is glucose, which derives from the depolymerisation of cellulose or hemicellulose. While performing an ECH, the carbonyl groups is preferred to be converted than the alcohol group[47], forming sorbitol as main product. Sorbitol is valuable compound in the food industry, and it is the precursor of important commodities such as vitamin C.

3. Alcohols and other oxygenate compounds: To increase the H/C ratio on biocrude, alcohols represent a suitable target. Both aromatic and aliphatic alcohols can be found, and they can derive

from further ECH or, in the case of aromatics, from a partial depolymerisation of lignin. Some important compounds are phenol, catechol, and derivatives. These aromatic alcohols are present in the Aarhus university biocrude in a notable percentage, and they are often taken as model molecules for ECH studies. The aromatic rings are usually a good target for hydrogenation to form the respective saturated alcohols and increase the H/C ratio of the molecules. Phenolic compounds can follow two main pathways when hydrogenated (see Figure 28)[47]. The first is a direct hydrogenation of the aromatic ring without attack the lateral chains, the second, instead, starts with the cleavage of the lateral group (methyl, butyl, ethyl) followed by the ring hydrogenation. The products are usually cyclohexanol or methyl-cyclohexanol.

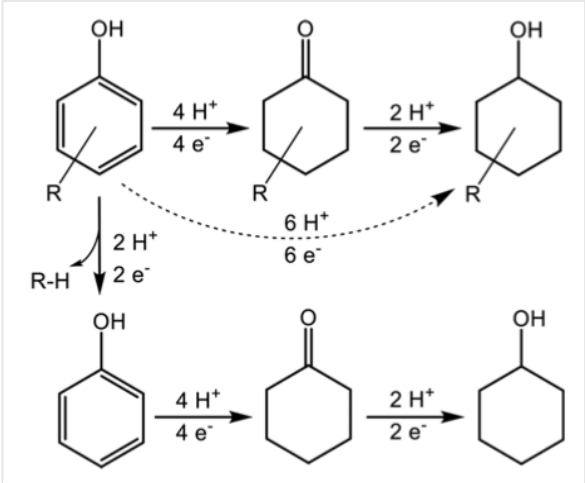

Figure 28: ECH pathways for phenolic compounds[47].

Another important molecule is guaiacol, which also results from lignin, and it has a more complex scheme of reduction. Indeed, it may undergo a hydrogenation to produce 2-methoxycyclohexanol or a demetehoxylation to form phenol. The reaction are current sensitive and they are also related to the position of the hydroxyl and methoxy group[43].

4. Long-chain fatty acid: the amount of long-chain fatty acids is related with the type of feedstock utilised for the biocrude production. Algae- based biocrudes usually present a higher percentage of fatty acids respect those from lignocellulosic biomasses. The most present are usually palmitic acid, linolelaidic acid, linoleic acid, oleic acid and steric acid. The hydrogenation of these compounds, and in particular on the PA and saturated long-chain fatty acid, is the target reaction of this study.

In this thesis the team has chosen the Palmitic Acid (PA) as model compound and as a relevant component of the biocrude. PA or hexadecanoic acid, is a C16 saturated carboxylic acid. It is one of the most common long chain fatty acids present in nature and it can be found in different plants, microorganisms, and animals. PA accounts for 20-30% of the total fatty acids in the human's phospholipid membrane, a 70 kg man is made up of 3.5 kg of PA. The human body can synthesize PA endogenously or it can be provided in diet; indeed, the PA is the major component of palm oil (40% of the total fats) but can be also found in dairy products (50-60%), breast milk (20-30%), meat, cocoa butter (26%) and olive oil (8-20%)[57]. Industrially, it can be produced by hydrolysis of triglycerides catalysed by a strong base such as NaOH or KOH.

As seen in the paragraph 1.2.2.2, PA is also an important component of the bio-crude derived from Aarhus HTL plant, mainly for the Spirulina and sewage sledge bio-crudes in which PA represents the 37.0 and 36.9 mg/g respectively. For this reason, the interest towards this chemical is rising and it has become an important model molecule for bio-crude upgrading studies.

The PA is a weak organic acid with a pK_a of almost 4,75[58]. Therefore, in presence of a strong base like NaOH or KOH, the PA is neutralised forming the associated salt that in this case is the Sodium palmitate (NaPal). The equilibrium is related to the pH and it has to be controlled since the two compounds have a different thermo-chemical behaviour.

1.5 Electrochemical theoretical background

In this paragraph a theoretical analysis on the electrocatalytic systems at lab scale will be done, coupling the theoretical principles useful to carrying out an electrochemical reductive process with the practical aspects of the lab-scale electrorefining. This section has been provided to be eventually consulted. For the sake of brevity, a description of the kinetics of the electrochemical reactions have been reported in the Annex 4, as an important part of the theory of electrochemistry.

1.5.1 Electrochemical cell and thermodynamic of electrochemical systems

The electrochemical cells are the reactors in which redox reactions occur. They can be customised in relationship with the final scope of the process and they can be distinguished in two main categories[59]:

1. Galvanic Cells: the reactions are spontaneous ($\Delta G < 0$) when the electrode is connected via a conductor. Like primary and secondary batteries.
2. Electrolytic Cells: they require a potential more than their open circuit potentials (OCP, the potential that exists in an open circuit) to carry out the non-spontaneous electrochemical reaction ($\Delta G \geq 0$). The potential needed is called overpotential.

In the case of biomass hydrogenation and in general biomass electrorefining, the reactions require an electrolytic cell since they are not spontaneous and required additional energy.

There are different types of electrolytic cell in relationship with the specific need of the experiment, but in general, two main categories can be defined[47]:

1. Bulk electrolysis cell: the most used in lab scale systems. They can be divided or undivided cells and are practically used for fundamental analysis of the reactions, potential analysis, and kinetics studies at mild conditions[47]. They can be designed for both batch and continuous processes and they usually exploit solid electrodes to carry out the reaction. The separator can be made by porous glass or ion-exchange membranes (e.g. Nafion) to allow the flux of ions (i.e. anions or cations) and to separate the anolyte and catholyte compartments and products. Figure 29

represents two schematic and representative example of bulk electrolysis cells[60], many designs and set-up are normally employed in electrochemical laboratories.

2. Electrochemical flow reactor: they are used mainly for continuous process, even though also batch system can be settled. They are used for the upscaling of electrochemical reactions, since enable the steady state conditions as well as ensuring higher throughput due to better fluid dynamics conditions. They can reach harsher conditions in term of pressure and temperature, and they can treat larger volumes of feedstock.

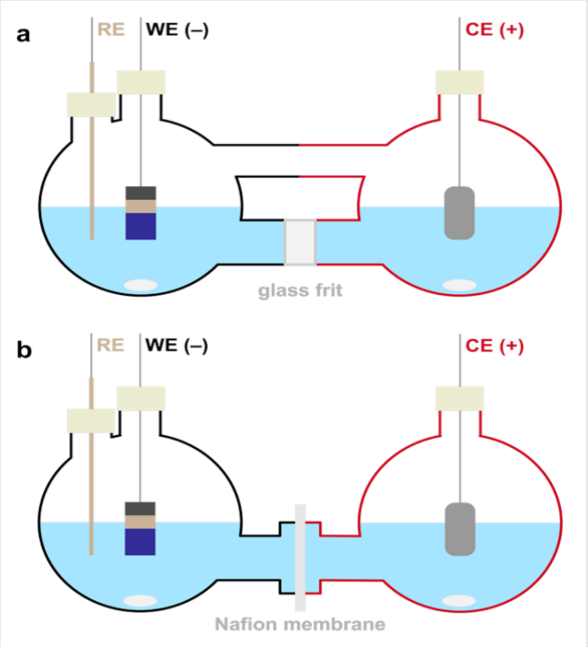

Figure 29: Bulk electrolysis cell with a glass frit membrane and linked headspace (a) and a divided H-cell with Nafion membrane[60].

In the case of this specific study, only the bulk electrolysis cell will be considered. The high versatility coupled with the simplicity of the set-up, make these systems suitable for a fundamental study as the one performed in the present work.

A classical electrochemical cell is composed by three electrodes: a working electrode, WE, where the reaction under investigation happens, a counter electrode, CE, and a reference electrode, RE which is a stable phase electrode with a fixed potential. The current is always supplied at the CE/WE pair, while the potential can be read either between the CE/WE or WE/RE. In the following, the potential will be always (if not stated otherwise) referred to the WE/RE. Thus, this potential difference is related to the potential at which the electrochemical reaction under investigation is taking place. However, it is also influenced by the resistivity of the solution.

This latter parameter is calculated from the potential drop in a region where no-faradic process (electrochemical reactions) are present. Hence, in this region the potential of the WE is observed respect the RE and the potential drop within them is given by Ohm's law:

$$E_{drop} = I \cdot R_s \quad (9)$$

It means that the real potential electrode (E_{el}) is different to the applied potential ($E_{applied}$) according to:

$$E_{el} = E_{applied} - E_{drop} = E_{applied} - I \cdot R_s \quad (10)$$

Related to this, there are the two-electrode cells (WE and RE), which are mainly used for polarography and in systems with low solution resistance. In fact, the polarographic experiments usually have $I < 1$ μA, $R_s < 100$ Ω and $iR_s < 1$ mV[59]. Otherwise, when the potential drop due to resistance is not negligible, the most used cells are the three-electrode cells, the RE is placed in close vicinity of the WE to eliminate the solution resistance, therefore only the so-called uncompensated resistance R_u remains (see Figure 30)[61]. The three-electrodes cells can have different shapes and designs, they might be made by different materials; the most common is the Pyrex glass or quartz, due to the low costs and easy manufacture, nevertheless, when corrosive environment is present (e.g. high pH, hydrofluoride), other plastic material such as Teflon, Kel-F or Nylon should be used[59]. These cells can have different compartments to separate the electrode and avoid contaminations events or selectivity loss, for this reason selective membrane in between the compartments plays and essential role for the overall efficiency and feasibility of the redox reactions. Hence, there are mono-compartment cells, H-cell, three-compartment cells, and specific designed cells. For the three-electrodes cell, a potentiostat must be used which controls the potential of the WE vs. RE by adjusting the current flow between WE and CE.

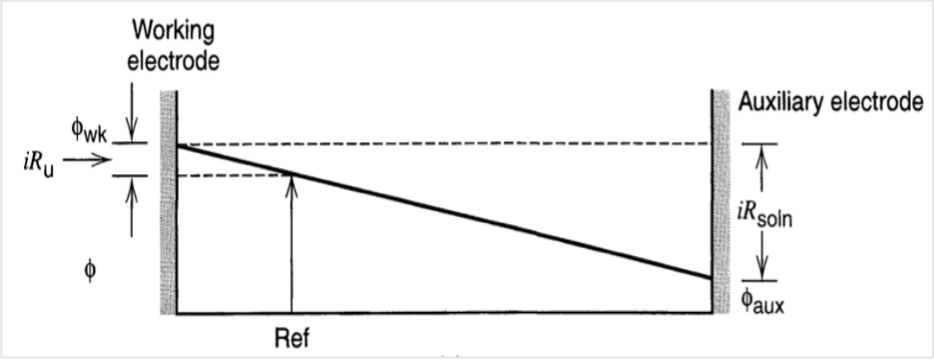

Figure 30: Potential drop between WE and CE and the relative iR_u measured at the RE[61].

In an electrochemical cell, the half-cell potentials are related to the free energy of Gibbs and with the equilibrium constant of the half-reactions as:

$$\Delta G_{cell} = -nFE \tag{11}$$

$$\Delta G_{cell} = \Delta G° + RT \ln\left(\frac{a_{red}}{a_{ox}}\right) \tag{12}$$

$$\Delta G°_{cell} = -RT \ln K \tag{13}$$

In which ΔG_{cell} is the cell's energy Gibbs variation, n mole of electrons involved in the redox reaction, F the Faraday constant, R the universal gas constant, the a_{red} and a_{ox} the activities of the redox species (the ratio is called also reaction quotient Q), K the equilibrium constant of a half reaction and E the electrode half-cell potential, which is related to the half reactions' redox potential at the anode and cathode.

Indeed, having E_{anode} and the $E_{cathode}$, the cell electrode potential is derived as

$$E_{cell}=E_{anode}-E_{cathode} \tag{14}$$

Combining the eq. (11) and eq. (12) yields to the Nernst equation[62]:

$$[E_{ox/red}]_{SHE}=[E°_{ox/red}]_{SHE}+\frac{RT}{nF}\ln\left(\frac{a_{red}}{a_{ox}}\right) \tag{15}$$

Here the subscript SHE stands for Standard Hydrogen Electrode, since the use of different reference electrodes influences the potential at which the WE works. By knowing the material of the reference electrode (e.g. Ag/AgCl as the one used in the present work) it is possible to calculate the potential referred to the SHE using the eq. (23). Since the activities are not always easy to calculate, or they are often unknown, the Nernst equation is written in base of the so-called formal potential (*E*°'):

$$[E°'_{ox/red}]_{SHE}=[E°_{red/ox}]_{SHE}+\frac{RT}{nF}\ln\left(\frac{\gamma_{ox}}{\gamma_{red}}\right) \tag{16}$$

The Nernst equation can be rewritten in terms of the species concentration (C) as:

$$[E_{ox/red}]_{SHE}=[E°'_{ox/red}]_{SHE}+\frac{RT}{nF}\ln\left(\frac{C_{ox}}{C_{red}}\right) \tag{17}$$

The formal potential of a redox species is related with the solvent and the electrolyte, hence it must be verified experimentally, using, for example, cyclic voltammetry methods.

The Nernst equation is the base of thermodynamic in electrochemical cells and it can be applied in all the electrolytic cells to evaluate the electrode half-cell potential at equilibrium.

1.5.2 Solvents

The solvent works has a medium of reaction. Indeed, it is chosen based on different parameters such as boiling point T_b [°C], freezing point T_f [°C], density ρ [g cm^{-3}], viscosity μ [mPa s], dielectric constant or relative permittivity ε_r, dipolar moment, toxicity expressed in medial lethal dose 50% (LD_{50}^f) and potential window (ECW)[63]. This last parameter is important in electroanalysis because it is the difference between E_{ox} and E_{red} of the solvent, and it defines the potentials at which the detected current is not related with the solvent redox activity.

In Table 7, some organic solvent with the related parameters has been highlighted[63]. The simplest and used solvent is water, due to its high relative permittivity, low viscosity, low LD_{50}^f and low costs (also in term of downstream treatment). In term of green chemistry, the aqueous system is the most studied and when analysing the feasibility of an electrochemical setup, the water is always the first option to implement. Sometimes different solvents are used in the same system, to enhance the

Table 7: Most important solvent parameters for electrochemical systems[63].

Solvent	T_f [a] (°C)	T_b [b] (°C)	d [c] (g cm^{-3})	μ [d] (mPa s)	ε_r [e] (—)	LD_{50} [f] (g_{oral} kg_{rat}^{-1})	p^* [g] (kPa)	E_{red} [h] (V *vs.* SHE)	E_{oxi} [i] (V *vs.* SHE)	ECW [j] (V)
N,*N*-Dimethylacetamide (DMAc)	−20	166	0.94	0.93	37.8	5.68	9.77			
N-Methyl-2-pyrrolidone (NMP)	−24	204	1.03	1.70	32.2	3.91	0.84			
Nitromethane (NM)	−29	101	1.13	0.61	36.7	0.94	4.88	−1.0	2.9	3.9
γ-Valerolactone (GVL)	−31	208	1.05	2.00	42.0	8.80	0.027	−2.8	5.4	8.2
Methoxyacetonitrile (MAN)	−35	120	0.96	0.70	36.0	0.98	2.50	−2.5	3.2	5.7
γ-Butyrolactone (GBL)	−43	204	1.13	1.73	39.1	1.54	0.43	−2.8	5.4	8.2
Acetonitrile (AN)	−44	82	0.79	0.34	35.9	6.69	11.81	−2.6	3.5	6.1
Trimethyl phosphate (TMP)	−46	197	1.07	2.20	21.0	0.84	0.13	−2.7	3.7	6.4
Propylene carbonate (PC)	−49	242	1.20	2.53	64.9	5.00	0.017	−2.8	3.8	6.6
1,2-Butylene carbonate (BC)	−53	240	1.14	3.20	53.0	5.00	0.0056	−2.8	4.4	7.2
3-Methoxypropionitrile (MPN)	−57	165	0.94	1.10	36.0	4.39	0.28	−2.5	3.3	5.8
N,*N*-Dimethylformamide (DMF)	−60	153	0.94	0.92	36.7	2.80	0.49			
Diglyme	−64	160	0.94	0.99	7.23	5.40	0.45			
1,2-Dimethoxyethane (DME)	−69	85	0.86	0.46	7.20	5.37	6.38			
4-Methyl-2-pentanone	−84	117	0.80	0.55	13.1	2.08	2.50			
Ethyl acetate (EA)	−84	77	0.89	0.43	6.02	5.62	12.57			
2-Propanol	−88	82	0.78	2.04	19.9	5.05	5.76			
Nitroethane (NE)	−90	115	1.05	0.68	28.0	1.10	2.08	−1.1	3.2	4.5
Toluene	−95	111	0.86	0.55	2.38	5.58	3.79			
Hexane	−95	69	0.65	0.29	1.88	25.00	20.12			
Acetone	−95	56	0.78	0.30	20.6	5.80	30.72			
Dichloromethane (DCM)	−95	40	1.32	0.39	8.93	2.00	57.99			
Methanol (MeOH)	−98	65	0.79	0.55	32.7	1.98	16.89			
Tetrahydrofuran (THF)	−108	66	0.89	0.46	7.58	2.45	21.55			
Ethanol (EtOH)	−115	78	0.78	1.08	24.6	10.47	7.85			
1-Propanol	−126	97	0.80	1.94	20.5	8.04	2.79			

[a] T_f: freezing point of pure solvent and data from ref. 52. [b] T_b: boiling point of pure solvent and data from ref. 52. [c] d: density and data from ref. 52. [d] μ: viscosity and data from ref. 52. [e] ε_r: relative permittivity and data from ref. 52. [f] LD_{50}: median lethal dose (50%), data from Material Safety Data Sheets of Sigma-Aldrich. [g] p^*: saturated vapour pressure at room temperature and data from ref. 52. [h] E_{red}: limiting reduction potential (0.65 M Et_4NBF_4, 25 °C, glassy carbon, 5 mV s^{-1}, and 1 mA cm^{-2} as threshold) and data from ref. 59. The potential is converted by SCE = 0.24 V *vs.* SHE. [i] E_{oxi}: limiting oxidation potential (0.65 M Et_4NBF_4, 25 °C, glassy carbon, 5 mV s^{-1}, and 1 mA cm^{-2} as threshold) and data from ref. 59. The potential is converted by SCE = 0.24 V *vs.* SHE. [j] ECW: electrochemical window (ECW = $E_{oxi} - E_{red}$).

solubility of the interested analyte or vary critical parameters such as viscosity. The final solution can be an azeotropic solution, which has the same composition of the vapour that distils when heated up, or non-azeotropic, which means that the two solvents cannot be seen as single mixed phase.

In the case of Palmitic acid, it has been verified that its solubility rises in azeotropic solutions such as acetone-heptane, ethanol-heptane and hexane-ethanol[64]. A good solvent, or mixed solvent solution, must have different essential characteristics: liquid at experimental conditions, good dissolution of the analyte and supporting electrolyte at high concentration, stable towards redox reactions in the experimental potential, not involved in deleterious reactions or side reactions with the supporting electrolyte or analyte, and, finally, it has to be safe, easy to purify, and with a low toxicity[65]. For biomass' treatment the solvents are, therefore, chosen in based on the solubilisation capabilities, since like in the case of palmitic acid, there could be compounds insoluble in aqueous systems. The choice of the solvent is, though, a very important step and it must follow the forth principle of green chemistry[66]. In this work, methanol and ethanol/water (70/30%) systems have been selected to be the appropriate solvent.

1.5.3 Supporting electrolyte

The supporting electrolytes instead are usually solvent-soluble salts that increase the conductivity of the solution, decreasing the resistance, and controlling the pH. They are usually in excess to neglect the migration phenomena, and, like the solvents, they have a specific potential window within which the current detected is not related with their redox reaction.

A good supporting electrolyte must have some characteristic: high solubility in the solvent chosen, chemically and electrochemically inertness in the reaction conditions, low toxicity and easy purification[65]. To analyse these characteristics, some important parameters must be considered such as the ionic radius [nm], the limiting molar conductivity of the ions in the selected solvent [S cm^2 mol^{-1}] and, as said before, the ECW of the ionic couple which is the difference between the E_{ox}^{anion} and the E_{red}^{cation} (see Table 8)[63].

Table 8: Most common ion pairs for organic systems[63].

			Λ_m [b] (S cm^2 mol^{-1})						
Supporting ion		r [a] (nm)	PC (μ: 2.53 mPa s)	GBL (μ: 1.73 mPa s)	H_2O (μ: 0.89 mPa s)	THF (μ: 0.46 mPa s)	AN (μ: 0.34 mPa s)	E_{red} [c] (V *vs.* SHE)	E_{oxi} [d] (V *vs.* SHE)
Anion	BF_4^-	0.229	20.43	30.77	75.1[93]		108.5[94]		3.6
	ClO_4^-	0.237	18.93	28.45	67.36	88.9[95]	103.6		3.1
	PF_6^-	0.254	17.86	26.70	65.5[93]	77.5[96]	102.8[97]		3.8
	AsF_6^-	0.260	17.58	25.92	32.4[98]		100.1[97]		3.8
	$CF_3SO_3^-$	0.270	16.89	24.93			96.3		3.0
	$(CF_3SO_2)_2N^-$	0.325	14.40	20.55	32.2[99]		83.72[99]		3.3
	$C_4F_9SO_3^-$	0.339	13.03	18.66					3.3
	BPh_4^-	0.419	8.52	11.67	19.8[100]		58.02		1.0
Cation	Li^+	0.076	8.43	13.99	38.68		69.97[97]	−3.0	
	Me_4N^+	0.283	14.50	21.52	44.9		94.52	−2.9	
	Et_4N^+	0.343	13.50	19.32	32.7		85.19	−2.8	
	Pr_4N^+	0.381	10.47[101]		23.45[102]		70.20[103]	−2.8	
	Bu_4N^+	0.415	9.09	14.03	19.5	43.8[96]	61.63	−2.8	
	Am_4N^+	0.467[101]	8.05[101]		17.13[102]		55.81[104]		
	Hex_4N^+	0.469[105]	6.14[105]				50.58[104]	−2.9	

[a] r: ionic radius and data from ref. 106. [b] Λ_m: limiting molar conductivity at 25 °C, data in solvents PC and GBL from ref. 106, solvents EtOH and AN from ref. 52. [c] E_{red}: limiting reduction potential, data from ref. 59 (BF_4^- as the supporting anion, 0.65 M, 25 °C, glassy carbon, 5 mV s^{-1}, and 1 mA cm^{-2} as the threshold). The potential is converted by SCE = 0.24 V *vs.* SHE. Caution is needed for using the potential conversion. [d] E_{oxi}: limiting oxidation potential, data from ref. 107 (Et_4N^+ as the supporting cation, 0.65 M, 25 °C, glassy carbon, 5 mV s^{-1}, and 1 mA cm^{-2} as the threshold). The potential is converted by Li^+/Li = −3.00 V *vs.* SHE.

From the Stokes law:

$$\Lambda_m = \frac{z^2 F^2 / \pi N_a}{k \mu r} \quad (18)$$

In which z is the charge number, F the Faraday constant, N_a the Avogadro constant, k the Stokes constant, μ the solvent viscosity and r the ionic radius. This equation states that the lower the viscosity, the more the solvent will have a higher ionic conductivity. Moreover, the lower the ionic

radii of the ions, the more the system will have a higher conductivity. This phenomena is not true for alkali metal such as Li^+ and Na^+ and halogens, in which the conductivity value is overestimated[63]. Following the Denisos-Ramsey law on the supporting electrolyte dissociation constant (K_d), high relative permittivity of the solvent is correlated with a higher solubility of the supporting electrolytes:

$$-\ln(K_d)=\frac{q_e^2}{\varepsilon_0\ \varepsilon_r\ L\ k_B\ T} \tag{19}$$

In which q^2_e is the elementary charge, ε_0 the void permittivity, ε_r the solvent permittivity, L the distance between the two ions in a salt, k_b the Boltzmann constant and T the absolute temperature. The most common supporting electrolyte in water systems are simple water-soluble salts such as KOH, NaOH, carbonates, KNO_3, Na_2SO_4, HCl, KOH, H_2SO_4 and HClO. For organic solvents, Figure 31 shows the ions couples most used in non-aqueous electrochemistry[59], furthermore also alkaline metal can be used as cations due to their short atomic radius and the most used are Li^+ and Na^+. In this work mainly NaOH and NaCl have been used to increase the conductivity of catholyte phase and to tune its pH.

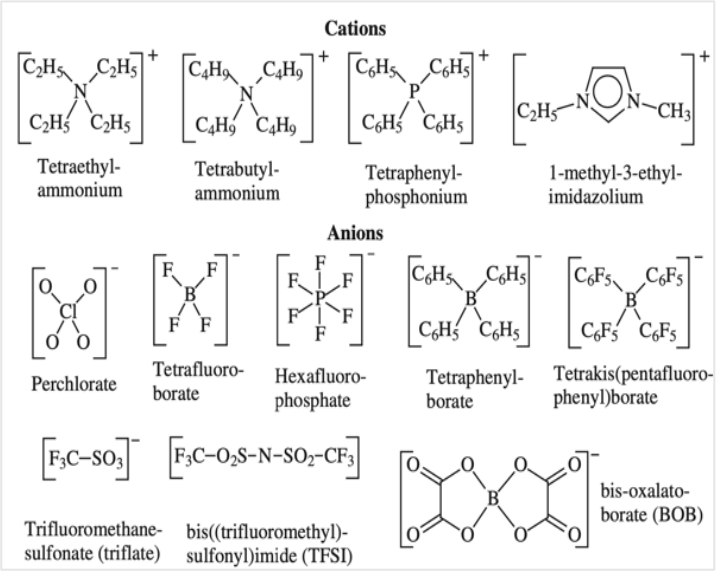

Figure 31: Anions and cations of salts commonly used in electrochemistry[59].

1.5.4 Mass transfer in electrochemical systems

The mass transfer of a certain ion in an electrochemical system can be due three phenomena:

Diffusion: related to the concentration gradient, hence the flow of mass goes in the directions of a lower electrochemical potential.

Migration: Related to the electric field (gradient of electrical potential), in this case the movement of charged particle goes in the direction of the electric field by applying a potential.

Convection: related to hydrodynamic flow of the electrode solution near the electrode surface, conditioned by the stirring or the rotating movement of the electrode (case of the rotating disk electrode).

These dynamics are combined in the Nernst-Plank equation, which assesses the unidirectional (x) flux (mass-transfer rate) of a species j in term of diffusion, migration and convection[59]:

$$J_j(x) = -D_j\left(\frac{\partial C_j(x)}{\partial x}\right) - \frac{z_j F}{RT} D_j C_j \frac{\partial \phi(x)}{\partial x} + C_j v(x) \qquad (20)$$

In which $J_j(x)$ is the flux of the species j [mol cm^{-2} s^{-1}] at distance x [cm] from the electrode, D_j the diffusion coefficient of j [cm^2 s^{-1}], C_i concentration of j [mol cm^{-2}], z_j the charge of j and v is the linear velocity of the solution flow [cm s^{-1}]. $\partial C_j(x)/\partial x$ is the concentration gradient and $\partial \phi(x)/\partial x$ is the potential gradient along the x axis.

The yellow part represents the Fick's law that governs the diffusion processes, the green term accounts for migration and the blue term represents the convection of the solution. Using a system with excess of supporting electrolyte (salts) makes the migration negligible, since the salts will take most of the solution migration. Furthermore, using a controlled stirring rate (rpm) or even a rotating disk electrode, the convection processes can be eliminated (or drastically reduced), leaving diffusion as the only way to transfer mass. Indeed, if j is charged, the flux J can be written in relationship with the electrode area (the flux is an amount per unit time per unit area) and the current, proportional to the concentration gradient (using the Faraday's law):

$$-J_{red} = \frac{I_{a,dif}}{nFA} \qquad (21)$$

$$I_{a,dif} = D_{red} nFA \left(\frac{\partial C_{red}(x,t)}{\partial x}\right) \text{ with } x=0 \qquad (22)$$

At the electrode-electrolyte interface the diffusion layer, where the mass transfer is due to diffusion, is limited by the so-called electrical double layer, which introduces a capacitive behaviour in the solution. The electrical double layer is divided in "sub-layers" (see Figure 32)[47]:

Inner Helmholtz plane (inner plane), in which solvated ions and solvent molecules are specifically adsorbed on the electrode surface at a certain distance x.

Outer Helmholtz plane (outer plane), in which the species involved are not specifically adsorbed.

Diffuse layer, which is in between the OHP and the bulk of the solution. It is present due to the thermal agitation in the solution.

The electrical double layer must be limited as much as possible because it can bring a local potential drop in the system (inner potential ϕ), that is the difference between

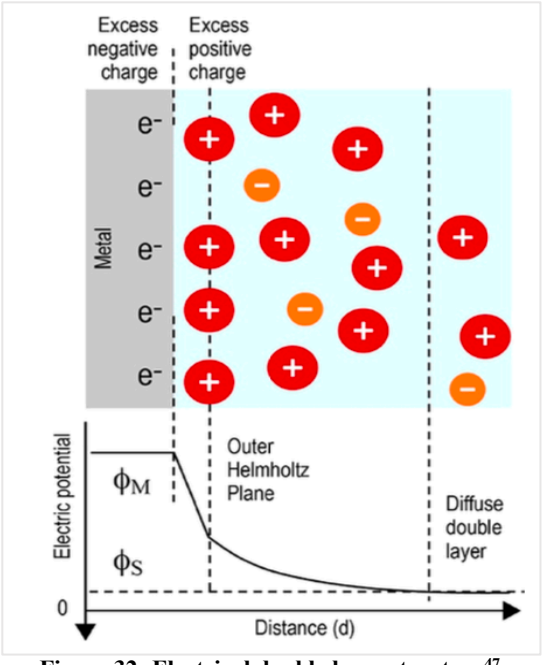

Figure 32: Electrical double layer structure[47].

the potential at the electrode surface ϕ_2 and the potential in the solution ϕ^s. Hence, it can influence the rate of reaction since the electroactive species are not able to be specifically adsorbed on the electrode surface. The most straightforward way to limit this phenomenon is to enhance the stirring of the solution and try to limit this capacitive aspect.

1.5.5 Electrodes and electrocatalysts

An essential part of the electrochemical system are the electrodes and the electrocatalysts. As said before, the three electrode cells are the most utilised for the laboratory scale experimentation on biomass, and they are composed by the working electrode (WE), the counter electrode (CE) and the reference electrode (RE). While the last two electrode are typically standardised and maintain constant during the different experiments, the WE is design ad-hoc to improve the kinetic of the target reaction and it can be changed and engineered to find the most suitable one.

Hence, the CE is usually an inert material used to counterbalance the reaction at the WE. It must be stable at the working potential and at the same time it doesn't have to catalyse parasitic reaction that could decrease the faradaic efficiency of the system. The most suitable materials to design the CE are the noble metal, in particular Pt is the most used since it presents a good stability even at more extreme potentials.

The RE, instead, is essential to carry out the reaction in the three-electrode cells; indeed, it must have an almost constant potential with low current passage, and it must be in the close vicinity with the WE to minimise the solution resistance. There are different types of reference electrodes according to the type of electrolyte and studies, but the most important ones are discussed below:

- **The Standard Hydrogen Electrode (SHE):** it is the primary reference in electrochemistry, and it consists in a Pt electrode in a proton solution and hydrogen gas with an ionic activity that is equal to one. The half-cell reaction is as follows[67]:

$$2H^+_{(aq)} + 2e^- \rightarrow H_2 \qquad (X)$$

  Usually the electrolyte is a hydrochloric acid solution[67].

- **The Silver-Silver Chloride Electrode:** it consists of silver covered by a solid silver chloride that is in contact with a solution containing the chloride anions. It is the most used in electroanalysis since it can be miniaturised, and it is very versatile since it can be used also with some soft organic solvents such as ethanol or methanol. The half-cell reaction is as follows[67]:

$$AgCl + e^- \rightarrow Ag + Cl^- \qquad (XI)$$

- **Saturated Calomel Electrode (SCE):** it is a second-kind electrode consisting of metallic mercury and excess of mercury chloride, highly soluble, with an addition of mercury paste with

calomel in contact with a KCl solution. The structure is not easy, and it is being increasingly replaced with the Silver-Silver Chloride Electrode. The half-cell reaction is as follows[67]:

$$Hg_2Cl_2 + 2e^- \rightarrow 2Hg + 2Cl^- \quad \text{(XII)}$$

When doing some potential operation, the results must be always presents versus the reference electrode, otherwise they cannot be validated. In this way, each data can be referenced also with another RE, with specific conversion equations in which the SCE has a potential V = 0. The SHE is pH dependent, so this parameter must be evaluated when converting the data. For example, for the conversion of E *vs*. Ag/AgCl to E *vs*. SHE the following equation must be used:

$$E_{(SHE)} = E_{Ag/AgCl} + 0{,}059pH + E^{\circ}_{Ag/AgCl} \quad (23)$$

In which the $E^{\circ}_{Ag/AgCl}$ is equal to 0,1976 V at 25°C.

Finally, the WE is the electrode where the target reaction takes place. It must be suitable to improve the rate as much as possible decreasing the overpotential required for the reaction to occur. The WE's aim is to transfer the electrons and carrying out the eventual chemical reactions. They must have some specific characteristics[59]: high electrical conductivity, low intrinsic overpotential for the desired reaction, high active surface, hardness and durability, electrochemical stability, homogeneous microstructure throughout the bulk and inexpensive costs of fabrication and recycling. There can be homogeneous and heterogenous electrocatalysts, but only the seconds will be evaluated in the study. In this category there are two main types: the so-called bulk electrocatalysts which are basically composed by the material of the electrode itself and the supported electrocatalysts which are formed by a modified electrode on which the active sites are coated/deposited. The active sites can be found in different materials:

- Metals: noble metals such as Pt, Ag, Pd, Au and Ru, transition metals like Cu, Ni, Fe, Ti, Mo, Co and Zn, as well as alloys.
- Metal hydroxides: like hydrotalcites, $Ni(OH)_2$, $Co(OH)_2$.
- Metal oxides: like RuO_2, TiO_2, MnO_2.
- Carbides: like Mo_2C.
- Sulphide: like Mo_2S.
- Carbonaceous materials: they have different crystal structure and orientation, as well as geometries. They are like carbon nanotube, carbon fiber, graphene-related materials, graphite, glassy carbon, amorphous powder, and diamond.

Instead, the most common supports are graphite-related material (highly conductive and porous), carbon nanotubes, graphene, and metals in different form such as foam, sponge, or gauze.

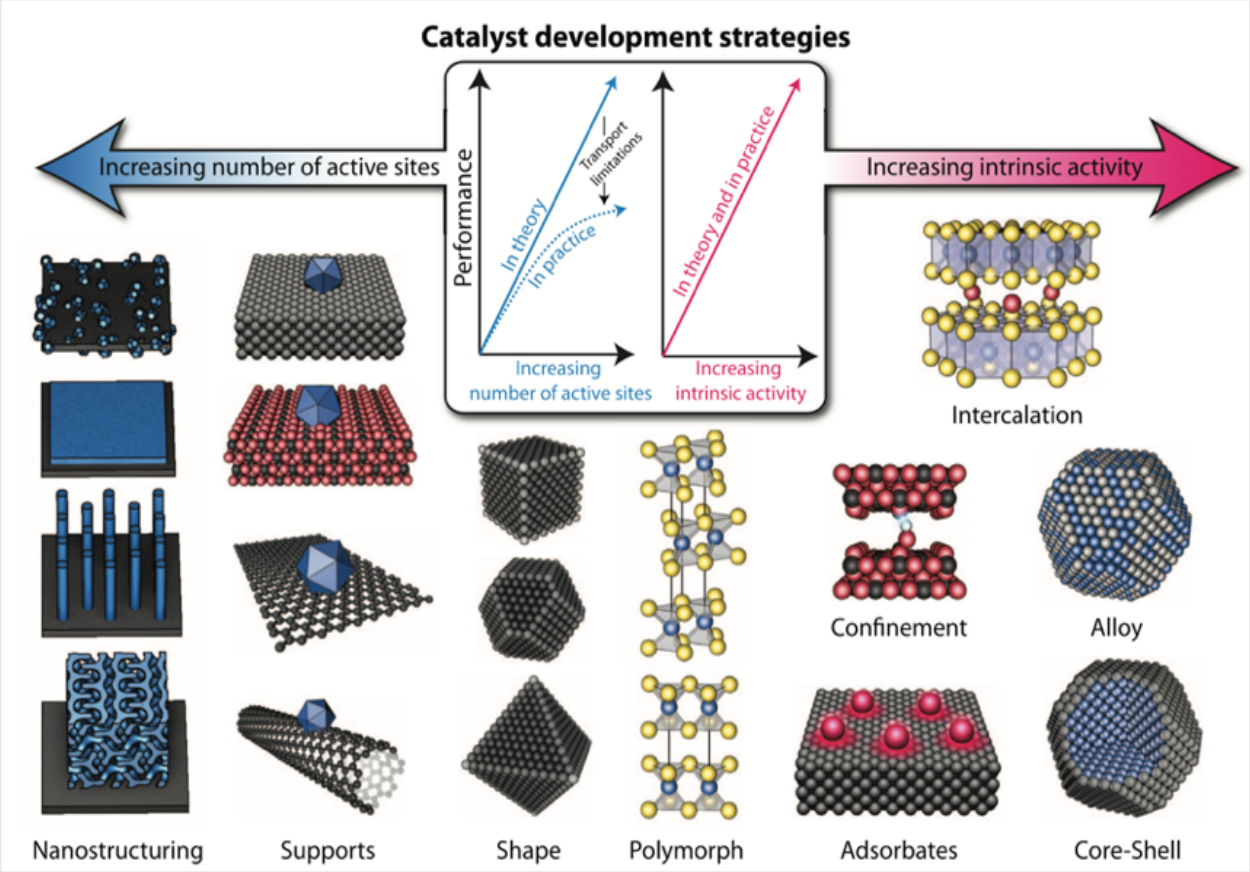

Figure 33: strategies to increase the activity of an electrocatalyst[49].

In order to improve the activity of a specific electrocatalyst, two strategies can be followed (see Figure 33)[49]: the first is focused on the increasing of the available active sites, by basically increase the surface area and the numbers of sites. This can be done by working on the nanoparticle shape, size and supports porosity. The second strategy seeks to increase the intrinsic activity of the nanoparticle by build engineered structures such as core-shell and alloys, as well as focusing on physical phenomena like intercalation and confinement. While the first strategy is limited by the mass transfer in the systems, the second one has the potential to improve the activity in theory and practice without notable limitations.

2. Material and methods

In this chapter the materials and the techniques used for the electrocatalytic hydrogenation of palmitic acid and for the tests on the biocrude, will be taken into account. The different experiments and analysis have been performed mainly in the Electrochemical Engineering Lab, located in Åbogade 40, Aarhus, 8200, under the Biological and Chemical Engineering Department of Aarhus University. First, the reagents and the chemicals used will be highlighted and the set-up of the experiments will be described, talking about the most important elements that allowed to perform all the experiments and the reactions. In this part, the followed protocol will be highlighted paying attention on the type of material used in the laboratory. After, the electrochemical analysis will be tackled. They are essentially investigations of the electrochemical set-up by exploiting some physical output or by carrying out the reactions and impose the conditions to the system. Afterwards, the products analysis will be divided in relationship with the different matrixes, starting from the liquid characterisation, and finishing with the gas sample analyses. In these two last steps, the techniques used for the analysis will be examined with some theoretical background, calculations and procedures for their implementation.

2.1 Reagents and chemicals

Hereby the list of all the reagents and chemicals used for the study: Palmitic acid 98% by Sigma-Aldrich, Na Palmitate 98,5% by Sigma-Aldrich, ethanol 70,3% (v/v) by TechniSolv, 100% assay methanol, acetonitrile CHROMASOLV for HPLC >99,99% by Sigma-Aldrich, isopropanol HPLC 100% assay by Sigma-Aldrich, acetone 100% assay by VWR Chemicals, Milli-Q water, NaOH 98,5% in pastilles by VWR Chemicals, KOH 85,2% in pellets by VWR Chemicals, NaCl >99,9% by Sigma-Aldrich, $LiBF_4$, $TBABF_4$ 99% by. Sigma-Aldrich, LiCl, Lauric acid, Myristic acid, decanoic acid, hexadecanol 99% pure by Sigma-Aldrich, H_2O_2 solution 3% in water, HCl solution 2 M in water, H_2SO_2 solution 0,5 M in water.

2.2 Electrochemical set-up

The electrochemical set-up has been changed during the experiments, but common features have been followed, to minimise variables and uncertainties. This paragraph will consider the different aspects that have been essential to perform the reactions and the electrochemical experiments. It will start with the electrochemical cell and the main components' evaluation. After, the pre-treatments used for

the WE and the implementation strategy will be highlighted and, finally, the reactions set-up with the cleaning and sample methods will be analysed.

2.2.1 Electrochemical cells and components

For the execution of the electrochemical experiments, a three-electrode set-up have been exploited. As stated in the paragraph 1.5.1, the three-electrode set-up allows to minimise the resistance of the solution leaving the uncompensated resistance as only factor to analyse. The potential drop associated to this phenomenon is then considered in order to understand the real applied potential in the cell (according to the eq. (10)).

Three types of cells have been used for the different tests:

1. **Mono-compartment cell (Mcell):** this cell is the simplest one and allows to perform the analysis of particular system such as the melted palmitic acid or the systems with acetonitrile as solvent. It has been also exploited for tests where a a stable pH was needed, not influenced by the eventual ionic transfer from the anolyte. The electrodes were usually introduced by using a single septum, that works also as plug to maintain the inert atmosphere and avoid the oxygen exchange (see Figure 34).
2. **H-cell with Nafion n117 (Hcell):** it has been the most used for the fundamental investigation of the ECH of Palmitic acid and it can be considered as the most suitable cell for ECH of bio-based model compounds. The cation exchange membrane allows the proton transport separating the cathode and the anode in an efficient way. The high thermal, mechanical and chemical stability of Nafion allows rising the temperature and achieving more extreme conditions in term of pH. In this case, three septa have been utilised: (1) top septum for the WE in the cathodic compartment, (2) lateral septum for the RE in the cathodic compartment as well and (3) top septum for the CE in the anodic compartment see Figure 34).

Figure 34: Mcell (left) and Hcell (right) used for the experiments.

3. **H-cell with fritted glass (HCF):** this type of cell has been used only for the initial analysis and after abounded for the H-cell with Nafion. The set-up is almost the same then the Hcell but the electrode chambers are linked with a gas bridge and the Nafion 117 is substituted by the friteed glass (porous glass).

About the electrodes utilised, as stated in the paragraph 1.5.5, the RE is usually chosen at the beginning and standardised in base of the type of solvent (organic, semi-organic or aqueous), the CE instead is used to enhance the counter reaction that in this case was the OER (see reaction (IV)). Both the CE and the RE were maintained constant in all the tests, while the WE has been changed after each reaction, and it was made mainly by industrial Ni foams.

For the following experiments the RE is shown in Figure 35. It is a micro leak-free Ag/AgCl electrode (see paragraph 1.5.5) and it has been found suitable to be used in both methanol-based and ethanol-based electrolyte, but also in other systems. Furthermore, the size and the versatility have been fundamental to perform the experiments in these types of cells and to try to maintain the same geometry (important for the ohmic drop).

The CE, instead, is a Pt mesh (Figure 35). The high surface area, coupled with the good stability and activity toward OER, makes this anodic electrocatalyst the best choice in almost all the ECH studies not coupled with target oxidation reactions (e.g. co-electrocatalysis). In the case of the Palmitic Acid ECH the Pt sponge allows the evaluation of the cathodic reaction only, without influence or even jeopardise the target reaction.

For the working electrode the study focuses on the utilisation of Ni as metal for the selective ECH of PA. Indeed, mainly industrial Ni foams have been used to perform fundamental and basic studies on the feasibility of the reaction (Figure 35). Figure 23 showed that Ni was a good compromise in term of relative activity towards ECH. Moreover, the tests were done mainly in neutral-alkaline conditions, where the Ni seems to be more active and stable.

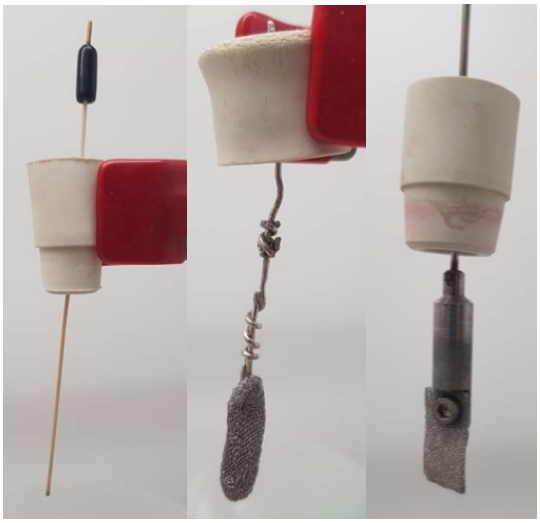

Figure 35: from the left. Ag/AgCl RE, Pt CE and an example of Ni foam WE 1x1.

In some cases, other materials have been used, but with no further studies. For example, the tests *13a* and *13b* (see test table as Annex 12), have been carried out in acidic pH, have been done with a Pt coil since the pH wasn't suitable for the Ni. Another example is the test *12c*, which has been performed with a Cu mesh, to compare the results and discuss for future material usage.

2.2.2 Electrode preparation and reaction set-up

In this paragraph, the protocol followed for the preparation and the pre-treatments of the single electrodes will be described. For the CE and RE no special preparation or cleaning treatments have been implemented.

The CE is washed with Milli-Q, before and after reaction and afterwards heated up in an oven until 100°C overnight. Due to its good stability and inertness, the Pt mesh was stored in a plastic cylinder with the proper septum without specific treatments. The RE is carefully washed with Milli-Q water before and after reaction as the CE; successively it has to be wiped with paper and put inside a proper potassium chloride 30 % (w/w)/silver chloride 1 % (w/w) aqueous solution, and storage until use. It is important to leave the electrode in the solution because it might readjust the eventual disequilibrium due to the activity during the reaction.

For the WE, instead, a customise path has been established and it is shown in Annex 5.

Regarding the reaction set-up, it refers to all the operations that must be done before the initialisation of the electrochemical investigations. It includes the implementation of the electrode and electrolyte in the cells, the set-up of the temperature and the inert atmosphere setting. In this phase, a protocol must be followed in order to standardise the method and decrease the uncertainties (see Annex 6).

2.2.3 Material for the electrochemical investigations

When the cell and the solutions have reached thermal equilibrium, the electrochemical investigations can be performed. As highlighted in the paragraph 1.5.1, the potentiostat is an essential element to perform most of the electrochemical techniques. In this study it has been used a CH Instruments Electrochemical Workstation (CHI660E) linked with a computer and cables for the electrodes.

Before starting the investigations, all the electrodes must be connected with the appropriate electrical cables with the crocodile plugs. Once the electrodes are all properly connected, the electrochemical investigations can start and have been performed according to the following scheme:

I. **Open Circuit Potential (OCP) analysis**.
II. **Resistance analysis**: in some cases, the ohmic drop associated to a specific solution resistance has been detected, but never implemented with compensations. The potential chosen for the resistance analysis was usually the OCP or the potential of the CA.
III. **Electrochemical investigations techniques:** the electrochemical techniques can be finally used in a proper and constant order: EIS (eventually), CV, DPV, CA and, if needed, a final CV.

2.2.4 Sampling and cleaning

In this paragraph the post reaction methodologies are explored, looking mainly on the sampling methods and the cleaning of the cell and the catalyst.

The sampling has been done mainly on the liquid phase and in some tests also on the headspace. For the liquid phase, three main samples have been collected:

I. **Raw sample:** It defines the liquid portion collected as it was after the reaction (Figure 36). The amount of this sample has been defined by the volume of the 8 ml vial where it has been stored. It was stored at room temperature for eventual further analysis or as a source to obtain additional samples for solid analysis.

II. **Filtered sample:** it is the liquid sample that, before being collected, it has been filtered by a 0,45 nm filter (Figure 36). 5 ml of the liquid solution has been withdrawn using a syringe and after the changing of the needle and the implementation of the filter it has been storage in a reagentsglas.

III. **Sample for solid analysis:** this sample have been collected in an aluminium plate without any filtration or pre-treatment (Figure 36). It is successively dried under the fume overnight. The solid residual has been used for the IR, TGA and DSC analyses. For the IR and DSC, they have been acidified with an aqueous solution of HCl 2 M to move the equilibrium toward the PA and avoid the presence of NaPal.

Figure 36: Different types of samples, from the left; raw samples, filtered samples and sample for solid analysis.

In some tests, also the gaseous phase has been analysed. To do that, a suitable syringe has been used in order to pick up a suitable volume of headspace. The specific methodology followed for the gas sampling is explained in paragraph 2.5.1.1 of the Material and Method chapter.

After the different samplings the electrocatalyst was washed with Milli-Q water, disassembled from the metal stick and storage in a plastic plate. The cell instead was emptied from the remaining liquid and it was treated twice with acetone and Milli-Q water. After, Milli-Q water heated up with a boiler, was added in the cell and kept it for half an hour. After the removal of the Milli-Q water, the cell was usually kept in Milli-Q water overnight or until the next usage.

Another important aspect to consider is the cleaning of the membrane. It must be done with a constant frequency (every 2-3 weeks), when the conditions of the system change (like from neutral to acid conditions) or when it has been jeopardised. Therefore, the electrochemical cell is disassembled and the Nafion 117 membrane is treated separately. The protocol is reported in Annex 7.

2.3 Electrochemical investigations

The concept of electrochemical investigations refers to a group of techniques and methods that can analyse electrochemical systems by studying different parameters involved such as potential, current, resistance, impedance, or time. Figure 37 shows the general classification of the most used electrochemical techniques divided by the type of parameter studied[59]. The electrochemical techniques used in the study of Palmitic acid ECH are mainly four: (1) Cyclic Voltammetry (CV), (2) Chronoamperometry (CA), (3) Electrochemical Impedance Spectroscopy (EIS) and (4) Differential Pulse Voltammetry (DPV). The CV and the CA have been often used; therefore, they will be tackled more in depth. The EIS will not be considered and the DPV will be only introduced generalising the purposes and the support that it gave for this study.

Controlled Potential	Potential Step	Amperometry	Chronoamperometry; Double Potential Step Chronoamperometry	
		Chronocoulometry; Double Potential Step Chronocoulometry		
		Sampled Current Voltammetry; Differential Pulse Voltammetry; Square Wave Voltammetry		
	Potential Sweep	Voltammetry	Stationary	Linear Scan Voltammetry
				Cyclic Voltammetry
			Hydro-dynamic	Stirred Solution/ Flow Cell
				Rotating Disk Electrode; Rotating Ring-Disk Electrode
			Anodic Stripping Voltammetry (Stationary/Hydrodynamic)	
	Constant Potential	Bulk Electrolysis	Stirred Solution	
			Flow Electrolysis	
Controlled Current	Chronopotentiometry		Constant-Current	
			Linearly Increasing Current	
			Current Reversal	
			Cyclic	
	Coulometry		Coulometric Titrations	
	Electrolysis			
Controlled Charge	Charge Step	Coulostatic Methods		
Impedance Techniques	ac Voltammetry (ac Polarography)			
	Electrochemical Impedance Spectroscopy			

Figure 37: General classification of electrochemical dynamic methods[59].

2.3.1 Cyclic Voltammetry

Cyclic Voltammetry (CV) is a fundamental technique for the investigation of electrochemical cells; it has proven useful in obtaining information about complicated electrode reactions, as well as on the overall system variables[61]. It is based on a three-dimensional i-t-E surface in which a triangular linear potential ramp E(t) is involved in function of the current recorded and time. However, more information can be extracted from the only two-dimensional study i-E, in which the current respond is highlighted in function of the potential variation[61]. The triangular linear potential ramp can be repeated in different cycles, and it is described by experimental parameters as the potential scan rate υ [mV/s], starting potential, higher potential and lower potential [V]. The output of CV is a voltammogram, in which is shown the characteristic current response of the analysed system changing the potential.

To analyse and understand the shape of the voltammogram, all the electrochemical system has to be evaluated. In the paragraph 1.5, the electrocatalytic systems have been described.

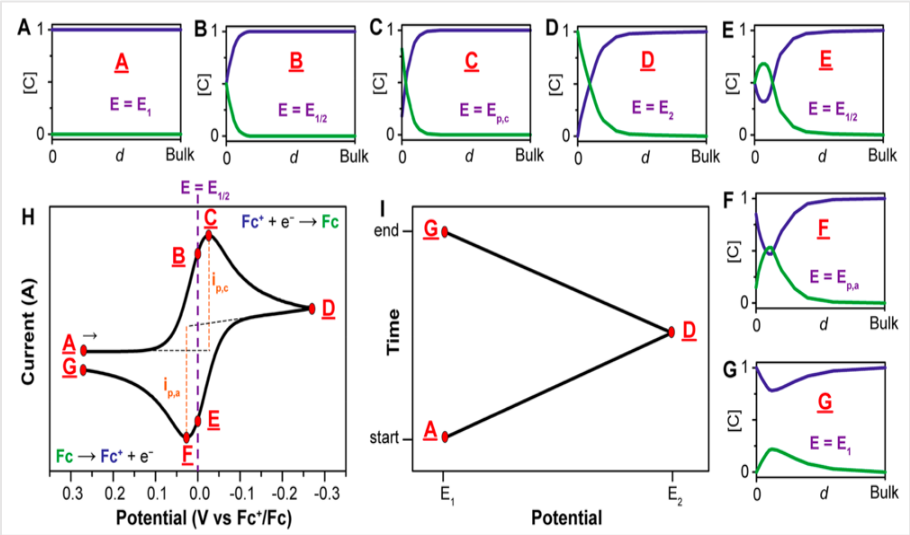

Figure 38: the graphs from A to G represent the concentration profile of Fc^+ and Fc in function of the distance from the electrode and in the different points of the voltammogram (H). The graph I shows the applied potential in function of time[65].

In general, the voltammogram is related with a heterogeneous redox reaction at the electrode-electrolyte interphase. The equilibrium between the oxidised and the reduced species is related with the Nernst equation (Eq. (15)). To understand, the classical example of the redox reversible couple ferrocenium (Fc^+) and ferrocene (Fc) has been shown. From the Figure 38, the concentrations profile of the two species changes in function of the potential applied and the time[65]. In this case, since the US convection is used, the *C* point defined the reduction peak of the redox couple and the point *F* the relative oxidation peak. The characteristic formal potential of the two compounds involved in the redox reactions, is defined by the point *B* and *E*, it can be written as:

$$E^{0'} = \frac{1}{2}\left(E_{p,a}+E_{p,c}\right) \qquad (24)$$

In which $E_{p,a}$ and $E_{p,c}$ represent the potential of the cathodic peak and the potential of the anodic peak, respectively. In this point, the concentrations of Fc^+ and Fc at the electrode surface (distance 0) are equal and the ratio of them (part of the Nernst equation) is equal to 1.

The determination of the formal potential is only one of the different evaluations that can be determined by the CV.

2.3.1.1 Analysis on the voltammogram

From the analysis on the Fc^+/Fc system, it has been analysed the formal potential of the redox species, but from a CV is possible to extrapolate other few different information.

The reversibility of a reaction can be explained using the CV; indeed, the electrochemical processes can be distinguished in electrochemical reversible, quasi-reversible and irreversible. The reversibility is analysed basically only on one electron transfer reaction ($O + e^- \rightarrow R$), since in complicated process is not feasible derive the equations of the current-potential relationship[61]. The reversible system (like

the Fc^+/Fc) follows the Nernst equation at the electrode surface and the electrochemical equilibrium is established at any time at the electrode surface.

The irreversible system instead, is characterised by a missing reduction or oxidation peak, that can be due to sluggish kinetics, or reactions (also homogeneous) that produced non-electroactive compound. This comprehends all those reactions that evolve products in a different phase such as gases, precipitates, dimers, or complexes.

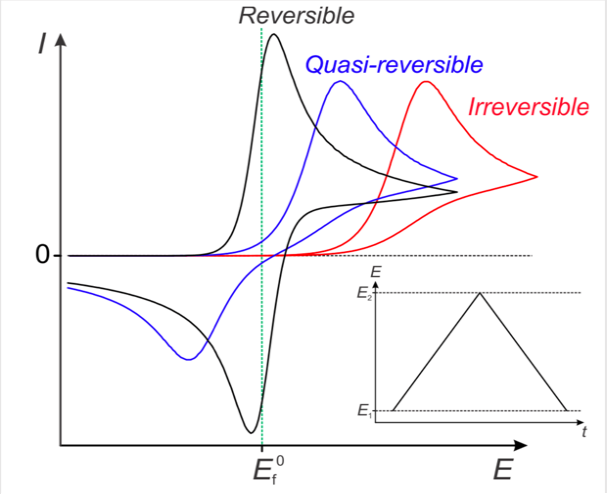

Figure 39: graphical comparison of cyclic voltammograms from reversible (black), quasi-reversible (blue) and non-reversible (red) systems[68].

The quasi-reversible system is established when the concentration ratio at the electrode surface do not follow the Nernst equation, but the cyclic voltammogram appears like that one of the reversible systems performed at slow scan rate. At larger scan rate instead, the voltammogram approaches more the appearance of a non-reversible system, therefore the oxidation and reduction peaks separate more from each other. The easiest way to have an idea on the reversibility, is performing a CV analysis at different scan rates and analyse graphically the results. Figure 39 represents the analysis of the reversible, quasi-reversible and non-reversible systems[68].

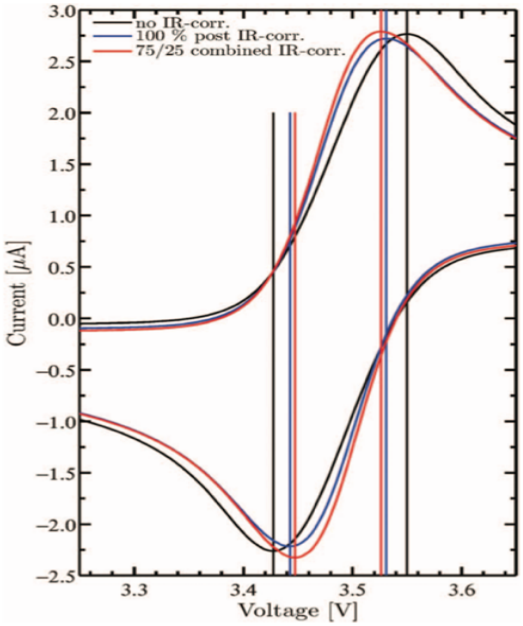

Figure 40: IR-compensation effect on the cyclic voltammogram. Before (black) and after (blue and red) IR-compensation[69].

The ohmic drop is an essential factor to analyse in a three-electrode electrolytic system, in fact, as stated by the equation (10) , the real electrode potential is influenced by the uncompensated resistance (R_u) of the solution. The CV can help with the R_u recognition, even though there would be more precise technique such as the EIS. To do that, the peak-to-peak separation (ΔE_p) must be introduced:

$$\Delta E_p = E_{p,a} - E_{p,c} \qquad (25)$$

In reversible systems, the peak-to-peak separation estimate the magnitude of the IR-drop and more the peaks are separated (bigger ΔE_p), higher will be the contribution of IR. The uncompensated resistance can be also analysed by the slope of a portion of the cyclic voltammogram where no faradaic contributions are present. Therefore, the steeper the slope, the higher the resistances will be. The IR-correction (or compensation) can be done directly on the software before performing the

analysis or after with a data processing method. In this study, the R_u have been analysed post-reaction. The overview on the calculations is highlighted in the paragraph 2.3.1.1. Figure 40 shows the cyclic voltammogram of a reversible system Fc^+/Fc before the software IR-compensation (in black) and after (blue and red). It is visible the shift of the peak-to-peak separation, which decreases after the IR-correction[69].

Another factor that can be analysed from a CV is the capacitance. It is the non-faradaic current contribution of the system, related to the accumulation of charges at the electrode-electrolyte interface over a certain time. The capacitive contribution is expressed as:

$$\left|I_{capacitive}\right| = \frac{dQ}{dt} = C_d \cdot \frac{dE}{dt} = A \cdot C_d^0 \cdot \upsilon \tag{26}$$

In which C_d is the differential capacitance of the double layer (μF), $C_d°$ is the differential capacitance of the double layer per area (μF cm^{-1}) and υ is the potential scan rate (mV s^{-1}). Therefore, the capacitance is the area between the two segments (negative and positive swaps) when no faradaic contributions are present. To calculate it the integral has to be done and after, having the $I_{capacitive}$ the formula has to be applied.

From the CV is also possible to analyse the concentration of the anolyte in the bulk. The Randles and Sevcik equation states that the peak current is proportional to the concentration of the redox species in the solution and to the square root of the scan rate:

$$I_p = 0{,}4463 \cdot nFAc(\infty)\sqrt{\frac{nFD}{RT} \cdot \sqrt{\upsilon}} \tag{27}$$

In which n is the number of electrons involved, F the Faraday constant, D is the diffusion coefficient (cm^2 s^{-1}), $c(\infty)$ the concentration of the redox species in the bulk, A the electrode area (cm^2) and υ the scan rate (mV s^{-1}). The Figure 41 shows the dependence of the CV from the scan rate, maintaining the concentration constant (in this case 2 mM FcMeOH) and leaving 100 mV s^{-1} as scan rate[70]. With smaller scan rate the peaks result less pronounced; the same behaviour is followed increasing the concentration from 0,25 to 2 mM keeping the scan rate constant. Therefore, with higher concentration of a redox species in the solution bulk, the concentration gradient $\partial c/\partial x$ is steeper, and the recorded

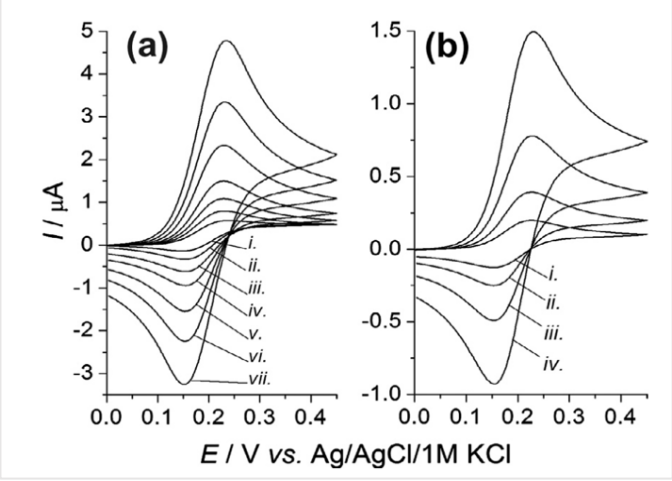

Figure 41: dependency of the CV from the scan rate (a) with 2 mM of FcMeOH and concentration (b) at 100 mV s^{-1}. In a, various υ has been used: 10 (i), 25 (ii), 50 (iii), 100 (iv), 250 (v), 500 (vi) and 1000 (vii) mV s^{-1}. Instead in b 0,25 (i), 0,5 (ii), 1 (iii) and 2 (iv) mM of FeMeOH[70].

current will be higher. Instead, with faster scan rate, the concentration gradient is steeper since the diffusion layer growth is slower than the change of concentration ratio at the electrode surface[70].

Cyclic voltammetry is also useful to perform some initial kinetic studies. The Nicholson method for quasi-reversible and reversible system can be applied. It is based on a dimensionless kinetic parameter Ψ that can be found in literature in relationship with the characteristic peek-to-peek separation value (ΔE_p). The equation associated to the method is[61]:

$$\Psi = \frac{(D_{Ox}/D_{Red})^{\alpha/2} k^0}{\sqrt{\pi D_{Ox}\, nF/RT}} \frac{1}{\sqrt{v}} \tag{28}$$

In this equation the ratio between the two diffusion coefficients can be assumed equal to 1, then the α value is useless and can be neglected. Hence, the standard rate constant k^0 can be derived.

Finally, an important information that can be derived from the CV is the potential window of the solvent used in the electrolyte. The aqueous systems are limited by the HER and the OER, instead the full organic system can be limited by the oxidation or reduction of the solvent itself (see Table 7). For example, acetonitrile is well used in electrochemistry due to the very wide potential window.

The CV is, therefore, a very important and essential analysis for the electrochemical system and, reassuming, the voltammogram shape is related from different factors like: (1) scan rate, (2) mass transport phenomena, (3) IR-drop and conductivity of the electrolyte, (4) solvent and potential window, (5) Anolyte concentration and type, (6) capacitance of the electrode-electrolyte interphase, (7) type of electrocatalyst.

2.3.2 Chronoamperometry

The chronoamperometry or constant potential bulk electrolysis is an essential electrochemical technique associated to the reaction parameters and dynamics. Indeed, it is a potential step method in which the characteristic current response of the electrochemical system at a certain potential is plotted

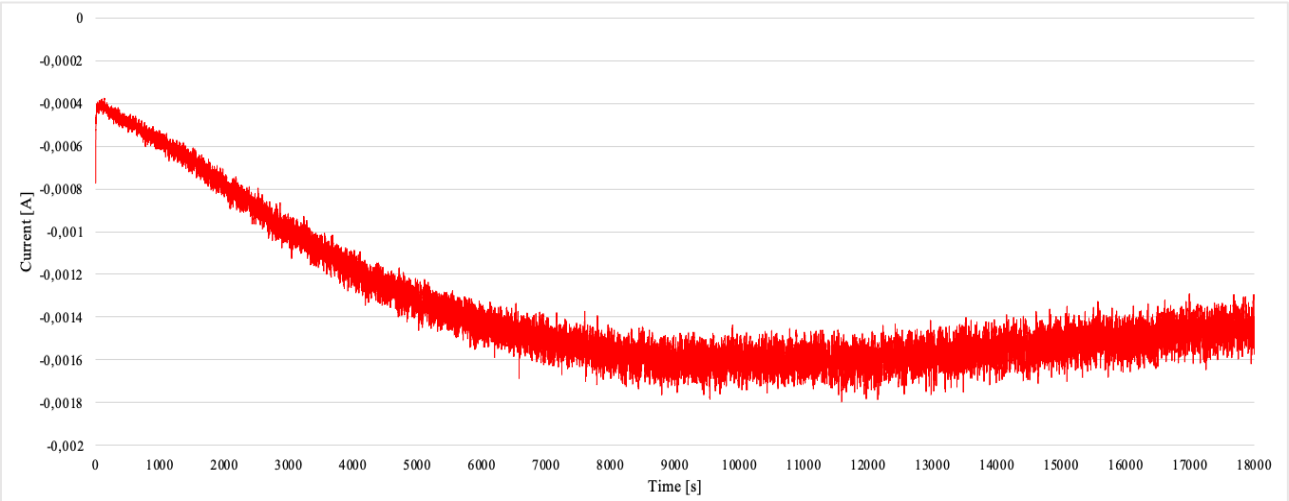

Figure 42: example of a typical chronoamperogram detected for the test *5h*.

versus time (Figure 42). It is also associated to chronocoulometry which is the integration of the current of the CA versus time (see Figure 43). This variant is useful to analyse the accumulated charge of the system due to the target reaction or other redox side processes. The CA is usually coupled with CV, and it can be carried out for seconds, hours or even days. The exiting graph is called chronoamperogram and it gives important information on the diffusion coefficient, the reaction mechanism and kinetic of reaction.

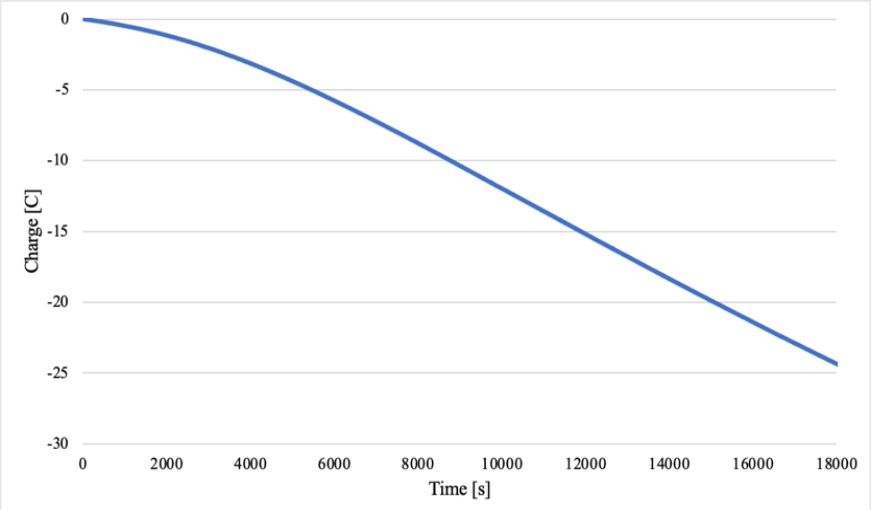

Figure 43: Integration of the current curve of the test *5i*.

While analysing this technique, it is usually assumed that the system depends on the diffusion phenomena only, eliminating migration and convection. Furthermore, a fast kinetic is usually assumed, even though it is not always the case. Considering these assumptions and analysing a reduction reaction, the chronoamperometry analysis is usually performed at the formal potential detected with CV tests or a more negative (in case of reduction) potentials. Therefore, at time 0, the only active species presents on the surface of the electrode is the oxidised one and the concentration at the surface of the electrode is equal to that one in the bulk. With time, the concentration decays with distance from the electrode and, as said before, the arrival of new active species is limited by only diffusion. Hence, the faradaic current near the electrode surface uses to decrease over time as the mass transport limit is reached and due to the increasing of the concentration gradient ($\partial C_{red}/\partial x$). The curve is an exponential decay that can be described by the Cottrell equation[61]:

$$I(t) = \frac{nFA\sqrt{D_o}\cdot C_{red}(\infty)}{\sqrt{\pi}} \cdot \frac{1}{\sqrt{t}} \qquad (29)$$

In which I is the current (A), n the number of electrons required for the redox reaction, A the planar electrode area, D_0 the diffusion coefficient of the active species ($cm^2\ s^{-1}$), $C_{red}(\infty)$ the active species concentration in the bulk solution and t is the time. The yellow part of the equation represents the slope of the line that fits the trend of the current response in the chronoamperogram (see Figure 44)[61]. During the CA experiments, the diffusion layer increases in direction of the solution bulk in relationship with the diffusion coefficient. The D_0 is indeed an important parameter that is characteristic for the specific electrochemical process that is happening at the electro-electrolyte

interphase. With the linearisation of the equation, the diffusion coefficient can be calculated, and from this parameter the thickness of the diffusion layer is calculated as follow:

$$\delta = \sqrt{\tau \cdot 2D_o} \tag{30}$$

In which δ is the thickness of the diffusion boundary layer and τ the characteristic time used to establish the diffusion layer. To limit the diffusion layer, the solution has to be stirred with a magnet. In more complex cases, a rotating disk electrode can be used or even a flow cell.

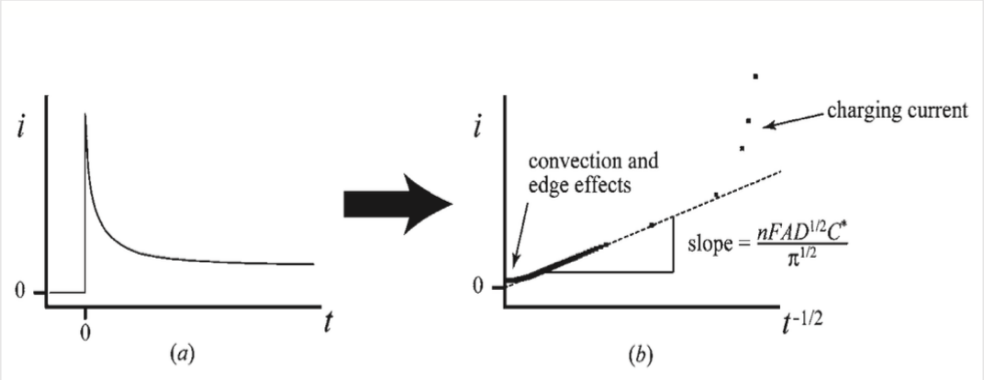

Figure 44: linearisation of the characteristic chronoamperometric curve using the Cottrell equation[61].

In the electrolytic cells, the current is related with the concentration of the active species in the solution and, therefore, the accumulated charges derive from the redox reactions at the surface of the electrode. The coulombs accumulated are the symbol of the overall electrochemical activity of the system during the experiments, at that certain potential. Applying the Faraday's law in a certain time in the CA experiment, the amount of reagents converted electrochemically can be assumed:

$$Q = n \cdot F \cdot N \tag{31}$$

In which Q are the charges accumulated during the CA test (C), n the number of electrons involved in the single redox reaction and N is the number of moles of the active species in the solution.
In this study the CA have been integrated to calculate the accumulated charges.

2.3.3 Differential Pulse Voltammetry

The DPV instead has been exploited when the peak of the PA was not or partially visible. Indeed, it helps to recognise the activity at a certain potential in situation in which it is not very clear. This technique is used to focus only on the faradaic processes, since it is able to preclude the capacitive contribution, focusing only on redox reactions. Indeed, when the peak is upwards, oxidation reactions are occurring, instead, downwards peaks are related with reductive reactions.

2.4 Solid-liquid sample characterisation

For the solid-liquid sample characterisation, four main techniques have been used:

1. Differential Scanning Calorimetry (DSC)

2. Thermal Gravimetric Analysis (TGA)
3. FTIR-Spectroscopy (IR-spectroscopy)
4. Gas Chromatography coupled with Mass Spectroscopy (GC-MS)

Below, each technique will be considered analysing some basic theoretical aspects and the methods used to implement them in this study.

2.4.1 Differential Scanning Calorimetry (DSC)

The Differential Scanning Calorimetry (DSC) is a technique for the analysis of the heat energy uptake of sample within a regulated increase or decrease of the temperature. The device is able to determine the heat flow related to the material transitions as a function of time and temperature[71]. Therefore, the output signal is a heat flow rate (mW) and with endothermic transitions (melting, evaporations) a positive peak will be detected, instead, with exothermic transitions (crystallisation), the peak will be negative. Here it is worth to note that the direction of the peaks refers to the specific configuration of the DSC unit used in the present work. There are different types of DSC in relationship with the specific application, but in this study the instrument used is a power-compensated Double Furnace DSC 8000 by PerkinElmer, equipped with an autosampler. In this type of DSC, the sample and the reference are placed in two different thermal chambers (furnaces) and they rely on different separated heaters and temperature sensors[72]. Indeed, in order perform the analysis, a reference is always needed. The difference in temperature of the two furnaces is maintained at the minimum thanks to a control lop that adapts the heating powers (P). Hence, the temperature difference ΔT_{SR} will be calculated as follow:

$$\Delta T_{SR} = T_S - T_R \ [°C] \tag{32}$$

In which T_S and T_R are the temperature of the sample and the reference respectively (see Figure 45)[72].

In DSC experiments energy is provided simultaneously in the sample and reference furnaces and the temperature is raised equally over time. The difference of the energy input required to maintain the temperature of the sample and the reference the same, will be the amount of excess heat absorbed (endothermic process) or released (exothermic process) by the sample[71].

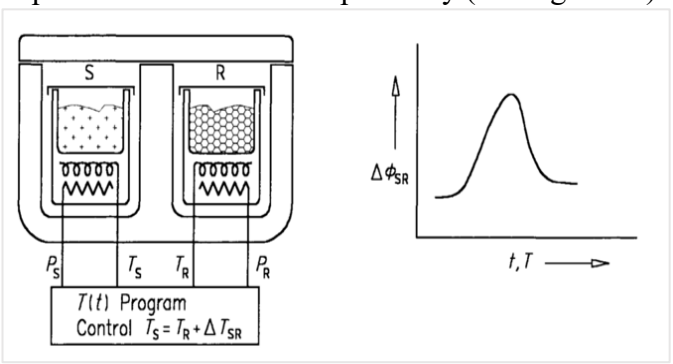

Figure 45: power-compensated DSC scheme[72].

The specific heat capacity (C_P), that is the heat required to raise of 1 °C the temperature of 1 kg of a material at constant pressure, is defined as:

$$C_P = \left(\frac{\Delta H}{\Delta T}\right)_p \quad [J\ K^{-1}\ kg^{-1}] \tag{33}$$

Therefore, the enthalpy of transition (ΔH_{trans}) will be the integration of C_p, and would be the area of the resulting peak (see Figure 46)[71]. The eq. (34) shows the integration of eq. (33), the enthalpy of transition.

$$\Delta H_{tran} = \int \frac{T}{T_0} C_p(T)\ dT + H(T_0) \tag{34}$$

Thus, the DSC can be used in different fields and with different purposes. Some examples are in protein biology for the denaturation temperatures, polymer science for melting points or glass transition T and for purity analysis and evaluation of fractions. In the case of study, the DSC has been used for purity and fraction analysis, in order to be compared with the data from TGA.

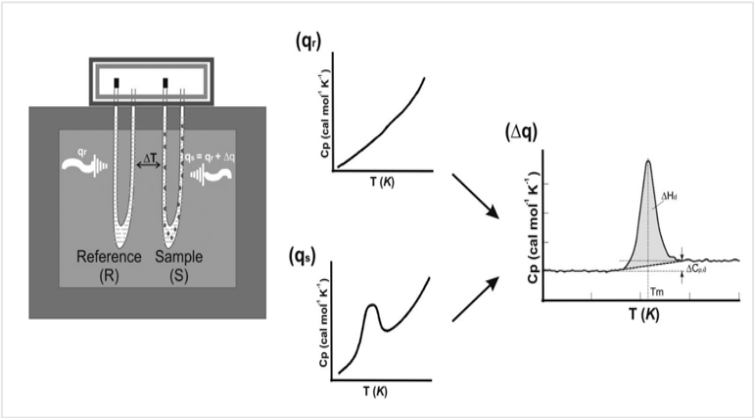

Figure 46: scheme of a DSC's set-up with visual explanation of the differential heat signal (Δq) on temperature[71].

In this study, the sample analysed from DSC was the solid phase, derived from the drying and the acidification with HCl 2 M of the mother solution. The acidification is an essential step, since it allows the movement of the equilibrium toward the PA instead NaPal. Indeed, the NaPal has a complex thermal behaviour with few isolated peaks and sometimes overlapped with the PA one (see Figure 71). The sample preparation and the analysis have been reported in the Annex 9.

2.4.2 Thermal Gravimetric Calorimetry (TGA)

The Thermal Gravimetric Calorimetry (TGA) is, like DSC, a technique in which the change in the sample mass is detected in function of an increasing temperature[72]. The instrument is based on a precision balance located in a furnace that is programmed for a linear increasing of the temperature. The resulted plot (thermography) is, therefore, the mass change (%) in relationship with the temperature or time. A purge gas controls the sample environment and it can be N_2, O_2, air or other gases. TGA can provide information on physical phenomena such as sublimation and evaporation, chemical phenomena related to solid-gas reactions, oxidative degradation or decomposition and on all those phenomena that occur with a change of mass[73]. Therefore, it can quantify loss of water, solvent, decarboxylation, pyrolysis, amount of metallic residues or carbonaceous residues.

Practically, in a thermography, when no mass is loosing, there will be a straight line paralel to the x axes. When there is mass loss associated to a certain phenomena, the slope of the line changes and there will be a descending trends until the mass is consumed. The residual mass is the unlost % of mass at the end of the analysis. TGA could be ideally coupled with IR, MS or GC-MS in order to understand and specified the reason of the weight loss. The TGA used for this study is a TG 209 f1 Libra by Netzsch, with autosampler, a vacuum-tight thermo-microbalance and a ceramic furnace.
In order to perform the analysis, an alumina crucible has been used. The Al_2O_3 has a melting point of 2072 °C and behaves like a total inert material even at the maximum temperature achievable by the instrument (1100 °C). The sample derived from the dried mother solution and usually without any acidification step (it is not required). The procedure is shown in the Annex 10.

2.4.3 FTIR Spectroscopy

The Fourier Transformation Infra-Red spectroscopy (here referred to IR spectroscopy) is the most used spectroscopic method analysis that studies the interaction of infrared radiation with the materials, exploiting the radiation absorbed, reflected, or emitted. The mid-infrared (IR or MIR) spectrum goes from 4000 cm^{-1} (λ = 2.5 μm) to 400 cm^{-1} (λ = 25 μm) and it surrounded by the near IR region (12500 cm^{-1} to 4000 cm^{-1}) and the far-IR region (400 cm^{-1} to 10 cm^{-1})[74]. In this study only the MIR will be analysed, and the instrument used is a Nicolet iS5 FTIR-spectrometer equipped with iD5 ATR accessory by Thermo-Fischer Scientific.
The reason why this technique has become very popular is related with the high versatility. Indeed, the IR method is fast, sensitive, and can be applied on gaseous, liquid and solid samples. The classical format of IR spectrum is transmittance % (or absorbance) versus the wavenumber (cm^{-1}). The wavenumber is defined as:

$$k = \frac{1}{\lambda} \ [cm^{-1}] \text{ and } E = h \cdot c \cdot k \qquad (35)$$

In which λ is the wavelength, E is the energy of an electromagnetic wave, h is the Planck constant and c the light velocity in vacuum.
The IR spectrum is like a footprint of a compound, and it derives from vibrations of bound atoms. Whenever these bound atoms vibrate, they are able to absorb IR energy[74]. Absorption bands can derive from two main origins: (1) fundamental vibrations of functional groups (C=O, C=C, C≡N, -CH_2 and -CH_3) and (2) fundamental vibrations of skeletal groups (C-C-C). Depending on the direction of the vibrational movement there can be: (a) stretching vibrations that involve bond length changes or (b) deformations vibrations which involve the bond-angle changes of the group. Usually, the stretching vibrations occur at higher frequencies (bigger wavenumber) than the deformations ones

because they need more energy. Both of them can be also be regarded as arising from symmetric or asymmetric vibrations[75]. Figure 47 shows the vibrations that could potentially happen on a methylene group CH_2.

Other absorption bands type are the overtones and combination bands. The overtones are detected at more or less twice the frequency of the strong fundamental absorption, instead the combination bands derive from the combination of two fundamental vibrations (addition or subtraction)[75].

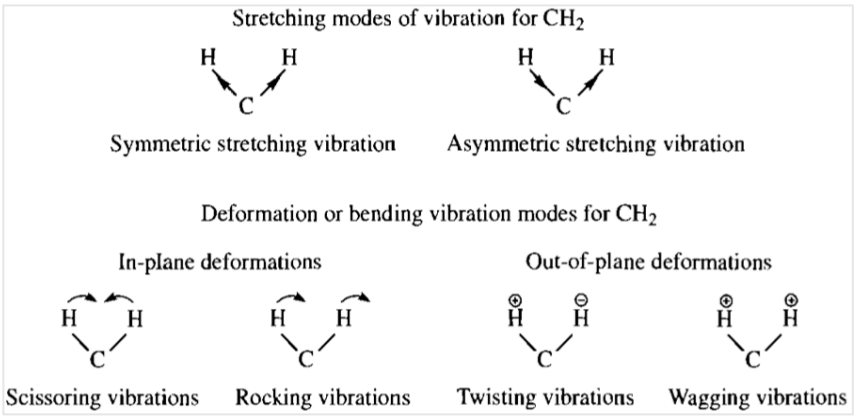

Figure 47: type of vibrations on the methylene group CH_2[75].

In organic compounds, characteristic vibrations of the functional groups occur usually between 4000 and 1500 cm^{-1}, while heavier atoms contained in the inorganic compound can be detected even at lower frequencies[74]. The intensities of the bands in pure compounds and mixtures are proportional to the concentration and, therefore, the number of functional groups present in the sample.

Generally, the absorption band are affected by the magnitude of the dipole change during vibration. It means that larger change, stronger absorption band. Nevertheless, any vibration is influenced by many factors that can be related with the molecule transformation or changing after a reaction[75]. For example, the C=O group stretching vibration is lower in CH_3COCH_3 than in CH_3COCl, this is due to the mass difference between CH_3 and Cl. The phase (condensed phase, solution or gas) and the grade of hydrogenation can influence the vibration frequency. Indeed, high hydrogenated compounds result with more vibrational coupling phenomena.

FTIR spectroscopy is based on the Fourier Transformation that is a mathematical procedure to pass from crude data to the spectra. In this study, the IR spectroscopy has been an essential technique for the confirmation of the electrochemical activity on the mother solution. Indeed, it helped to perform a qualitative analysis on the grade of hydrogenation of the sample, studying the ratio between the -CH_3 and the -CH_2 peaks. The sampling has been done from the solid fraction of the sample, that has been submitted to drying process. Initially the sample were not acidified, but after, in order to have cleaner spectra the acidification become essential. The protocol followed is highlighted in Annex 11.

2.4.4 Gas Chromatography – Mass Spectroscopy

The GC-MS is a fundamental characterisation technique for the recognition of compounds in unknown sample. In this study, the technique has not been directly used, therefore, only a brief introduction will be done.

In the GC, the mixture to be analysed is introduced in inert gas stream which carry the sample in a column (or tube) packed with solid supports and coated with the specific liquid phase[76]. The interactions (mainly absorptive) between the gas stream and the coating generates a differential separation of the components of the mixture, which are swept in a progressive order through a specific detector. Very often, volatile compounds may have the same retention time on the specific column, resulting in overlapped or non-visible peaks. Therefore, it is usually coupled to MS, which results a very power instrument for the analysis of single compound. The MS takes the injected materials, and it ionizes them in a vacuum. The fragmentation products are, then, focused on a magnetic mass analyser, collected, and analysed by an ion detector (see Figure 48)[76].

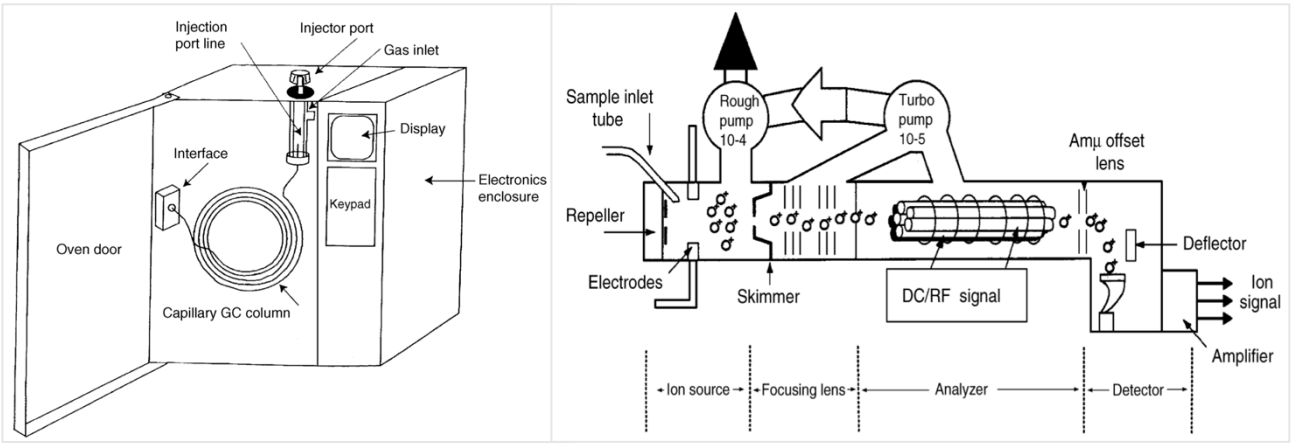

Figure 48: GC and MS simplified scheme and main components[76].

The GC chromatograms are displayed in relationship with the retention time, nevertheless the GC/MS analyses are in three-dimensions [77]. At the dimensions of the retention time (s) on the x-axis and the intensity (% related to the total ion current or voltage) on the y-axis, the mass/charge on the z-axes (m/z) is implemented[77].

For the GC aspect, there are different parameters related to the separation and the resolution. They are based on the plates-theory, which is used to fractionate the column in theoretical plate in order to analyse the efficiency. The main ones are shown below[76].

$$K_A = \frac{t_A - t_0}{t_0} \tag{36}$$

In which K_a is the characteristic retention factor of the compound, t_a the on-set time of the peak and t_0 the retention time linked to a non-retained solvent, from which the other retention times are calculated.

$$\alpha = \frac{t_B - t_0}{t_A - t_0} = \frac{K_B}{K_A} \tag{37}$$

The parameter α is called separation factor and it is established between two different and consecutive peaks.

$$n = 5{,}4 \cdot \left(\frac{t_B}{W_{1/2}}\right)^2 \text{ with } h = \frac{L}{n} \tag{38}$$

In which the *n* is the efficiency factor, $W_{1/2}$ the half of the peak's width, *h* the height of the theoretical plate (Also H or HETP) and *L* the is the length of the column (cm or mm). The efficiency factor analyses how sharp the peaks are and the overlap that is occurring between adjacent peaks, it defines the number of theoretical plates[76].

The GC, therefore, depends on different variables such as (1) stationary phase chemistry, (2) stationary phase thickness, (3) column internal diameter, (4) column length, (5) carrier gas chemistry, (6) carrier gas pressure, (7) injection temperature and (8) column temperature.

The MS, instead, is equipped in series with the GC apparatus. It is composed by six components[76]:

1. **Pumping system:** it provides high vacuums for the analyses.
2. **Interface to the gas chromatograph:** it links the capillary column with the ionization chamber, and it guarantees the separation of the GC phases thank to a series of pumping system designed ad-hoc.
3. **Ionization chamber with electron source:** in this part, the sample is bombarded with ions thanks to an ion source under a specific voltage. They can derive from different sources, and they are able to fragmentate the molecules ionizing them.
4. **Focusing lens:** they focus the single fragments into the analyser.
5. **Quadrupole analyser:** it is the most used and is formed by four cylindrical quartz rods clamped in pair by ceramic collars. A DC/RF (Direct current/radio frequency) electromagnetic field is generated around the rods charging them in opposite charges. Based on the field strength and frequency the single masses can follow a stable path onto the ion detector, otherwise they end up colliding with the walls of the quadrupole rods without being detected.
6. **Detector:** it is an ion detector, and it relies on the so called amu-offset, which is a lens that deflect the ions in a straight path, while separating them from the gamma radiations derived from the ionization phenomena. This step is needed because the gamma radiation uses to interfere with the ion detector creating noises and backgrounds that may decrease the quality of the final data.
7. **Data/control system:** it monitors the trend of the analysis and the different parameters.

2.4.4.1 Case of study and sampling procedure

In this study, has said before, the technique was not directly usable by the team. The liquid sample have been delivered to the central quarter of the Biological and Chemical Engineering Department located in Hangøvej, Aarhus C, 8000.

For the GC-MS, the method is not already fully implemented. The tests using standard methods failed to detect the PA in the solution, therefore future research must be done in order to have a reliable GC-MS analysis. For the qualitative analysis with the biocrude, instead, the classical method followed for the results shown in Figure 12, has been used without any issue. Nevertheless, some samples on the PA have been analysed, and only one showed some results. Below, the sampling is explained.

The sampling procedure has been done on two different samples: (1) the solid sample and (2) the filtered liquid sample. In the first case the solids are diluted in pure methanol for the GC-MS and a volume of 1,5 ml is filtered with a 0,45 μm filter directly in the vial. For the filtered liquid sample, since the actual GC-MS method does not run-in presence of water or ethanol, the liquid sample is dried overnight and the solid has followed the same procedure of the solid samples.

2.5 Gas sample characterisation

2.5.1 Micro-Gas Chromatography

For the in-situ headspace analysis of the electrochemical cell, a Micro-GC has been utilized. The theoretical aspects are quite similar to those ones of the classical GC, but in this case at micro-scale. The Micro-GC is useful as in-situ analysis to monitor the gaseous stream over time; indeed, the good portability and the good sensitivity make this technique essential for gaseous phase processes and reactions, as well as for the analysis of molecules that at room temperature are in gas phase.

2.5.1.1 Case of study and sampling procedure

In this specific study, the Micro-GC is a model 490 Micro GC by Agilent Technologies integrated with an appropriate software where the chromatograms are shown. It was used for analysis on closed system, but for this study, the sample was directly injected from an injection port.

In this specific set-up, the gaseous sample (20-50 μL) is injected at 1,5/1,8 bar and split in two different compartments. The 50% of the sample passes through an MS5 type packed column by Agilent, in which the so-called permanent gases such as O_2, N_2, CO, CH_4, H_2 and H_2O vapour can be detected and separated efficiently. The other 50% of the sample is injected in a PPU type packed column by Agilent that is able to the detect the polar fractions like CO_2, “air” (no differentiation

between O_2 and N_2) and volatile hydrocarbon from C2 to C5. Each column relies on separate thermal conductivity detector; therefore, two different chromatograms are produced.

For the sampling procedure, a suitable plastic syringe for gases has been used. First, it has been cleaned with nitrogen in order to remove the air in the internal space, usually for 3-4 times. The sample has been done thank to a needle put on the cathodic chamber of the electrochemical cell and consists in a volume from 30 to 60 ml of headspace. After the sampling, the gas phase is injected directly in the Micro-GC achieving a pressure from 1,5 to 1,8 bar. The analysis is qualitative, aimed to detect the presence of some specific gases or volatile compounds.

3. Results and discussion

In this chapter the results of the analysis on the ECH of palmitic acid will be shown. Each study and result from the different techniques used will be contextualised and discussed in order to create a general logic and make the comprehension easier. In the logic followed, three main steps can be distinguished:

1. **Analysis on the feasibility of the process**: the aim of this step is to accumulate proofs on the effective realisation of the process. Since no literature reference were present, these studies must be carried out. In order to do that, almost all the techniques have been utilised.
2. **Qualitative characterisation on the products**: in this phase the products are analysed. Since no protocol was present yet, the assessments can be considered qualitative and further studies on the systems will be done. This step relies on different techniques and on the chromatography analysis like GC-MS.
3. **Analysis on the possible reaction pathway**: this step is the last and most difficult step. The characterisation of the possible products is always followed by the various pathways analysis, coupled with the study of the efficiency parameters. In this case, due to the limited time and lack of data, the pathways will be only recognised and assumed. The quantitative analysis will be done as soon as a reliable and standardised protocol will be found.

Table 9 shows the most relevant tests performed in this study, focusing on the different set-ups (cell type, electrolyte, supporting electrolyte, anolyte, analyte, and pH before electrochemistry). This table have been extracted from the Annex 12, deleting the failed tests and the ones not discussed in the present work. The electrocatalyst (WE) is Ni foam for all the test unless the *12c* test that has been carried out with a Cu mesh and the *13a*/*13b* tests that have Pt coil as WE.

In order to create a logic scheme, the electrochemical studies will be considered first, analysing the most relevant and important results from the electrochemical investigations. Afterwards, all the techniques used for the sample's characterisation will be tackled, dividing them in based on the phase analysed. For the sake of brevity and clarity, in this section only the most important tests will be discussed. In any case, for all the performed tests all the techniques discussed above (CV, CA, TGA, DSC, IR) have been used.

Table 9: most relevant tests with relative set-up and aims (from the table of the test).

n°	Aim of the test	Validity	Cell type	Electrolyte solution (catholyte)	Supporting electrolyte	Anolyte	Analyte concetration [mM]	Apparent initial pH
5b	EtOH system testing, pH analysis post membrane cleaning	Valid	H cell, Nafion n117	30ml - 70% EtOH, 30% H2O	10mM NaOH	H2O - 10mM NaOH	Variable, additions with relative CV: 0, 3, 7, 10 mM PA	From 12,30 (EtOH), 10,98 (H2O) to 6,45 (EtOH) and 10,85 (H2O) with 10 mM PA
5c	EtOH system testing, pH analysis post membrane cleaning	Valid	H cell, Nafion n117	30ml - 70% EtOH, 30% H2O	10mM NaOH	H2O - 10mM NaOH	Variable, additions with relative CV: 0, 10 mM PA	From 11,98 EtOH to 6,30 with 10 mM PA
5d	EtOH system testing, pH analysis post membrane cleaning	Valid	H cell, Nafion n117	30ml - 70% EtOH, 30% H2O	10mM NaOH	H2O - 10mM NaOH	Variable, additions with relative CV: 0, 7, 10 mM PA	From 12,38 (EtOH) to 6,64 (10 mM)
5e	EtOH system testing, pH analysis post membrane cleaning	Valid	H cell, Nafion n117	30ml - 70% EtOH, 30% H2O	10mM NaOH	H2O - 10mM NaOH	Variable, additions with relative CV: 0, 7, 10, 13, 16, 19 mM PA	From 12,50 (EtPH) to 6,25 (19 mM)
5f	EtOH system testing, pH analysis post membrane cleaning	Valid	H cell, Nafion n117	30ml - 70% EtOH, 30% H2O	10mM NaOH	H2O - 10mM NaOH	Variable, additions with relative CV: 0, 7, 10, 16, 22, 25 mM PA	From 12,60 (EtPH) to 6,23 (25 mM)
5g	Chemical blank, Understand if there some non-electrochemical reactionl	Valid	H cell, Nafion n117	30ml - 70% EtOH, 30% H2O	10mM NaOH	H2O - 10mM NaOH	25 PA	/
5h	EtOH system testing (5f)	Valid	H cell, Nafion n117	30ml - 70% EtOH, 30% H2O	10mM NaOH	H2O - 10mM NaOH	25 PA	6,7-7,06
5i	EtOH system testing (5f)	Valid	H cell, Nafion n117	30ml - 70% EtOH, 30% H2O	10mM NaOH	H2O - 10mM NaOH	25 PA	6,6-7
5j	Electrochemical blank of 5f, 5h, 5i with NaCl in more or less same ionic strenght and pH	Valid	H cell, Nafion n117	30ml - 70% EtOH, 30% H2O	25mM NaCl	H2O - 10mM NaOH	/	EtOH: 6,6-7; H2O: 6,3-6,7
5k	Electrochemical blank 2 of 5f, 5h, 5i with NaCl in more or less smae ionic strenght and pH, 40 min N2 purging	Valid	H cell, Nafion n117	30ml - 70% EtOH, 30% H2O	25mM NaCl	H2O - 10mM NaOH	/	/
5l	Electrochemical blank 2 of 5f, 5h, 5i with NaCl in more or less smae ionic strenght and pH, 36 min N2 purging	Valid	H cell, Nafion n117	30ml - 70% EtOH, 30% H2O	25mM NaCl	H2O - 10mM NaOH	/	/
5m	Chemical blank of 5f, 5h, 5i with NaOH, 25mN PA , 40 min N2 purging	Valid	H cell, Nafion n117	30ml - 70% EtOH, 30% H2O	10mM NaOH	H2O - 10mM NaOH	25 PA	/
5n	Chemical blank for CO analysis, no catalyst, but in T	Valid	H cell, Nafion n117	30ml - 70% EtOH, 30% H2O	10mM NaOH	H2O - 10mM NaOH	/	/
5o	Chemical blank for CO analysis, no catalyst, 25°C	Valid	H cell, Nafion n117	30ml - 70% EtOH, 30% H2O	10mM NaOH	H2O - 10mM NaOH	/	/
5p	Same condition as 5i	valid (low corrent passage)	H cell, Nafion n118	30ml - 70% EtOH, 30% H2O	10mM NaOH	H2O - 10mM NaOH	25 PA	/
5r	EtOH system testing (5f)	Valid	H cell, Nafion n117	30ml - 70% EtOH, 30% H2O	10mM NaOH	H2O - 10mM NaOH	25 PA	6,54
5s	EtOH system testing (5f)	Valid	H cell, Nafion n117	30ml - 70% EtOH, 30% H2O	10mM NaOH	H2O - 10mM NaOH	20 PA	6,05 (20mM)
7b	Repeat 7a but in M cell and with 5mM NaCl	Valid	M cell	40ml - 70% EtOH, 30% H2O	5mM NaCl	/	10 NaPal	8,043
7c	Chemical blank, Understand if there some non-electrochemical reactionl	Valid	M cell	40ml - 70% EtOH, 30% H2O	5mM NaCl	/	10 NaPal	/
7d	Reversibility test, from 7b	Valid	M cell	40ml - 70% EtOH, 30% H2O	5mM NaCl	/	10 NaPal	/
7e	Change the [NaPal] maintening the some ionic strenght, try to also analyse the pH	Valid	M cell	40ml - 70% EtOH, 30% H2O	10mM NaCl	/	5 NaPal	7,7±
7f	Change the [NaPal] maintening the some ionic strenght, try to also analyse the pH	Valid	M cell	40ml - 70% EtOH, 30% H2O	14mM NaCl	/	1 NaPal	7,6±
7g	Change the [NaPal] maintening the some ionic strenght, try to also analyse the pH	Valid	M cell	40ml - 70% EtOH, 30% H2O	5mM NaCl	/	20 NaPal	8,5± (??)
7h	Blank of 7b	Valid	M cell	40ml - 70% EtOH, 30% H2O	5mM NaCl	/	/	/
8a	Test or comparison with 7a, but using NaPal	Valid	H cell, Nafion n117	25ml - 70% EtOH, 30% H2O	10μl sol 0,1M KOH	10μl sol 0,1M KOH in H2O	10 NaPal	9,4
9a	Test at basic pH (9-10) for comparison with 5f.	Valid	H cell, Nafion n117	25ml - 70% EtOH, 30% H2O	10mM NaOH	H2O - 10mM NaOH	9 PA	8,5
10a	System in hydrogenation, comparison with 5f and related tests.	Valid	H cell, Nafion n117	25ml - 70% EtOH, 30% H2O	10mM NaOH	H2O - 10mM NaOH	20 PA	6,9
11a	System in hydrogenatio, comparison with 7a or 10a	Valid	M cell	40ml - 70% EtOH, 30% H2O	5mM NaCl	/	10 NaPal	8,5
12a	system in hydrogenation, and alkaline pH, comparison with 11a, 10a and 9a.	Valid (no perfect range of pH)	H cell, Nafion n117	30ml - 70% EtOH, 30% H2O	10mM NaOH	H2O - 10mM NaOH	8,5 PA	8,3 (difficult to achieve 9-10, unstable)
12b	system in hydrogenation, and alkaline pH, comparison with 11a, 10a and 9a.	Valid (problem with pH of the anolyte and catholyte)	H cell, Nafion n117	30ml - 70% EtOH, 30% H2O	10mM NaOH	H2O - 10mM NaOH	12 PA	8,9 (difficult to achieve 9-10, unstable)
12c	system in hydrogenation, and alkaline pH, comparison with 11a, 10a and 9a.	Valid (problem with pH of the anolyte and catholyte)	H cell, Nafion n117	30ml - 70% EtOH, 30% H2O	10mM NaOH	H2O - 10mM NaOH	10 PA	8,4 (difficult to achieve 9-10, unstable)
12d	system in hydrogenation, and alkaline pH, comparison with 11a, 10a and 9a.	Valid	H cell, Nafion n117	30ml - 70% EtOH, 30% H2O	10mM NaOH	H2O - 10mM NaOH	10 PA	9,04
13a	test for the study of the acid conditions	Valid	H cell, Nafion n117	30ml - 70% EtOH, 30% H2O	10mM NaOH	H2O - 10mM NaOH	25 PA	6,54
13b	test for the study of the acid conditions	Valid	H cell, Nafion n117	30ml - 70% EtOH, 30% H2O	0,1M NaCl	H2O - 0,1M NaCl	10 PA	EtOH: 4,22; H2O: 5,46

3.1 Electrochemical studies

In this study the CV has represented an essential technique for the recognition of the potential in which there was electrochemical activity toward the PA. Therefore, the results from CV must be analysed first.

The CVs have been performed with different parameters in terms of initial potential, final potential, scan rate and number of segments. The data have been processed and, from the characteristic voltammogram, the uncompensated resistance (R_u) and the capacitance have been extrapolated (see Table 10). For each test done, both the resistance and the capacitance have been evaluated on the same potential window. The interval has been taken around the OCP and with a potential window of 0,1 V and a total of 0,2 V (see Figure 49). This choice has been taken to standardise the method and have a more reliable comparison between the different analyses. The segment used for the resistance analysis was the second-to-last (usually the fifth or the seventh) and the slope has been calculated in the potential window. One divided by the angular coefficient is an estimation of the R_u of the solution analysed. The capacitance instead has been calculated by assessing the integral between the segment used for the resistance's analysis and the successive one, always in the limits of the same potential window. The capacitance has been calculated dividing the integral between curves (J s^{-1}) by the scan rate (V s^{-1}) and dividing as well by the factor 0,1*2 which represents the potential window around the OCP (V). These calculations are explained in the Annex 8, which represent an extract of the excel work file.

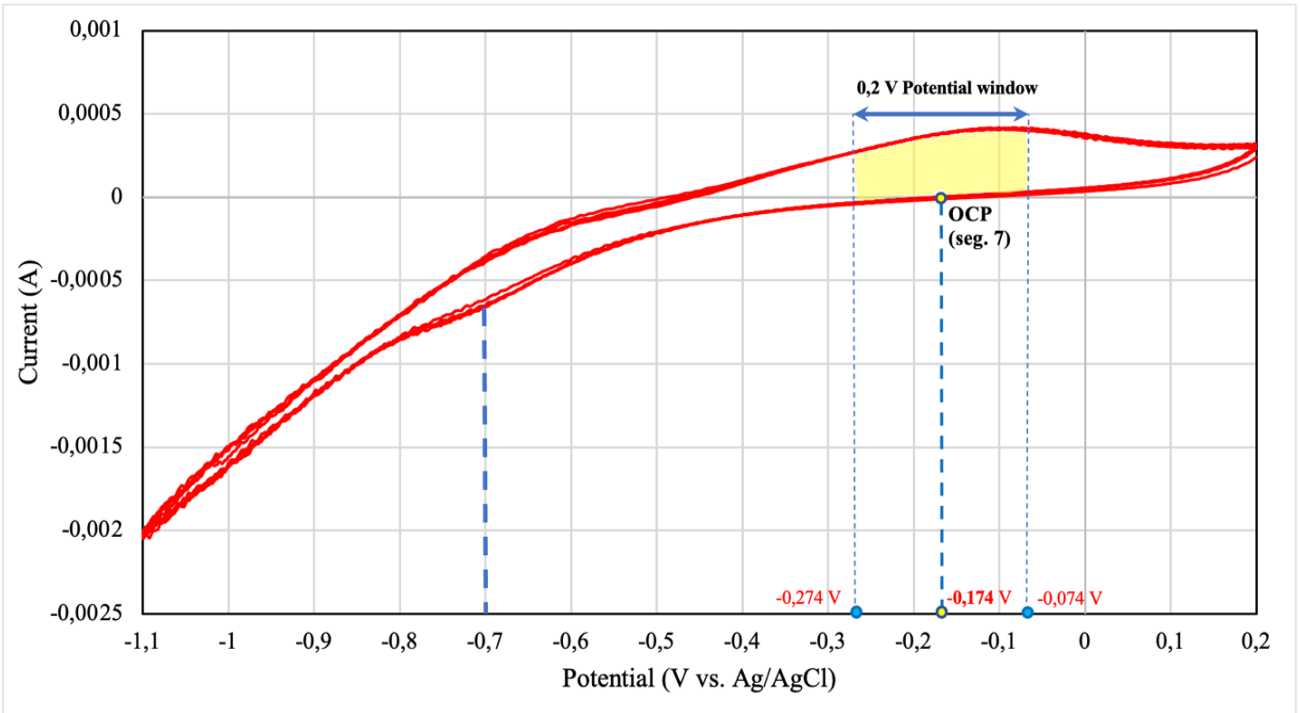

Figure 49: CV of the test *7b*. The dotted lines represent from the left, the on-set potential of the NaPal/PA electrochemical activity, the lower limit of the potential window, the OCP and the upper limit of the potential window.

Figure 49 represents the cyclic voltammogram of the test *7b*, performed in M cell with 10 mM of NaPal and 5 mM of NaCl as supporting electrolyte, achieving a pH equal to 8,04. In this plot is evident the peak at -0,7 V, which was the first signal related to the electrochemical activity of Palmitic acid. After the peak at -0,7 V the voltammetry shows an almost linear increase in the absolute value of the current with the voltage. This coupled to the fact that no capacitive behaviour is found in this window (reductive and oxidative scans are overlapping at current lower than -0,9 V) suggests the presence of the hydrogen evolution reaction. This behaviour has been found in several tests and it is important to say that the position of the peak at -0,7 V is related to pH of the electrolyte solution and therefore different tests changing the pH in the range of alkaline to neutral/acid have been performed. On the graph is also highlighted the potential window around the OCP in which the resistance and the capacitance have been evaluated.

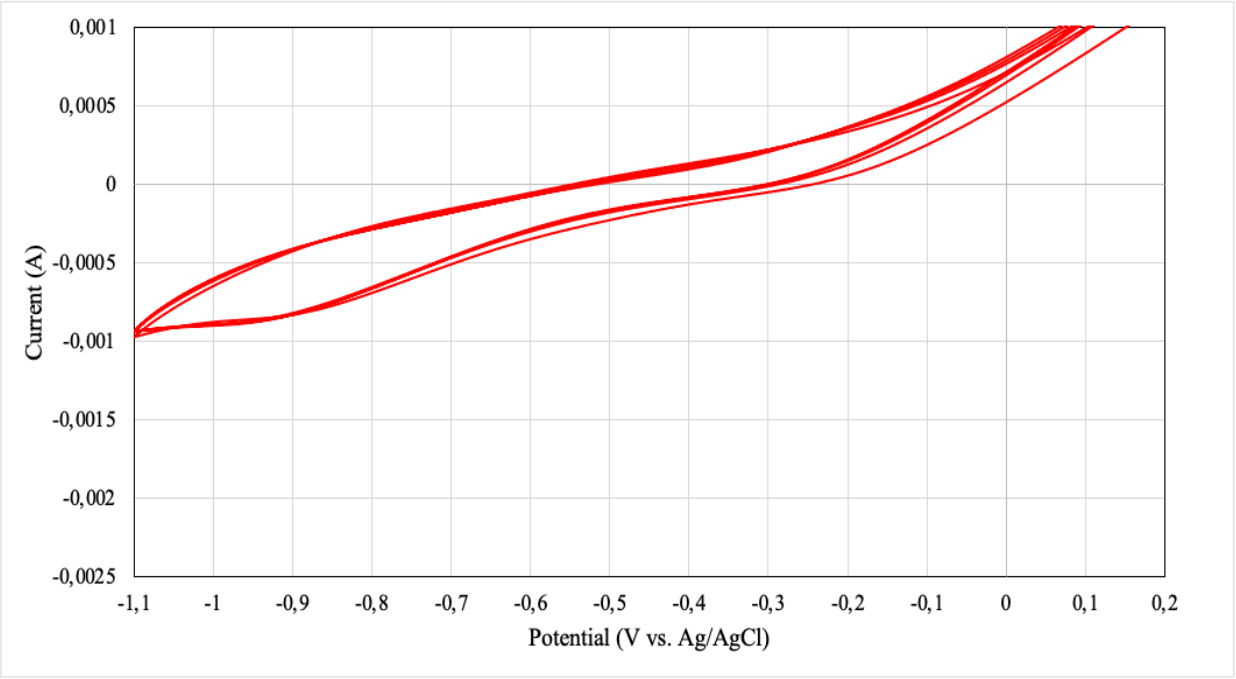

Figure 50: CV of the blank with no NaPal (*7h*).

In the same conditions, but without the NaPal, the *7h* has been carried out. The cyclic voltammogram of this electrochemical blank is shown in the Figure 50. As it is visible, in the potentials around -0,7 V, no activity has been detected, symbol that the peak at 0,7 V found in the experiments with PA or NaPal were possibly related the reactivity of these compounds. Also, the current drawn in the system is clearly higher (twice as high) in the presence of PA with respect to the blank, which is a direct confirmation of the electrochemistry happening in the presence of the acid.

Clearer evidence of the PA's reactivity can be seen by using Differential Pulse Voltammetry (DPV). It has been used to try to magnify the electrochemical trace. Figure 51 shows a differential pulse voltammogram of a test in which, at the target potential, it did not have a visible and determined peak. Nevertheless, an electrochemical activity at -0,7 V is clearly visible.

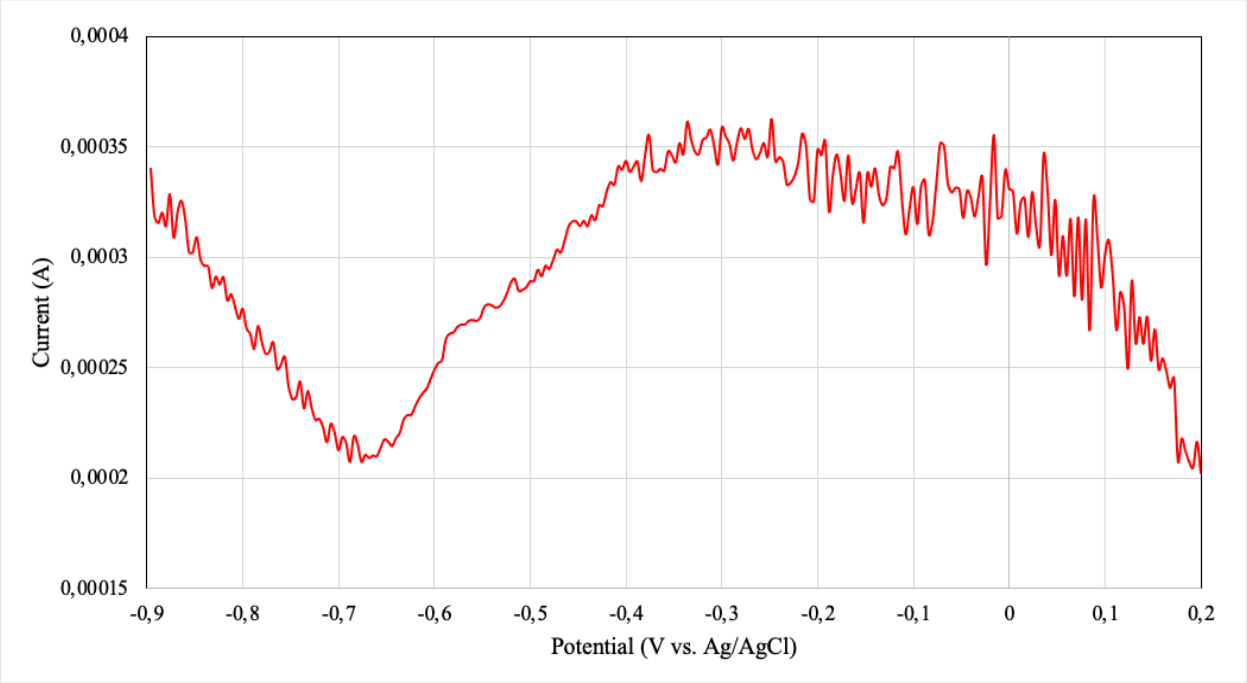

Figure 51: Example of a Differential Pulse Voltammogram.

An important aspect to analyse is the reversibility. Since one oxidative peak and one reductive peak have been detected, in order to prove that they do not derive on the same activity (on PA), an analysis at different scan rate has been carried out. As said in the paragraph 2.3.1.1 the CV is a powerful technique to assess the electrochemical reversibility of a redox process, and depending on that, different analysis can be carried out. Figure 52 shows the CVs of test performed at different scan rates (from 0,01 V to 0,1 V) and shows that the peak at -0,7 V decreases in amplitude by reducing the scan

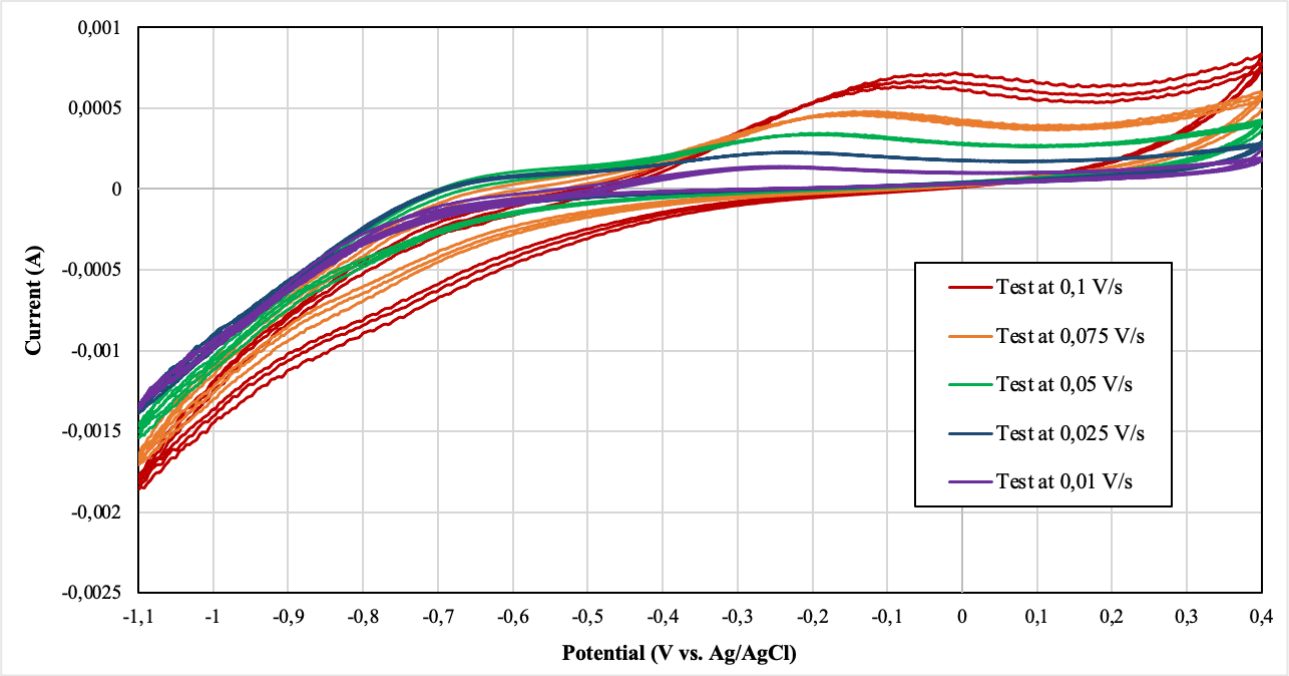

Figure 52: reversibility study in the *7b* system. The scan rate has been changed in five different tests.

rate. This seems to point toward an irreversible or quasi-reversible electrochemical activity, possibly having a sluggish kinetic.

Figure 53, instead, reports different CVs performed with the same set-up of the *7b*, but with different concentration of NaPal. The analysis has been done starting from the blank (*7h*) with no NaPal, 1 mM (*7f*), 5 mM (*7e*), 10 mM (*7b*) and 20 mM (*7g*) of analyte. Considering the *7b* has reference, the *7e* and *7f* have been carried out with different concentration keeping however a similar ionic strength. In other words, in those tests NaPal was replaced with an equal amount of NaCl to keep a similar ionic (i.e. Na+) concentration thus a similar solution conductivity and cell resistance. On the other hand the test *7g* could not been performed at the same ionic strength of the other tests due to the larger amount of NaPal used. Looking the singular CVs and the currents achieved in reduction (negative potential), by increasing the concentration of NaPal, the current tends to be more and more negative.

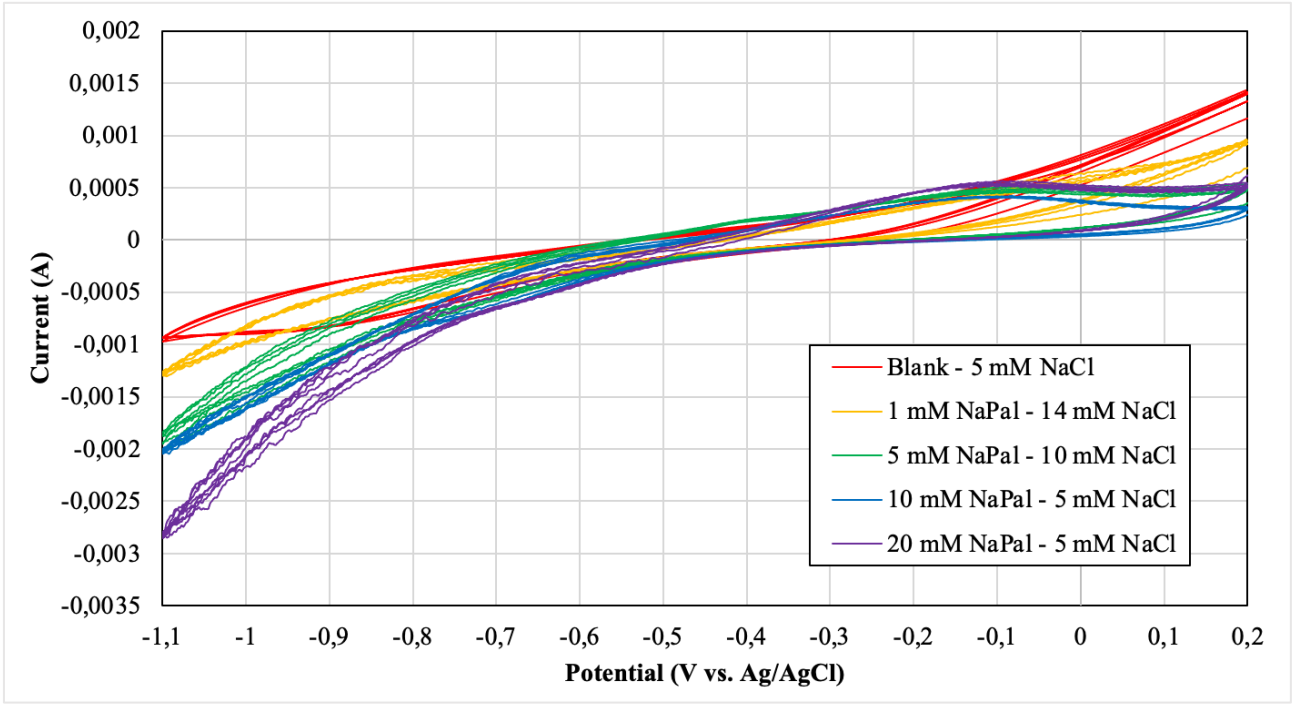

Figure 53: CVs of tests performed with a different concentration of NaPal and a trying to maintain the same ionic strength with the concentration of the supporting electrolyte, in this case NaCl.

Table 10 reports the resistance and capacitance of these tests. Here is it clear that all the tests have the same order of magnitude for the resistance. Here it is worth to notice that some deviations and data scattering is to be expected because of the experimental uncertainties. The parameter that has the most impact on the calculated solution resistance is the distance between the working and reference electrode; which influence dramatically the results. Even though a difference in resistance can be partially responsible for a larger current drawn in the system, it has been excluded that this parameter has an important role here. To support this claim, just consider the test performed at 10 mM and 20 mM of NaPal. For these tests, the lower resistance was found at 10mM however the larger current (around 50% more) was registered in the experiment with 20 mM.

It is also clear from the same table that the capacitance is very similar between tests. This latter parameter is a proxy of the electrode surface area hence these results show that a very similar mass of Ni was used in the electrochemical experiments. Thus, also the amount of catalysts does not play a role in the larger activity of found by increasing the NaPal content. Hence, all these information point strongly in the direction that the larger current found in the more concentrated samples are related to the electrochemical activity of NaPal.

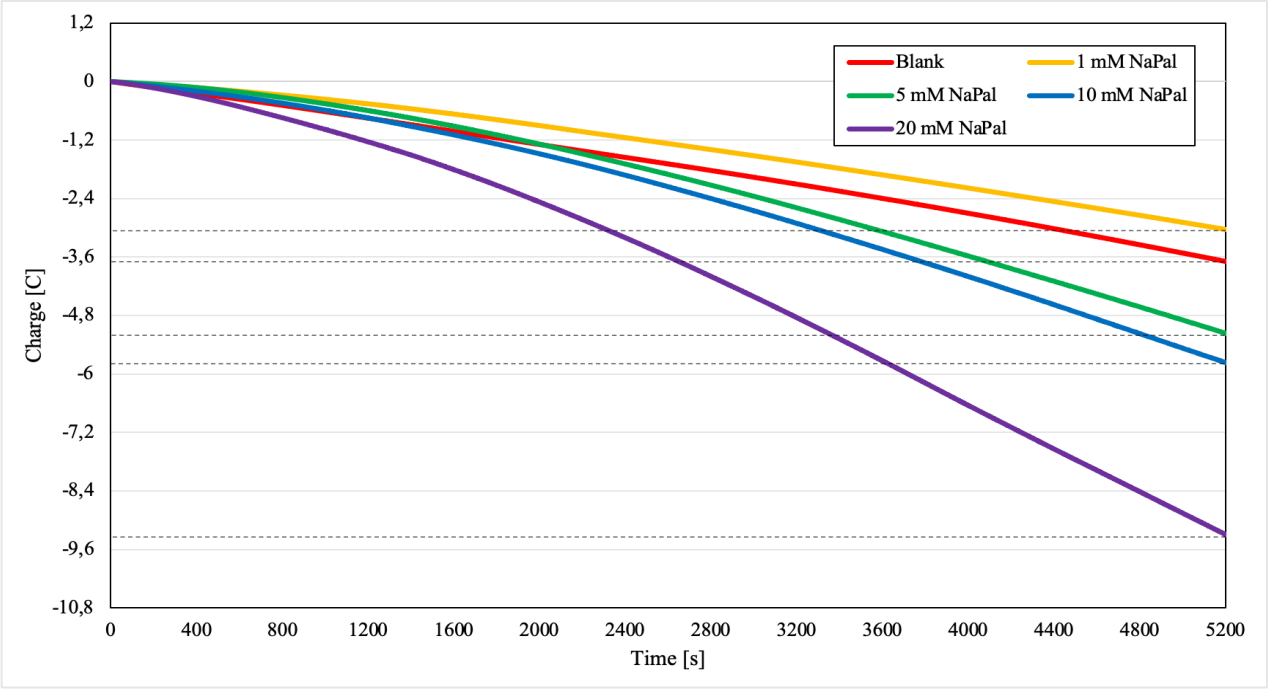

Figure 55: chronocoulograms of the tests performed at different NaPal concentration.

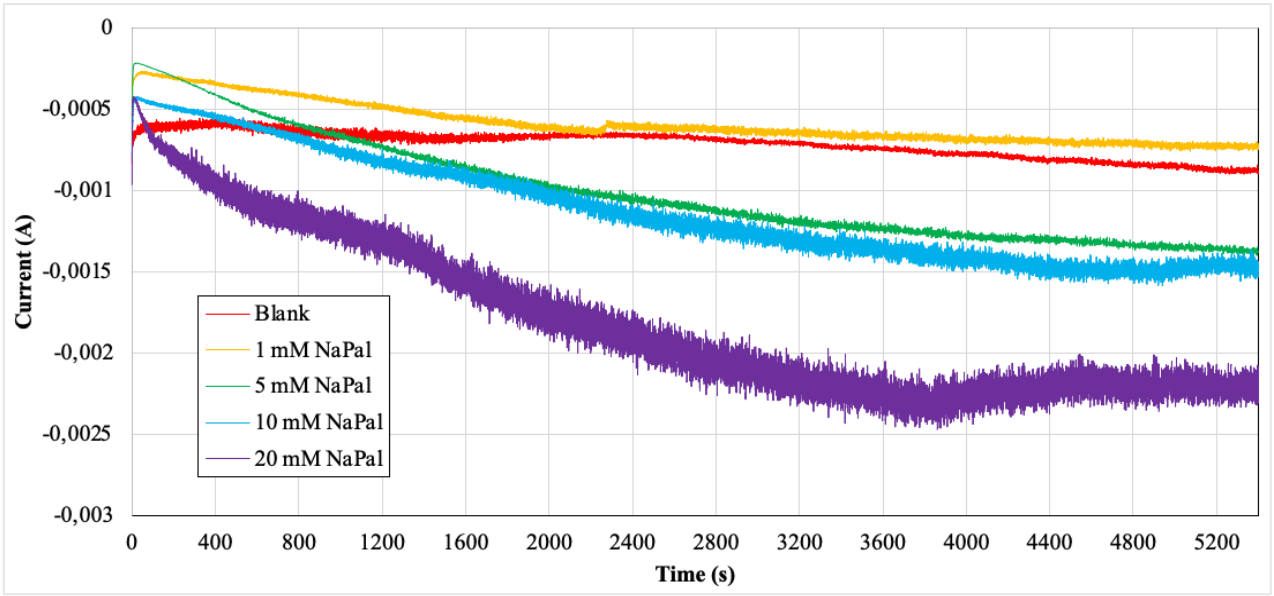

Figure 54: chronoamperograms of the test performed with different NaPal concentration in the Mcell.

The same trend has been found in the chronocoulogram in Figure 55 and the related chronoamperograms in Figure 54. The CAs were performed at a potential fixed at -0,7 V, where the activity was detected, and carried out for 1,5 hours.

Similarly, to the trend observed in the analysis of the CVs, also the CA show that higher the NaPal concentration, more negative values the current reaches. It is also important to point out that the electrical current seems to approach a steady state after approximately one hour, meaning that the system is somehow arriving to steady state condition within this characteristic time.

The integrations of these curves confirm, as predicted, that the accumulated charge is also correlated with the concentration of NaPal. Indeed, the blank test (*7h*) has accumulated -3,9 C, the 1 mM (*7f*) -3,2 C, the 5 mM (*7e*) -5,4 C, the 10 mM (*7b*) -6,1 C and the 20 mM (*7g*), with different ionic strength, achieved -9,7 C.

Table 10: electrochemical data and results of the most important tests.

n°	System resistance [mΩ]	System capacitance [mW]	Apparent initial pH	CA	Reaction Potential [V]	Reaction time [s]	Apparent final pH (after reaction)	Accumulated charges [C]
5f	2041,694	4,805	6,23	yes	-0,65	14500	6,95	/
5h	914,674	6,135	6,90	yes	-0,65	21600	EtOH: 7,3-7,6; H2O: 6,3-6,8	-28,27
5i	655,146	6,960	6,80	yes (2)	-0,7	75520	EtOH: 7,4-7; H2O: 3,3-3,8	-36,58
5j	275,156	8,714	EtOH: 6,8; H2O: 6,5	yes	-0,7	10800	/	-1,32
5k	186,219	40,466	/	yes	-0,7	61200	/	-16,44
5r	248,256	15,741	6,54	yes (2)	-0,7	10800	/	-10,765
5s	3593,930	3,343	6,05	yes	-0,65	11040	6,63	/
7a	5126,553	6,781	8,35	yes	-0,7	5400	9,0±	-28,27
7b	3101,083	8,552	8,04	yes	-0,7	5400	7,8	-6
7e	2177,131	8,201	7,7±	yes	-0,7	5400	8,08±	-5,362
7f	1250,114	7,189	7,6±	yes	-0,7	5400	7,5±	-3,181
7g	2358,067	8,796	8,5± (??)	yes	-0,7	10800	8,4	-9,738
7h	2039,372	1,549	/	yes	-0,7	5400	/	-3,868
8a	3027,037	3,581	9,40	yes	-0,7	5400	10,85±	-1,45
9a	4712,604	5,408	8,50	yes	-0,8	5400	11,2±	-1,778
10a	2022,662	5,854	6,90	yes	-1,5	5400	8±	-18,94
11a	2992,300	4,257	8,50	yes	-1,5	5400	8,75	-35,69
12a	4845,253	6,764	8,30	yes	-1,5	5400	/	-19,2
12b	4780,354	5,774	8,90	yes	-2	14400	EtOH: 11,5; H2O: 5	-53,38
12c	452,878	3,184	8,40	yes	-2	14400	EtOH: 11,23; H2O: 5	-32,27
12d	2947,082	6,187	9,04	yes	-1,4	14400	EtOH: 11,60; H2O: 6,60	-37,16
13a	15365,205	0,490	6,54	yes	-0,7	10800	6,22	-0,9471
13b	6167,146	1,619	EtOH: 4,2 H2O: 5,4	yes	-0,7	10800	EtOH: 4,90 H2O: 2,98	-3,531

Table 10 shows the results of the most important electrochemical tests. The system resistance referred to the uncompensated resistances. Here the capacitance, the initial apparent pH, the applied potential, the final apparent pH and the accumulated charged are shown.

From this tab, another signal of the possible electrochemistry performed to the NaPal or PA is shown. This signal is coming from the analysis of the pH before and after the bulk electrolysis (e.g. CA). In

general, it has been observed an evident increase in the pH after the CA indicating a lower presence of the acid content. Although this indication is relatively strong evidence of the electrochemical activity of the PA, it is worth to notice that the readings of this parameter were sometimes unstable even though reproducible.

In conclusion, the electrochemical analysis coupled with the pH measurements indicate that under the experimental conditions adopted in this work, the PA can be attacked via electrochemical methods.

3.2 Products analysis

The product analysis has been done on two different phases:

- Gaseous phase: mainly the micro-GC has been used.
- Liquid/solid phase: the IR-spectroscopy, TGA, DSC and GC-MS techniques have been exploited.

3.2.1 Gas phase analysis

For the gaseous phase the Micro-GC has been able to perform qualitative analysis. This instrument is versatile and allows the team to have qualitative information on the gaseous compounds' presence in the electrochemical cells after and in-between the PA or biocrude reactions.

In standard condition, after a suitable baking of the columns, the peaks result stable at one specific retention time, the peak area is, therefore, the only parameter that changes base on the concentration. The Figure 56 shows the two chromatograms, the permanent one (a) and the polar (b). Starting with the permanent column, the water vapour exits at 31 s, H_2 at 32 s, O_2 at 41 s, N_2 at 51,5 s and CO at 101 s. In the column of the polars, the air, which is the sum of N_2 and O_2 is visible after 29,5 s, CO_2 at 32 s and the C2+ volatile compounds exit in the time range after the 32 s in relationship with the number of carbons.

From the study of the PA, the Micro-GC showed the presence of an anomalous O_2 content. After 10 min of N_2 purging, O_2 should have been at minimum, which was not the case. Moreover, after a general checking on the possible gaseous losses and with 40 min of N_2, the O_2 content resulted to be notable, but lower than before. Therefore, an attempt was made to reduce the magnitude of this phenomenon, conscious that the headspace was not totally O_2-free. As a consequence, a direct estimation of the presence of O_2 after the CA experiment due to some electrochemical activity cannot be conducted, and any conclusions based on the O_2 concentration cannot be drown.

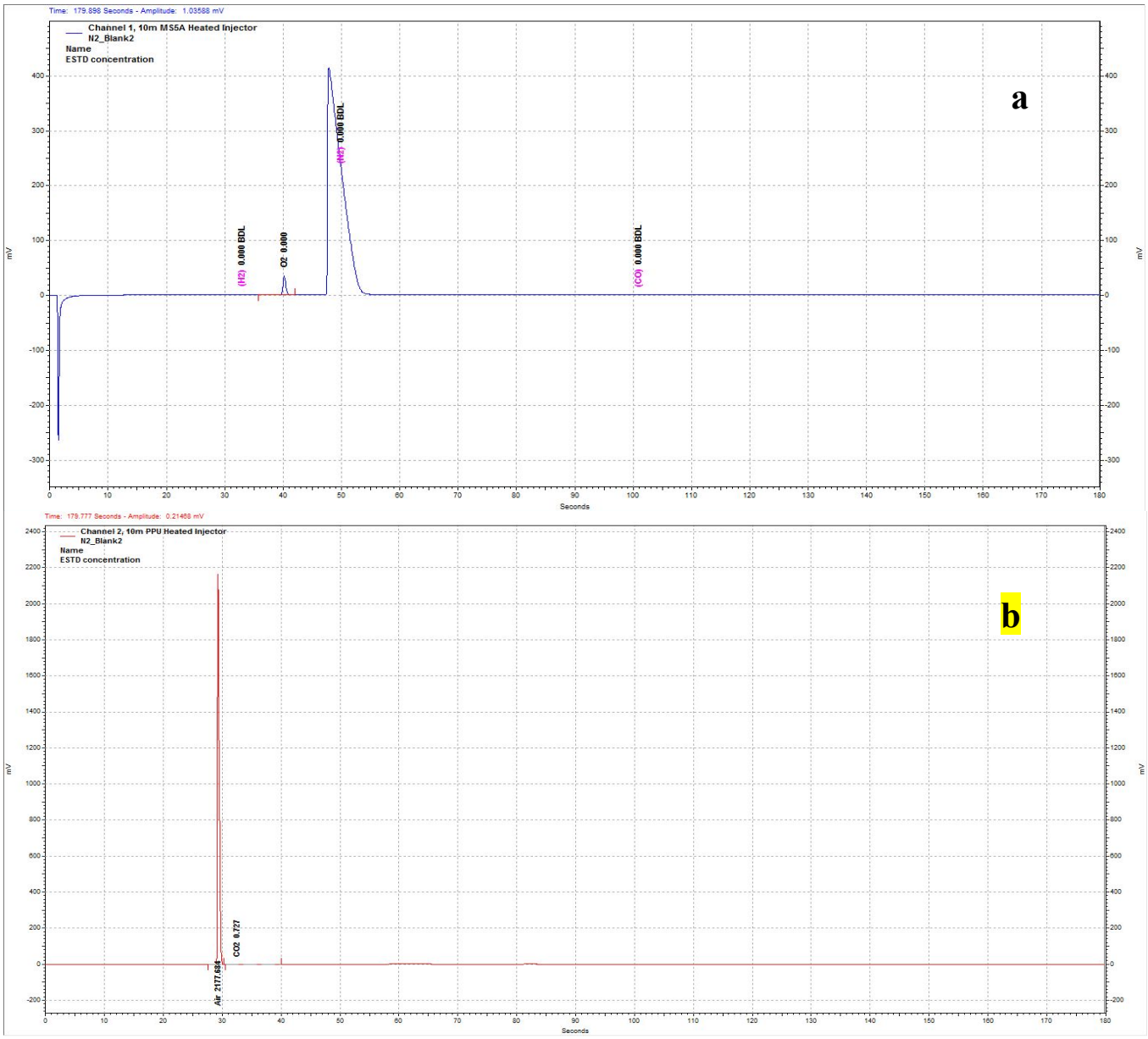

Figure 56: Chromatograms of the permanent and polar columns of the Micro-GC, general overview.

Furthermore, an unexpected CO peak has been detected in almost all the tests. It has been investigated using several blank and eventually changing the concentration of the PA to see if it would have an influence on it. From the blank analysis it is possible to conclude that the CO peak was a permanent peak derived from a side non-electrochemical reaction that happens in the electrochemical cell. Indeed, the blank without the PA shows the peak as well, but only after 3 hours at the temperature of 65°C and with the catalyst in the cell. The same result has been reached removing the Ni foam from the electrochemical cell. Only lowering the temperature from 65 to 25°C, the peak of the CO disappeared. This result can be related to a partial oxidation of the solvent or other side unwanted reactions happening at 65°C. Thus, also the peak related to the CO cannot be used for drawing conclusions regarding the composition of the head space.

The only remaining peak associated to the presence of O atoms is the CO_2. In general, it has been observed a larger concentration of the CO_2 after the CA experiments. This might point out at a reaction of the PA, which can produce CO_2; in further studies this aspect will be investigated in more details by using a novel GC-MS which was not operative at the time of performing this thesis.

3.2.2 Solid/liquid phase analysis

3.2.2.1 IR-spectroscopy results

IR spectroscopy was used to gather insights regarding the possible products present after CA. To have comparable data, the absorbance has been used. Therefore, the spectrum detected (in transmittance) has been recalculated in form of absorbance and, using the software of the IR spectrometer, the automatic baseline has been calculated for each test. After, due to the high quantity of tests and the lack of time, the normalisation has been automatized via an Excel calculation file. This process has been done in relationship with the reference spectrum of pure palmitic acid. Following the study of

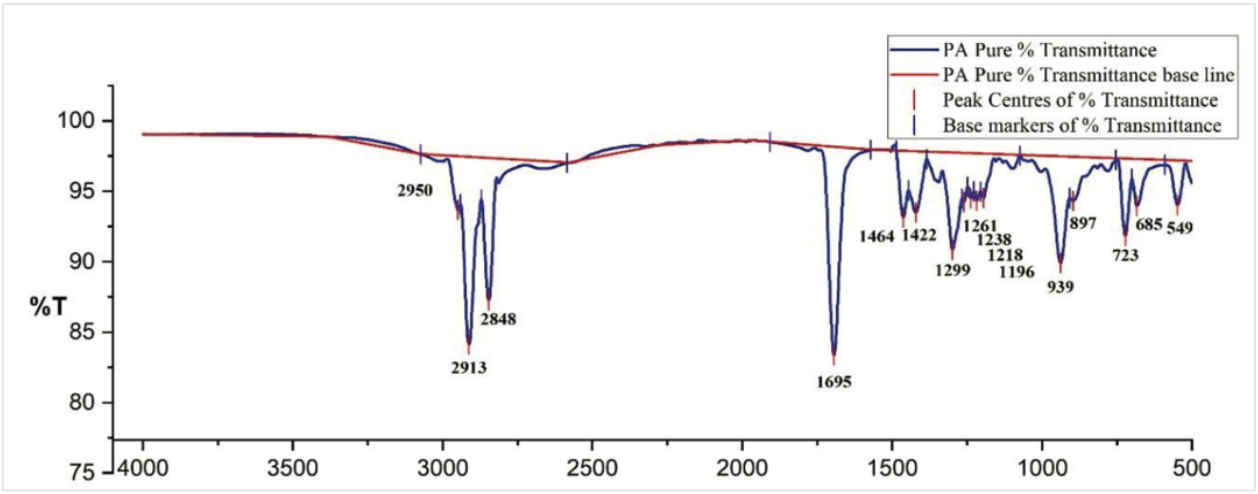

Figure 57: IR spectrum of pure Palmitic Acid by Krishna et al[78].

Krishna *et al*. entitled "Enhancing the thermal properties of organic phase change material (palmitic acid) by doping MXene nanoflakes"[78], the peak analysis have been evaluated (see Figure 57).

The most important, notable, and recurrent peaks in palmitic acid are basically ten. They have been shown in Figure 58, which is the IR spectrum of pure palmitic acid derived from this study. Hence, from higher frequency there are (1) symmetrical stretching vibration of $-CH_3$ group, (2) symmetrical stretching vibration o $-CH_2$ group, (3) C=O group stretching vibration, (4) (5) (6) deformation vibration of $-CH_2$ and CH_3 groups, (7) in plane vibration of the -OH group, (8) out-plane vibration of the -OH group, (9) swinging vibration of the -OH group and (10) swinging vibrations of the -OH group[78]. Alongside each peak there is the wavenumber associated that has been taken as reference

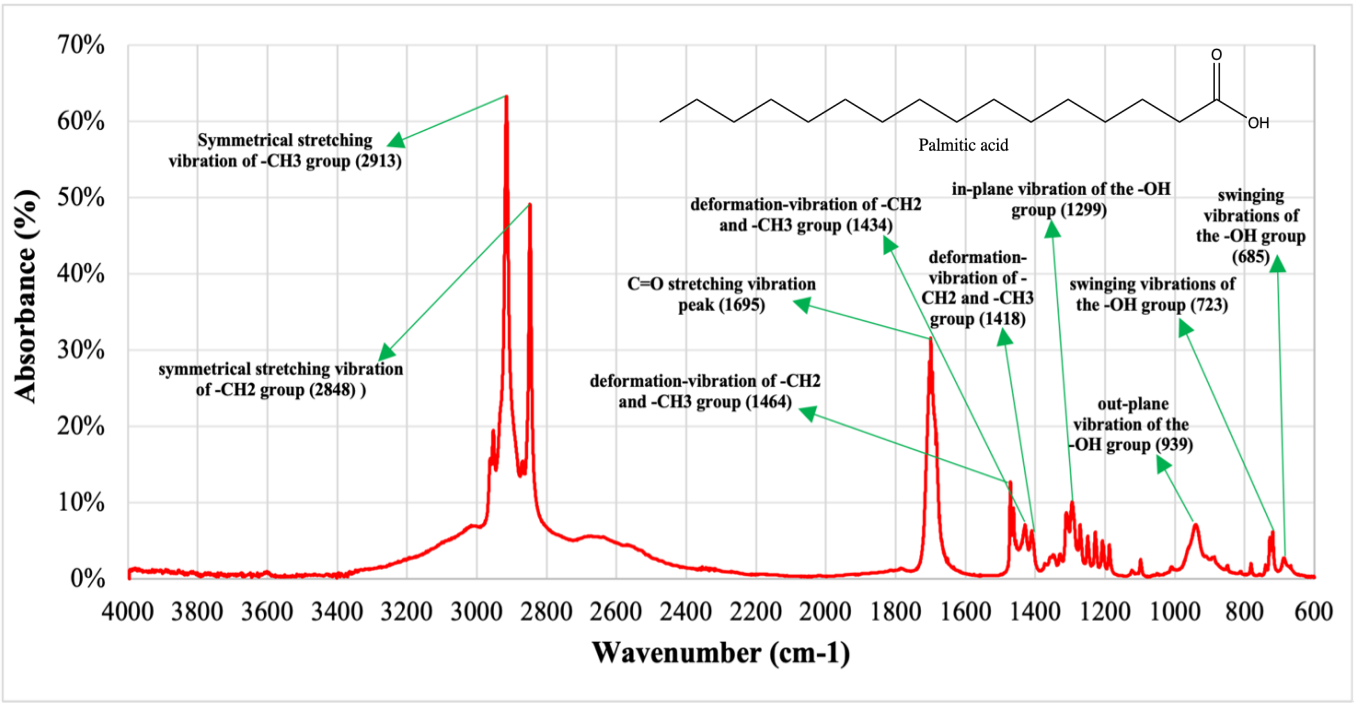

Figure 58: Reference IR spectrum of pure Palmitic Acid.

and they derived from the study cited above. The real wavenumbers of the peaks are reported in the Annex 11.

The normalisation has been done on the peak 2, the symmetrical stretching vibration of -CH_2 group, since it was the most stable at a certain wavenumber.

Furthermore, the samples have been acidified before the analysis since the spectrum of PA is remarkably different than that one of the NaPal. Therefore, in order to have reproducible results, the equilibrium toward PA had to be moved. The Figure 59 shows the two IR spectra of pure PA and

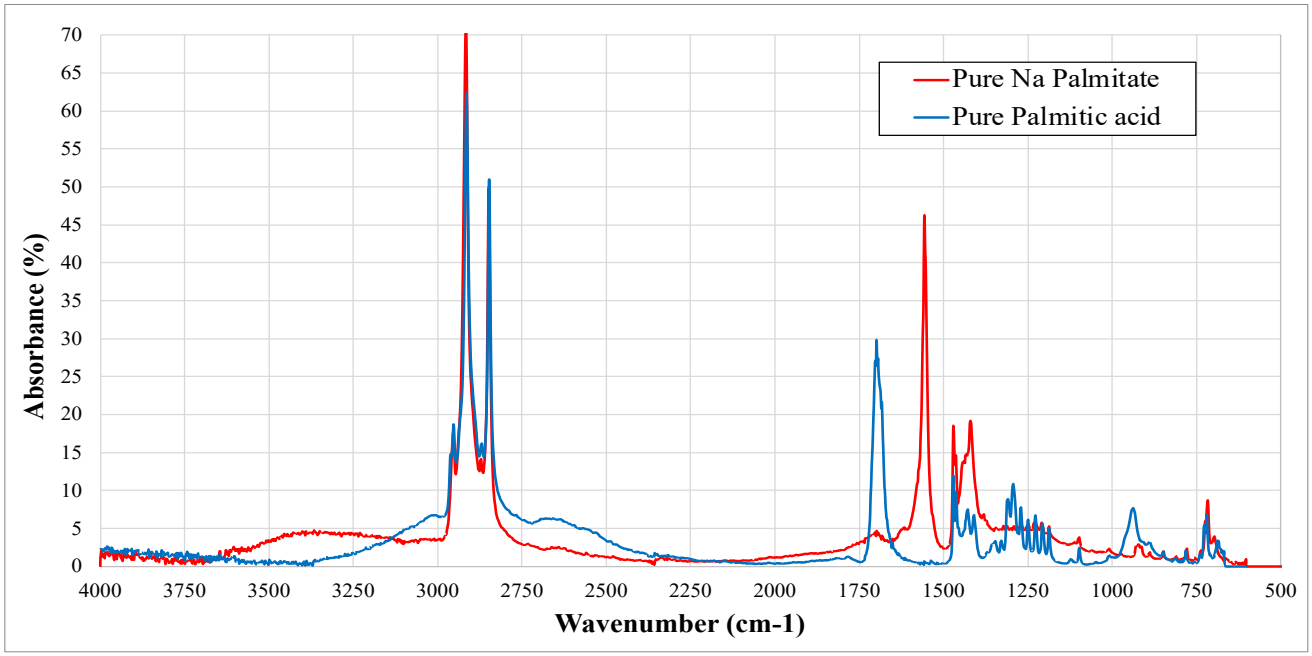

Figure 59: Comparison between the pure Na palmitate and the pure Palmitic acid IR spectra.

pure NaPal; as it is visible, they are different, mainly in the C=O, -OH part, probably due to the variation of the atomic mass (Na presence).

Due to the high amount of data and analyses with the IR spectrometer, further data processing was not performed. The deconvolution of the peaks would have been an essential tool to analyse in a more accurate way the spectra, and it will be part of future studies. In any case, the ratio of the peaks is a good approximation to retrieve information regarding the relative abundance of a specific group. Here the rational is to compare the ratio between peak heights, which can be compared between different samples. A statistical difference of the values of the peak ratios would therefore give important information on the structure of the products.

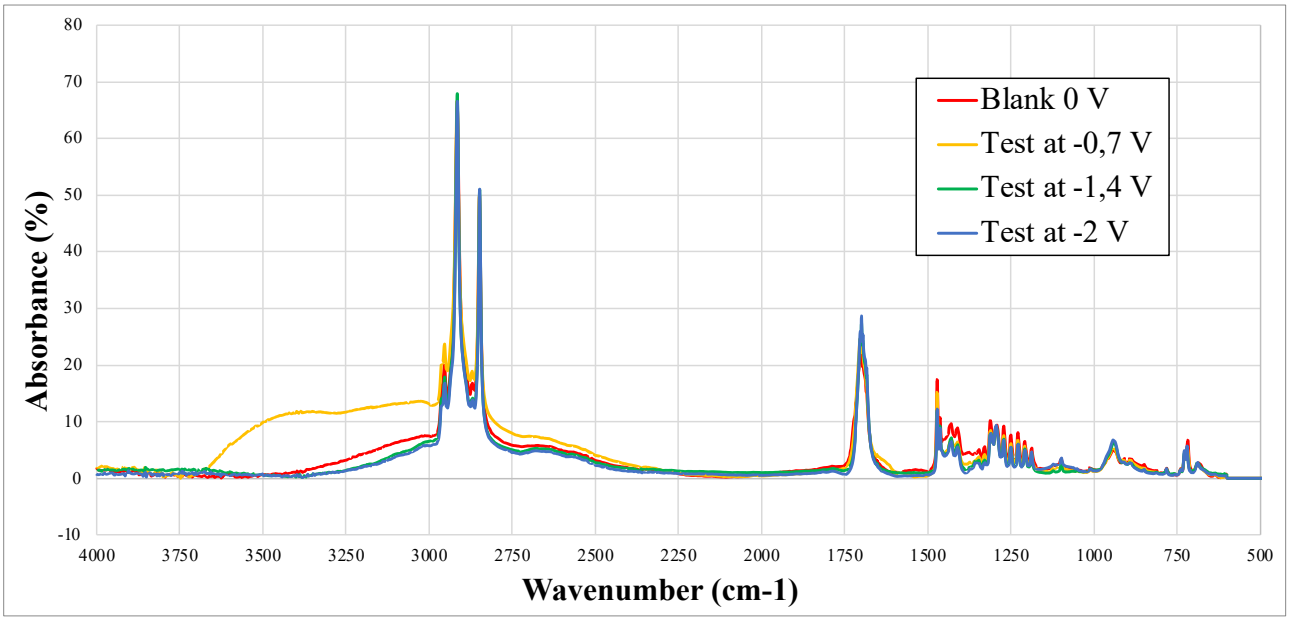

Figure 60: IR spectra's comparison of different test performed changing the applied potential.

In particular, some comparisons to analyse the grade of hydrogenation and the CH_3/CH_2 ratio have been performed. For almost all the tests, an IR analysis has been done.

Figure 60 shows the comparison between normalised spectra of CA carried out at different voltage. Figure 62 focuses on the most important peaks analysed. Following the reference spectrum of Palmitic acid (Figure 58), the two major peaks in the range of 3000-2800 cm^{-1} represent the symmetrical stretching vibration of $-CH_3$ group (*c*) and the symmetrical stretching vibration of $-CH_2$ group (*b*), which it has been use as normalisation peak. The graphs *d* represents the C=O stretching vibration, the graph *e*, the out-plane vibration of the -OH group and the graph *f* magnifies the series of peak in the range 1500-1150 cm^{-1} related to both the deformation vibration of the CH_3 - CH_2 and the in-plane vibration of the -OH group.

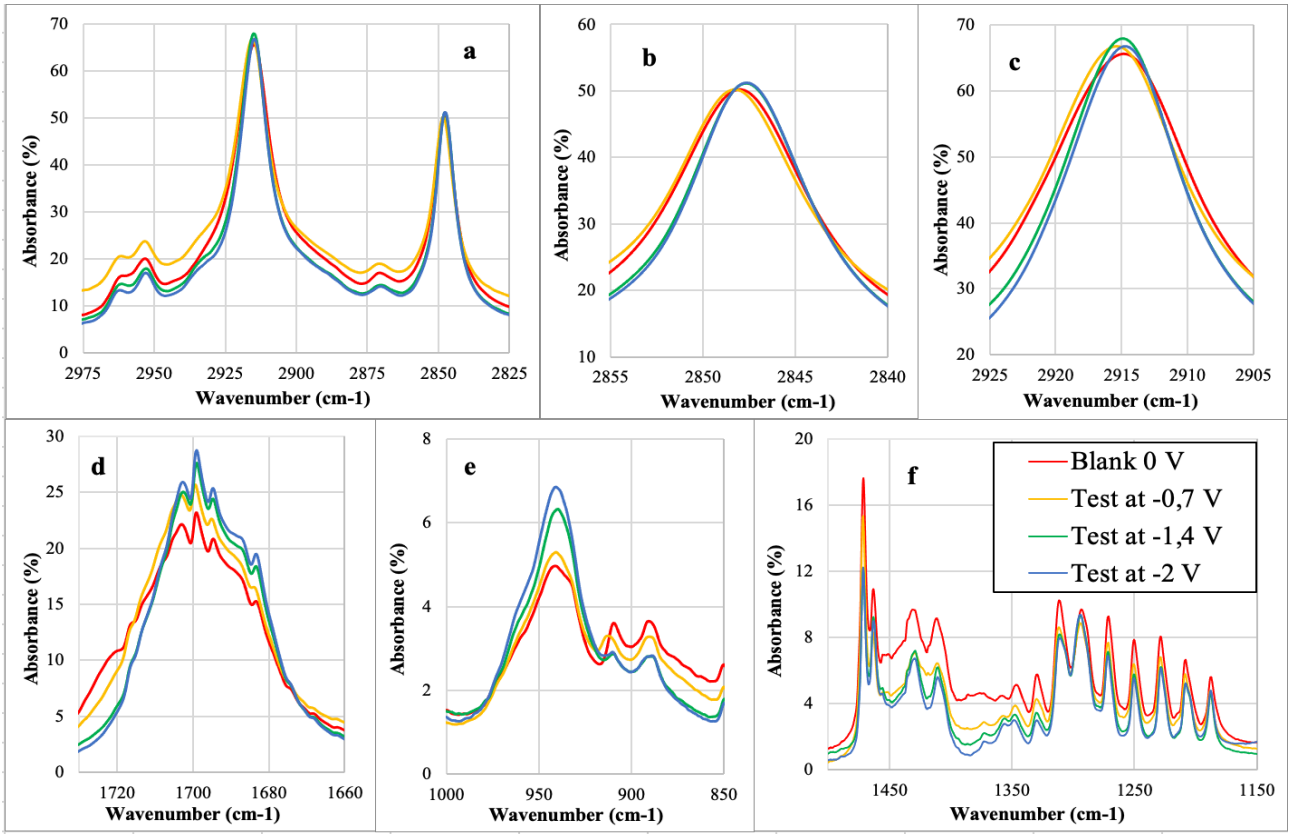

Figure 62: Magnifications of the most important peaks related to the PA.

The aim of this analysis was to find some correlation or trend that would have explained or even confirmed the effective hydrogenation of PA. In Figure 62 only some representative spectra have been used, however the IR analysis have been performed for all the CA carried out in this work. All the duplicated test performed in the same conditions showed very similar results.

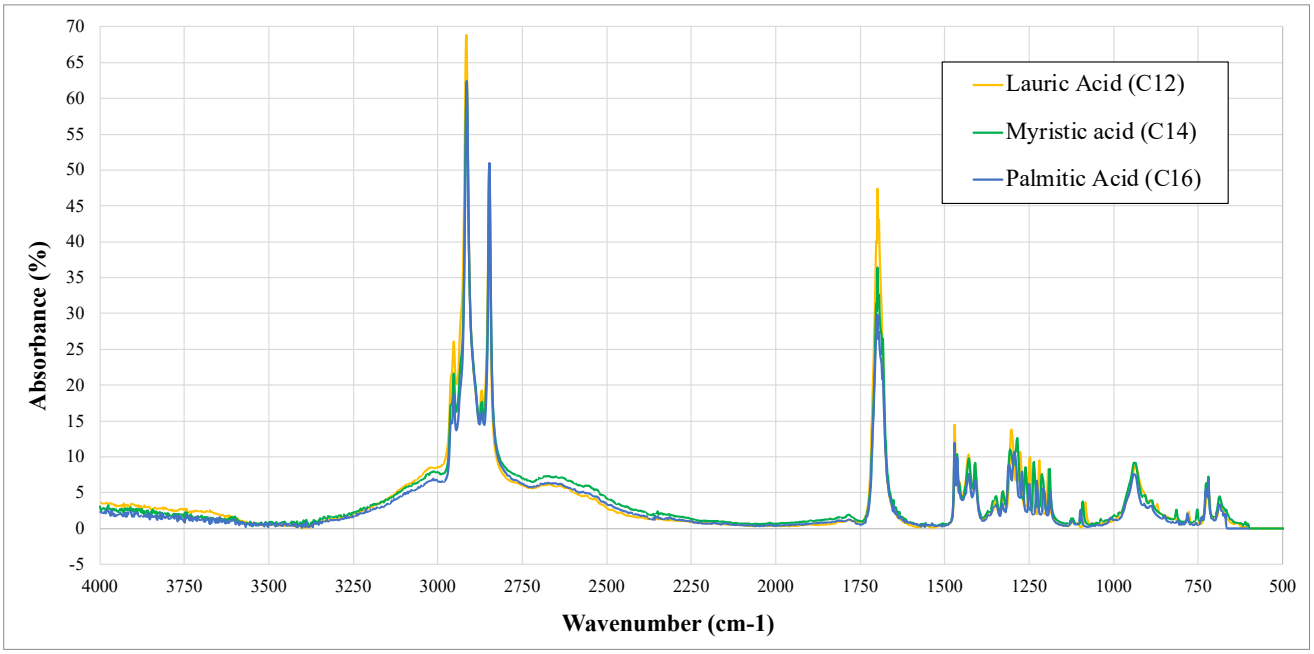

Figure 61: IR spectra's comparison of different long chain fatty acid with different C-chain length.

These data have been cross checked versus model compound having different ratio of the CH_2/CH_3 gorup. In this respect Figure 61, shows the comparison among different long-chain fatty acid in term of carbon content. This study aimed to find a correlation between the peak of the CH_3 and CH_2, as well as C=O and –OH groups approximating the grade of hydrogenation and the length of the fatty acid chain, respectively.

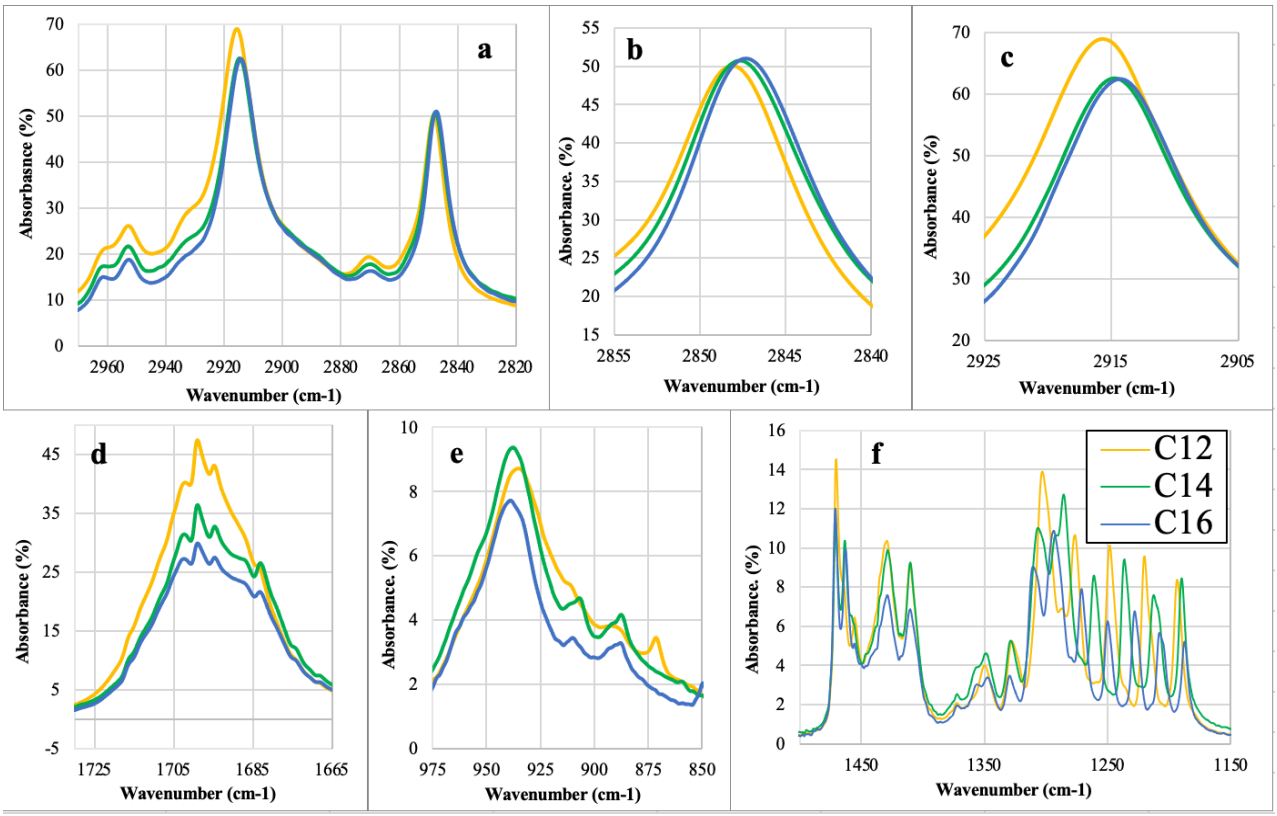

Figure 63: Magnifications of the most relevant peaks for the comparison between the different peaks of the long chain fatty acids.

Looking the peaks in Figure 63 related to the analogous peaks of Figure 62, decreasing the number of carbon in the chain, the peak related to the CH_3 vibrations should increase as consequence of the CH_3/CH_2 ratio change (panels *a* and *c*). This is observed in general both for the model compounds (fatty acids with different chain length) as well as for the sample after bulk electrolysis.

Another important information can be inferred from the analysis of the C=O stretching vibration peak (panel *d*) and the peak related to the out-plane vibration of the -OH group (panel *e*). For what concern the C=O stretching vibration it is rather clear that the trend observed in the model compounds is retrieved also in the samples after bulk electrolysis. Clearly, the samples that were exposed at the higher voltage difference (in this case -2 V) have higher peaks intensity and mimic the expected behaviour of a shorter fatty acids (see panel *d* in Figure 61). In a similar way also the -OH group peak appear more evident in the sample exposed at higher voltage difference (see panel e on Figure 62) and again this is in very stringent analogy with the model compound tested (see panel e in Figure 61). This evidence clearly indicates that the samples after bulk electrolysis show an IR spectrum

compatible with shorter chains, and it seems quite evident that the higher the voltage difference applied to the system (and as a consequence the higher the charge accumulated, see results on the CA tests) more abundant the group related to the –OH and CH_3 groups. It is worth to notice that most probably the products are a mixture of different compounds and therefore the IR cannot be used to fully characterize the product. In other words, these results show the presence of smaller chain fatty acids, but cannot be used to quantify the real length of the carbon chain.

In any case, the analysis on the different spectra of tests at different voltage and reference compounds with different carbon chain length, the ratio between the major peaks of the CH_3 and CH_2 groups confirms the effective hydrogenation of the PA (or NaPal) contained in the sample. It also seems that the higher the voltage difference applied in the system the larger is the fraction(s) of smaller chain fatty acids present as products. The Table 11 highlights the ratio of the considered peaks for the most important acidified tests. The experiements have been divided in base on the type and the set-up used.

Table 11: Results of the CH_3/CH_2 ratio analysis on the most relevant tests. Notice that the wavenumber and the height of the CH_2 symmetrical vibration peak is constant for all the tests. This is due to the fact that the spectra have been normalized on that specific peak.

Peaks (wn)	symmetrical stretching vibration of -CH3 group (2913)		symmetrical stretching vibration of -CH2 group (2848)		Ratio
Sample	Wavenumber (cm-1)	Height	Wavenumber (cm-1)	Height	
P. Acid ref	2914,29	62,406	2848,345	50	1,248
C14 acid ref	2914,91	62,534	2848,345	50	1,251
C12 acid ref	2915,67	68,930	2848,345	50	1,379
5c	2915,070	63,907	2848,345	50	1,278
5f	2914,490	59,930	2848,345	50	1,199
5g (blank 5f)	2914,83	65,585	2848,345	50	1,312
5h (5f bis)	2915,14	59,624	2848,345	50	1,192
5i (5f tris)	2914,83	67,414	2848,345	50	1,348
5s	2914,700	67,928	2848,345	50	1,359
10a (Test 6)	2914,620	67,174	2848,345	50	1,343
11a (Test 7)	2914,940	66,059	2848,345	50	1,321
12b	2914,74	66,753	2848,345	50	1,335
12c	2914,47	55,820	2848,345	50	1,116
12d	2914,92	67,944	2848,345	50	1,359
13b	2914,780	65,052	2848,345	50	1,301

3.2.2.2 TGA results

Figure 64 represents an exemple of thermograph of the sample 5i (after bulk electrolysis) in N_2 atmosphere. The change in mass detected can have different shapes and therefore can be associated to different phenomena[79]. In complex systems such as biomass based samples or biocrudes, the single

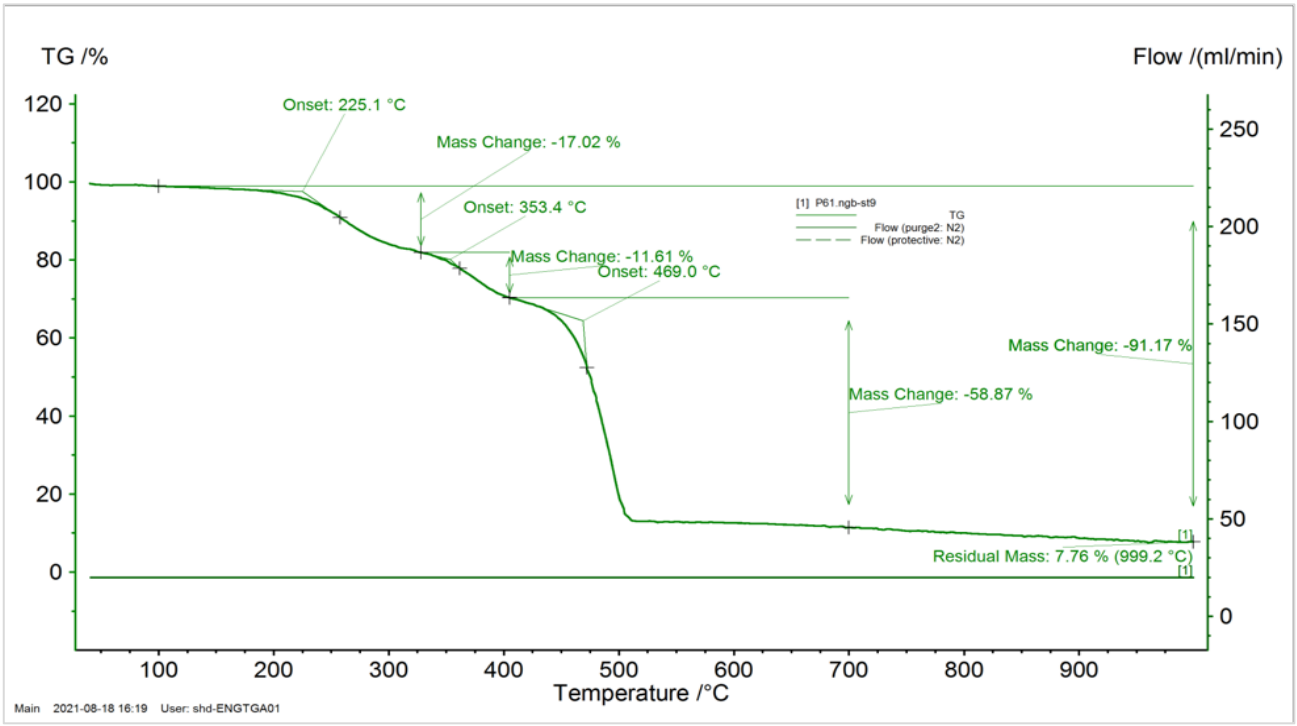

Figure 64: TGA after analysis of the sample *5i* in N_2 atmosphere.

peaks have to be associated and analysed very carfully in order to define the possible phenomenon associated. In the case of PA the system was relativelly known and the TGA has been exploited to understand the residual mass and the eventual losses associate to products or impurities.

The TGA has been used to analyse the fractions of the solid sample and, at the same time, the residual mass that remained after the thermal treatments.

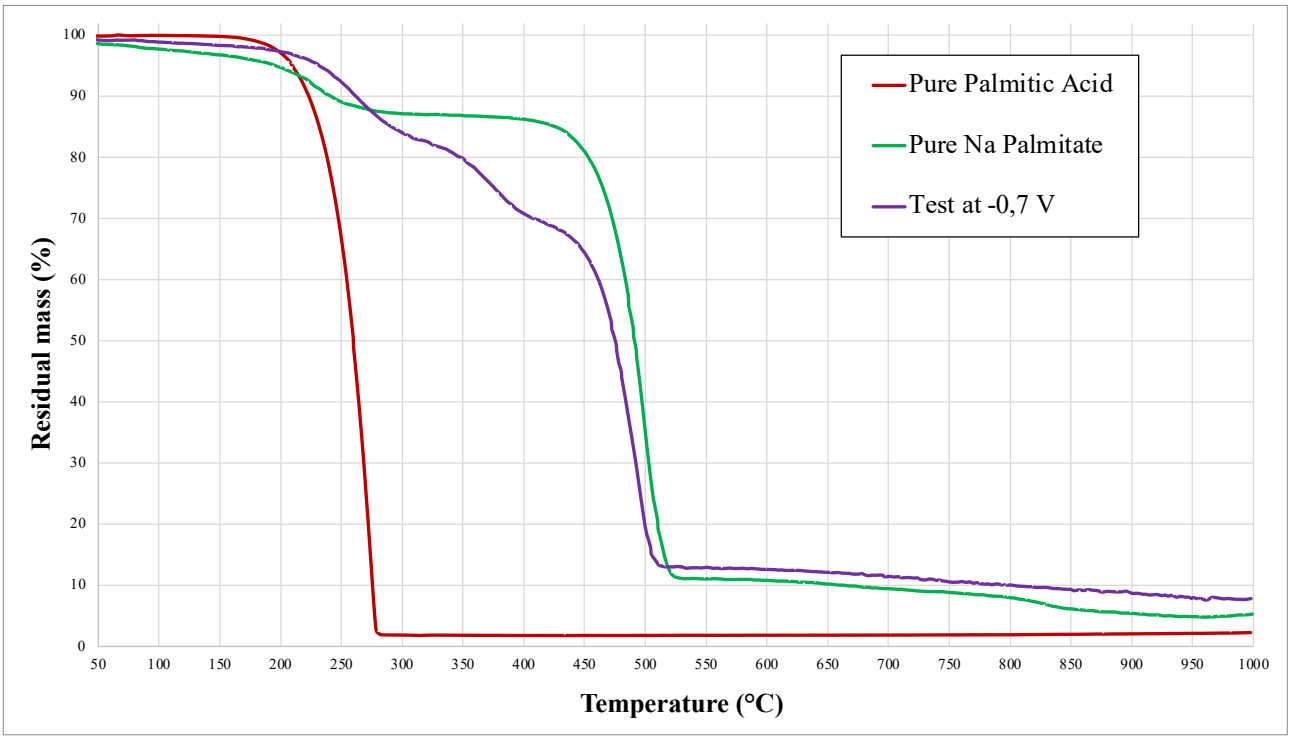

Figure 65: Thermograms of the pure PA, pure NaPal and the *5i* test at –0,7 V.

Figure 65 shows three TGA thermograms derived from pure Palmitic acid, pure Na Palmitate and a representative test performed at -0,7 V. The mass of the pure Palmitic acid is lost at 254 °C and the average on-set temperature of the tests was 220,98 °C. The curve approaches the zero, symbol that no residues have been produced. The pure NaPal, instead, has an on-set temperature of 479,9 °C and the average of the tests was 465,14 °C. In this case, the curve does not achieve the zero, due to the Na presence (ash). In the case of the tests *5i*, usually the curve highlights the equilibrium PA/NaPal after the reaction. This is calculated by the ratio between the % of PA mass and NaPal. Other anomalous peaks, not detected either in the pure PA and pure NaPal, have been found, symbol of presence of additional products, possibly coming from the electrolysis of the reactants (see Annex 15). From the onset temperature of the anomalous mass changes, it is in theory possible to infer which products can be generated from the electrolysis. However, this procedure can be extremely complicated, and it would require a TGA coupled with MS analysis, which is not available in the laboratory at Aarhus University.

In any case the attention was focused on the residual mass, which is an indication of pyrolized products that can be either coming from hydrocarbon or from ashes. Our analysis shows that after the electrochemical reaction, usually, a higher amount of residual mass was detected. A portion of the mass was associated to the metal ion of the supporting electrolyte (NaOH, NaCl or KOH) or to the NaPal, but the anomalies had a more relevant magnitude, sometimes achieving values above 28 %. The systems with both NaPal and the Na ions present achieved a 11,13 % of residual mass.

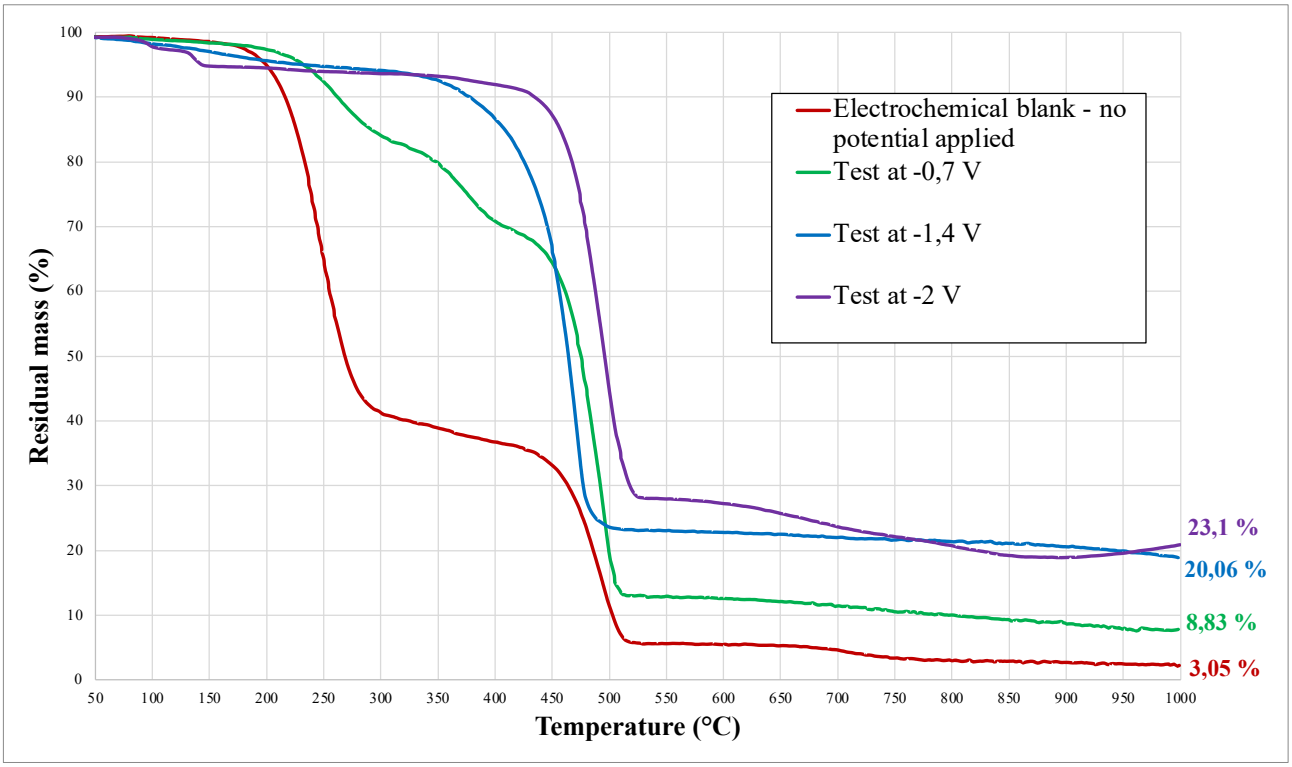

Figure 66: Thermograms of the four different tests performed changing the applied potential.

The analysis of the data has been done directly on the instrument software. The aim is to define the onset temperature and the mass change (%) associated to the peak, but also the final residual mass (see Figure 64). The analysis has been done manually: firstly, the onset temperature has been calculated, afterwards the mass change was analysed by choosing two points P1 and P2 around the peaks (if possible, the same range of the onset T should be used) and making the difference between them. From the TGA data it has been also possible to recognise the equilibrium between the PA and the NaPal and which is correlated with the pH of the sample. All the curves' analyses and the mass losses are reported in the Annex 14 and Annex 15.

While investigating this phenomenon, a trend has been discovered. The Figure 66 presents four different TGA thermograms on the electrochemical blank with no potential (*5g*) and three tests, *5*i, *12d* and *12b*, performed at various potential of -0,7 V, -1,4 V and -2 V respectively. The numbers at the end of the curves refer to the residual mass after 1000°C and as it is displayed, there is a linear relationship between the potential applied and the residual mass. Indeed, rising the voltage in the system, the residual masses increase linearly. This phenomenon is an important discover to consider for the future optimisation and up-scaling studies.

Performing a statistical analysis on different tests gathered in base in the potential applied, the Figure 67 is the result. It graphically shows the linear relationship between the potential applied and the residual mass with the systemic error calculated with the standard deviations.

Once confirmed the linear trend, the next step was to understand if the residual mass was carbonaceous material. To verify that, TGA analyses in air instead N_2, have been done. In an oxidizing atmosphere like air the carbonaceous materials are fully oxidised in CO_2. The Figure 68

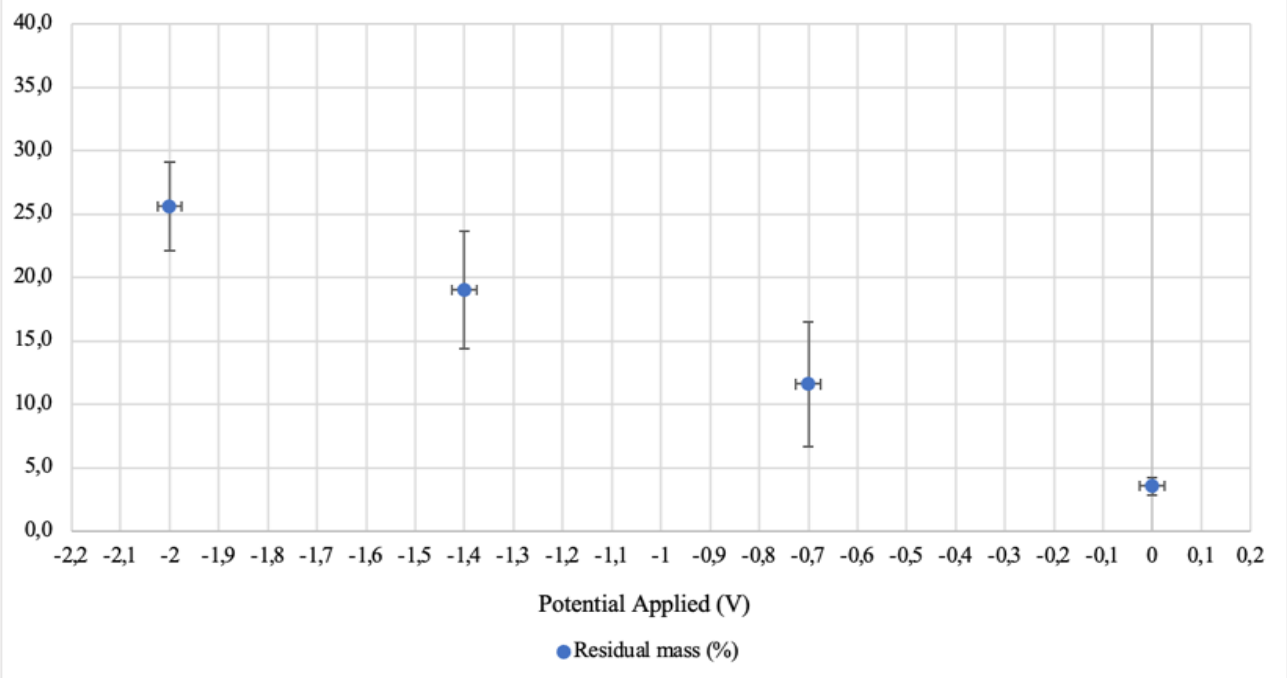

Figure 67: residual masses (%) of the different group of tests performed at various potentials.

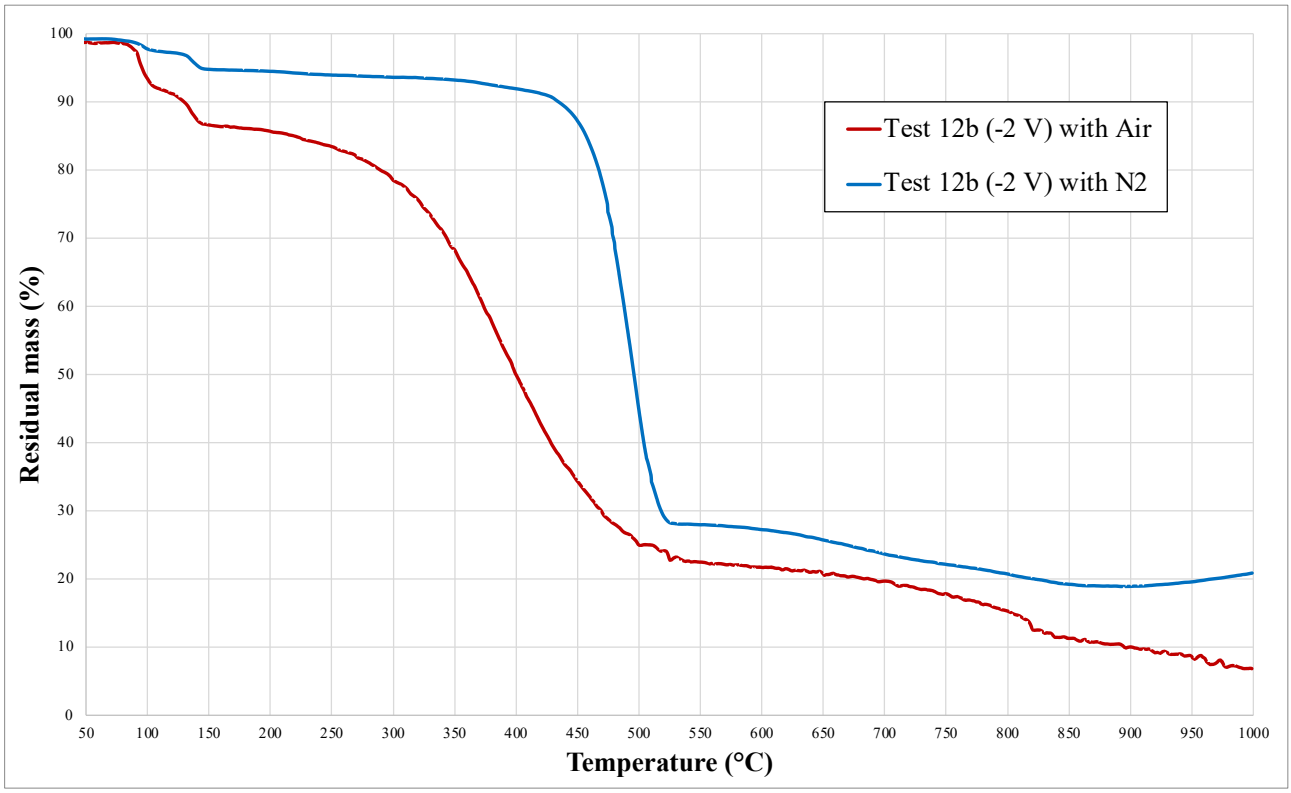

Figure 68: thermograms of the *12b* under N_2 atmosphere (blue) and air atmosphere (red).

demonstrates that a substantial part of the residual mass can be associated to carbonaceous materials formed during the electrochemical reaction. The blue curve is the *12b* (-2 V) test performed in N_2 and it has a residual mass of 23,1 %. The red curve instead refers to the same test but treated in air. In this case the residual mass drastically drops, achieving 7,25 %, in line with the residual mass derived from the Na present in the solution used for this specific experiment.

In summary, the TGA results show that the bulk electrolysis produced some compounds having onset temperatures for their decomposition below the one of the NaPal and in some cases below 100 °C. This information should be coupled with a non-negligible presence of carbonaceous compounds found in all the samples after bulk electrolysis. This can be interpreted as the bulk electrolysis

Table 12: TGA results of the most relevant tests, gathered (colour) by the potential applied for the CA.

Test	Potential applied [V]	Mass loss [%]	Residual mass [%]	Mass PA [%]	Mass NaPal [%]	PA conc. [mM]	Reaction time (h)	Initial pH
Palmitic acid blank	none	98,18	1,82	98,18	/	/	/	/
Na palmitate blank	none	92,5	7,5	10,84	77,52	/	/	/
5g (5f blank)	none	96,95	3,05	61,52	33,05	25	4	/
5f	-0,65	80,99	19,01	42,86	32,91	25	4 + 13 in cell	6,23
5s	-0,7	88,29	11,71	48,25	34,84	20	3 + 12,6 in cell	6,05
5h	-0,65	94,12	5,88	16,21	58,45	25	6 + overnight	6,8
5i	-0,7	91,17	8,83	17,02	58,87	25	20	6,8
5r	-0,65	87,46	12,54	8,74	57,69	25	3	6,54
7b	-0,7	91,58	8,42	15,08	66,69	10 NaPal	2	8,04
7e	-0,7	81,1	18,9	14,05	46,67	5 Na Pal	2	7,8
7g	-0,7	88,53	11,47	7,3	78,27	20 Na Pal	3	8,4
12a	-1,5	72,86	27,14	3,38	60,68	8,5	2	8,3
12d	-1,4	79,4	20,6	/	72,55	10	4	9,04
12c	-2	71,91	28,09	/	68,73	10	4	8,4
12b	-2	76,9	23,1	/	65,81	12	4	8,9

performed produced shorter chain fatty acids, alcohol or hydrocarbons. The most relevant results can be found in the Table 12, the tests have been gathered (different colour) based on the potential.

3.2.2.3 DSC results

The DSC technique is another fundamental thermal analysis that can give information on the enthalpy of transition of the compound present in the sample, in this case solid. At the same time, indirectly, it can also study the grade of purity of the PA in the sample after reaction, or in other words can give information of the amount of unreacted PA (or NaPal).

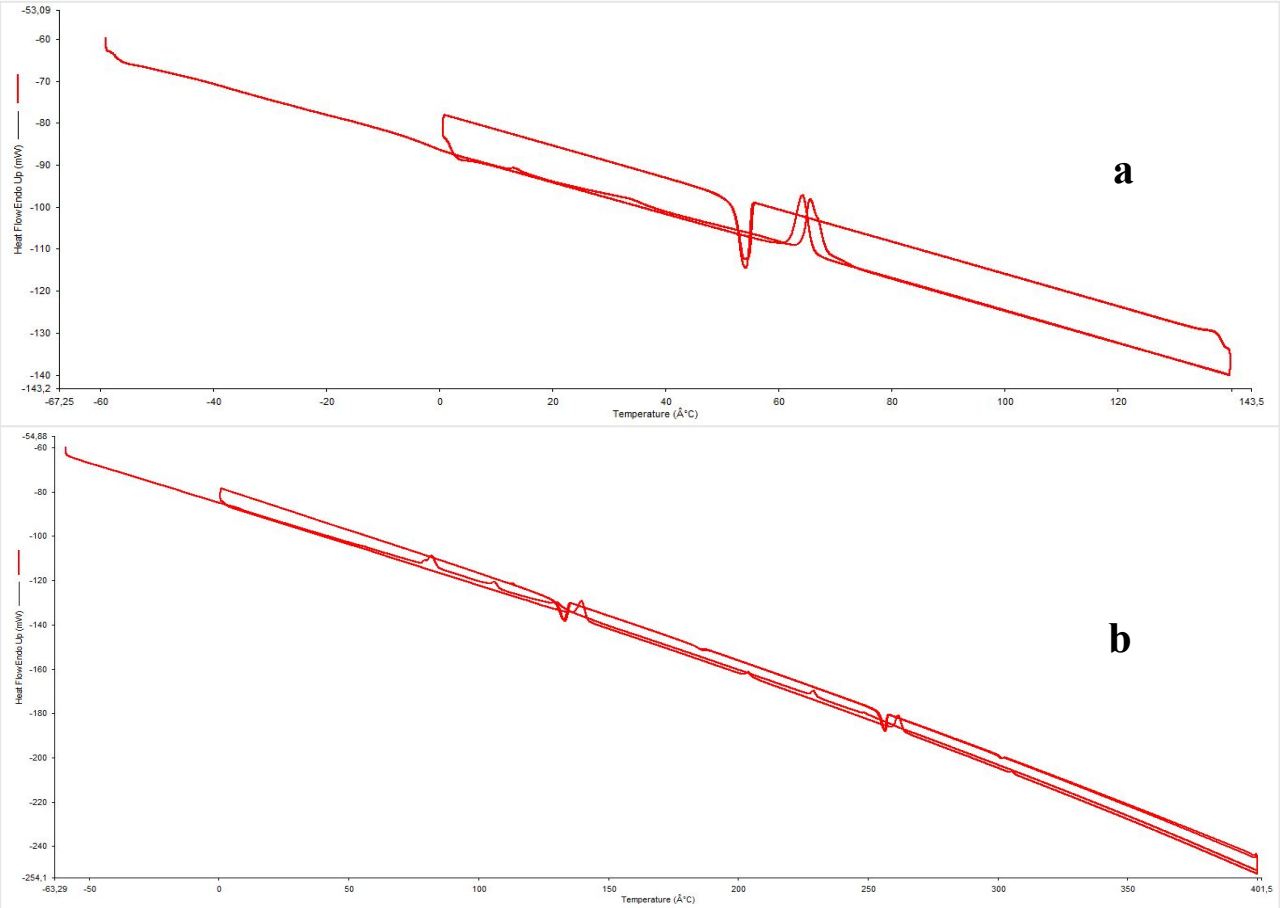

Figure 69: Overview of two unprocessed DSC curve of an acidified test (a) and the NaPal (b).

The output of a DSC analysis is a graph of the heat flow (mW) versus the temperature (°C). In base of the method, different number of segments can be performed. Figure 69 represents two DSC curves without any data processing. The curve *a* refers to an acidified test performed from -60 to 140°C for four thermal segments. The curve *b*, instead, refers to the NaPal reference test done from -60 to 400 °C and 4 segments, in order to analyse the multiple peaks of the compound even at higher temperatures. Form these plots the temperatures of the peaks with the relative ΔH_{trans} have been evaluated. This process has been done directly on the DSC's software, with a manual analysis of every segment of the graph; Annex 16 reports all the results obtained from DSC.

The raw data are suitable for the peak analysis, but they cannot be used for comparative evaluation. The slope changes in each test and the mass of the samples is different. Therefore, in order to make comparable analysis, different steps for the data processing have been implemented:

I. **Linearisation of the graph:** the data saved, must be linearised in term of slope in order to be visually comparable. To do that, the single data of heat flow at certain T is corrected following the eq. (39):

$$Q_{corr} = T \cdot m + a + Q_{uncorr} \quad (39)$$

In which Q_{corr} is the linearised heat flow value, T the temperature at which the heat flow data has been detected, m and a the arbitrary slope and zero-point of the heat flow, and Q_{uncorr} the non-linearised data of heat flow.

II. **Baseline respect an arbitrary point**: after having found the right compromise with the slope, the zero baseline is done by fixing a temperature point (in this case -50 °C) and the value of heat flow of that point is subtracted or summed to all the other points.

III. **Mass normalisation**: the last step is the normalisation in based on the mass of the sample picked up. For this step, all the heat flow data are divided by the mass of the sample.

After these three steps, the graphs were ready to be analysed and compared. Usually, only the first segment has been analysed and since most of the tests have been done until 140°C, this temperature has been chosen as maximum limit. The Figure 70 shows the DSC graph of the pure NaPal after the steps of linearisation, baseline and mass normalisation. In this case, on the *y* axis the specific heat flow is normalised on a gram of sample.

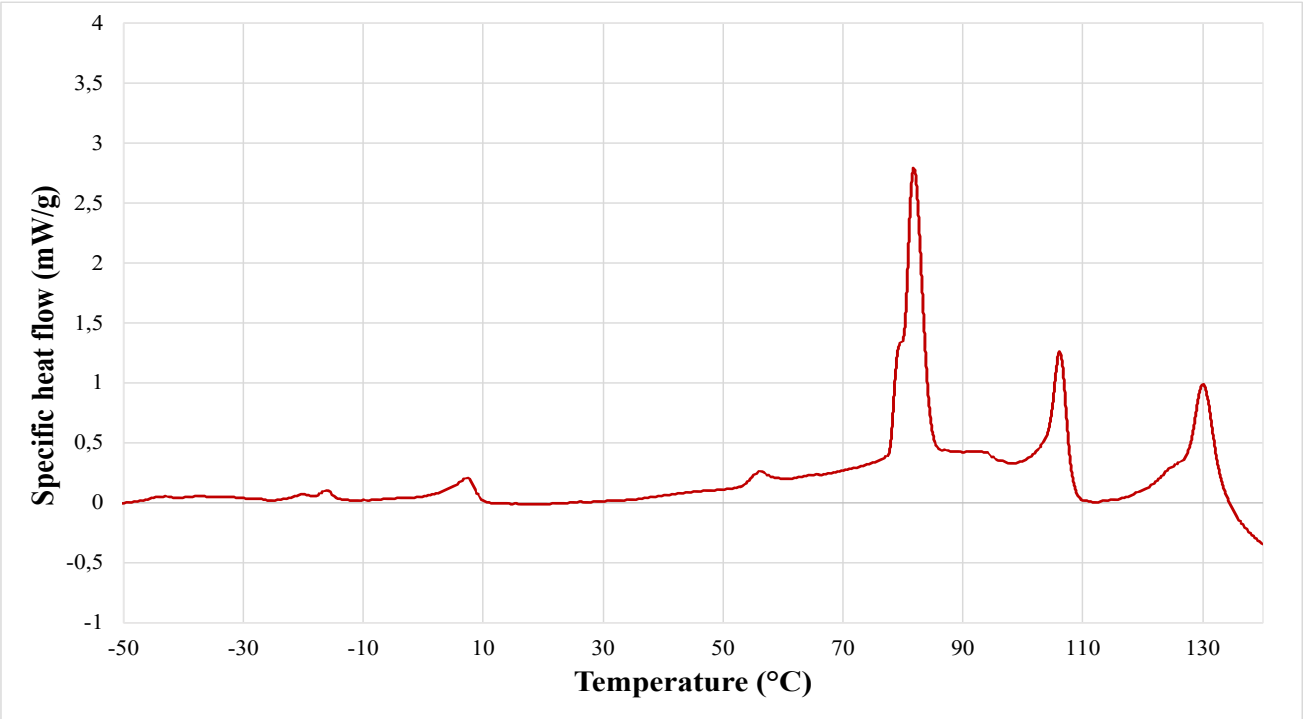

Figure 70: DSC curve of the pure Na Palmitate after data processing.

Figure 71 represents the first segment of the DSC analysis (from -60 to 140 °C) of pure Palmitic acid, pure Na Palmitate and the pure Na Palmitate after acid. While the PA results in a single and well-defined peak at 67,87 °C constant in all the tests, the NaPal presents multiple peaks at very different temperature and not always constant and present in the tests. Therefore, the acidification treatments were needed in order to move the equilibrium towards the PA and maintain the well-defined peak for further analysis. The area behind the pure PA's curve defines the melting enthalpy of the compound and it has been used as reference. The blue segment, related to the pure NaPal acidified, presents some peaks at low temperatures that appear only after the acid treatment. These peaks must be analysed carefully since they are recurrent in few tests. Thus, the peak analysed at those temperatures can be due to impurities in the solutions, products derived from the electrochemical reaction or residual peaks of the acidified NaPal.

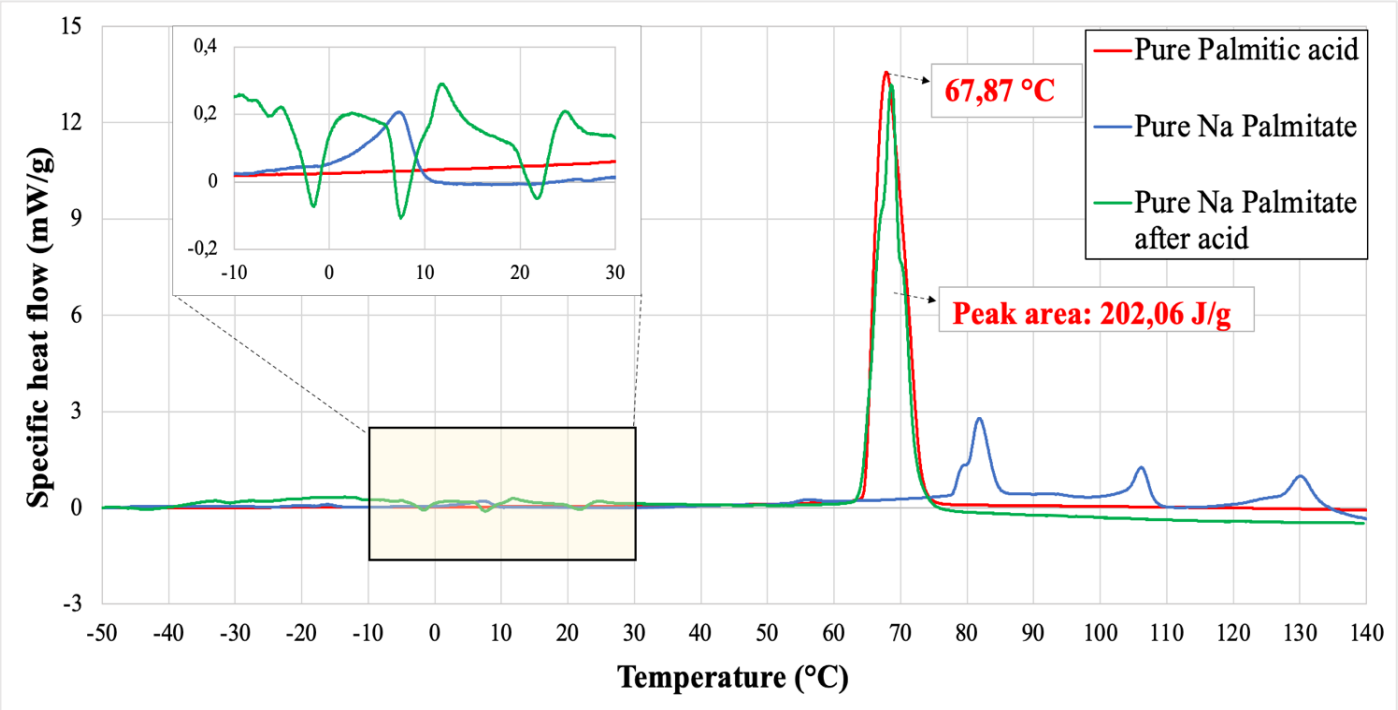

Figure 71: DSC curves of the first ascendent segment related to the pure PA (red), pure NaPal (blu) and the pure NaPal after acid treatment. The red numbers refer to the on-set temperature and the peak area of the reference PA peak. The highlighted portion has been done to show the presence of anomalous peaks in the NaPal after acid curve.

While the detection of peaks at lower temperature is a strong indication of the presence of additional compound in the mixture, their quantitative analysis and the precise identification of the possible products is very difficult to perform.

Therefore, an opposite strategy has been followed. In fact, moving the equilibrium toward the PA, it has been possible to calculate the grade of unreacted PA in the sample.

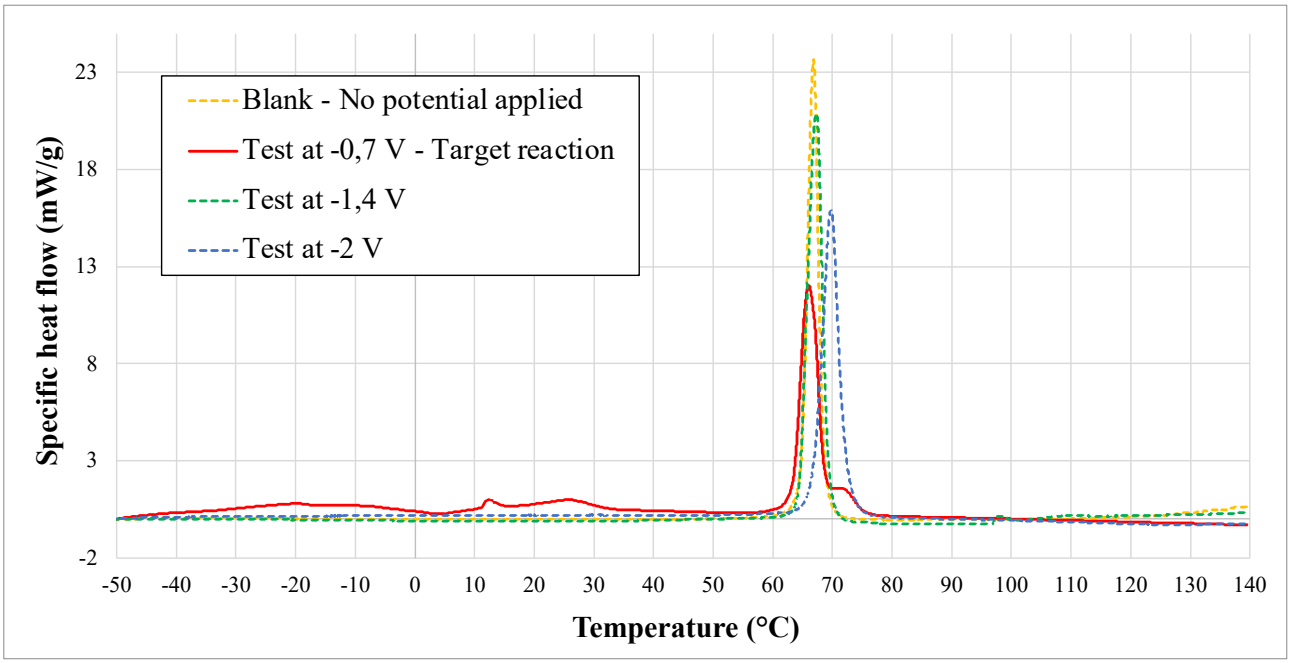

Figure 73: DSC curves of the first ascendent segment of the blank test *7c* (yellow dotted line), the test *5h* at target potential of -0,7 V(red line), the test *12d* at -1,4 V (green dotted line) and the test *12b* at -2 V (blue dotted line).

Figure 73 shows the first segment of the DSC analysis of the pure Palmitic acid and the tests performed at different potentials, the *5h* (-0,7 V), *12d* (-1,4 V), *12b* (-2 V) and the blank with no potential applied (*7c*). As it is visible, in the target potential (-0,7 V) there is a lower heat flow than the other tests and that can be related to the lower content of palmitic acid due to a probable reaction. Indeed, in the target test, some activities have been detected at lower temperatures, which could be related to products of the electrochemical reaction.

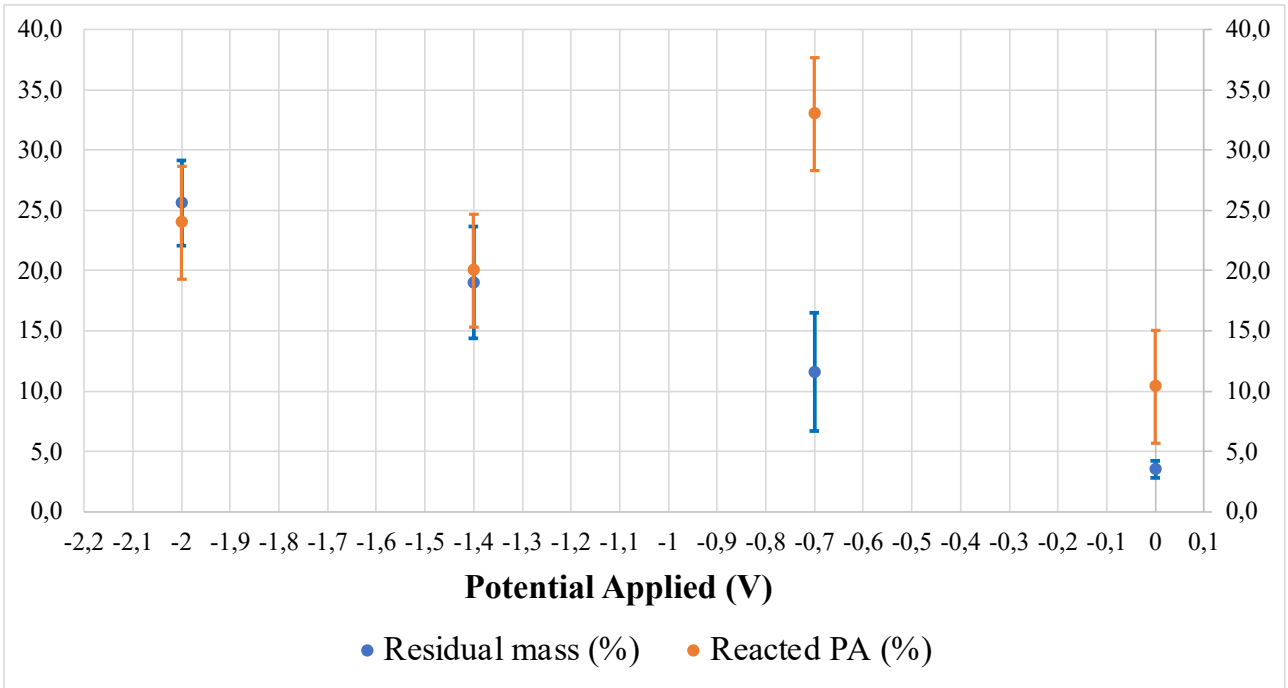

Figure 72: correlation between the residual mass (%) and the PA reacted (%) of the most important test divided by the potential applied.

Figure 72 represents the statistical analysis on the TGA residual mass *vs*. potential applied (Figure 67), overlapped with the analysis on the PA purity derived from the integration of the area behind the PA peak and normalised with the melting enthalpy of the reference. This graph shows that also in the case of the PA residual mass analysis, there is a correlation between the impurity (%) and the potential applied. Indeed, the tendence is similar to that one of the residual masses. Only one point seems to be an outlier compared to a liner trend. This is the point at the target potential (-0,7 V). This is related to the PA reaction, and therefore, it represents an important proof that the PA can be attacked electrochemically.

Table 13: results of the DSC analysis, the purity has been calculated doing the average of the PA's specific *ΔH* of transition of all the four segments (when they were present).

Palmitic. Acid								
Sample	**Mass [mg]**	**T (seg 1-3) [°C]**	**T (seg 2-4) [°C]**	**Specific ΔH (seg 1-3) [J/g]**	**Specific ΔH (seg 2-4) [J/g]**	**Average of the segments in absolute value**	**Purity [%]**	**Purity average**
5g	1,48	67,45	58,71	/	-171,58	171,58	85%	90%
7c	1,61	66,48	56,58	158,655	-148,6025	153,62875	76%	
PA reference	4,65	67,87	/	202,06	/	202,06	100%	
Na palm acid ref	2,10	67,26	57,92	175,46	-218,14	196,80	97%	
5h	0,87	64,74	54,07	115,44	-123,44	119,44	59%	67%
5h bis	1,05	64,74	51,52	105,37	-103,25	104,31	52%	
5i	1,26	65,79	54,46	170,50	-186,79	178,65	88%	
5r	2,40	67,57	50,11	144,83	-130,78	137,81	68%	
12a (-1,5V)	2,01	66,30	52,67	159,34	-154,72	157,03	78%	80%
12d (-1,4)	1,86	68,04	58,17	153,71	-142,88	148,29	73%	
10a (-1,5)	1,78	67,17	54,92	180,93	-179,24	180,09	89%	
12b (-2V)	1,65	69,64	57,71	155,63	-150,36	153,00	76%	76%
12c	1,03	67,93	54,68	148,11	-133,83	140,97	70%	

Table 13 shows the statistical analysis of the DSC data and PA's peaks of the tests divided by the potential applied. The red rectangle is the PA's reference transition enthlapy.

In summary the test performed with DSC shows that the residual mass of the PA after the bulk electrolysis is lower (up to 35%) with respect of the initial mass. In particular the highest conumption of PA was found when the bulk electrolysis was performed at – 0,7 V which corresponds well with the peak seen during the cylic voltammetry. This is a strong indication that -0,7 V is indeed where the selective electrochemistry over the PA can be performed. In addition, some compounds having low thermal transition temperatures have been detected.

3.2.2.4 GC-MS results

Only partial results can be shown from GC-MS analysis. At the moment of submitting this thesis only few samples have been correctly analysed. As said before, the GC-MS method is unreliable, further optimisation must be implemented in the future, therefore below only the GC chromatograms will be considered. Nevertheless, Figure 74 shows the chromatograms of the hexadecanol reference (a), test *5i* after electrolysis (b) and test before electrolysis (c).

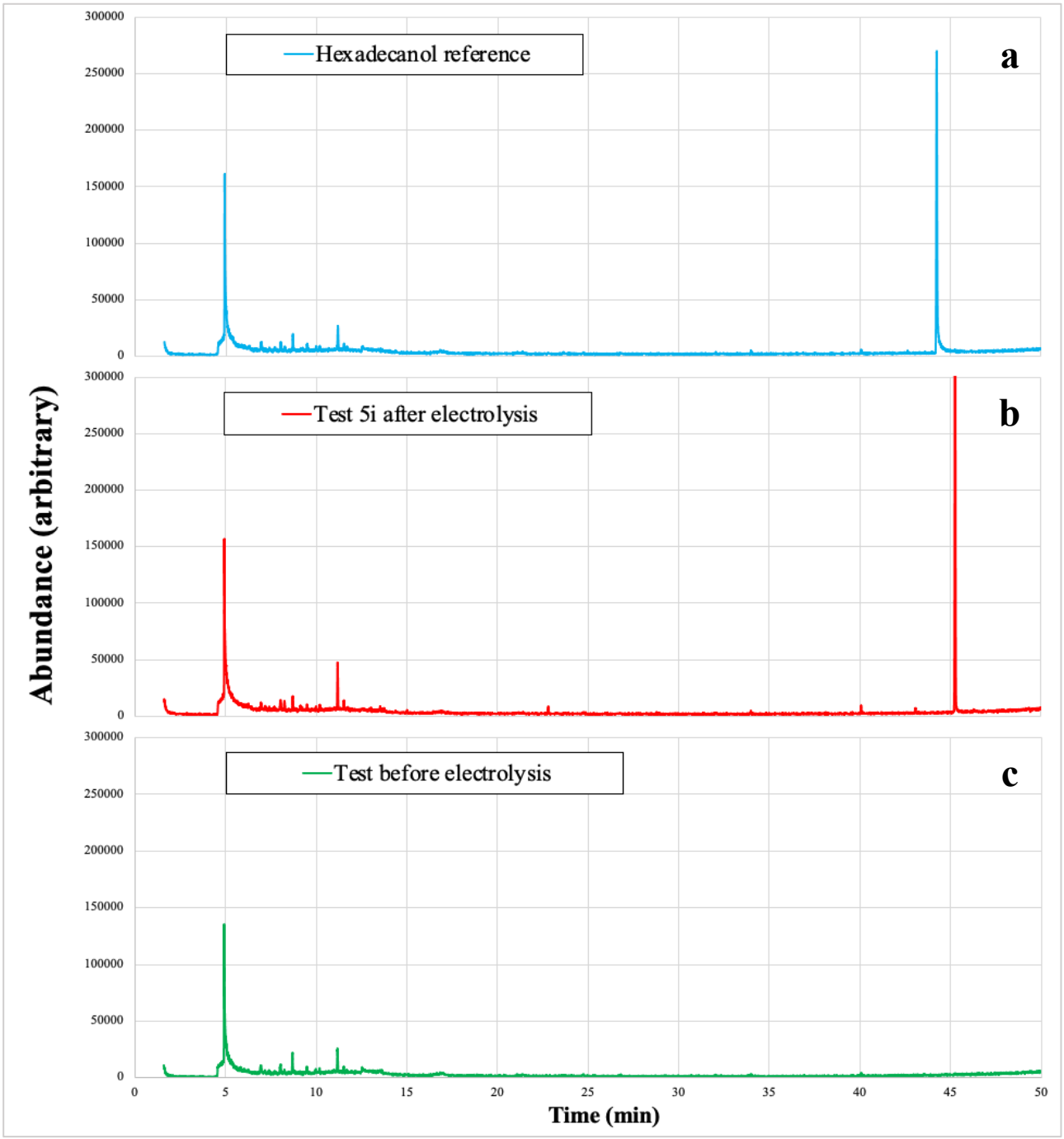

Figure 74: Chromatograms of the hexadecanol reference (a), test *5i* after electrolysis (b) and test before electrolysis (c).

The results show that after the bulk electrolysis at –0,7 V (again the same voltage where the peak has been found in the CV analysis) there is the presence of a significant peak which is compatible, both

from the retention time, and the MS abundance analysis, to an alchool, most probably a C15 or C16. This peak is not present in the chromatograms of the test before electrolysis. Hence, this compound could be related with hexadecanol or pentadecanol.

These results even if incomplete suggest that one of the possible reaction path must bring to alchools.

3.3 Possible reaction schemes

This paragraph aimed to assume a possible reaction pathway. It is an assumption because not enough studies have been performed and a protocol for the product characterisation must be found yet. Therefore, based on the thermochemical behaviour and some qualitative GC analyses, the paths have been identified.

PA can undergo different reactions that must be taken into account while performing ECH. The reactions involving the PA/NaPal in the electrochemical system under study can be different, but only few are suitable with the working conditions or with the results of the analyses. Below the reactions considered, with the explanation on why one must be considered or not:

I. Fischer Esterification: the reaction involves a carboxylic acid and an alcohol in presence of an acid catalyst (H_2SO_4) forming the relative ester and water.

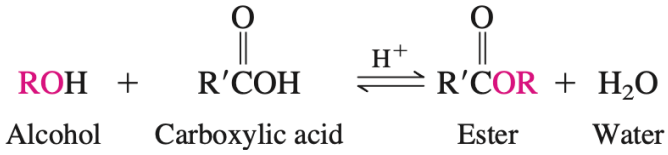

(XIII)

It is a reversible reaction and the equilibrium is established by two main factors: (1) the excess concentration of alcohol or carboxylic acid which would favour the reaction, (2) the water removal, which would move the equilibrium to the right[80].

In order to avoid this reaction, the water has been maintained at the 30% in the electrolyte and the pH at alkaline, neutral or basic-acid values. Nevertheless, the protonic movements due to the electrode redox reactions is always present and this reaction must be monitored. Therefore, some checks on the possible production of Palmitic acid methyl ester or other esters had to be done. The Fischer esterification can be also exploited for a fast indirect analysis for the quantification of unreacted carboxylic acids. Breton et al. used the esterification for the GC-MS detection of carboxylic acids[81].

This reaction has been excluded. Esters are not compatible with the analyses results and the reaction conditions (alkalinity and water content) should block this path.

II. Saponification: It is the counter reaction of esterification, and it is basically a hydrolysis reaction. Unlike the Fischer Esterification, it is a base irreversible reaction, carried out in aqueous phase[80].

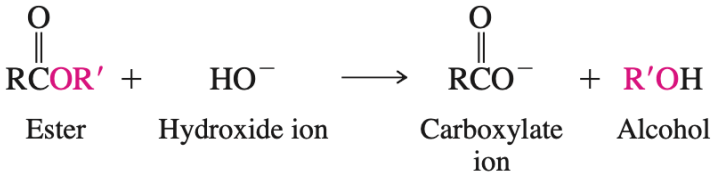

(XIV)

The reaction, therefore, generate the relative carboxylate ion and alcohol. In this case the hydroxide ion is a reagent and not a catalyst. This reaction has not been considered since the esters have not been detected and the solvent is only 30% of water.

III. Kolbe/Non-Kolbe electrolysis: In electrochemical systems the dimerization of carboxylic acid has been confirmed in literature only with the so-called anodic Kolbe electrolysis, an oxidative decarboxylation process[82]. Figure 75 refers to the Kolbe electrolysis of a carboxylic acid. The electrode mechanism is related with the adsorbed carboxylate ion, which, after decarboxylation,

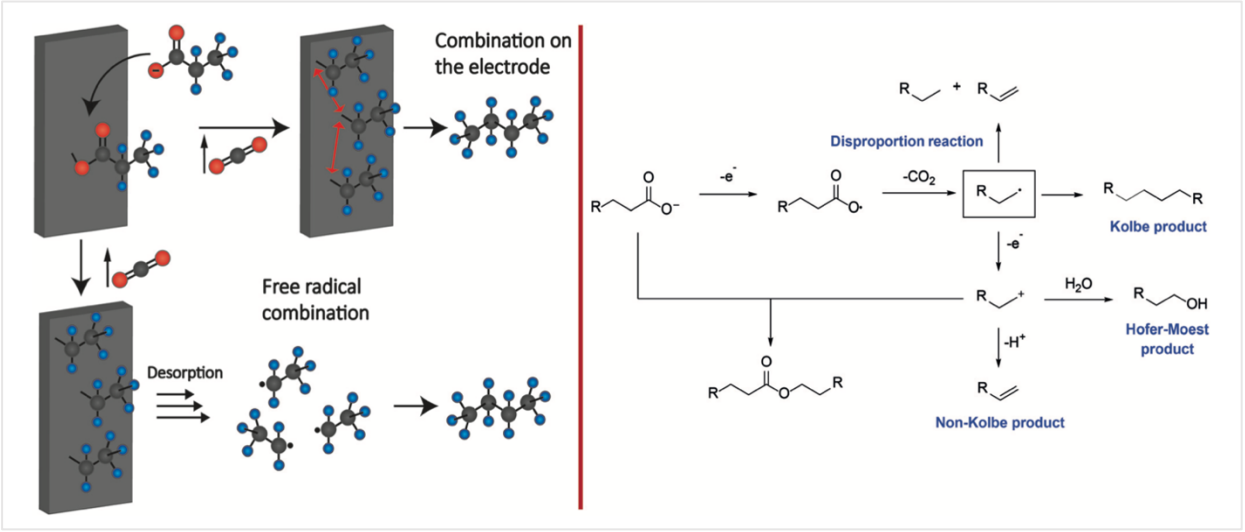

Figure 75 In the left-hand side, two electrode mechanisms for Kolbe electrolysis. On the right-hand side the reaction mechanism of Kolbe, Non-Kolbe and Hoer-Moest pathways[83].

can perform a free radical combination or a dimerization at the electrode surface. Moreover, from the adsorbed carboxylic radical, different pathways a part the Kolbe one, can be followed:[83]

- Disproportion reaction: two radicals perform a redox reaction in which one is oxidised and the other reduced.
- Non-Kolbe reaction: the radical is oxidised and deprotonated.
- Hofer-Moest reaction: the radical is, also in this case, oxidised another time and after hydrated to form the relative alcohol.

Due to the anodic nature of this reactions, it has been excluded. In addition, the OCP of our system was at negative voltages before and after the bulk electrolysis.

IV. Electrocatalytic hydrogenation of Palmitic acid: Palmitic acid as carboxylic acid represents one of the most oxidised species, therefore it requires more electrons, and the electrocatalytic hydrogenation reactions are difficult to perform. Particularly, the presence of saturated C-C bonds, like in the case of Palmitic acid, makes the hydrogenation reduction potential more negative, decreasing the affinity to electrons.[51] In heterogenous electrochemical reactions, and in particular in electrocatalytic hydrogenation processes, the target compound is usually firstly hydrogenated forming a complex with the active site on the surface of the electrocatalyst. The radical intermediate can undergo to further hydrogenation or can eventually react with another radical to produced dimers[53]. In the case of carboxylic acids, this mechanism has been assumed. The natural chemical dimerization can be done with two hydrogen bonding between the hydroxy and the carbonyl groups. Most of the carboxylic acid are dimerised naturally, which explain the higher boiling point than, for example, alcohols. For the acid reduction, the first reaction to carry out is the conversion of the carboxylate group via deoxygenation to an aldehyde, which is more reactive and can be more easily reduced to alcohol. Saturated long chain fatty acids are difficult to attack electrochemically, different attempts have been done, mainly in room conditions, but without any result[38]. Only the unsaturated C=C have been confirmed to be reducible[81]. Hence, the hydrogenation of long fatty acids into valuable chemicals for biofuels has resulted feasible only thermo-catalytically or using anodic non-Kolbe processes. An example is done by X. Liu et al. which used a 5% Pt/C catalyst to perform a hydrothermal hydrodeoxygenation of Palmitic acid with formic acid as hydrogen donor[84].

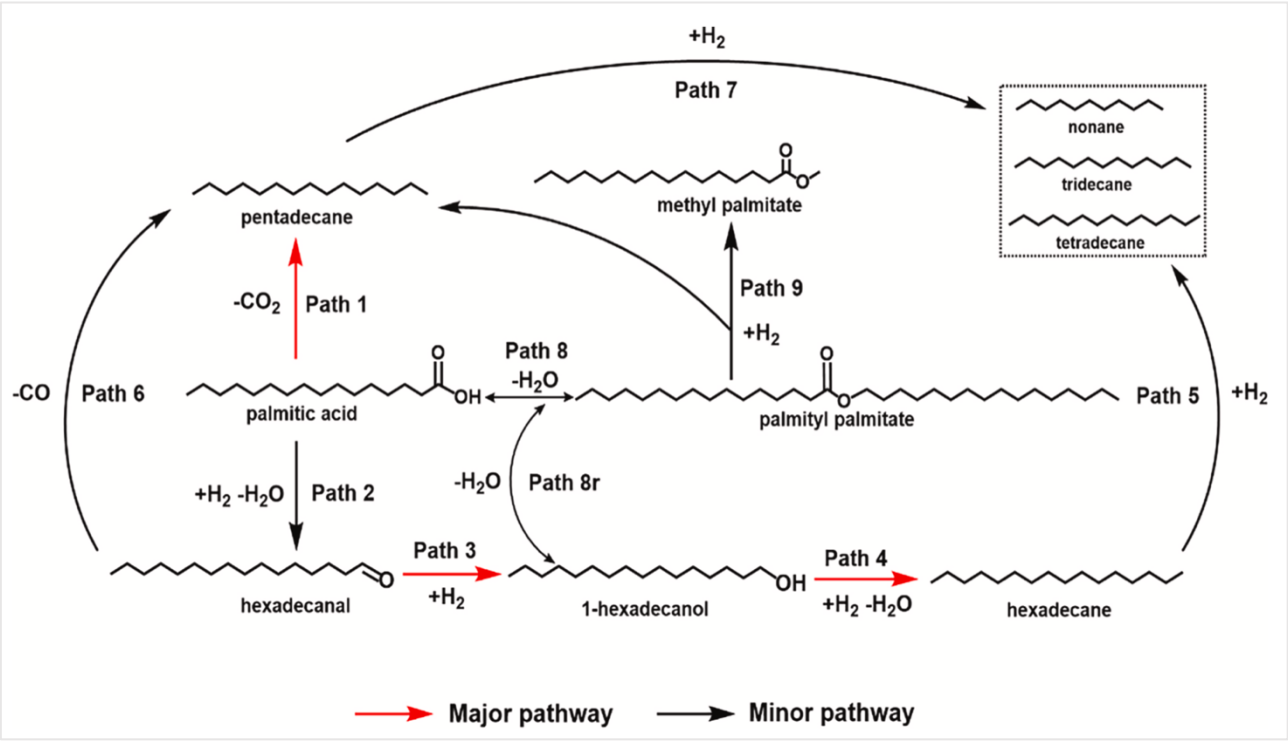

Figure 76: possible pathway for the thermo-catalytic reduction of Palmitic acid[84].

Figure 76 shows the pathways that have been recognised and the selectivity is directed to the production 1-hexadecanol, hexadecane and pentadecane. This pathway is assumed as reference also in the electrochemical hydrogenation. More detailed studies have to be done in order to generate the electrochemical reaction scheme. Anyway, from the thermo-catalytic scheme, the path 8 can be excluded since the palmityl palmitate would have been easily detected by TGA and DSC and it is not compatible with IR analysis. In the same vein, path 1 to pentadecane can be denied. However, the combination of the path 2 to hexadecanal and to the 1-hexadecanol are possible and compatible with the finding of this thesis. The path 6 is excluded since no anomalous CO concentration has been detected.

V. Other reactions: one reaction can be the cleavage of the long chain of fatty acid. It is not well known the dynamic and the products that could ideally produce in the system under study. It cannot be excluded that these reactions have happened, since some shorten fatty acids have been detected in the IR analysis and partially confirmed also in the DSC and TGA analysis.

In summary of the potential reaction pathways considered in this study, the possible paths selected are: 1) electrochemical assisted chemical esterification (reaction (XIII)); 2) direct hydrogenation to pentadecanal and to the 1-hexadecanol, and, finally, (3) cleavage of the fatty acid chain, which are possible and compatible with the finding of this thesis. Further studies on this direction must be done.

3.4 Summary of the results

This paragraph summarised the results obtained by the different techniques:

I. From the CVs, an electrochemical activity of PA/NaPal at -0,7 V (depending on the pH, concentration of PA and other reaction conditions) has been clearly identified. It has been found recurrent in many tests with different set-up and even with different supporting electrolytes. Furthermore, thanks to DPV analyses, this electrochemical activity was detected even though it wasn't always evident from the CV. From the blank test instead, no peaks have been detected. The reaction has been found to be irreversible or quasi-reversible, as expected. The currents related to the peaks are modest but acceptable.

II. From the bulk electrolysis or chronoamperometry at the target potential, the studies at different concentration of palmitic acid (Figure 54 and Figure 55) with almost constant conditions, highlights that the current is dependent on the PA concentration. Indeed, the accumulated charges were sensibly higher by increasing the PA concentration. Moreover, the pH of the solution tends to averagely increase, signal that could be associated to the PA transformation.

III. From the analyses on the headspace, no notable compounds have been detected. The oxygen content was unsuspectingly higher, but the hydrogen was present in a small portion, meaning that the current detected from the CA derives from the electrochemistry of PA.

IV. From IR-spectroscopy the comparison between the CH_3 and CH_2 symmetrical stretching vibrations shows that the sample treated electrochemically have a relatively higher ratio with respect to the PA reference. This can be due to electrolyte interaction (solvent or supporting electrolyte), but mainly because of the grade of hydrogenation and eventually a cleavage of the carbon chain. IR spectroscopy also showed that the ratio of the C=O bonds and –OH are very different between the pristine samples and the one after bulk electrolysis. This is compatible with fatty acids with shorter chains or the presence of alcohols.

V. From TGA analyses, the curves respect the equilibrium between PA/NaPal, related to the solution pH. Furthermore, a linear relationship between potential applied and residual mass has been found. The tests in air show that residual mass is mostly a carbonaceous mass, that can be oxidised. The curves also show that other compounds are present in the sample, which sometimes have on-set temperature between the PA and NaPal or even below the PA (Annex 15).

VI. The DSC analyses confirm that at the target potential, the purity of PA decreases nonlinearly respect the other studies performed at non-target potential. This is the most important fact that confirm that the PA has been attacked. Moreover, different peaks, not correlated with the NaPal acidification, have been detected (Annex 16).

VII. For the GC-MS, a precise and reliable method is still under investigation. Nevertheless, the chromatograms of the positive tests, present a peak that fits with reduced compound derived from PA, such as hexadecanol.

VIII. The possible reaction pathway is related mainly on two branches: (1) direct hydrogenation to hexadecanal and to 1-hexadecanol or pentadecanol; eventually the (2) cleavage of the fatty acid chain to produce unknown compounds.

4. Conclusions

HTL is a promising process for the treatment of wet biomass without costly and energy expensive pre-treatments. The derived biocrude is a source of energy that could potentially be used as drop-in fuel. From the other hand, electrocatalytic processes for bio-based chemicals upgrading rely on a very high energy efficiency and a good versatility in term of space, cost and easy implementation, as well as low impacts due to the possible integration with delocalised renewables energy sources.

The aim of this study was born with the necessity to integrate these two processes in order to have a feasible and cost-effective processes for the direct production of biofuels. The ambitious project started with a feasibility study with a model compound, Palmitic acid. As said at the beginning, this work is an innovative approach, sometimes even with no literature support; therefore, the aim was to perform fundamental analysis on the electrocatalytic hydrogenation, analysing the reactivity and the potential problems of future developed and up-scaled systems.

PA represents a good and suitable model compound for this study since it represents a notable fraction in the reference biocrudes. Moreover, PA/NaPal is also one of the most unreactive compounds present in the biocrude, due to the saturated chain, the carboxylic group and its oxidation state; the study could hypothetically be applied for biocrude solutions, which should be more reactive and easier to hydrogenate with these systems.

From this study, important conclusions have been found. From the point of view of the feasibility of the electrochemical process, different proofs and analysis have confirmed the possibility to attack electrochemically the PA and perform an electrocatalytic hydrogenation (see the paragraph 3.4). The identification of a linear relationship between the potential applied and the carbonaceous mass produced *in-situ,* represents an important insight for future studies. Moreover, the pH has proved to be an essential parameter to monitor in order to analyse the dynamics in the electrolyte solution.

In summary, the work of this thesis has shown that an upgrading of one of the most relevant components of the biocrude is possible, even though a series of improvements and test must be considered. The reduction of the PA to 1-hexadecanol or hexadecanal could ideally stabilise a PA-based biocrude in term of pH, viscosity and calorific power, as well as in term of distillation temperature (decreasing the boiling point). This reaction could represent a considerable improvement on the energy efficiency of the overall HTL process. In fact, electrocatalytic upgrading processes, coupled with HTL, could represent a simple, reliable and sustainable alternative for the biocrude production from wet biomass.

4.1 Future Studies

This study is at the initial phase, the potential still has to be exploited and further analysis must be implemented in order to empower the overall work. Future studies will focus on the optimisation of the overall electrochemical systems, the exploration of other set-up, the recognition of the possible products by a solid protocol, and the implementation of a suitable catalyst in term of activity and stability. Based on this work, different study lines can be followed:

I. One direction must focus on the improvement of the electrochemical set-up. It can be done using suitable implementations for the in-situ-analysis of the gases, pressure detection or methods to standardise the electrode geometry and limited the uncompensated resistances.

II. The second direction aims to evaluate the suitable electrocatalyst for the ECH of PA or the biocrude directly. The investigations of new active and stable material should be the priority, in order to try to perform quantitative analyses. In this optic, there will be more studies with catalysts produced in the University of Bologna. They are optimised electrocatalysts synthetised by electrodeposition of metal nanoparticle (Ag, Ni, Cu, In, Zn) on highly porous metal foams mainly made of Ni or Cu (see Figure 77). The enhanced surface area with the nano-scale coating of active sites should, in theory increase the activity of the catalyst toward electrochemical reactions.

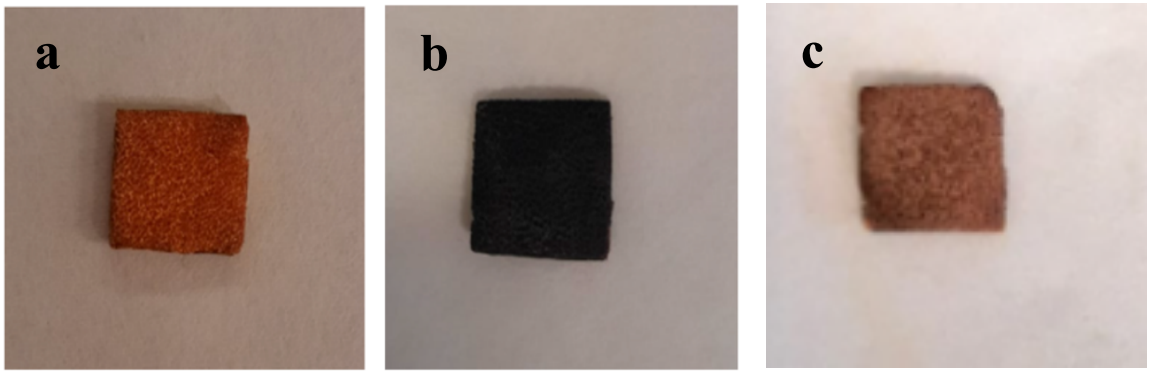

Figure 77: Example of a 1x1 Cu foam before (a) and after (b) electrodeposition with Ag nanoparticles and after Cu nanoparticles (c). University of Bologna.

Figure 78 shows the SEM images of a successful Cu foam with Cu nanoparticles electrodeposited. As suggested by Figure 33, another strategy to increase the activity could be related with the enhancement of the intrinsic activity of the electrocatalyst with engineered nanostructures. From this point of view, there are many potential improvements that could be applied to the study. This work used only an industrial and standard Ni foam, since it was available, cheap and very versatile for the feasibility analysis that had to be done.

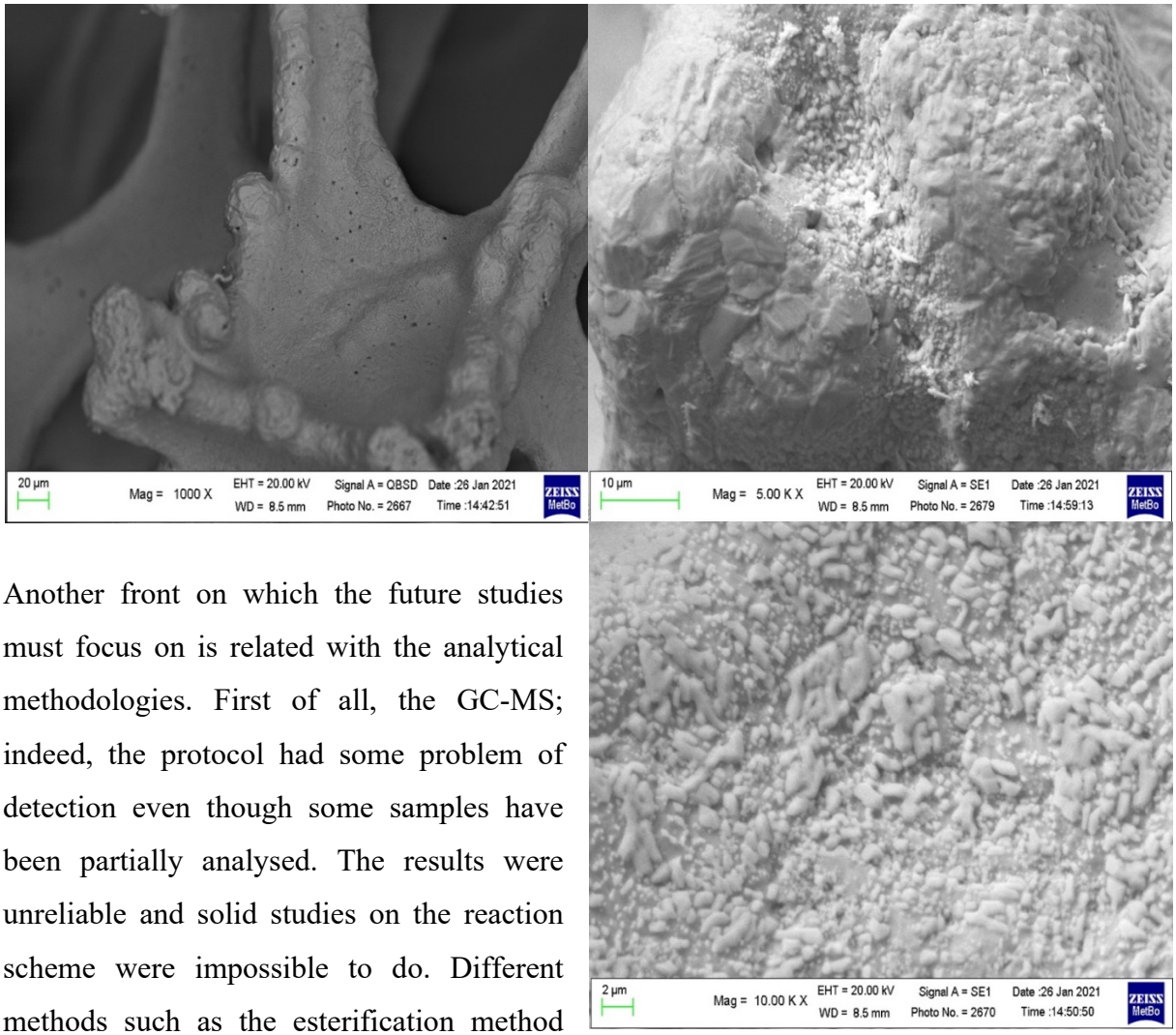

Figure 78: SEM images of a Cu foam electrodeposited with Cu nanoparticles. University of Bologna.

III. Another front on which the future studies must focus on is related with the analytical methodologies. First of all, the GC-MS; indeed, the protocol had some problem of detection even though some samples have been partially analysed. The results were unreliable and solid studies on the reaction scheme were impossible to do. Different methods such as the esterification method described by Breton e*t al.* for the fatty acid detection at the GC.MS[81] must be explored and implemented. Also the FTIR-spectroscopy analysis has to be improved; the deconvolution of the peaks must be done in order to have more reliable results.

IV. Another study line is related with the tests on the biocrude. In fact, the final aim is to produce a relatively simple electrochemical set-up for the biocrude ECH. The composition is variable, and with that also the electrochemistry. Therefore, it is essential to perform test with different type of biocrudes and in different conditions. The work was focused on the activity of PA, nevertheless, some tests on a woody biocrude have been performed. Since, the feedstock from which the biocrude has been produced wasn't one of the three target ones (*Miscanthus, Spirulina* and sewage sludge), the results from these analyses are explained only in term of future directions which the study can undertake. Therefore, Figure 79 shows the chromatograms

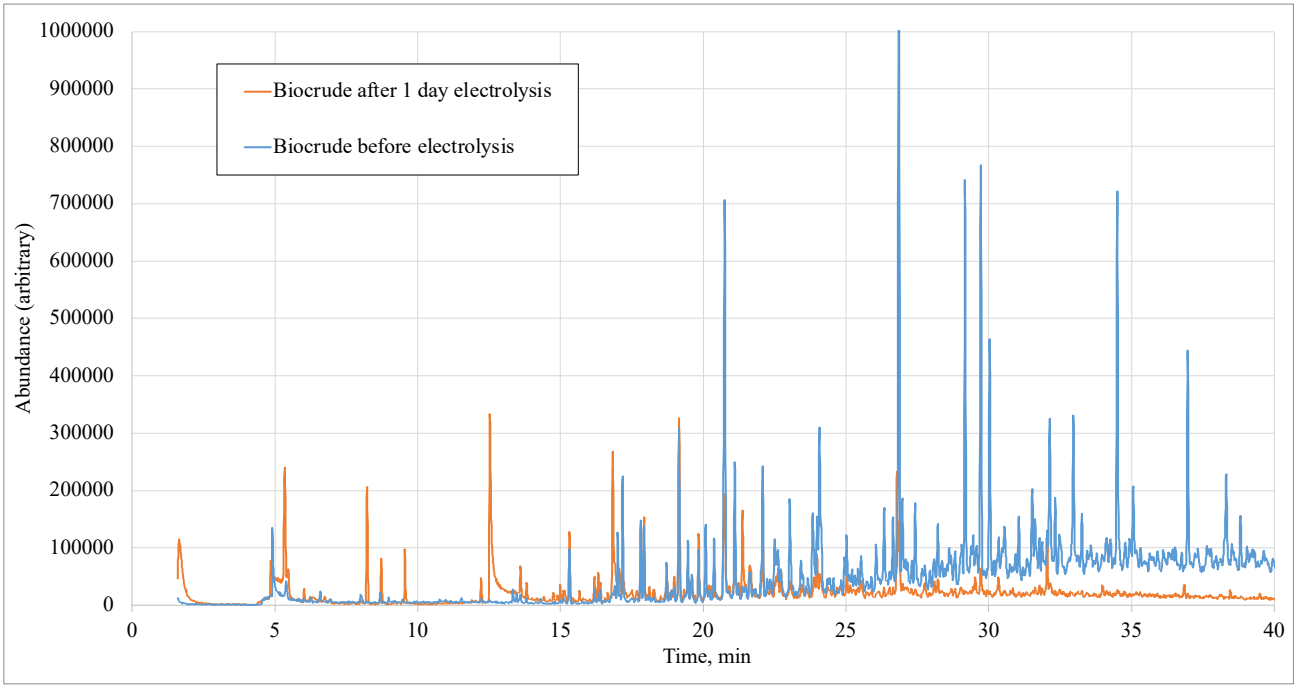

Figure 79: Chromatograms of the biocrude before electrolysis and after one day electrolysis.

resulted from the unreacted biocrude (blue) and the biocrude after one day of bulk electrolysis (orange). It is visible that the high molecular weight components present in the unreacted biocrude are practically eliminated or lowered with the ECH, creating new and higher peaks at lower retention times, symbol of lower molecular weight. This study has been displayed to underline the potential of this study.

These future lines highlight the huge unexploited potential of this study. A lot of work must be done, and the different lines can be followed. This work represents only the beginning.

Acknowledgments

One last word must be spent for all those who will treasure this work, even only for a sentence read or for a sense of curiosity. I would like to share a small thought with you, a personal vision, which I hope you can appreciate after all these impersonal and analytical pages.

"*Remember that any contribution, even though minimal, makes you a change maker. Because the worthy things derived from small pieces that only united can form an amazing picture; a picture of a new world. A living world full of energy, green energy, globally available without discriminations. A world where energetic systems run by local resources will help to fight poverty and inequality. In this world, the waste becomes the first resource, and innovations interact with people's life creating progress and wellbeing.*
No more third-party interests, only one: our planet, Mother Earth.
Piece by piece this world will arise, but no one will tell you what the final image of the puzzle will be, it will be up to all of you to choose which path to follow and which future to pursue. It will be difficult, many obstacles must be faced and overcome, but once arrived, you will recognise the mistakes made; you will just realise that you were not alone; it will be just the darker chapter of our history".

Just as it is not possible to solve the world's worst problems alone, this thesis has been the fruit of many people, collaborations, and support. For this reason, I would like to thank firstly my two supervisors, Patricia, and Jacopo. Thank you for the time and the availability you have dedicated to me, you have been a source of inspiration and motivation. Thank you also for the patience and support you have shown during these uncertain periods when it would have been very easy to get lost. Sincere thanks also go to all those with whom I share my experience in the laboratories, especially to Monica, Paolo and Prime.

It was not easy to get to this step; a pandemic in the way, a few months delay, a new country to discover and all the consequent problems. But despite of this, I can finally say that I made it! And this is surely also thanks to those who always believed in me even if from distance. Thanks therefore to my whole family; my parents, my brothers, my grandparents and all the other members. Words are not enough to show all my gratitude for the constant support and for the sacrifices they have made to let me achieve this point.

Thanks also to all my friends. They have been my strength, the constant presence that has helped me even in the most difficult moments of this journey. In particular to Giulia, Fabrizio, my daily motivators, Caroline, Lara, Silvia, Sara and Luca. But also to Dott. Brogis, with whom I shared moments of joy, fun and indecision in one of the most beautiful cities I have ever experienced, Bologna. The time has passed very fast, but I am sure we will have the chance to empower the beautiful things we have created, together.

And with these acknowledgements, a chapter of my life is about to end. But, as I usually remind myself: “do not be afraid of changes, they bring fresh air, they bring progress”.
Who knows where I will end up next?

Francesco

Bibliography

(1) Ritchie, H.; Roser, M. CO_2 and Greenhouse Gas Emissions - Https://Ourworldindata.Org/Co2-and-Other-Greenhouse-Gas-Emissions.
(2) Steffen, W.; Richardson, K.; Rockstrom, J.; Cornell, S. E.; Fetzer, I.; Bennett, E. M.; Biggs, R.; Carpenter, S. R.; de Vries, W.; de Wit, C. A.; Folke, C.; Gerten, D.; Heinke, J.; Mace, G. M.; Persson, L. M.; Ramanathan, V.; Reyers, B.; Sorlin, S. Planetary Boundaries: Guiding Human Development on a Changing Planet. *Science* **2015**, *347* (6223), 1259855–1259855. https://doi.org/10.1126/science.1259855.
(3) Poore, J.; Nemecek, T. Reducing Food's Environmental Impacts through Producers and Consumers. *Science* **2018**, *360* (6392), 987–992. https://doi.org/10.1126/science.aaq0216.
(4) of the United Nations, F. and A. O. *The State of the World's Land and Water Resources for Food and Agriculture*, 0 ed.; Routledge, 2013. https://doi.org/10.4324/9780203142837.
(5) Naik, S. N.; Goud, V. V.; Rout, P. K.; Dalai, A. K. Production of First and Second Generation Biofuels: A Comprehensive Review. *Renew. Sustain. Energy Rev.* **2010**, *14* (2), 578–597. https://doi.org/10.1016/j.rser.2009.10.003.
(6) Nazari, M. T. Biofuels and Their Connections with the Sustainable Development Goals: A Bibliometric and Systematic Review. 18.
(7) Abdullah, B.; Syed Muhammad, S. A. F.; Shokravi, Z.; Ismail, S.; Kassim, K. A.; Mahmood, A. N.; Aziz, M. M. A. Fourth Generation Biofuel: A Review on Risks and Mitigation Strategies. *Renew. Sustain. Energy Rev.* **2019**, *107*, 37–50. https://doi.org/10.1016/j.rser.2019.02.018.
(8) Bharathiraja, B.; Yogendran, D.; Kumar, R. R.; Chakravarthy, M.; Palani, S. Biofuels from Sewage Sludge- A Review. 12.
(9) Kamm, B.; Kamm, M. Principles of Biorefineries. *Appl. Microbiol. Biotechnol.* **2004**, *64* (2), 137–145. https://doi.org/10.1007/s00253-003-1537-7.
(10) Ong, H. C.; Chen, W.-H.; Singh, Y.; Gan, Y. Y.; Chen, C.-Y.; Show, P. L. A State-of-the-Art Review on Thermochemical Conversion of Biomass for Biofuel Production: A TG-FTIR Approach. *Energy Convers. Manag.* **2020**, *209*, 112634. https://doi.org/10.1016/j.enconman.2020.112634.
(11) Abdulyekeen, K. A.; Umar, A. A.; Patah, M. F. A.; Daud, W. M. A. W. Torrefaction of Biomass: Production of Enhanced Solid Biofuel from Municipal Solid Waste and Other Types of Biomass. *Renew. Sustain. Energy Rev.* **2021**, *150*, 111436. https://doi.org/10.1016/j.rser.2021.111436.
(12) Chen, W.-H.; Lin, B.-J.; Lin, Y.-Y.; Chu, Y.-S.; Ubando, A. T.; Show, P. L.; Ong, H. C.; Chang, J.-S.; Ho, S.-H.; Culaba, A. B.; Pétrissans, A.; Pétrissans, M. Progress in Biomass Torrefaction: Principles, Applications and Challenges. *Prog. Energy Combust. Sci.* **2021**, *82*, 100887. https://doi.org/10.1016/j.pecs.2020.100887.
(13) Aragón-Briceño, C. I.; Pozarlik, A. K.; Bramer, E. A.; Niedzwiecki, L.; Pawlak-Kruczek, H.; Brem, G. Hydrothermal Carbonization of Wet Biomass from Nitrogen and Phosphorus Approach: A Review. *Renew. Energy* **2021**, *171*, 401–415. https://doi.org/10.1016/j.renene.2021.02.109.
(14) Canabarro, N.; Soares, J. F.; Anchieta, C. G.; Kelling, C. S.; Mazutti, M. A. Thermochemical Processes for Biofuels Production from Biomass. *Sustain. Chem. Process.* **2013**, *1* (1), 22. https://doi.org/10.1186/2043-7129-1-22.
(15) Klaimy, S.; Lamonier, J.-F.; Casetta, M.; Heymans, S.; Duquesne, S. Recycling of Plastic Waste Using Flash Pyrolysis – Effect of Mixture Composition. *Polym. Degrad. Stab.* **2021**, *187*, 109540. https://doi.org/10.1016/j.polymdegradstab.2021.109540.
(16) Anastasakis, K.; Biller, P.; Madsen, R.; Glasius, M.; Johannsen, I. Continuous Hydrothermal

Liquefaction of Biomass in a Novel Pilot Plant with Heat Recovery and Hydraulic Oscillation. *Energies* **2018**, *11* (10), 2695. https://doi.org/10.3390/en11102695.
(17) Wang, C.; Kong, Y.; Hu, R.; Zhou, G. *Miscanthus* : A Fast-growing Crop for Environmental Remediation and Biofuel Production. *GCB Bioenergy* **2021**, *13* (1), 58–69. https://doi.org/10.1111/gcbb.12761.
(18) Ge, S.; Brindhadevi, K.; Xia, C.; Salah Khalifa, A.; Elfasakhany, A.; Unpaprom, Y.; Doan, H. V. Enhancement of the Combustion, Performance and Emission Characteristics of Spirulina Microalgae Biodiesel Blends Using Nanoparticles. *Fuel* **2022**, *308*, 121822. https://doi.org/10.1016/j.fuel.2021.121822.
(19) Chen, W.-T.; Zhang, Y.; Lee, T. H.; Wu, Z.; Si, B.; Lee, C.-F. F.; Lin, A.; Sharma, B. K. Renewable Diesel Blendstocks Produced by Hydrothermal Liquefaction of Wet Biowaste. *Nat. Sustain.* **2018**, *1* (11), 702–710. https://doi.org/10.1038/s41893-018-0172-3.
(20) Guo, Y.; Yeh, T.; Song, W.; Xu, D.; Wang, S. A Review of Bio-Oil Production from Hydrothermal Liquefaction of Algae. *Renew. Sustain. Energy Rev.* **2015**, *48*, 776–790. https://doi.org/10.1016/j.rser.2015.04.049.
(21) Seshasayee, M. S.; Savage, P. E. Oil from Plastic via Hydrothermal Liquefaction: Production and Characterization. *Appl. Energy* **2020**, *278*, 115673. https://doi.org/10.1016/j.apenergy.2020.115673.
(22) Jia, P.; Wang, J.; Zhang, W. Catalytic Hydrothermal Liquefaction of Lignin over Carbon Nanotube Supported Metal Catalysts for Production of Monomeric Phenols. *J. Energy Inst.* **2021**, *94*, 1–10. https://doi.org/10.1016/j.joei.2020.09.014.
(23) Yang, J.; Chen, H.; Liu, Q.; Zhou, N.; Wu, Y.; He, Q. (Sophia). Is It Feasible to Replace Freshwater by Seawater in Hydrothermal Liquefaction of Biomass for Biocrude Production? *Fuel* **2020**, *282*, 118870. https://doi.org/10.1016/j.fuel.2020.118870.
(24) Xue, Y.; Chen, H.; Zhao, W.; Yang, C.; Ma, P.; Han, S. A Review on the Operating Conditions of Producing Bio-Oil from Hydrothermal Liquefaction of Biomass: Producing Bio-Oil from Hydrothermal Liquefaction of Biomass. *Int. J. Energy Res.* **2016**, *40* (7), 865–877. https://doi.org/10.1002/er.3473.
(25) Saber, M.; Nakhshiniev, B.; Yoshikawa, K. A Review of Production and Upgrading of Algal Bio-Oil. *Renew. Sustain. Energy Rev.* **2016**, *58*, 918–930. https://doi.org/10.1016/j.rser.2015.12.342.
(26) Xiu, S.; Shahbazi, A. Bio-Oil Production and Upgrading Research: A Review. *Renew. Sustain. Energy Rev.* **2012**, *16* (7), 4406–4414. https://doi.org/10.1016/j.rser.2012.04.028.
(27) Watson, J.; Wang, T.; Si, B.; Chen, W.-T.; Aierzhati, A.; Zhang, Y. Valorization of Hydrothermal Liquefaction Aqueous Phase: Pathways towards Commercial Viability. *Prog. Energy Combust. Sci.* **2020**, *77*, 100819. https://doi.org/10.1016/j.pecs.2019.100819.
(28) Xu, D.; Lin, G.; Guo, S.; Wang, S.; Guo, Y.; Jing, Z. Catalytic Hydrothermal Liquefaction of Algae and Upgrading of Biocrude: A Critical Review. *Renew. Sustain. Energy Rev.* **2018**, *97*, 103–118. https://doi.org/10.1016/j.rser.2018.08.042.
(29) Venteris, E. R.; Skaggs, R. L.; Wigmosta, M. S.; Coleman, A. M. A National-Scale Comparison of Resource and Nutrient Demands for Algae-Based Biofuel Production by Lipid Extraction and Hydrothermal Liquefaction. *Biomass Bioenergy* **2014**, *64*, 276–290. https://doi.org/10.1016/j.biombioe.2014.02.001.
(30) Bhagwandas, J. This Experimental Research (August – November 2014) Is Done in Commission of SINTEF Energy Research, Located in Trondheim (Norway). It Is Done by Jina Charissa Bhagwandas, Author of This Report, for the Completion of Her Internship (20 European Credits) of the Study Mechanical Engineering with as Specialization Thermal Engineering at the University of Twente, Located in Enschede (Netherlands). 30.
(31) Gollakota, A. R. K.; Kishore, N.; Gu, S. A Review on Hydrothermal Liquefaction of Biomass. *Renew. Sustain. Energy Rev.* **2018**, *81*, 1378–1392. https://doi.org/10.1016/j.rser.2017.05.178.

(32) Pedersen, T. H.; Jensen, C. U.; Sandström, L.; Rosendahl, L. A. Full Characterization of Compounds Obtained from Fractional Distillation and Upgrading of a HTL Biocrude. *Appl. Energy* **2017**, *202*, 408–419. https://doi.org/10.1016/j.apenergy.2017.05.167.
(33) Nagappan, S.; Bhosale, R. R.; Nguyen, D. D.; Chi, N. T. L.; Ponnusamy, V. K.; Woong, C. S.; Kumar, G. Catalytic Hydrothermal Liquefaction of Biomass into Bio-Oils and Other Value-Added Products – A Review. *Fuel* **2021**, *285*, 119053. https://doi.org/10.1016/j.fuel.2020.119053.
(34) Akhtar, J.; Amin, N. A. S. A Review on Process Conditions for Optimum Bio-Oil Yield in Hydrothermal Liquefaction of Biomass. *Renew. Sustain. Energy Rev.* **2011**, *15* (3), 1615–1624. https://doi.org/10.1016/j.rser.2010.11.054.
(35) Rothenberg, G. *Catalysis: Concepts and Green Applications*; WILEY-VCH: Weinheim, Bergstr, 2008.
(36) Chen, Y.; Mu, R.; Yang, M.; Fang, L.; Wu, Y.; Wu, K.; Liu, Y.; Gong, J. Catalytic Hydrothermal Liquefaction for Bio-Oil Production over CNTs Supported Metal Catalysts. *Chem. Eng. Sci.* **2017**, *161*, 299–307. https://doi.org/10.1016/j.ces.2016.12.010.
(37) Djandja, O. S.; Wang, Z.; Chen, L.; Qin, L.; Wang, F.; Xu, Y.; Duan, P. Progress in Hydrothermal Liquefaction of Algal Biomass and Hydrothermal Upgrading of the Subsequent Crude Bio-Oil: A Mini Review. *Energy Fuels* **2020**, *34* (10), 11723–11751. https://doi.org/10.1021/acs.energyfuels.0c01973.
(38) Lu, J.; Wu, J.; Zhang, L.; Liu, Z.; Wu, Y.; Yang, M. Catalytic Hydrothermal Liquefaction of Microalgae over Mesoporous Silica-Based Materials with Site-Separated Acids and Bases. *Fuel* **2020**, *279*, 118529. https://doi.org/10.1016/j.fuel.2020.118529.
(39) Castello, D.; Haider, M. S.; Rosendahl, L. A. Catalytic Upgrading of Hydrothermal Liquefaction Biocrudes: Different Challenges for Different Feedstocks. *Renew. Energy* **2019**, *141*, 420–430. https://doi.org/10.1016/j.renene.2019.04.003.
(40) Hansen, S.; Mirkouei, A.; Diaz, L. A. A Comprehensive State-of-Technology Review for Upgrading Bio-Oil to Renewable or Blended Hydrocarbon Fuels. *Renew. Sustain. Energy Rev.* **2020**, *118*, 109548. https://doi.org/10.1016/j.rser.2019.109548.
(41) Lian, X.; Xue, Y.; Zhao, Z.; Xu, G.; Han, S.; Yu, H. Progress on Upgrading Methods of Bio-Oil: A Review: Upgrading Progress of Bio-Oil. *Int. J. Energy Res.* **2017**, *41* (13), 1798–1816. https://doi.org/10.1002/er.3726.
(42) Jiang, X.; Ellis, N. Upgrading Bio-Oil through Emulsification with Biodiesel: Mixture Production. *Energy Fuels* **2010**, *24* (2), 1358–1364. https://doi.org/10.1021/ef9010669.
(43) Lam, C. H.; Deng, W.; Lang, L.; Jin, X.; Hu, X.; Wang, Y. Minireview on Bio-Oil Upgrading via Electrocatalytic Hydrogenation: Connecting Biofuel Production with Renewable Power. *Energy Fuels* **2020**, *34* (7), 7915–7928. https://doi.org/10.1021/acs.energyfuels.0c01380.
(44) Li, Z.; Kelkar, S.; Raycraft, L.; Garedew, M.; Jackson, J. E.; Miller, D. J.; Saffron, C. M. A Mild Approach for Bio-Oil Stabilization and Upgrading: Electrocatalytic Hydrogenation Using Ruthenium Supported on Activated Carbon Cloth. *Green Chem* **2014**, *16* (2), 844–852. https://doi.org/10.1039/C3GC42303D.
(45) ASTM D5291-16, Standard Test Methods for Instrumental Determination of Carbon, Hydrogen, and Nitrogen in Petroleum Products and Lubricants, ASTM International, West Conshohocken, PA, 2016, Www.Astm.Org.
(46) Harnisch, F.; Urban, C. Electrobiorefineries: Unlocking the Synergy of Electrochemical and Microbial Conversions. *Angew. Chem. Int. Ed.* **2018**, *57* (32), 10016–10023. https://doi.org/10.1002/anie.201711727.
(47) Akhade, S. A.; Singh, N.; Gutiérrez, O. Y.; Lopez-Ruiz, J.; Wang, H.; Holladay, J. D.; Liu, Y.; Karkamkar, A.; Weber, R. S.; Padmaperuma, A. B.; Lee, M.-S.; Whyatt, G. A.; Elliott, M.; Holladay, J. E.; Male, J. L.; Lercher, J. A.; Rousseau, R.; Glezakou, V.-A. Electrocatalytic Hydrogenation of Biomass-Derived Organics: A Review. *Chem. Rev.* **2020**, *120* (20), 11370–11419. https://doi.org/10.1021/acs.chemrev.0c00158.
(48) Pala, M.; Guo, K.; Prins, W.; Ronsse, F.; Rabaey, K. Electrochemical Upgrading of Bio-Oil:

A Proof-of-Principle Investigation. 21.
(49) Seh, Z. W.; Kibsgaard, J.; Dickens, C. F.; Chorkendorff, I.; Nørskov, J. K.; Jaramillo, T. F. Combining Theory and Experiment in Electrocatalysis: Insights into Materials Design. *Science* **2017**, *355* (6321), eaad4998. https://doi.org/10.1126/science.aad4998.
(50) Song, Y.; Chia, S. H.; Sanyal, U.; Gutiérrez, O. Y.; Lercher, J. A. Integrated Catalytic and Electrocatalytic Conversion of Substituted Phenols and Diaryl Ethers. *J. Catal.* **2016**, *344*, 263–272. https://doi.org/10.1016/j.jcat.2016.09.030.
(51) Lister, T. E.; Diaz, L. A.; Lilga, M. A.; Padmaperuma, A. B.; Lin, Y.; Palakkal, V. M.; Arges, C. G. Low-Temperature Electrochemical Upgrading of Bio-Oils Using Polymer Electrolyte Membranes. *Energy Fuels* **2018**, *32* (5), 5944–5950. https://doi.org/10.1021/acs.energyfuels.8b00134.
(52) Mayer, J. M. PROTON-COUPLED ELECTRON TRANSFER: A Reaction Chemist's View. *Annu. Rev. Phys. Chem.* **2004**, *55* (1), 363–390. https://doi.org/10.1146/annurev.physchem.55.091602.094446.
(53) Andrews, E.; Lopez-Ruiz, J. A.; Egbert, J. D.; Koh, K.; Sanyal, U.; Song, M.; Li, D.; Karkamkar, A. J.; Derewinski, M. A.; Holladay, J.; Gutiérrez, O. Y.; Holladay, J. D. Performance of Base and Noble Metals for Electrocatalytic Hydrogenation of Bio-Oil-Derived Oxygenated Compounds. *ACS Sustain. Chem. Eng.* **2020**, *8* (11), 4407–4418. https://doi.org/10.1021/acssuschemeng.9b07041.
(54) Zhang, B.; Zhang, J.; Zhong, Z. Low-Energy Mild Electrocatalytic Hydrogenation of Bio-Oil Using Ruthenium Anchored in Ordered Mesoporous Carbon. *ACS Appl. Energy Mater.* **2018**, *1* (12), 6758–6763. https://doi.org/10.1021/acsaem.8b01718.
(55) Wang, X.; Deng, W.; Lam, C. H.; Xiong, Y.; Xiong, Z.; Xu, J.; Jiang, L.; Su, S.; Hu, S.; Wang, Y.; Xiang, J. Coke Formation and Its Impacts during Electrochemical Upgrading of Bio-Oil. *Fuel* **2021**, *306*, 121664. https://doi.org/10.1016/j.fuel.2021.121664.
(56) dos Santos, T. R.; Nilges, P.; Sauter, W.; Harnisch, F.; Schröder, U. Electrochemistry for the Generation of Renewable Chemicals: Electrochemical Conversion of Levulinic Acid. *RSC Adv.* **2015**, *5* (34), 26634–26643. https://doi.org/10.1039/C4RA16303F.
(57) Carta, G.; Murru, E.; Banni, S.; Manca, C. Palmitic Acid: Physiological Role, Metabolism and Nutritional Implications. *Front. Physiol.* **2017**, *8*, 902. https://doi.org/10.3389/fphys.2017.00902.
(58) National Center for Biotechnology Information (2021). PubChem Compound Summary for CID 985, Palmitic Acid. Retrieved September 26, 2021 from Https://Pubchem.Ncbi.Nlm.Nih.Gov/Compound/Palmitic-Acid.
(59) *Handbook of Electrochemistry*, 1st ed.; Zoski, C. G., Ed.; Elsevier: Amsterdam ; Boston, 2007.
(60) Lamagni, P. Carbon Cioxide: C1 Synthon over MOF-Modified Electrodes, Electron Mediator in Photocatalysis - PhD Thesis. 245.
(61) Bard, A. J.; Faulkner, L. R. *Electrochemical Methods: Fundamentals and Applications*, 2nd ed.; Wiley: New York, 2001.
(62) Ho, J.; Coote, M. L.; Cramer, C. J.; Truhlar, D. G. Theoretical Calculation of Reduction Potentials. 50.
(63) Gong, K.; Fang, Q.; Gu, S.; Li, S. F. Y.; Yan, Y. Nonaqueous Redox-Flow Batteries: Organic Solvents, Supporting Electrolytes, and Redox Pairs. *Energy Environ. Sci.* **2015**, *8* (12), 3515–3530. https://doi.org/10.1039/C5EE02341F.
(64) Calvo, B.; Collado, I.; Cepeda, E. A. Solubilities of Palmitic Acid in Pure Solvents and Its Mixtures. *J. Chem. Eng. Data* **2009**, *54* (1), 64–68. https://doi.org/10.1021/je8005979.
(65) Elgrishi, N.; Rountree, K. J.; McCarthy, B. D.; Rountree, E. S.; Eisenhart, T. T.; Dempsey, J. L. A Practical Beginner's Guide to Cyclic Voltammetry. *J. Chem. Educ.* **2018**, *95* (2), 197–206. https://doi.org/10.1021/acs.jchemed.7b00361.
(66) Anastas, P.; Eghbali, N. Green Chemistry: Principles and Practice. *Chem Soc Rev* **2010**, *39*

(1), 301–312. https://doi.org/10.1039/B918763B.
(67) *Handbook of Reference Electrodes*; Inzelt, G., Lewenstam, A., Scholz, F., Eds.; Springer Berlin Heidelberg: Berlin, Heidelberg, 2013. https://doi.org/10.1007/978-3-642-36188-3.
(68) Lee, J. Electrochemical Sensing of Oxygen Gas in Ionic Liquids on Screen Printed Electrodes. 266.
(69) Landesfeind, J.; Ehrl, A.; Graf, M.; Wall, W. A.; Gasteiger, H. A. Direct Electrochemical Determination of Thermodynamic Factors in Aprotic Binary Electrolytes. *J. Electrochem. Soc.* **2016**, *163* (7), A1254–A1264. https://doi.org/10.1149/2.0651607jes.
(70) Lesch, A.; Cortés-Salazar, F.; Prudent, M.; Delobel, J.; Rastgar, S.; Lion, N.; Tissot, J.-D.; Tacchini, P.; Girault, H. H. Large Scale Inkjet-Printing of Carbon Nanotubes Electrodes for Antioxidant Assays in Blood Bags. *J. Electroanal. Chem.* **2014**, *717–718*, 61–68. https://doi.org/10.1016/j.jelechem.2013.12.027.
(71) Gill, P.; Moghadam, T. T.; Ranjbar, B. Differential Scanning Calorimetry Techniques: Applications in Biology and Nanoscience. **2010**, *21* (4), 27.
(72) *Handbook of Thermal Analysis and Calorimetry*; Gallagher, P. K., Brown, M. E., Kemp, R. B., Eds.; Elsevier: Amsterdam [Netherlands] ; New York, 1998.
(73) Coats, A. W.; Redfern, J. P. Thermogravimetric Analysis. A Review. *The Analyst* **1963**, *88* (1053), 906. https://doi.org/10.1039/an9638800906.
(74) Front Matter. In *Handbook of Spectroscopy*; Gauglitz, G., Vo-Dinh, T., Eds.; Wiley-VCH Verlag GmbH & Co. KGaA: Weinheim, FRG, 2005; pp i–xxxii. https://doi.org/10.1002/3527602305.fmatter.
(75) Socrates, G. *Infrared and Raman Characteristic Group Frequencies: Tables and Charts*, 3. ed., repr. as paperback.; Wiley: Chichester, 2010.
(76) McMaster, M. C. *GC/MS: A Practical User's Guide*, 2nd ed.; Wiley-Interscience: Hoboken, N.J, 2008.
(77) Hübschmann, H.-J. *Handbook of GC/MS: Fundamentals and Applications*, 2nd, completed rev. and updated ed ed.; Wiley-VCH: Weinheim, 2009.
(78) Krishna, Y.; Saidur, R.; Aslfattahi, N.; Faizal, M.; Ng, K. C. Enhancing the Thermal Properties of Organic Phase Change Material (Palmitic Acid) by Doping MXene Nanoflakes; Selangor Darul Ehsan, Malaysia, 2020; p 020013. https://doi.org/10.1063/5.0001366.
(79) Olatunji, O. O.; Akinlabi, S. A.; Mashinini, M. P.; Fatoba, S. O.; Ajayi, O. O. Thermo-Gravimetric Characterization of Biomass Properties: A Review. *IOP Conf. Ser. Mater. Sci. Eng.* **2018**, *423*, 012175. https://doi.org/10.1088/1757-899X/423/1/012175.
(80) Atkins, R. C.; Carey, F. A. *Student Solutions Manual to Accompany Organic Chemistry*, 7. ed.; MacGraw Hill higher education; McGraw Hill: Boston, 2008.
(81) Breton, S.; Brisach-Wittmeyer, A.; Rios Martín, J. J.; León Camacho, M.; Lasia, A.; Ménard, H. Selective Electrocatalytic Hydrogenation of Linolenic Acid on Pd / Al 2 O 3 and Pd-Co / Al 2 O 3 Catalysts. *Int. J. Electrochem.* **2011**, *2011*, 1–9. https://doi.org/10.4061/2011/485194.
(82) Chen, N.; Ye, Z.; Zhang, F. Recent Progress on Electrochemical Synthesis Involving Carboxylic Acids. *Org. Biomol. Chem.* **2021**, *19* (25), 5501–5520. https://doi.org/10.1039/D1OB00420D.
(83) Holzhäuser, F. J.; Mensah, J. B.; Palkovits, R. (Non-)Kolbe Electrolysis in Biomass Valorization – a Discussion of Potential Applications. *Green Chem.* **2020**, *22* (2), 286–301. https://doi.org/10.1039/C9GC03264A.
(84) Liu, X.; Yang, M.; Deng, Z.; Dasgupta, A.; Guo, Y. Hydrothermal Hydrodeoxygenation of Palmitic Acid over Pt/C Catalyst: Mechanism and Kinetic Modeling. *Chem. Eng. J.* **2021**, *407*, 126332. https://doi.org/10.1016/j.cej.2020.126332.
(85) Girault, H. H. *Analytical and Physical Electrochemistry*; Fundamental sciences; EPFL ; Marcel Dekker: Lausanne, Switzerland : New York, 2004.

Annexes

Annex 1: most relevant advantages, disadvantages, and issues regarding the different generation of biofuels

Topic	First generation biofuel	Second generation biofuel
Competition with food crops	Made from edible oil and starch feedstock	No food-energy conflict
Land footprint	Requires arable land	Require arable land or forests
Conversion to biofuels	Easy conversion	Need sophisticated downstream processing technologies due to high contents of hemicelluloses and lignin
Water footprint	Potable water is required for cultivation	Potable water is required for cultivation
Environment-friendliness	Using pesticides and fertilizers are of the main concerns	No expenditure on fertilizer, or pesticides; however deforestation is a concern
Commercialization	Commercially produced	Commercially produced
Sustainability	Is not conservative in use of natural resources such as water and land	Do not preserve ecology due to deforestation concerns
Nutrient requirements	Using pesticides and fertilizers are of the main concerns	No need for any fertilizer treatment
Harvesting	Harvesting is done by hand or machine picking	Harvesting is done by hand or machine picking
Regulation	The regulations are fairly clear	The regulations are fairly clear
Financial input	The capital cost is fairly low	The capital cost is fairly low
Environmental condition	Parameters such as temperature and humidity must be within a suitable range	Parameters such as temperature and humidity must be within a suitable range

Topic	Third generation biofuel	Fourth generation biofuel
Competition with food crops	No food-energy conflict	No food-energy conflict
Land footprint	Non-arable land can be used for cultivation	Non-arable land can be used for cultivation
Conversion to biofuels	Easy conversion due to increased hydrolysis and/or fermentation efficiency	Easy conversion due to increased hydrolysis and/or fermentation efficiency
Water footprint	Waste, saline and non-potable water also can be used	Waste, saline and non-potable water also can be used
Environment-friendliness	CO_2 fixation, waste water treatment, no expenditure on fertilizer are pros and ecological concerns such as marine eutrophication cons	Medium (CO_2 fixation, waste water treatment, are of the pros but release of GM organisms, is the main concern
Commercialization	Insufficient biomass production for commercialization	Insufficient biomass production for commercialization
Sustainability	Do not have favorable economics	There are concern about leaking of GMO to environment and ecological risks
Nutrient requirements	Large carbon and nitrogen sources are required. Solar energy is only available at day time. Nutrients can be recycled in the process	Large carbon and nitrogen sources are required. Solar energy is only available at day time. Nutrients can be recycled in the process
Harvesting	Harvesting of microalgae is expensive, and complicated	Harvesting of microalgae is expensive, and complicated
Regulation	No regulation is available for marine cultivation	No regulation is available for marine cultivation furthermore strict regulation are for the intended release of GM algae
Financial input	The initial cost for large scale cultivation is too high	The initial cost for large scale cultivation is too high
Environmental condition	Can be cultivated in harsh environmental condition such high pH, salinity high light intensities	Can be cultivated in harsh environmental condition such high pH, salinity high light intensities

Annex 2: elemental composition, HHV and biocrude yield of some HTL feedstocks.

S.No	Feedstock	Elemental composition of product species after HTL								
		C (%)	H (%)	N (%)	O (%)	S (%)	Ash (%)	Moisture (%)	HHV	% Yield
1	Spirulina algae	68.9	8.9	6.5	14.9	0.86	–	–	33.2	32.6
2	Swine manure	71.2	9.5	3.7	15.6	0.12	–	–	34.7	30.2
3	Anaerobic sludge	66.6	9.2	4.3	18.9	0.97	–	–	32.0	9.4
4	Arthrospira platensis	74.5	10.2	6.8	7.5	1.0	–	–	38.65	30
5	Tetraselmis	71.4	9.5	5.7	12.3	1.1	–	–	35.58	29
6	Nannochloropsis gaditana	76.1	10.3	4.5	8.8	0.4	–	–	38.00	
7	Scenedesmus almeriensis	74.9	9.1	5.9	9.6	0.7	–	–	36.20	
8	Nannochloropsis Sp	77.2	9.9	4.7	8.2	0.5	–	–	39	
9	Almeriansis	73.2	9.3	5.1	0.8	11.7	35.8	20.0	–	42.6
10	Gaditana	74.2	9.3	4.0	0.6	11.8	36.2	12.4	–	50.8
11	Nannochloropsis Oceana	77.6	4.9	3.4	–	0.3	–	–	37.70	54.2
12	Derbesia	73	7.5	6.5	10.6	0.7	–	–	33.2	
13	Ulva	72.6	8.2	5.8	11.0	0.4	–	–	33.8	
14	Chaetomorpha	70.9	7.7	6.8	11.4	0.1	–	–	32.5	
15	Cladophora	71.6	8.0	7.1	10.6	0.9	–	–	33.3	
16	Oedogonium	72.1	8.1	6.3	10.4	1.3	–	–	33.7	
17	Cladophora FW	71.1	8.3	6.8	10.6	1.3	–	–	33.5	
18	Aspen wood	75.2	8.2	0.5	15.8	0.3	0.48	3.8	34.3	
19	Scenedesmus	72.6	9.0	6.5	10.5	1.35	–	–	35.5	
20	Defatted scene	72.2	8.9	7.8	10.5	0.90	–	–	35.3	
21	Spirulina	72.2	9.1	8.1	9.2	1.41	–	–	35.8	
22	Nutrient depleted Oedogonium	65.8	8.5	1.5	18.3	–	–	–		
23	Spent coffee grounds	71.2	7.1	3.0	18.7	–	–	–	31.00	
24	Pinus	60.1	6.0	1.2	32.7	0.1	–	–	23.1	
25	Cupressus funebris	62.0	6.6	1.6	29.8	0.1	–	–	25.1	
26	Platanus	70.0	6.3	0.7	23.0	0.01	–	–	28.6	
27	Cinnamomum Camphora	74.0	8.4	1.5	16.1	0.01	–	–	34.2	
28	Pittosporum tobira	71.0	8.5	1.5	19.0	0.01	–	–	32.9	
29	Distylium racemosum	64.1	6.8	0.7	28.4	0.01	–	–	26.3	
30	Viburnum odoratissimum	71.7	8.1	1.2	19.0	0.01	–	–	32.5	
31	Salix alba	73.7	9.2	3.1	14.1	0.01	–	–	35.6	
32	Algal waste of Indiana polis	71.4	8.36	4.92	15.4	–	–	–	33.3	
33	Swine manure	71	8.9	4.1	0.21	14.2	35	–	–	61
34	Garbage	73.6	9.1	4.6		12.7	36	–	–	21
35	Indonesian biomass residue	67–80	6–8	0–2		11–23	30	–	–	21–36
36	Sawdust, rice husk, lignin						–	–	–	8
37	Beech wood	76.7	7.1	0.1		16.1	34.9	–	–	28
38	Phytomass	76.6	7.6	2.1	0.1	13.6	–	–	–	
39	Algae Dunaliella tertiolecta	63.55	7.66	3.71		25.8	30.7	–	–	25.8
40	Porphyridium	66–83	5–11	0–12	0–1	8–27	22.8–36.9	–	–	5–25
41	Nannochloropsis	51	7	9	0.6	28.8		3	–	46
42	Acid mine drainage	68.8	7.9	7.1			–	–	29.70	
43	Cyanobacteria sp.	76.02	9.10	6.29	7.44	1.15	–	–	36.51	
44	Bacillariophyta sp.	76.09	9.11	5.60	8.28	0.92	–	–	36.45	
45	Seaweed	75.54	9.16	3.65	11.66	0.62	–	–	35.97	
46	L.digitata	70.5	7.8	4.0	17	0.7	–	–	32	17.6
47	L.hyperbore	72.8	7.7	3.7	14.9	0.8	–	–	33	9.8
48	L.saccharina	74.5	7.9	3.0	14.0	0.6	–	–	33.9	13
49	A.esculenta	73.8	8	3.8	14	0.8	–	–	33.8	17.8
50	L.Saccharina	31.3	3.7	2.4	26.3	0.7	24.2	9.2	12	
51	Taihu cyanophyta	77.30	12.08	1.10	9.01		–	–	41.73	
52	Coffee Husk	43.13	5.02	1.55	32.78	0.67	7.4	8.44	16.79	
53	Tucuma Seed	48.83	6.12	0.88	32.20	–	5.97	6.08	20.77	
54	Sugarcane	45.05	5.57	0.25	37.91	–	3.21	6.95	20.77	
55	Peanut shell	41.52	7.43	2.12	27.96	0.60	12.80	7.98	16.52	
56	Rice husk	31.47	6.67	1.04	23.03	0.50	29.53	8.19	15.39	
57	Pine sawdust	45.95	7.47	0.32	34.32	0.57	4.71	6.90	17.03	
58	Pond water algae biomass	46.09	6.22	9.70	37.35	0.64				
59	Spirulina	48.10	6.97	10.14	34.13	0.66				
60	Chlorella	51.33	7.90	9.80	30.38	0.59				
61	Pond water algae oil	59.94	11.57	0.11	28.37	0.31				
62	Spirulina oil	66.73	12.40	0.50	20.21	0.16				
63	Cladophora glomerata	26.8	3.53	2.14	20.48	0.22	36.5	9.1	10.29	
64	Posidonia Oceanica	35.5	3.60	0.27	28.85	0.18	26.1	5.5	12.82	
65	Nannochloropsis gaditana	40.3	5.97	6.30	14.49	0.37	28.3	4.1	18.53	
66	Microcystis	42.26	6.27	7.88	43.07	0.52	6.14	9.59	16.2	
67	Almeriensis	41.78	6.81	7.94	42.93	0.55	14.5		17.6	
68	S.japonica	34.7	5.5	1	41.6	0.3	18.3	7.4	12.1	
69	S.pallidum	22.64	4.90	2.96	21.34	1.42	36.44	10.30	9.63	
70	P.elongata	35.81	5.93	6.86	51.40		27.45	11.55	12.54	
71	Sargassum sp	26.70	4.23	1.35	67.53		36.82	9.34	10.10	
72	U.fasciata	25.64	5.75	3.13		5.52	16	19.86		

Annex 2 continues

S.No	Feedstock	Elemental composition of product species after HTL								
		C (%)	H (%)	N (%)	O (%)	S (%)	Ash (%)	Moisture (%)	HHV	% Yield
73	Xuzhou SS	47.4	7.9	8.2	35.2	1.3	56.8	5.6		
74	S.patens C.Agardh						17.7	14.38	15.47	
75	E.grandis	47.19	5.77	0.21	46.59	0.24	0.09		18.07	
76	T.suesica	43.32	7.27	5.75	40.55	3.11	12.20	7.88		
77	Dunaliella tertiolecta	53.3	5.2	9.8	31.7	–			19.8	
78	Chlorella vulgaris	52.6	7.1	8.2	32.2	0.5			23.2	
79	Nannochloropsis oculata	57.8	8.0	8.6	25.7	–			17.9	
80	Botryococcus braunii	77.04	12.40	1.23	9.86	0.18			35.6	
81	Fucus vesiculosus	32.88	4.77	2.53	35.63	2.44	11.8		15.0	
82	Chorda filum	39.14	4.69	1.42	37.23	1.62	9.9		15.55	
83	Laminaria digitata	31.59	4.85	0.90	34.16	2.44	10		17.60	
84	Fucus Serratus	33.5	4.78	2.39	34.44	1.31	18.6		16.66	
85	Laminaria hyperborea	34.97	5.31	1.12	35.09	2.06	11.2		16.54	
86	Macrocystis pyrifera	27.3	4.08	2.03	34.8	1.89	18.5		16.0	
87	Miscanthus	46.32	5.58	0.56	41.79	0.2	2.1		19.08	
88	Nannochloropsis Salina	55.16	6.87	2.73	33.97	1.27	2.48	4.95	25.40	
89	Mougeotia	41.51	5.59	5.40	27.03	0.51	19.96	5.14	16.63	
90	Cladophora	33.79	4.73	6.35	21.27	1.57	32.29	5.09	14.53	
91	Seaweed meal	43.99	5.95	5.21	36.13	1.02	7.7	7.92	18.35	
92	Synechococcus/Anabaena	42.78	7.74	7.91			38.1	7.4	9.61	
93	Synechocystis	46.12	7.98	3.52			11.2	4.5	15.37	
94	A.azuera	40.82	5.56	0.63	52.99		10.61	6.03	52.99	
95	Chlorella.sp	47.54	7.1	6.73	38.63		5.93	6.8	18.59	
96	E.prolifera	35.20	5.20	2.10	32.98		15.91	8.61	13.4	
97	Datura Stramonium L	43.55	5.98	0.77	49.70		6.38	3.73	14.39	
98	E.Spectabilis	39.27	6.54	1.28	52.91		4.6	5.6	13.17	
99	Brewers spent grain	46.6	6.85	3.54	42.26	0.74	4.5	8	20.39	
100	Laurel algae	48.97	6.38	3.02	41.63		10.53	9.95	19.77	

Annex 3: Reaction pathway of the feedstock macromolecules to the final HTL products. (a) hydrolysis; (b) decomposition; (c) dehydration; (d) polymerization; (e) deamination; (f) Maillard reaction; (g) decarboxylation; (h) aminolysis; (i) cyclization; (j) halogenation; (k) dehydrohalogenation and (l) condensation + pyrolysis.

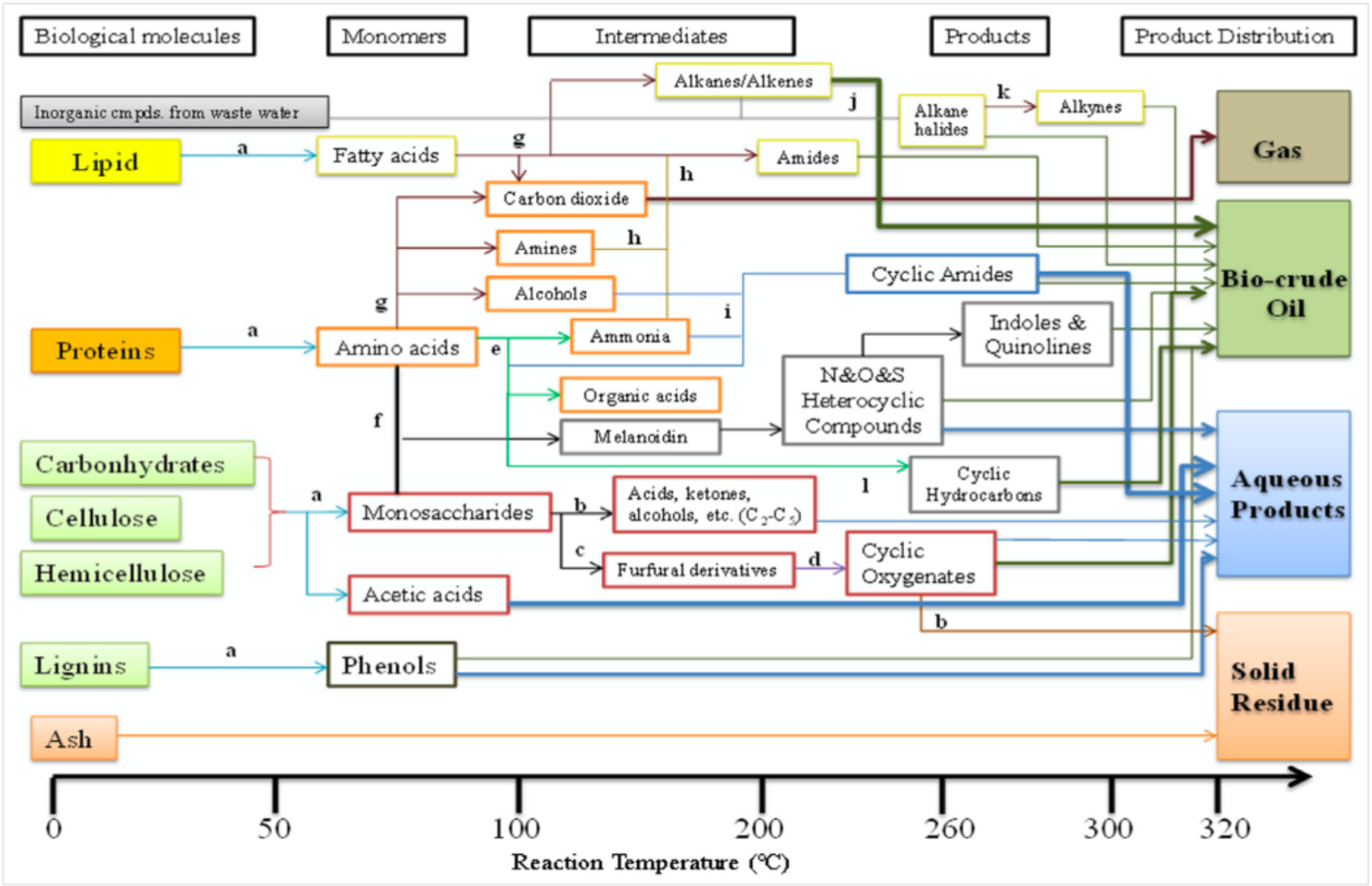

Annex 4: Kinetic theoretical background.

Electrolytic cells are complex system in which different factor can influence the overall rate of a reaction. As shown in the Figure 80, there are different types of variables related to the electrode design, mass transfer in the cell, electrolyte's characteristics, electrical parameters, and external factors such as T, P or time. In this complicated system, the faraday current is usually connected to heterogeneous reactions that occur at the electrode-electrolyte interphase. Eq. (40) relates the current density with the rate of a certain heterogeneous reaction at the electrode-electrolyte region:

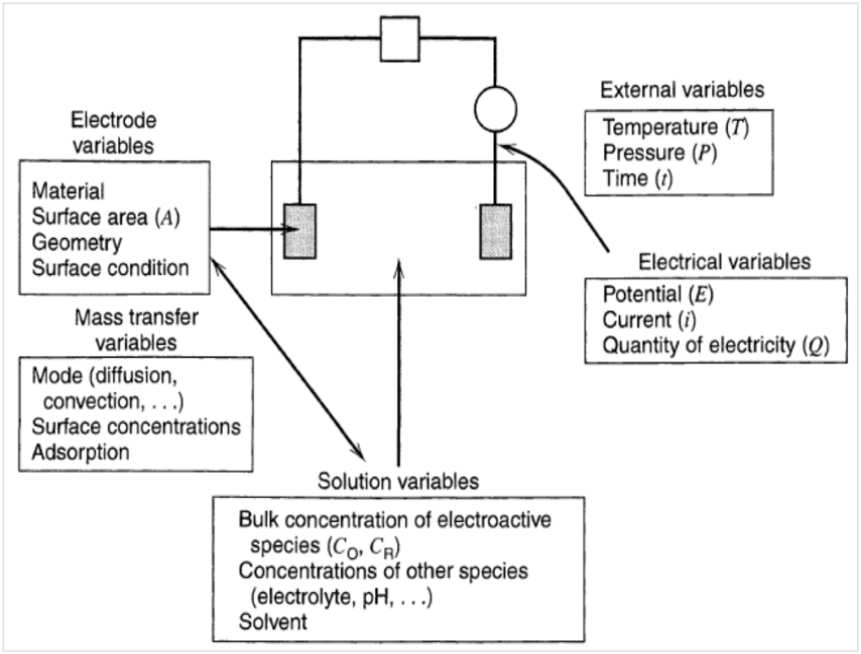

Figure 80: parameters affecting the rate of a target reaction.

$$\text{Rate}[\text{mol sec}^{-1}] = \frac{i}{nFA} = \frac{j}{nF} \qquad (40)$$

In which i is the faradaic current or the dQ/dt [A], n the electron transferred, F the Faraday constant, A the surface area of the electrode (cm^2) and j is the current density [A cm^{-2}].

There are four mains factors that are related with the reaction rate and the electrode current (see Figure 81)[59]: (1) mass transfer to the electrode surface (see paragraph 1.5.4); (2) kinetics of the redox reaction and the electron transfer; (3) eventual successive or preceding reactions; (4) surface reactions related to adsorption, desorption or crystallization dynamics[59]. The electron transfer rate is related to the double layer capacitance and the solution resistance:

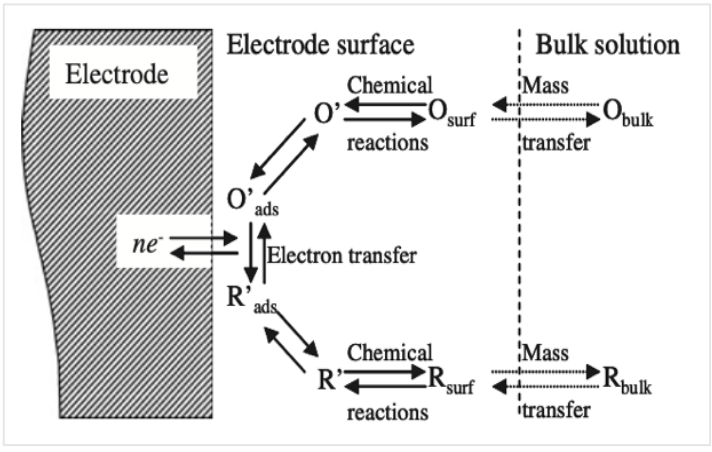

Figure 81: Processes involved in electrode reaction and kinetic.

$$\tau = R_s C_d \tag{41}$$

In which τ is non-faradaic electrode time constant, the R_s the solution resistance and C_d the double layer capacitance. Having τ, the double layer charging will be completed at 95% in a time equal to 3τ. Therefore, it is important to analyse the rate-determining step, which is the slowest process among all. In the non-spontaneous reactions, like the case of biomass upgrading, the potential [V] that you must applied to carrying out the reaction is called overpotential [η]. Electrocatalysis works with the aim to decrease this parameter and the consequent activation energy of the target reaction. The overpotential can be seen as:

$$\eta = E - E_{eq} \tag{42}$$

In which E is the equilibrium potential [V], which can be obtained with the Nernst equation, and the E is the potential applied [V]. Hence, the voltage that can be detected from two electrode in a circuit is formed by different contributions:

$$V = \Delta E_{eq} \pm \sum |\eta_{ct}| \pm \sum |\eta_{conc}| \pm IR \tag{43}$$

In which η_{ct} refers to the activation energies of the reactions occurring at the electrode, η_{conc} is the concentration profiles at the electrode due to mass transport limitations and IR is the ohmic loss. In electrolytic cell there will be the minus sign instead for the galvanic cells the contributions will be always positive.

To understand the kinetic of an electrochemical heterogeneous reaction at the electrode-electrolyte interphase, the Butler-Volmer model equation is often used. Since the purpose of this paper is not a kinetical study, only the complete equation will be highlighted:

$$i = i_0 \left[e^{\frac{-\alpha_a nF\eta}{RT}} - e^{\frac{\alpha_c nF\eta}{RT}} \right] \tag{44}$$

$$i = i_a + i_c \tag{45}$$

In which i_0 is the exchange current [A] that can be derived experimentally from the Tafel plot, α_a and α_c are the electrode dimensionless charge transfer coefficient parameter that can have a value in between 0 to 1 (usually it is equal to 0.5) and η is the overpotential [V] with a value shown in the eq. (42). In yellow is highlighted the anodic contribution, instead in green the cathodic one. This equation can be used to predict the current resulted from an overpotential[59] and it is based on different kinetic concepts, taking in consideration the difference of cathodic and anodic currents, the

Arrhenius equation, the Gibbs activation energies in form of overpotential and the reaction rate constant. The Butler-Volmer equation can be also written using the exchange current density j_0 [A c

m^2] and in general, high J_0 indicates a facile electrochemical reaction, instead with a low j_0 there will be a sluggish kinetic of the electrochemical reaction and a higher overpotential must be applied to achieve a certain current. The Figure 82[85] shows the current density-overpotential curves in relationship with the anodic (positive) and cathodic (negative) current density; notice that increasing the exchange current density (A m^{-2}) the overpotential is reduced, signal of fast redox kinetic.

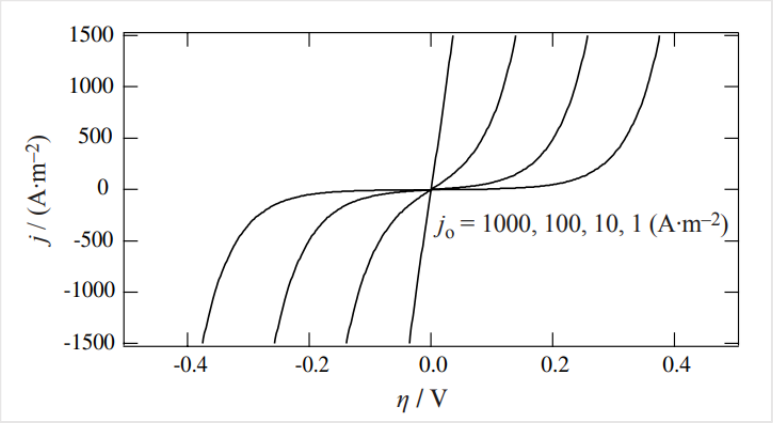

Figure 82: Influence of the exchange current density on the overpotential-current density curves, calculated at n=1, α=0,5 and T=298K

To validate the Butler-Volmer equation some assumptions must be done:

- Mass-transfer limitations are negligible and the concentration at the surface of the electrode is equal to the concentration at the bulk.
- n is often assumed equal to one.
- The volume of the solution is large enough so that the concentrations in the solution remain constant.

To extend the validity of the Butler-Volmer equation, it can be also written considering the mass transfer limitation, hence the eq. (46) is obtained:

$$j = j_0\left[\frac{c_0(0,t)}{c_0^*} e^{\frac{-\alpha_a nF\eta}{RT}} \frac{c_r(0,t)}{c_r^*} - e^{\frac{\alpha_c nF\eta}{RT}}\right] \quad (46)$$

In which the C_o and C_r are the concentration of the species that have to be oxidized or reduced instead the c(0,t) parameters are the species time depending concentration at distance 0 from the electrode's surface.

The Butler-Volmer equation is often displayed as the log|I| or log|j| in function of the overpotential in the so-called Tafel plots (see Figure 83)[85]. Indeed, further

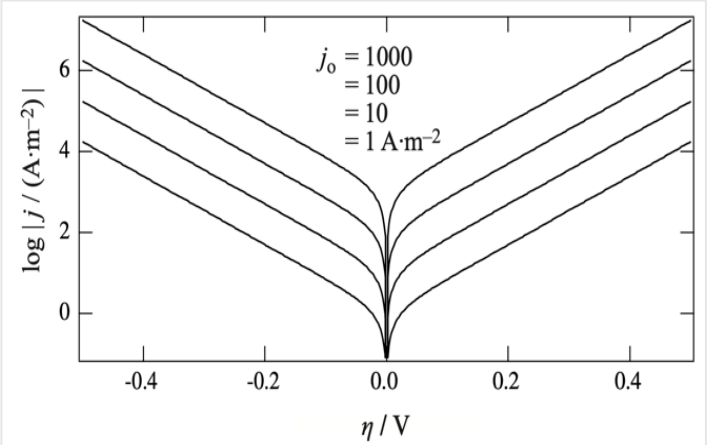

Figure 83: Tafel plot at n=1, α=0,5 and T =298K.

from the equilibrium, usually only one term of the Butler-Volmer equation dominates, therefore it can be simplified as followed:

$$i_a = i_0 \exp\left(\frac{\eta}{b}\right) \quad (47)$$

$$i_c = -i_0 \exp\left(-\frac{\eta}{b}\right) \quad (48)$$

In which b is the Tafel slope and:

$$\eta = a + b \log i \quad (49)$$

The Taffel equation allows to determine graphically the exchange current or the exchange current density by the extrapolation of the two lines at $\eta = 0$ V. Furthermore, by analysing the slope the charge transfer coefficient can be predicted[85].

Annex 5: working electrode preparation procedure.

The WE, before being implemented in the electrochemical cell, undergoes two main phases: (1) preparation phase followed by the (2) pre-treatments phase.

The preparation phase can be divided in two main steps:

I. **Cutting and shaping:** the Ni foam (main electrocatalyst used) has been taken from an industrial roll. The cutting has been done using scissors and calibre achieving a rectangular shape of 2cm x 1cm.

II. **Electrode assembling:** the shaped Ni foam is then assembled on a metallic conductive stick from the side not immersed in the electrolyte solution (using only 1x1cm of the cut). This side is then covered with inert Teflon material to avoid the possible influence on the gas phase and on the solution. The capillary phenomenon that would carry the solution in the upper part of the catalyst by the pores, has been neglected.

The second phase consists in all the pre-treatments necessary to clean and avoid contaminations phenomena. The reliability of results also depends on the capabilities of a method to avoid or to remove any impurities in the electrochemical system. The WE is always treated, since the reaction will occur on its surface or pores. In the case of this study, this phase can be divided in five main steps:

I. **Isopropanol immersion:** the metal stick with the electrocatalyst has been gently immersed and relieved in a pure solution of HPLC isopropanol 100% assay. It has to be done for a dozen of times, to be sure that the eventual organic residuals can dissolve.

II. **Milli-Q rinsing:** the foam has been washed with Milli-Q water to remove the remaining isopropanol.

III. **Acid treatment:** the electrocatalyst was then subjected to an acid treatment. The acid used is an HCl 2M in Milli-Q water. The stick has been immersed in a baker with the acid solution and left in immersion for 5 minutes.

IV. **Milli-Q rinsing:** it has been done in order to remove the gross part of the acidic solution that could actually remain in the pores.

V. **Ultrasonic treatments:** after some struggles regarding the incoherent changing of the pH, this step has been implemented. The aim is therefore to have certainty about the effective acid removal. Hence, the electrocatalyst, after the second rinsing, is put in a backer with Milli-Q water. The backer is than immersed for 10 minutes in the Ultrasonic bath for the treatment.

With these five steps, the pre-treatments can guarantee an elimination of almost all the most frequent contaminations. This step has been done for all the electrocatalysts that would later be used to perform the reactions.

Annex 6: reaction set-up protocol.

The reaction set-up procedure presents different steps:

I. **Preheating of the cell:** using clamps, the cell is put for minimum 10 minutes in a crystallizer located on a heating plate at maximum 55 °C (depending on the solvent used). A thermocouple has been used to monitor the temperature and a magnetic stirrer to homogenise the heat transfer.

II. **Electrolyte adding and preparation:** Depending on the type of test, each electrolyte solutions have been prepared ad hoc. The logic followed can be generalised in two main approaches: (1) for isolated tests, the right volume of solvent (methanol, ethanol/H_2O, or acetonitrile) was firstly added in the cell and after the amount of the suitable supporting electrolyte (NaOH, NaCl, $LiBF_4$ or LiCl) has been added directly in the cell; (2) for repeated tests, instead, the electrolyte solutions (catholyte or anolyte) have been mixed in 100 ml flasks in order to be stored for the next reaction and decrease the accidental errors.

Also in this case, in based on the type of cell, the electrolyte solution has been added in the cell using a graduated cylinder. For the Mcell, 40 ml of the electrolyte solution of interest has been used. For the Hcell and the HCF, 30 ml (or 25 ml) of the catholyte has been added in the cathodic chamber and after the anolyte has been progressively added to reach the same level of the catholyte, or, in some cases, the same volume (30 ml or 25 ml) has been just used. Also in this case, depending on the logic followed to prepare the electrolyte, the volume measured with the graduated cylinder might be only the solvent (isolated tests) or the electrolyte already mixed

(repeated tests). After the electrolyte solution's adding, a magnetic stirrer has been placed only in the cathodic compartment.

III. **Palmitic Acid addition:** after, the suitable amount of PA has been added as anolyte.

IV. **Time of solubility:** sometimes the PA do not solubilise immediately, for this reason a waiting time has been established. This time interval was variable in based on the PA concentration, type of solvent and set-up.

V. **Analysis of the pH:** in most of the tests, the pH has been measured using a portable pH meter pre calibrated. In the Hcell the pH has been evaluated in both the compartments, in particular when the system was new. These values will be compared with the pH measurements after CA, or they have been analysed for other observations.

VI. **Electrode's implementation:** after the pH measurements the electrode have been implemented in the cell. For the Mcell a single septum has been used, instead for the Hcell any electrode had a septum (see paragraph 2.2.1).

VII. **N_2 purging:** this step is fundamental. Indeed, the purging is used to set an inert atmosphere in the headspace removing oxygen and other reactive gaseous species. The removal of the oxygen is very important because the reductive environment is guarantee. Furthermore, oxygen can undergo side reaction that might decrease the overall faradaic efficiency (FE) or even jeopardise the target reaction pathway. For this reason, it has been used a N_2 purging system, in which the gas inlet needles were coupled with outlet in order to do maintain the atmospheric pressure while purging the other gases away. This treatment used to last 10 minutes, but after the Micro-GC analysis on the headspace, the timing has been increased to 40 minutes, since the value of oxygen was too high.

VIII. **Reaction temperature setting:** only 3-4 minutes before the finish of the N_2 purging, the reaction temperature has been settled. This why it happens that sometimes, during the purging at reaction temperature (60°C or above) the catholyte, that is based on organic solvents, used to evaporate decreasing the level of the cathodic compartment. This phenomenon can generate some disequilibrium of mass between the two compartments, generating a possible mass flow, as well as change the concentration and all the further analyses.

After these few steps the system is ready to be electrochemically analysed by techniques such as EIS, CV, DPV or CA. Some tests may exit on this scale, but the most important ones have been followed it. reassumes all the main parameters and treatments that each test has been subjected.

Annex 7: Nafion membrane cleaning procedure.

The protocol followed to clean the Nafion membrane is shown above:

I. **Hydrogen peroxide bath:** the membrane is put in a Becker with 30 ml of a solution of H_2O_2 3% in water for 1 hour at 80°C.

II. **Milli-Q water bath:** in another backer, the membrane is put in 30 ml of Milli-Q water for 1 hour at 80 °C.

III. **Sulfuric acid bath:** the Nafion membrane is then left to soak for 1 hour, at 80°C, in an aqueous solution of H_2SO_4 0,5 M.

IV. **Milli-Q water treatment:** in order to re-establish the grade of protonation of membrane and avoid that once implemented in the cell it could acidified the environment, further water baths must be done. Therefore, a glass plate is used and 3 baths of 10 min have been done. A backer with Milli-Q water is also prepared and using a pH meter, the pH is detected. After any bath the pH of the solution in the glass plate is analysed. This step finish when the pH is more or less the same of the Milli-Q water in the backer.

Annex 8: extrapolation of the excel file used for the calculation of capacitance and resistance.

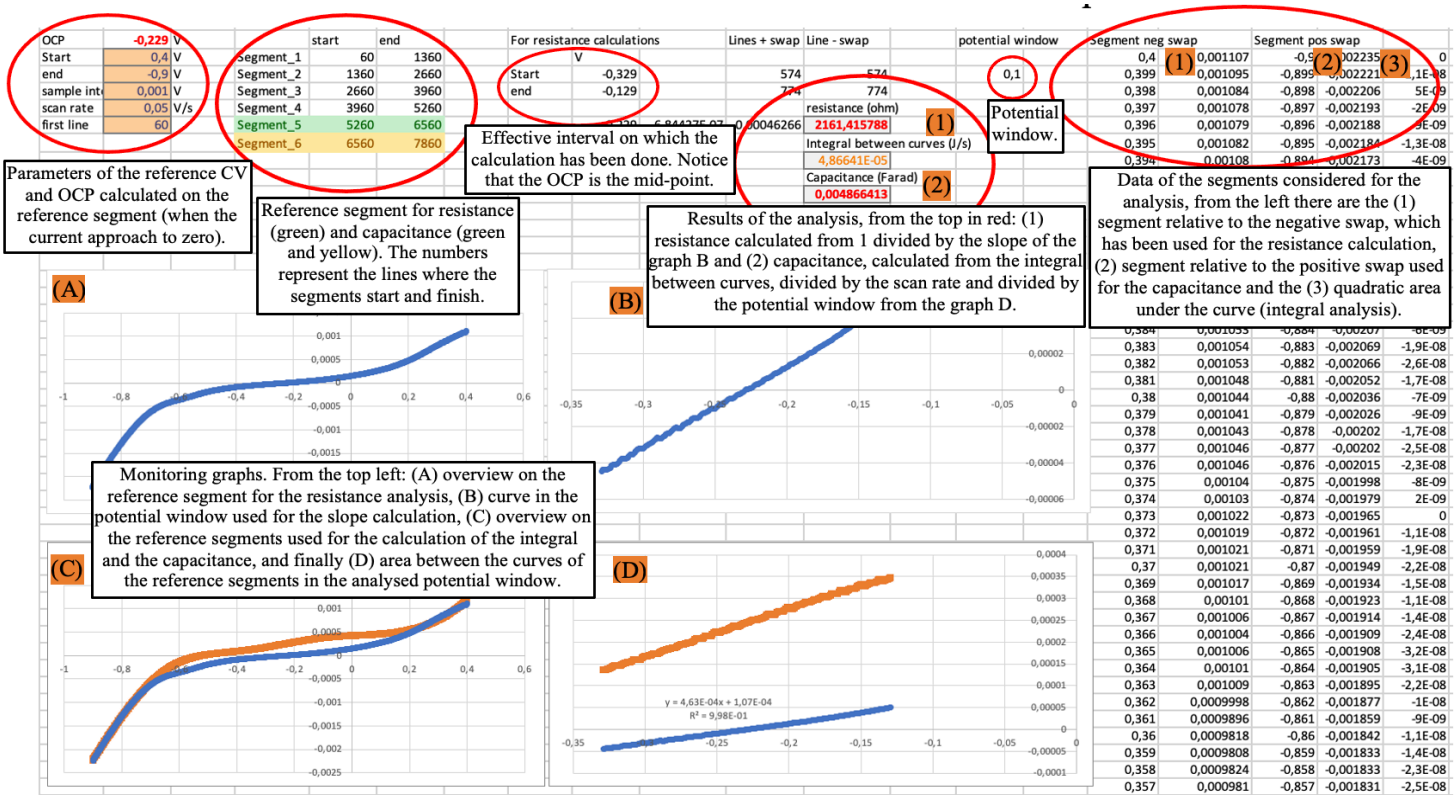

Annex 9: DSC sampling and analysis.

The acidified sample has followed a standard method of preparation:

I. **Sample weighing:** a mass in the range of 1-2 mg of the solid sample has been weighted with a 5-decimal analytical scale directly on the specific 50 µL pan with holes.

II. **Sample covering:** the sample is then transported in the appropriate compartment on the specific crimper and covered with the suitable cover.

III. **Cutting and pressing** using the crimper the boarder of the plate has been cut, obtaining a circular sample that suits the size of the chamber.

IV. **Initial T setting:** in order to set the initial temperature of the first segment, the cooler has been turned on and the temperature has been set at -60°C.

V. **Method setting:** before the sample injection, the method must be defined. In this case of study, it is based on four segments, from -60 to 140, 140 to 0, 0 to 140 and 140 to 0 °C. In some cases, the higher temperature could be 200 or 400 °C. This range has been found suitable for the PA evaluation and the target product analysis.

VI. **Data specifics:** the sample name and mass has been set in the software.

VII. **Sample and reference injection:** when the chamber has achieved -60 °C, it has been opened and using a vacuum stick, the sample is put in the left furnace and the reference in the right one. The two samples must be covered with the suitable covers. When the chamber is closed the analysis can be initialised by the software.

Annex 10: TGA sampling and analysis.

The standard procedure was:

I. **Sample weighing:** like in the case of the DSC, a mass of 1-2 mg of sample has been weighted with a 5-decimal analytical scale directly on the alumina crucible. Any residues outside the crucible had to be removed since it could jeopardise the analysis or even ruin the furnace.

II. **Sample injection:** the crucible with the sample is carefully put in the TGA's autosampler and the plastic cover is closed in order to avoid the entrance of dusts and particulates.

III. **Software set-up:** the sample is analysed by the autosampler, and all the parameters have been set on the software. Usually, the thermal scan is 40 °C/min for an interval that goes from 0 °C to almost 1000 °C.

Annex 11: IR sampling and analysis procedure.

The protocol followed for the IR analysis is divided in five steps:

I. **Cleaning of the crystal plate**: the plate where the sample is put has been cleaned with ethanol and dried up with a special lens-cleaning tissue.

II. **Background detection**: before the analysis and every 5 minutes, the background has been detected. Practically, no sample is put on the crystal and the analysis is carried out. The background spectrum will be the sum of all the gaseous or solid/liquid impurities present in between the sensor and crystal. The characteristic background's IR spectrum has been saved and the following analysis will be corrected in base on it.

III. **Sample analysis**: an unquantified amount of solid sample has been put on the crystal. The upper part of the spectrometer with the sensor must be carefully lowered until it blocks. The sample was than ready to be analysed and the run launched.

IV. **Cleaning of the plate**: the crystal plate has been cleaned properly for the next sample with ethanol and the special lens-cleaning tissue.

Annex 12: table of the tests.

n°	Aim of the test	Validity	Cell type	Electrolyte solution (catholyte)	Supporting electrolyte	Anolyte	Analyte concetration [mM]	Apparent initial pH	CV	System resistance	System capacitance [W]	CA	Reaction Potential [V]	Reaction time [s]	Apparent final pH (after reaction)	Accumulated charges [C]
1a	Bologna cond. Emulation	Failed N2 purg	H cell, frit	20ml - 85% MeOH, 15%H2O	0.1M NaOH	H2O - 0,1M NaOH	10 PA	/	/	/	/	/	/	/	/	/
1b	Bologna cond. Emulation	Failed N2 purg	H cell, frit	20ml - 85% MeOH, 15%H2O	0.1M NaOH	H2O - 0,1M NaOH	10 PA	/	/	/	/	/	/	/	/	/
1c	Bologna cond. Emulation	Failed N2 purg	H cell, frit	20ml - 85% MeOH, 15%H2O	0.1M NaOH	H2O - 0,1M NaOH	10 PA	/	yes	/	/	/	/	/	/	/
1d	Bologna cond. Emulation	Failed N2 purg	H cell, frit	20ml - 85% MeOH, 15%H2O	0.1M NaOH	H2O - 0,1M NaOH	10 PA	/	yes(4)	/	/	/	/	/	/	/
1e	Bologna cond. Emulation	Valid	H cell, frit	20ml - 85% MeOH, 15%H2O	0.1M NaOH	H2O - 0,1M NaOH	10 PA	/	yes (4)	/	/	/	/	/	/	/
1f	Bologna cond. Emulation	Valid. (problem with RE)	H cell, frit	20ml - 85% MeOH, 15%H2O	0.1M NaOH	H2O - 0,1M NaOH	10 PA	/	yes (4)	/	/	/	/	/	/	/
1g	Bologna cond. Emulation	No N2 purging	H cell, frit	20ml - 85% MeOH, 15%H2O	0.1M NaOH	H2O - 0,1M NaOH	0	/	yes	/	/	/	/	/	/	/
1h	Bologna cond. Emulation	No N2 purging	H cell, frit	20ml - 85% MeOH, 15%H2O	0.1M NaOH	H2O - 0,1M NaOH	10 PA	/	yes (2)	/	/	/	/	/	/	/
2a	PA formal potential study, liquified PA	Failed, no current	H cell, frit	Liqueied PA	/	H2O - 0,1M NaOH	/	/	/	/	/	/	/	/	/	/
2b	PA formal potential study, liquified PA	Failed, no current	M cell	Liqueied PA	/	/	30ml - 25,56g PA	/	/	/	/	/	/	/	/	/
2c	PA formal potential study, liquified PA	Failed, sup. electr. No soluble	M cell	Liqueied PA	0,1M LiBF4	/	10ml - 8,52g PA	/	/	/	/	/	/	/	/	/
2d	PA formal potential study, liquified PA	Failed, No relevant current	M cell	Liqueied PA	0.1M LiCl	/	20ml - 17,05g PA	/	/	/	/	/	/	/	/	/
2g	PA formal potential study, liquified PA	Failed, supp. Elect. No soluble	M cell	Liqueied PA	0.25M LiCl	/	20ml - 17,05g PA	/	/	/	/	/	/	/	/	/
3a	EtOH system, PA in excess	Valid	M cell	30ml - 70% EtOH, 30% H2O	0.1M NaOH	/	7,17g. PA	Acid pH	yes	/	/	/	/	/	/	/
3b	EtOH system, PA in excess	Valid	M cell	30ml - 70% EtOH, 30% H2O	0.1M NaOH	/	/	/	yes	/	/	/	/	/	/	/
3c	EtOH system, PA in excess	Valid	M cell	30ml - 70% EtOH, 30% H2O	0.1M NaOH	/	3,585g PA	Acid pH	yes	/	/	/	/	/	/	/
4d	EtOH system testing, pH analysis at neutralisation	Failed, no N2 purging after additions	M cell	40ml - 70% EtOH, 30% H2O	10mM NaOH	/	Variable, additions with relative CV: 0, 3, 7, 10 mM PA	From basic (blank), to neutral (10mM PA)	yes (5), 4 after additions, 1 after CA	/	/	yes (first 30 min missed)	-0,5	10800	Neutral/alkaline	/
4e	EtOH system testing, pH analysis at neutralisation	Failed, at 10mM the CV was no sense	M cell	40ml - 70% EtOH, 30% H2O	10mM NaOH	/	Variable, additions with relative CV: 0, 3, 7, 10 mM PA	From 12,06 (blank) to 7,66 (10mM PA)	yes (4), 4 after additions	/	/	/	/	/	/	/
4f	EtOH system testing, pH analysis at neutralisation	Valid	M cell	40ml - 70% EtOH, 30% H2O	10mM NaOH	/	Variable, additions with relative CV: 0, 3, 7, 10, 13, 16, 19, 25, 30, 35 mM PA	From 12,46 (blank) to 6,11 (35mM AP)	yes (11), 10 after additions and 1 after CA	/	/	yes	-0,5	5400	/	/
4g	EtOH system testing, pH analysis, direct neutralisation	Valid	M cell	40ml - 70% EtOH, 30% H2O	10mM NaOH	/	Variable, additions with relative CV: 0, 10, 16 mM PA	from 12,30 (blank) to 6,87 (16mM)	yes (3), after additions	/	/	yes	-0,6	10800	6,87	/
4h	EtOH system testing, pH analysis	Failed, pH problem, after 10mM the pH was 5,22	H cell, Nafion n117	40ml - 70% EtOH, 30% H2O	10mM NaOH	H2O - 10mM NaOH	Variable, additions with relative CV: 0, 10 mM PA	From 13 (EtOH), 11,70 (H2O) to 5,22 (EtOH) and 10,75 (H2O) with 10 mM PA	yes (2), after additions	/	/	/	/	/	/	/
4i	EtOH system testing, pH analysis	Failed, positive OCP and no reaction has been carried out	H cell, Nafion n117	40ml - 70% EtOH, 30% H2O	10mM NaOH	H2O - 10mM NaOH	10 PA	6,14 EtOH and 10,82 H2O	yes (2), Blank + 10mM	/	/	yes	-0,4	10800	/	/
4j	EtOH system testing, pH analysis	Failed, pH problem	H cell, Nafion n117	40ml - 70% EtOH, 30% H2O	10mM NaOH	H2O - 10mM NaOH	10 PA	Wrong pH	yes (2), Blank + 10mM	/	/	/	/	/	/	/

Annex 12 continues

n°	Aim of the test	Validity	Cell type	Electrolyte solution (catholyte)	Supporting electrolyte	Anolyte	Analyte concetration [mM]	Apparent initial pH	CV	System resistance	System capacitance [W]	CA	Reaction Potential [V]	Reaction time [s]	Apparent final pH (after reaction)	Accumulated charges [C]
5a	EtOH system testing, pH analysis post membrane cleaning	Failed, OCP too high	H cell, Nafion n117	30ml - 70% EtOH, 30% H2O	10mM NaOH	H2O - 10mM NaOH	10 PA	/	/	/	/	/	/	/	/	/
5b	EtOH system testing, pH analysis post membrane cleaning	Valid	H cell, Nafion n117	30ml - 70% EtOH, 30% H2O	10mM NaOH	H2O - 10mM NaOH	Variable, additions with relative CV: 0, 3, 7, 10 mM PA	From 12,30 (EtOH), 10,98 (H2O) to 6,45 (EtOH) and 10,85 (H2O) with 10 mM PA	yes (3), after additions	/	/	yes	-0,6 (-0,2/-0,3 positive current, -0,4/-0,5 low current)	5400	/	/
5c	EtOH system testing, pH analysis post membrane cleaning	Valid	H cell, Nafion n117	30ml - 70% EtOH, 30% H2O	10mM NaOH	H2O - 10mM NaOH	Variable, additions with relative CV: 0, 10 mM PA	From 11,98 EtOH to 6,30 with 10 mM PA	yes (2), Blank + 10mM	/	/	yes	-0,65	5400	/	/
5d	EtOH system testing, pH analysis post membrane cleaning	Valid	H cell, Nafion n117	30ml - 70% EtOH, 30% H2O	10mM NaOH	H2O - 10mM NaOH	Variable, additions with relative CV: 0, 7, 10 mM PA	From 12,38 (EtOH) to 6,64 (10 mM)	yes (3), after additions	/	/	/	/	/	/	/
5e	EtOH system testing, pH analysis post membrane cleaning	Valid	H cell, Nafion n117	30ml - 70% EtOH, 30% H2O	10mM NaOH	H2O - 10mM NaOH	Variable, additions with relative CV: 0, 7, 10, 13, 16, 19 mM PA	From 12,50 (EtPH) to 6,25 (19 mM)	yes. (6)	/	/	/	/	/	/	/
5f	EtOH system testing, pH analysis post membrane cleaning	Valid	H cell, Nafion n117	30ml - 70% EtOH, 30% H2O	10mM NaOH	H2O - 10mM NaOH	Variable, additions with relative CV: 0, 7, 10, 16, 22, 25 mM PA	From 12,60 (EtPH) to 6,23 (25 mM)	yes (5), after addition	2041,693542	0,004805239	yes	-0,65	14500	6,95	/
5g	Chemical blank, Understand if there some non-electrochemical reactionl	Valid	H cell, Nafion n117	30ml - 70% EtOH, 30% H2O	10mM NaOH	H2O - 10mM NaOH	25 PA	/	/	/	/	/	/	14500	/	/
5h	EtOH system testing (5f)	Valid	H cell, Nafion n117	30ml - 70% EtOH, 30% H2O	10mM NaOH	H2O - 10mM NaOH	25 PA	6,7-7,06	yes(1)	914,674167	0,006134631	yes	-0,65	21600 and let overnight in T	EtOH: 7,3-7,6; H2O: 6,3-6,8	-28,27
5i	EtOH system testing (5f)	Valid	H cell, Nafion n117	30ml - 70% EtOH, 30% H2O	10mM NaOH	H2O - 10mM NaOH	25 PA	6,6-7	yes(1)	655,1457144	0,006959861	yes(2, divided)	-0,7	75520 total	EtOH: 7,4-7; H2O: 3,3-3,8	-16,44 after 15750 (CA1), -20,14 after 60770 (CA2)
5j	Electrochemical blank of 5f, 5h, 5i with NaCl in more or less same ionic strenght and pH	Valid	H cell, Nafion n117	30ml - 70% EtOH, 30% H2O	25mM NaCl	H2O - 10mM NaOH	/	EtOH: 6,6-7; H2O: 6,3-6,7	yes(1)	275,1559439	0,008713606	yes	-0,7	10800	/	-1,32
5k	Electrochemical blank 2 of 5f, 5h, 5i with NaCl in more or less smae ionic strenght and pH, 40 min N2 purging	Valid	H cell, Nafion n117	30ml - 70% EtOH, 30% H2O	25mM NaCl	H2O - 10mM NaOH	/	/	yes(1)	186,2194333	0,040465994	yes	-0,7	61200	/	-16,44
5l	Electrochemical blank 2 of 5f, 5h, 5i with NaCl in more or less smae ionic strenght and pH, 36 min N2 purging	Valid	H cell, Nafion n117	30ml - 70% EtOH, 30% H2O	25mM NaCl	H2O - 10mM NaOH	/	/	/	/	/	/	/	/	/	/
5m	Chemical blank of 5f, 5h, 5i with NaOH, 25mN PA , 40 min N2 purging	Valid	H cell, Nafion n117	30ml - 70% EtOH, 30% H2O	10mM NaOH	H2O - 10mM NaOH	25 PA	/	/	/	/	/	/	10800	/	/
5n	Chemical blank for CO analysis, no catalyst, but in T	Valid	H cell, Nafion n117	30ml - 70% EtOH, 30% H2O	10mM NaOH	H2O - 10mM NaOH	/	/	/	/	/	/	/	10800	/	/
5o	Chemical blank for CO analysis, no catalyst, 25°C	Valid	H cell, Nafion n117	30ml - 70% EtOH, 30% H2O	10mM NaOH	H2O - 10mM NaOH	/	/	/	/	/	/	/	10800	/	/
5p	Same condition as 5i	valid (low corrent passage)	H cell, Nafion n118	30ml - 70% EtOH, 30% H2O	10mM NaOH	H2O - 10mM NaOH	25 PA	/								
5q	EtOH system testing (5f)	Low current, blocked	H cell, Nafion n117	30ml - 70% EtOH, 30% H2O	10mM NaOH	H2O - 10mM NaOH	25 PA	6,5	/	/	/	/	/	/	/	/
5r	EtOH system testing (5f)	Valid	H cell, Nafion n117	30ml - 70% EtOH, 30% H2O	10mM NaOH	H2O - 10mM NaOH	25 PA	6,54	yes (1)	248,2564554	0,015740708	yes (2, divided)	-0,7	10800	/	-7,043 after 10800 (CA1), -3,722 after 55870 (CA2)
5s	EtOH system testing (5f)	Valid	H cell, Nafion n117	30ml - 70% EtOH, 30% H2O	10mM NaOH	H2O - 10mM NaOH	20 PA	6,05 (20mM)	yes (2), Blank + 20mM	3593,93044	0,003342529	yes	-0,65	11040	6,63	/

Annex 12 continues

n°	Aim of the test	Validity	Cell type	Electrolyte solution (catholyte)	Supporting electrolyte	Anolyte	Analyte concetration [mM]	Apparent initial pH	CV	System resistance	System capacitance [W]	CA	Reaction Potential [V]	Reaction time [s]	Apparent final pH (after reaction)	Accumulated charges [C]
6a	Try to enlarge the potential window of the system to isolare the peak	Failed, problem with acid pH and Ni	H cell	25ml - 100%. AcNi (98% pure)	5mM TBABF4	100%. AcNi (98% pure) + 5mM. TBAB4	5 PA	4,30 (blank), 3,70 (5mM)	yes (2), Blank + 5mM	/	/	/	/	/	/	/
6b	Try to enlarge the potential window, addition of H2O,	Failed, invalid CV2 and OCPs	M cell	40ml - 100%. AcNi (98% pure)	5mM LiBF4	/	10 initialy PA	/	/	/	/	/	/	/	/	/
6c	Try to enlarge the potential window, addition of H2O	/	M cell	40ml - 100%. AcNi (98% pure)	5mM LiBF4	/	20 PA	From 1,3 (no water) to 5,3 (with 20% H2O added)	yes (7)	/	/	/	/	/	/	/
7a	Evaluate the Na palmitate at neutral pH with no supporting electrolyte	Failed, problem with the pH	H cell, Nafion n117	25ml - 70% EtOH, 30% H2O	/	H2O - 5mM NaOH	10 NaPal	8,35	yes(1)	5126,552742	0,006780752	yes	-0,7	5400	9,0±	-28,27
7b	Repeat 7a but in M cell and with 5mM NaCl	Valid	M cell	40ml - 70% EtOH, 30% H2O	5mM NaCl	/	10 NaPal	8,043	yes(1)	3101,083322	0,008552088	yes	-0,7	5400	7,8	6
7c	Chemical blank, Understand if there some non-electrochemical reactionl	Valid	M cell	40ml - 70% EtOH, 30% H2O	5mM NaCl	/	10 NaPal	/	/	/	/	/	/	5400	/	/
7d	Reversibility test, from 7b	Valid	M cell	40ml - 70% EtOH, 30% H2O	5mM NaCl	/	10 NaPal	/	yes at different scan rate	9421,78046	0,002383312	/	/	/	/	/
7e	Change the [NaPal] maintening the some ionic strenght, try to also analyse the pH	Valid	M cell	40ml - 70% EtOH, 30% H2O	10mM NaCl	/	5 NaPal	7,7±	yes(2), the first is valid	2177,130945	0,008200938	yes	-0,7	5400	8,08±	-5,362
7f	Change the [NaPal] maintening the some ionic strenght, try to also analyse the pH	Valid	M cell	40ml - 70% EtOH, 30% H2O	14mM NaCl	/	1 NaPal	7,6±	yes(1)	1250,114433	0,007189211	yes	-0,7	5400	7,5±	-3,181
7g	Change the [NaPal] maintening the some ionic strenght, try to also analyse the pH	Valid	M cell	40ml - 70% EtOH, 30% H2O	5mM NaCl	/	20 NaPal	8,5± (??)	yes(1)	2358,066659	0,008796061	yes	-0,7	10800	8,4	-9,738 (after 5400s)
7h	Blank of 7b	Valid	M cell	40ml - 70% EtOH, 30% H2O	5mM NaCl	/	/	/	yes	2039,372282	0,001549273	yes	-0,7	5400	/	-3,868
8a	Test or comparison with 7a, but using NaPal	Valid	H cell, Nafion n117	25ml - 70% EtOH, 30% H2O	10μl sol 0,1M KOH	10μl sol 0,1M KOH in H2O	10 NaPal	9,4	yes(1)	3027,037396	0,003581027	yes	-0,7	5400	10,85±	-1,45
9a	Test at basic pH (9-10) for comparison with 5f.	Valid	H cell, Nafion n117	25ml - 70% EtOH, 30% H2O	10mM NaOH	H2O - 10mM NaOH	9 PA	8,5	yes(1)	4712,603513	0,005408047	yes	-0,8	5400	11,2±	-1,778
10a	System in hydrogenation, comparison with 5f and related tests.	Valid	H cell, Nafion n117	25ml - 70% EtOH, 30% H2O	10mM NaOH	H2O - 10mM NaOH	20 PA	6,9	yes(1)	2022,662119	0,005854376	yes	-1,5 (hydrogenation)	5400	8±	-18,94
11a	System in hydrogenatio, comparison with 7a or 10a	Valid	M cell	40ml - 70% EtOH, 30% H2O	5mM NaCl	/	10 NaPal	8,5	yes(1)	2992,299541	0,004257225	yes	-1,5	5400	8,75	-35,69
12a	system in hydrogenation, and alkaline pH, comparison with 11a, 10a and 9a.	Valid (no perfect range of pH)	H cell, Nafion n117	30ml - 70% EtOH, 30% H2O	10mM NaOH	H2O - 10mM NaOH	8,5 PA	8,3 (difficult to achieve 9-10, unstable)	yes(1)	4845,252783	0,006763748	yes	-1,5	5400	/	-19,2
12b	system in hydrogenation, and alkaline pH, comparison with 11a, 10a and 9a.	Valid (problem with pH of the anolyte and catholyte)	H cell, Nafion n117	30ml - 70% EtOH, 30% H2O	10mM NaOH	H2O - 10mM NaOH	12 PA	8,9 (difficult to achieve 9-10, unstable)	yes(1)	4780,354326	0,005773926	yes	-2	14400	EtOH: 11,5; H2O: 5	-53,38
12c	system in hydrogenation, and alkaline pH, comparison with 11a, 10a and 9a.	Valid (problem with pH of the anolyte and catholyte)	H cell, Nafion n117	30ml - 70% EtOH, 30% H2O	10mM NaOH	H2O - 10mM NaOH	10 PA	8,4 (difficult to achieve 9-10, unstable)	yes(1)	452,8778009	0,003183689	yes	-2	14400	EtOH: 11,23; H2O: 5	-32,27
12d	system in hydrogenation, and alkaline pH, comparison with 11a, 10a and 9a.	Valid	H cell, Nafion n117	30ml - 70% EtOH, 30% H2O	10mM NaOH	H2O - 10mM NaOH	10 PA	9,04	yes(1)	2947,081821	0,006186667	yes	-1,4	14400	EtOH: 11,60; H2O: 6,60	-37,16
13a	test for the study of the acid conditions	Valid	H cell, Nafion n117	30ml - 70% EtOH, 30% H2O	10mM NaOH	H2O - 10mM NaOH	25 PA	6,54	Yes (1)	15365,20524	0,000490488	yes	-0,7	10800	6,22	-0,9471
13b	test for the study of the acid conditions	Valid	H cell, Nafion n117	30ml - 70% EtOH, 30% H2O	0,1M NaCl	H2O - 0,1M NaCl	10 PA	EtOH: 4,22; H2O: 5,46	yes (3), 2 before CA and 1 after CA	6167,145607	0,001619203	yes	-0,7	10800	EtOH: 4,90 H2O: 2,98	-3,531

Annex 13: table of the IR results.

Peaks (wn)	symmetrical stretching vibration of -CH3 group (2913)		symmetrical stretching vibration of -CH2 group (2848)		C=O stretching vibration peak (1695)		deformation-vibration of -CH2 and -CH3 group (1464)		deformation-vibration of -CH2 and -CH3 group (1434)	
Sample	**Wavenumber (cm-1)**	**Height**	**Wavenumber (cm-1)**	**Height**	**Wavenumber (cm-1)**	**Height**	**Wavenumber (cm-1)**	**Height**	**Wavenumber (cm-1)**	**Height**
P. Acid ref	2914,29	62,406	2848,345	50,000	1698,95	29,803	1462,98	9,896	1428,96	7,592
P. Acid ref 2	2915,14	65,203	2848,345	50,000	1699,28	32,522	1463,10	9,676	1429,17	7,280
C14 acid ref	2914,91	62,534	2848,345	50,000	1699,00	36,427	1463,19	10,152	1429,07	9,866
C12 acid ref	2915,67	68,930	2848,345	50	1699,00	47,462	1470,58	14,529	1429,26	10,366
C10 acid ref	2915,20	66,592	2848,345	50	1705,39	36,765	1471,11	12,294	1429,01	8,455
5c	2915,070	63,907	2848,345	50,000	1699,060	26,014	1471,240	14,065	1429,020	6,691
5f	2914,490	59,930	2848,345	50,000	1699,070	19,782	1471,380	15,032	1429,020	8,005
5g (blank 5f)	2914,83	65,585	2848,345	50,000	1699,06	23,176	1471,26	17,636	1431,19	9,687
5h (5f bis)	2915,14	59,624	2848,345	50,000	1699,14	19,782	1471,3	15,032	1428,96	7,994
5i (5f tris)	2914,83	67,414	2848,345	50,000	1698,93	26,355	1471,39	12,110	1428,85	7,192
5s	2914,700	67,928	2848,345	50,000	1698,730	22,192	1462,550	7,901	1429,500	5,408
10a (Test 6)	2914,62	67,174	2848,345	50,000	1698,93	31,580	1471,58	9,497	1429,11	6,670
11a (Test 7)	2914,94	66,059	2848,345	50,000	1699,03	28,040	1471,45	10,941	1429,38	6,341
12b	2914,74	66,753	2848,345	50,000	1699,02	28,739	1471,37	12,176	1429,29	6,750
12c	2914,47	55,820	2848,345	50,000	1698,95	29,956	1471,38	12,373	1429,23	10,560
12d	2914,92	67,944	2848,345	50,000	1699,01	27,617	1471,35	12,042	1429,09	7,202
13b	2914,78	65,052	2848,345	50,000	1698,95	25,953	1471,38	11,884	1429,33	6,625

Annex 13 continues

Peaks (wn)	deformation-vibration of -CH2 and -CH3 group (1418)		in-plane vibration of the -OH group (1299)		out-plane vibration of the -OH group (939)		swinging vibrations of the -OH group (723)		swinging vibrations of the -OH group (685)		Quality of baseline
Sample	Wavenumber (cm-1)	Height	Wavenumber (cm-1)	Height	Wavenumber (cm-1)	Height	Wavenumber (cm-1)	Height	Wavenumber (cm-1)	Height	
P. Acid ref	1410,48	6,875	1293,85	10,881	938,87	7,724	719,68	6,815	687,42	3,441	Good
P. Acid ref 2	1410,67	6,466	1294,29	10,364	940,39	7,334	719,92	6,401	688,17	2,905	
C14 acid ref	1410,22	9,258	1306,89	11,020	940,02	9,234	719,89	7,228	687,37	4,512	Good
C12 acid ref	1410,61	9,190	1303,09	13,900	935,19	8,719	720,34	5,018	685,31	3,471	
C10 acid ref	1410,89	8,293	1294,15	11,412	939,79	8,181	719,87	6,396	688,05	2,575	
5c	1410,290	7,353	1293,360	10,376	940,740	6,502	719,680	6,629	689,020	2,834	Good
5f	1410,980	8,108	1293,610	9,112	943,700	5,846	718,190	5,531	689,080	3,114	Good
5g (blank 5f)	1411,52	9,172	1293,15	9,705	941,11	4,972	717,32	6,741	686,74	2,814	Good
5h (5f bis)	1410,71	8,095	1293,68	9,112	940,48	5,648	719,04	5,496	688,74	3,100	Good
5i (5f tris)	1410,68	6,730	1293,69	9,317	940,07	5,800	719,73	5,095	688,23	2,580	Good
5s	1406,510	5,640	1293,310	8,611	941,740	4,981	719,500	4,984	688,090	2,051	Good
10a (Test 6)	1410,48	5,000	1294,43	10,474	940,27	8,051	719,98	6,578	688,45	3,895	Good
11a (Test 7)	1410,68	5,360	1294,38	8,958	940,61	6,297	719,88	5,421	688,53	2,746	Good
12b	1410,57	5,604	1294,16	9,386	940,87	6,861	719,79	5,809	688,32	2,840	Good
12c	1410,85	7,482	1295,45	12,057	940,19	12,208	719,78	9,217	688,66	7,967	Good
12d	1410,71	6,218	1293,85	9,325	939,76	6,333	719,81	5,629	688,32	2,960	Good
13b	1410,72	5,880	1293,89	8,894	941,4	6,117	719,68	5,524	688,08	2,583	Good

Annex 14: table of TGA results of Palmitic acid curves, Na Palmitate curves and residual mass. In red the sample treated in air.

Sample	Mass sample	T onset palmitic acid (°C)	Mass palmitic acid (%)	T onset Na palmitate (°C)	Mass Na palmitate (%)	Overall mass (%)	Residual mass (%)
Palmitic acid blank	5,9	254,8	98,18	/	/	98,18	1,82
Na palmitate blank	1,12	205,9	10,84	479,9	77,52	92,5	7,5
Carbon Black ref.	3,24	/	/	/	/	99,21	0,79
5f before reaction	3,56	224,2	81,86	470,9	14,37	96,72	3,28
5f after reaction	2,37	257,9	42,86	481,8	32,91	80,99	19,01
5f before reaction, air treatment	1,76	209,3	87,39	/	/	100,52	-0,52
5f after reaction, air treatment	1,34	217	50,57	340,9	23,6	90,34	9,66
5s	1,85	224,3	48,25	484	34,84	88,29	11,71
5g (5f blank)	1,7	231	61,52	462,4	33,05	96,95	3,05
5h	2,17	222,4	16,21	465,1	58,45	94,12	5,88
5i	1,6	225,1	17,02	469	58,87	91,17	8,83
5i after acid	0,51						
5m (chem. Blank 5f)	2,13	221,9	61,86	463,3	27,37	91,51	8,49
5m (chem. Blank 5f) bis	1,9	227,7	65,54	461,5	28,32	95,68	4,32
5m after acid	1,94						
5r	2,23	238	8,74	459,6	57,69	87,46	12,54
12a	1,71	213,5	3,38	460,5	60,68	72,86	27,14
12b	1,6	/	/	470,1	65,81	76,9	23,1
12b air treatment	0,8	/	/	323	64,05	92,75	7,25
12c	1,47	/	/	461,7	68,73	71,91	28,09
12c air treatment	1,86	207,2	8,43	299,7	63,91	80,79	19,21
12d (-1,4)	1,7	/	/	443,1	72,55	79,4	20,6
12d after acid	2	204,8	75,72	/	/	95,36	4,64
12d (-1,4) - air	1,54	214,1	4,65	338,8	57,36	70,46	29,54
12d after acid - air	1,78	208,4	-66,9	354,3	1,56	92,05	7,95
7b	1,66	201	-15,08	471,7	66,69	91,58	8,42
7c (chem. blank 7b)	1,56	202,8	8,76	468,4	70,57	89,63	10,37
7e	0,59	205,9	14,05	461,2	46,67	81,1	18,9
7g	2	209	7,3	461,3	78,27	88,53	11,47
7g after acid	1,35	207,9	52,31	460,4	36,4	93,49	6,51
13a	1,8	231,9	58,53	459,6	35,22	94,7	5,3
13b	2,93	209,7	31,65	453,6	2,42	36,62	63,38
13b air	2,12	209,4	44,12	301	4,55	50,98	49,02
10a (test 6) -1,5	1,66	224,8	8,06	463,9	68,39	90,73	9,27
11a (test 7)	1,63	217,1	35,83	488,,8	41,1	90,99	9,01

Annex 15: TGA results on the anomalous curves. In red the samples treated in air.

Sample	T onset 1 (°C)	Mass 1 (%)	T onset 2 (°C)	Mass 2 (%)	T onset 3 (°C)	Mass 3 (%)	T onset 4 (°C)	Mass 4 (%)	T onset 5 (°C)	Mass 5 (%)	T onset 6 (°C)	Mass 6 (%)	T onset 7 (°C)	Mass 7 (%)	T onset 8 (°C)	Mass 8 (%)	T onset 9 (°C)	Mass 9 (%)	T onset 10 (°C)	Mass 10 (%)	T onset 11 (°C)	Mass 11 (%)	T onset 12 (°C)	Mass 12 (%)
Palmitic acid blank																								
Na palmitate blank																								
Carbon Black ref.																					697,9	99,25		
5f before reaction																								
5f after reaction																								
5f before reaction, air treatment																	412,6	11,31						
5f after reaction, air treatment																	450	6,99						
5s																								
5g (5f blank)																								
5h													357,9	11,61										
5i													353,4	11,61										
5i after acid																								
5m (chem. Blank 5f)																								
5m (chem. Blank 5f) bis																								
5m after acid																								
5r													357,7	18,11										
12a			124	3,22															Present					
12b	91,4	1,83	131,5	2,56									343	1,87										
12b air treatment	91	7,88	128,8	7,94																				
12c	Present		Present																					
12c air treatment																								
12d (-1,4)			125,3	3,67																				
12d after acid											307,2	4,98	343	4,86									841,1	-9,75
12d (-1,4) - air	85,5	2,29																						
12d after acid - air							261,3	1,51	279,8	2,41					386,1	1,56							848,3	-17,56
7b																								
7c (chem. blank 7b)																			619,6	4,47				
7e																								
7g																								
7g after acid																			Present				831,1	4,59
13a																								
13b													330	1,03										
13b air	56,5	0,22									301	4,55												
10a (test 6) -1,5													345,4	9,27										
11a (test 7)																							850	10,04

Annex 16: table of the DSC results, until 140°C and with only the first segment.

Sample	Mass sample (g)	Starting T (°C)	Final T (°C)		T Peak	Transition ΔH (J/g)	T Peak	Transition ΔH (J/g)	T Peak	Transition ΔH (J/g)	T Peak	Transition ΔH (J/g)	T Peak	Transition ΔH (J/g)	T Peak	Transition ΔH (J/g)	T Peak	Transition ΔH (J/g)	T Peak	Transition ΔH (J/g)
Palmitic acid reference	4,65	-60	400																	
Na palmitate reference	2,1	-60	400																	
Na Palmitate after acid	1,27	-60	140		-1,69	-0,862			7,46	-0,945	11,83	0,642	24,37	0,705						
Decanoic acid reference	2	-60	140								10,53	0,824			37,43	110,322				
C12 reference low T	1,5	-60	140														47,93	167,796		
C14 reference low T	3,62	-60	140																	
1-Hexadecanol reference low T	1,32	-60	140																	
1-Hexadecanol reference high T	1,32	-60	400																	
5f after reaction 1	1,8	-20	150																	
5f after reaction 2	1,8	-20	150																	
5f after reaction, after acid	0,3	-60	140																52,77	20,444
5f after reaction, afrer acid high T	0,3	-60	400																	
5f after reaction high T	1,4	-60	400								13,3	1,313	26,7	1,217						
5f before reaction	2,5	-20	150																	
5s acid	2	-60	200				3,9	8,758			12,03	8,818								
5h acid	0,87	-60	140								13,3	4,071			33,69	10,279				
5h acid 2	1,05	-60	140								11,14	0,541	25,99	4,241						
5h low T	1,83	-60	140								12,34	1,753								
5i acid	1,26	-60	140								11,53	2,442								
5m acid	1,17	-60	140						7,92	-0,83	17,13	-985								
5r	2,01	-60	200						8,05	-1,146	11,51	0,766	26,54	1,88						
5r acid	2,4	-60	200																	
5g acid	1,48	-60	200		0,18	-0,078			8,08	-0,599	12,73	0,203	23,81	-1,724						
5r acid	2,4	-60	200																	
7b acid	1,03	-60	200		0,23	-1,549	3,39	0,589	8,39	-4,294										
7c acid (chemical balnk 7b)	1,61	-60	200																	
7g acid	2,4	-60	200										22,44	0,164						
12b	1,65	-60	200								12,15	3,56			35,84	12,593				
12b acid	1,71	-60	200																	
12c	1,55	-60	400																	
12c acid	1,42	-60	200				4	0,828			11,73	0,735			30,4	3,667				
12a acid	2,01	-60	200																	
12d acid	1,86	-60	200																	
10a	1,78	-60	200																	
11a	1,88	-60	200																	
13a acid	1,68	-60	200																	
13b acid	2,2	-60	200				2,71	0,315	7,42	0,076	11,73	1,609			32,35	18,32				

Annex 16 continues

Sample	Mass sample (g)	Starting T (°C)	Final T (°C)		T Peak	Transition ΔH (J/g)	T Peak	Transition ΔH (J/g)	T Peak	Transition ΔH (J/g)	T Peak	Transition ΔH (J/g)	T Peak	Transition ΔH (J/g)	T Peak	Transition ΔH (J/g)	T Peak	Transition ΔH (J/g)	T Peak	Transition ΔH (J/g)
Palmitic acid reference	4,65	-60	400						67,87	202,06										
Na palmitate reference	2,1	-60	400								81,8	23,859			106,2	7,039			130,12	6,258
Na Palmitate after acid	1,27	-60	140						68,63	174,333										
Decanoic acid reference	2	-60	140																	
C12 reference low T	1,5	-60	140																	
C14 reference low T	3,62	-60	140				59,73	183,01												
1-Hexadecanol reference low T	1,32	-60	140		54,5	202,102														
1-Hexadecanol reference high T	1,32	-60	400		52,7	199,23														
5f after reaction 1	1,8	-20	150						66,39	1,085	83,86	2,621	99,9	10,445	109,96	88,494				
5f after reaction 2	1,8	-20	150						62,55	13,163			97,94	10,976	107,73	53,937				
5f after reaction, after acid	0,3	-60	140		54,65	7,499			63,72	29,955										
5f after reaction, afrer acid high T	0,3	-60	400																	
5f after reaction high T	1,4	-60	400										97,34	10,128	106,955	84,564				
5f before reaction	2,5	-20	150						68,63	132,172			97,94	0,616						
5s acid	2	-60	200						66,63	133,651										
5h acid	0,87	-60	140						65,58	111,989										
5h acid 2	1,05	-60	140						66	112,031										
5h low T	1,83	-60	140																	
5i acid	1,26	-60	140						66,53	173,386										
5m acid	1,17	-60	140						63,47	37,519	75,3	44,375								
5r	2,01	-60	200								83,61	45,287			105,45	12,551			131,12	14,385
5r acid	2,4	-60	200						68,64	151,076	80,5	0,611								
5g acid	1,48	-60	200						67,95	60,918	79,18	63,829							146,22	-0,391
5r acid	2,4	-60	200						68,64	151,964	80,69	0,65								
7b acid	1,03	-60	200						68,52	155,009										
7c acid (chemical balnk 7b)	1,61	-60	200						66,82	163,375										
7g acid	2,4	-60	200				61,27	1,988	68,16	73,167	81,17	32,608								
12b	1,65	-60	200												104,29	19,006			138,98	52,396
12b acid	1,71	-60	200						69,74	156,02										
12c	1,55	-60	400												105	11,891			141,79	29,3
12c acid	1,42	-60	200						69,01	112,987			89,86	17,127						
12a acid	2,01	-60	200						67,3	167,587	75,47	0,123	97,94	1,997						
12d acid	1,86	-60	200						68,35	151,288	77,66	11,688								
10a	1,78	-60	200						67,88	180,514										
11a	1,88	-60	200						66,6	150,04										
13a acid	1,68	-60	200						66,2	173,039										
13b acid	2,2	-60	200						67,59	63,069			92,23	0,247						